TECHNISCHE UNIVERSITÄT MÜNCHEN

Department Chemie
Lehrstuhl für Biochemie

Combating Bacterial Infections with Novel Small-Molecule Therapeuticals – Target Identification, Assay Development and Compound Screening

Christina Daschkin, M.Sc. (TUM)

Vollständiger Abdruck der von der Fakultät für Chemie der Technischen Universität München zur Erlangung des akademischen Grades eines Doktors der Naturwissenschaften (Dr. rer. nat.) genehmigten Dissertation

Vorsitzender: Univ.-Prof. Dr. Stephan A. Sieber

Prüfer der Dissertation: 1. Univ.-Prof. Dr. Michael Groll
                                               2. Univ.-Prof. Dr. Markus Gerhard
                                               3. Univ.-Prof. Dr. Anja Hoffmann-Röder
                                                   Ludwig-Maximilians-Universität München

Die Dissertation wurde am 01.07.2015 bei der Technischen Universität München eingereicht und durch die Fakultät für Chemie am 09.11.2015 angenommen.

Table of contents

1 Abstract

Bacterial infections are once again life threatening conditions since rising resistances against established drugs compromise their treatment. Therefore, novel agents against bacterial infections are urgently needed. One such approach is the development of species-specific anti-virulence agents.

Nosocomially transmitted and community acquired Methicillin-resistant strains of *S. aureus* (MRSA) threaten public health due to their capability of causing severe systemic and deep-tissue infections. Especially hospitalized patients with indwelling medical devices and immuno-compromised patients are affected. *H. pylori*, on the other hand, is a gastric pathogen colonizing half the world's population. Since *H. pylori* infection is associated with more than 700,000 cancer cases per year worldwide, eradication is an important means of reducing cancer risk. However, although such therapies comprising combinations of up to four active agents are available, antimicrobial resistance is also increasing for this infectious disease. Consequently, the medical need for alternative therapeutic agents against *S. aureus* and *H. pylori* justifies efforts in the development of virulence inhibitors to obtain promising therapeutic options for combating these highly resistant pathogens. Such species-specific anti-virulence approaches promise decreased risk of resistance development and will spare the healthy microbiota from unwanted alterations, thus reducing side effects. As an alternative to antibiotic treatments, such new therapeutic strategies will help to control antimicrobial resistance and to spare advanced drug regimens for the most severe infectious conditions. The pivotal roles of *S. aureus* Sortase A (SaSrtA) and *H. pylori* γ-glutamyl transpeptidase (HPG) in multiple virulence mechanisms underline their suitability as novel drug targets.

This doctoral thesis presents assay development and validation of the two anti-virulence targets SaSrtA and HPG according to recognized criteria. Both assays performed excellently and were used for screening of compound selections.

Two initial hits were identified with the SaSrtA transpeptidation assay in a natural compound library. However, they could not be validated in subsequent experiments. Future screening endeavors need also to extend the platform for SaSrtA inhibitor validation with additional counter-screening assays and physical binding determination.

For the HPG, a tailored approach yielded 34 confirmed actives corresponding to a hit-rate of 33.33 %. IC_{50}-determination of the tailored compounds justified prioritization of one scaffold for structure-activity-relationship (SAR) studies. 40 derivatives based on this scaffold were submitted to IC_{50}-determination and inhibitory compounds were tested in specificity assays. Two substituents of the chosen scaffold were evaluated for their SAR. The highest inhibitory potency was achieved with compound #39 containing N-(*m*-chlorophenyl)-2-(dimethylamino)acetamide as R1 and *p*-phenoxyphenyl as R2. However, this compound was not selective for HPG and inhibited the human and *E. coli* gGTs as well. Therefore, compound #35 (R1= N-(*p*-methoxyphenyl)-2-(dimethylamino)acetamide) with slightly decreased potency but better selectivity was chosen for subsequent investigations. Physical interaction of HPG with inhibitory compounds of this scaffold class was investigated with MST, NMR-spectroscopy, crystal-soaking, and co-crystallization

experiments to provide a basis for further development efforts. Yet, compound solubilities were limited and thwarted this crucial assessment, thus questioning the compounds' suitability for development. Therefore, complementary approaches such as fragment-based drug discovery are required both to generate new hit compounds as well as provide information on relevant compound characteristics.

In an approach perpetuating the inhibitor identification efforts for SaSrtA and HPG, potential surface-exposed proteins from *H. pylori* were examined to enable prioritization of candidates for comprehensive validation as novel drug targets. Seven out of eight HP candidates identified via surface shaving (by Tobias Kruse) were recombinantly produced and purified. These proteins were used to generate specific murine antisera for investigating the HP candidates' cellular localization in a flow cytometry based approach. With these, the surface localization of six candidates could be confirmed, which is a favorable characteristic for drug targets. For an initial investigation of HP candidate involvement in *in vitro* viability and growth, *H. pylori* knock-out mutants were constructed for five HP candidates. However, only two constructs yielded mutant strains. Three HP-candidates, for which no knock-out mutants could be obtained, can thus be assumed to be essential for *in vitro* viability. Two clones of each obtained knock-out mutant strain were analyzed in liquid culture for growth in comparison to the wild-type strain. The knock out of candidate HP5 did not affect *in vitro* growth whereas the knock out of candidate HP2 reduced the growth of *H. pylori* in the chosen culture conditions. Furthermore, seven recombinant candidate proteins were tested as antigens for serological detection of *H. pylori* positive patient sera in a Luminex® assay. With the set cut-off, a selectivity of up to 97.5 % was obtained. In contrast, the sensitivity was highly variable and ranged from 5.0 % to 45.0 %. This indicated poor antigenicity of the HP candidates or low patient exposure.

In summary, two enzymatic assays have been validated for screening applications and inhibitory compounds were identified. The assays for both targets, SaSrtA and HPG, will be used in future inhibitor discovery approaches to support efforts in combating rising resistant infectious diseases. The SAR described with a class of compounds for HPG will help defining the pharmacophore for this anti-virulence target. Protein candidates from *H. pylori* have been assessed for their suitability as drug targets. Data on their surface-exposure, involvement in *in vitro* growth and viability as well as patient response will help prioritize the most promising candidates for in depth biological validation.

2 Zusammenfassung

Bakterielle Infektionen können heute weiterhin lebensbedrohliche Erkrankungen hervorrufen, da steigende Resistenzen gegen etablierte Medikamente ihre Behandlung erschweren. Folglich werden neuartige Wirkstoffe gegen bakterielle Infektionserkrankungen dringend benötigt. Ein möglicher Ansatz ist die Entwicklung von spezies-spezifischen Anti-Virulenz-Wirkstoffen.

Aufgrund ihrer Fähigkeit schwere systemische oder tiefliegende Gewebeinfektionen zu verursachen bedrohen nosokomial und ambulant erworbene Methicillin-resistente Stämme von *S. aureus* (MRSA) die Gesundheit und das Leben vieler Patienten. Insbesondere im Krankenhaus stationäre Patienten mit im Körper verweilenden medizinischen Vorrichtungen oder immungeschwächte Patienten sind betroffen. *H. pylori* hingegen ist ein im Magen ansässiger Erreger, welcher die halbe Weltbevölkerung kolonisiert. *H. pylori* Infektionen können mit mehr als der Hälfte der eine Million Magenkrebsfälle jährlich assoziiert werden. Daher stellt die Eradikation eine wichtige Methode zur Reduktion des Krebsrisikos dar. Obwohl bei Eradikationstherapien bis zu vier Wirkstoffe kombiniert werden, nehmen auch bei dieser Infektionskrankheit Antibiotikaresistenzen zu. Dementsprechend rechtfertigt der medizinische Bedarf nach alternativen Wirkstoffen gegen *S. aureus* und *H. pylori* Anstrengungen zur Entwicklung von Virulenzinhibitoren, um so vielversprechende therapeutische Möglichkeiten im Kampf gegen diese resistenten Erreger zu erhalten. Derartige spezies-spezifische Anti-Virulenz-Ansätze lassen ein vermindertes Resistenzentwicklungsrisiko erwarten und vermeiden ungewollte Veränderungen der gesunden mikrobiellen Flora, die ihrerseits zu Nebenwirkungen führen kann. Als Alternative zum Einsatz von Antibiotika ermöglichen es diese neuen Strategien, Antibiotika-resistenzen einzudämmen und kritische Behandlungsmöglichkeiten für die bedrohlichsten Infektionen vorzubehalten. Aufgrund der zentralen Funktionen der Sortase A aus *S. aureus* (SaSrtA) und der γ-Glutamyltranspeptidase aus *H. pylori* (HPG) in diversen Virulenzmechanismen sind diese Faktoren als Zielstrukturen für neuartige Wirkstoffentwicklungen bestens geeignet.

In dieser Doktorarbeit werden Assayentwicklung und –validierung zu den beiden Anti-Virulenz-Targets, SaSrtA und HPG, anhand anerkannter Kriterien präsentiert. Beide Assays erfüllen die Validierungskriterien in herausragender Weise und konnten zum Screening ausgesuchter Verbindungen verwendet werden.

Zwei initiale Hits konnten mit dem SaSrtA-Transpeptidierungsassay in einer Sammlung von Naturstoffen identifiziert werden. Diese konnten jedoch in Folgeexperimenten nicht weiter bewertet werden. Zukünftige Bemühungen zur Inhibitoridentifizierung müssen auch die Assayplattform für SaSrtA in Hinblick auf Spezifitätstests und Bindungsassays erweitern.

Für die HPG wurden 34 inhibitorische Verbindungen in einer Auswahl maßgeschneiderter Substanzen identifiziert, was einer Trefferquote von 33,33 % entspricht. IC_{50}-Bestimmungen der maßgeschneiderten Substanzen rechtfertigten die Priorisierung einer Gerüstklasse, um die Struktur-Aktivitäts-Beziehung (SAR) zu untersuchen. Die IC_{50}-Werte von 40 Derivaten sowie die Spezifität inhibitorischer Verbindungen wurden bestimmt. Zwei Substituenten konnten in Hinblick auf ihre SAR ausgewertet werden. Das höchste inhibitorische Potential wurde mit Verbindung #39 erzielt, welche N-(*m*-Chlorophenyl)-2-(dimethylamino)acetamid in Position R1 und *p*-Phenoxyphenyl in Position R2

enthält. Diese Verbindung inhibierte die HPG jedoch nicht spezifisch, sondern zeigte auch einen Effekt auf die humane und die *E. coli* gGT. Daher wurde Substanz #35 (R1 = N-(*p*-Methoxyphenyl)-2-(dimethylamino)acetamid), welche eine etwas geringere Potenz aber eine gute Selektivität aufwies, für nachfolgende Untersuchungen ausgewählt. Die physikalische Interaktion der HPG mit den inhibitorischen Verbindungen sollte mittels MST, NMR-Spektroskopie, Kristall-Soaking und Co-Kristallisation untersucht werdend, um so eine Grundlage für weitere Entwicklungsanstrengungen zu legen. Die Löslichkeit der Substanzen war jedoch begrenzt, sodass die Untersuchungen zur Interaktion mit der HPG kein eindeutiges Ergebnis lieferten. Somit war die entscheidende Beurteilung der Verbindungen im Hinblick auf deren Eignung zur Weiterentwicklung nicht möglich. Daher werden ergänzende Methoden, wie die Fragment-basierte Wirkstoffentwicklung, benötigt, um die Pipeline zu füllen und relevante Eigenschaften inhibitorischer Verbindungen offenzulegen.

In einem Ansatz, der die Bemühungen zur Inhibitoridentifizierung für SaSrtA und HPG weiterführt, wurden potentiell oberflächenexponierte Proteine aus *H. pylori* untersucht, um eine Priorisierung dieser Kandidaten für eine umfassende Bewertung als neue Wirkstoff-Targets zu ermöglichen. Sieben von acht HP-Kandidaten, die in einem Surface-Shaving (von Tobias Kruse) identifiziert worden sind, wurden rekombinant hergestellt und gereinigt. Diese Proteine konnten zur Erzeugung muriner Antiseren verwendet werden, um mit diesen die zelluläre Lokalisation der HP-Kandidaten in einem Durchflusszytometrie-basierten Experiment zu ermitteln. Somit wurde die Oberflächenlokalisation, welche eine bevorzugte Eigenschaft für Wirkstoff-Targets darstellt, von sechs Kandidaten bestätigt. Für eine erste Untersuchung der Beteiligung der Kandidaten an *in vitro* Lebensfähigkeit und Wachstum von *H. pylori* wurden Knock-out-Mutanten von fünf HP-Kandidaten konstruiert. Nur mit zwei dieser Konstrukte konnten jedoch Knockout-Stämme erzeugt werden. Die drei Kandidaten, von denen keine Knock-out-Mutanten erhalten werden konnten, können demnach als essentielle Faktoren für *in vitro* Lebensfähigkeit betrachtet werden. Je zwei Klone der erzeugten Knock-out-Mutantenstämme wurden in Flüssigkultur analysiert, um ihr Wachstumsverhalten mit dem Wildtypstamm zu vergleichen. Der Knockout des Kandidaten HP5 hatte keinen Einfluss auf das *in vitro* Wachstum, wohingegen der Knockout von HP2 zu signifikant reduziertem Wachstum in den gewählten Kultivierungsbedingungen führte. Weiterhin wurden die rekombinant produzierten Kandidatenproteine als Antigene für den serologischen Nachweis von *H. pylori* positiven Patientenseren im Luminex®-Assay getestet. Mit dem gewählten Cut-Off-Wert wurde eine Selektivität von bis zu 97,5 % erzielt. Die Sensitivität war im Gegensatz dazu sehr variabel und schwankte zwischen 5,0 % und 45,0 %. Dieses Ergebnis weist auf eine schwache Antigenität der HP-Kandidaten oder eine geringe Exposition der Patienten hin.

Zusammenfassend wurden zwei enzymatische Assays für Screening-Anwendungen validiert und inhibitorische Verbindungen identifiziert. Die Assays beider Targets, SaSrtA und HPG, werden in weiteren Projekten zur Inhibitoridentifizierung Anwendung finden und folglich die Anstrengungen im Kampf gegen resistente Infektionen unterstützen. Die SAR einer Substanzklasse, welche im Rahmen der vorliegenden Arbeit für die HPG beschrieben werden konnte, wird helfen den Pharmakophor dieses Anti-Virulenz-Targets zu definieren. Kandidaten aus *H. pylori* wurden im Hinblick auf ihre Eignung als Wirkstoff-Target untersucht. Daten bezüglich ihrer Oberflächenlokalisation, Beteiligung

an *in vitro* Lebensfähigkeit und Wachstum sowie Patientenimmunantworten werden helfen, diese Kandidaten für eingehende biologische Bewertung zu priorisieren.

3 Introduction

3.1 Challenges in the treatment of bacterial infections

Only since the first half of the twentieth century, infectious diseases are not the major cause for disease associated death determining human life span any more.[1] However, the initial success of antibiotic development is fading rapidly due to increasing bacterial resistance to antibiotics. In the United States, more than two million patients are newly infected with multi-drug-resistant bacteria every year, leading to eight million additional hospitalization days and about 22,500 death cases per year. Beside such alarming increase in patients' morbidity and mortality, bacterial infections also cause up to 35 billion US$ excess medical costs and additional 35 billion US$ loss of productivity in the United States.[2] A projection predicts 10 million additional deaths per year worldwide caused by rising antimicrobial resistant infections for the year 2050 compared to today. This would also lead to a loss of 2.0 to 3.5 % in the gross domestic product, which corresponds to about 100 trillion US$.[3] Moreover, rising prevalence of a variety of antibiotic-resistant pathogens and a reduction in newly developed and approved drugs is threatening many achievements of modern medicine (Figure 1). Especially the care of premature infants, cancer therapy and transplantation therapy are at stake because of virtually incurable infections in the already immune-compromised patients, who often cannot be treated with back-up antibiotics.[4] Thus, antimicrobial resistance is recognized as a threat to global health and safety.[5]
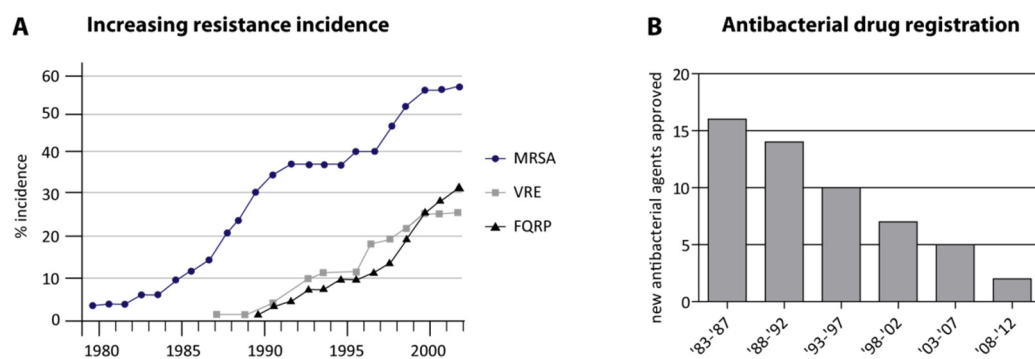
Figure 1: Antibiotic resistance incidence and antibacterial drug registration

Graph A illustrates data collected from hospital intensive care units that participated in the National Nosocomial Infections Surveillance System of the Centers for Disease Control.[6] MRSA: Methicillin-resistant *S. aureus*; VRE: Vancomycin-resistant *Enterococci*; FQRP: Fluoroquinolone-resistant *P. aeruginosa*
Graph B depicts the number of new molecular entity systemic antibiotic per 5-year interval. (Data taken from Infectious Diseases Society of America (IDSA), 20115)

There are classes of antimicrobials that present a comparably slow rate of resistance development due to the fact that multiple targets are being addressed. This prevents fast endogenous resistance development by a single genetic change leading to reduced target affinity or cell permeability, or by up-regulating endogenous enzymes capable of inactivating the compound.[7] As multiple steps of mutation and selection might be needed to lead to infection persistence in this case, a prolonged

phase of drug effectiveness can be anticipated, and these drugs are preferentially used as second line therapies for challenging infections like tuberculosis.[8] Examples are the synthetic antibiotics of the quinolone class, which target both DNA-gyrase and DNA-topoisomerase. Nevertheless, eleven years after being introduced to the market, clinically significant resistance arose.[9]

Another source of resistance development is posed by exogenous elements, which can be acquired via horizontal gene transfer. This mechanism is by itself aggravated in the presence of several antibiotics, in particular in sub-therapeutic concentrations.[10] The resulting resistance can be accomplished by class-specific efflux mechanisms, degradation of the drug or protection of the target structure.[8] Exogenous resistances can arise from environmental sources as was observed e.g. in the transmission of extended spectrum β-lactamases (ESBLs).[11, 12] This fact stresses the point that antimicrobials developed from natural sources may be most susceptible to such kind of resistance development because defense mechanisms could have developed in the environment even before discovery of the drug.[9]

Accordingly, the time lapse between market introduction and the development of significant resistance is multifactorial and can thus vary between less than a year and multiple decades. Important parameters are, furthermore, the quantity of prescriptions and the frequency of sub-therapeutic exposure that drive the selection pressure in favor for resistant organisms. Additionally, the aforementioned reservoir of existing resistance in the environment, the number of endogenous mutations needed to achieve resistance and the overall fitness of resistant bacteria promote resistance development.[13] An overview of market introduction and the time passing until clinically significant resistance arose is given in Figure 2.
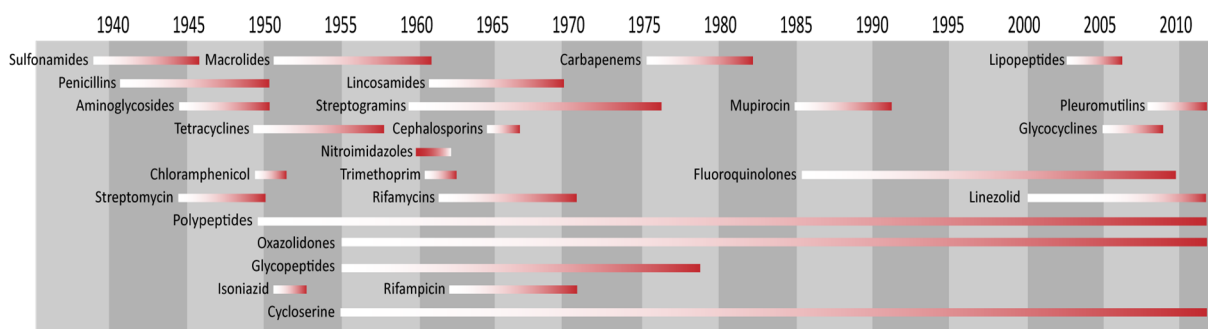
Figure 2: Timeline of market introduction and emerging resistance for anti-bacterials

Market introduction (white) of novel anti-bacterials is followed by clinically significant resistance (red) depending on multiple factors. (Adapted from Nugent, 2010[14])

Despite many discovery programs in pharmaceutical companies and academia, there is a void in the discovery of novel antibacterial drug classes since 1987 (Figure 3). Even though, several new drugs have been approved since. These were either described and patented before, or represent improved versions of previously registered classes. Improvements mainly addressed aspects of safety, bacterial spectrum, dosing regimens and most importantly, circumventing existing resistances and restoring antimicrobial activity. This route may be practicable due to the already suitable pharmacological properties of the known antibacterial. However, regulatory difficulties may arise due to the need of

proving non-inferiority with the existing drug. Moreover, improved drugs of already existing classes are prone to rapidly lead to pre-existing resistance-development problems.[9]

Since many of the highly resistant infections are nosocomially transmitted, efforts in novel drug development have to be accompanied by preventive measures like improving the use of antibiotics, hygiene management and resistance surveillance.[2]
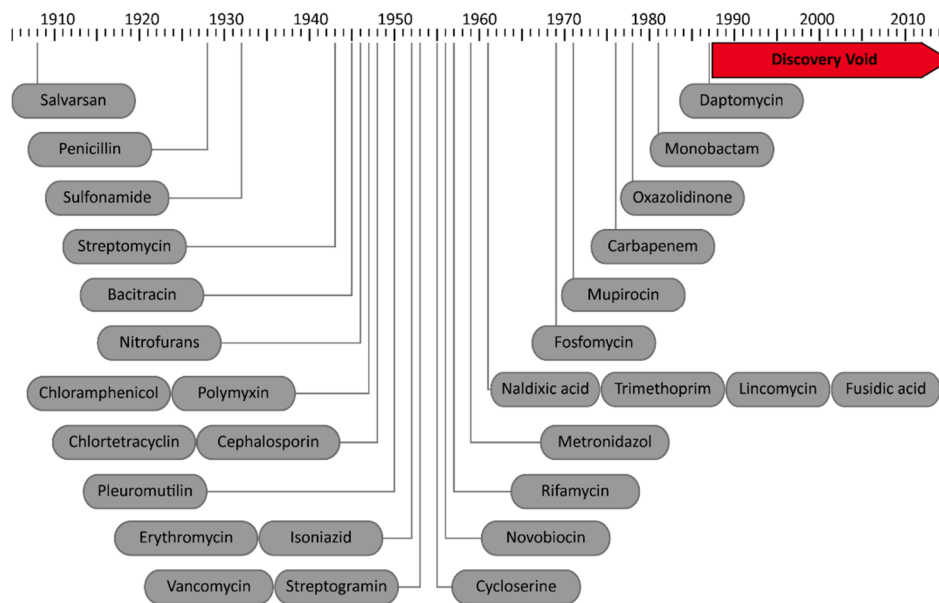
Figure 3: The anti-bacterial discovery-void

The dates indicated for novel systemic anti-bacterial classes correspond to the date of initial discovery or patent. The "Golden Age" of empirical antibiotic discovery (1945-1960) is followed by an ever declining discovery rate and finally the discovery void from 1987 until today. (Adapted from Silver, 2011[9])

Taken together, resistance development and the discovery void for new classes of antimicrobials underline urgent medical need for innovative strategies in anti-bacterial drug development.

3.2 Development of novel antibacterial drugs

Novel targets for antibiotic development have to fulfill several criteria. Firstly, they have to be essential for the organism with respect to their structure or enzymatic activity with the result that blocking the function leads to bacterial death or loss of viability. Secondly, targets need to be conserved across species in order to provide a useful spectrum of the drug. Thirdly, the target structure may have no or only low homology with equivalents in the mammalian host to avoid mechanism-based toxicity. And finally, the target should present sites that can be addressed by small drug-like molecules to obtain biological effects. For anti-virulence agents, those criteria are similar. However, the corresponding targets will only be essential for bacterial survival in the infection setting and inhibition of such targets may not lead to bacterial death or growth inhibition. Therefore, drug effects are targeted at infection-mechanisms and can be inhibition of colonization, spreading, and virulence or immune-evasion mechanisms. Faced with the urgent need for novel therapeutic options, all promising routes of development should be executed in academia and industry.[9, 15]

3.2.1 Novel antibiotics and further use of established antibiotics

Becker and coworkers suggested in 2006, that all the classes of broad-spectrum antibiotics might have already been discovered and no further general metabolic pathways exist that could be addressed by novel drugs (Figure 4).[16] This statement coincided well with the overall reduced interest and investments in general antimicrobial development by the pharmaceutical industry and academia as well as the resulting inappropriately empty antibiotic pipeline.[17]

For the pharmaceutic industry, the easiest way to progress was to modify existing antibiotics to circumvent arising resistances and broaden the anti-bacterial spectrum. This approach usually leads to compounds with suitable pharmacological properties but is eventually limited by the number of analogues that can be developed from the parent core-structure or to the number of analogues, which can overcome existing class specific resistances. The most successful classes to date with regard to the number of marketed analogues are the penicillins and cephalosporins.[17]

A further advance was a combinational therapy with the β-lactam analogue clavulanic acid as resistance inhibitor in combination with the established β-lactam amoxicillin (developed as Augmentin by Beecham Pharmaceuticals, patent document GB 2 005 538 A[18]). This therapy led to mechanism-based inhibition of β-lactamase-conferred resistance and restored the β-lactam efficacy.[19] The newest addition to the β-lactamase inhibitor combination therapy is Avibactam[20], which is a non-β-lactam Serine-β-lactamase inhibitor. It was approved by the FDA in combination with Ceftazidime[21] as treatment for complicated urinary tract and intra-abdominal infections in February 2015.
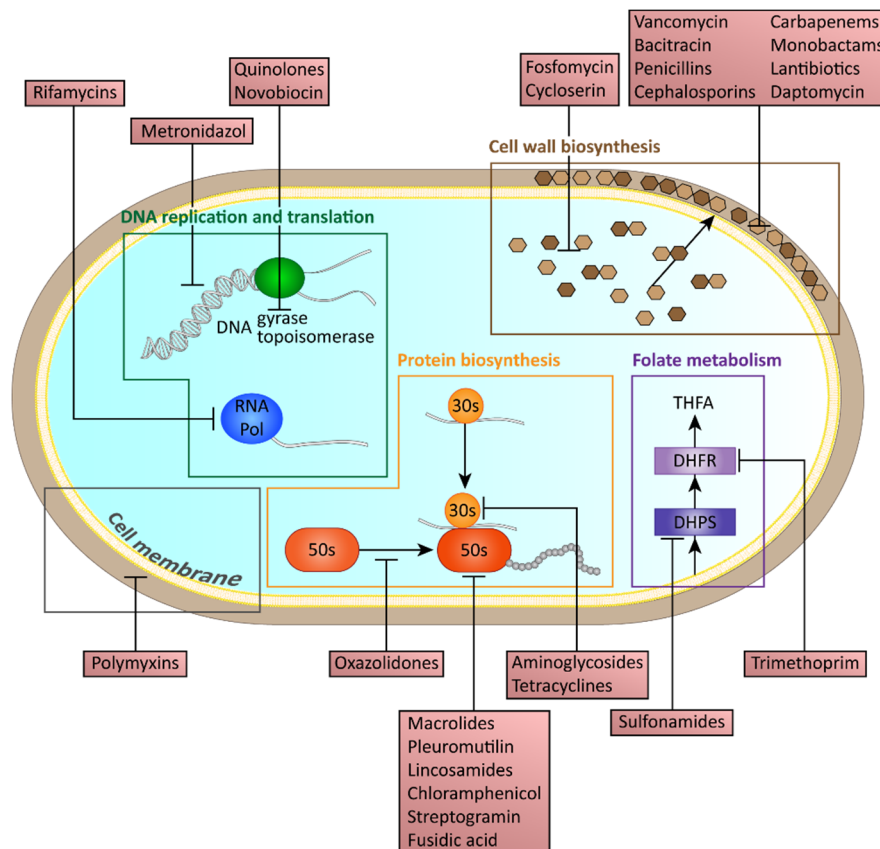
Figure 4: Bacterial targets of antibiotics

Bacterial targets of antibiotics are summarized by their associated function. The classes of antibiotics active against them are indicated in red boxes. DNA replication and translation, protein biosynthesis and cell wall biosynthesis are targeted by nearly all antibiotics in use.

30s and 50s correspond to the ribosomal subunits; DHPS: dihydropteroate synthase; DHFR: dihydrofolic-acid reductase; THFA: tetrahydrofolic acid

(Adapted from Lewis, 2013[22] and Walsh, 2003[13])

Another novel approach is the combination of classical antibiotics with agents that hijack facilitated uptake in bacteria. The most promising mechanism for this is the iron-uptake, which is essential for pathogens in the iron-depleted host environment. Here, siderophores (catecholates, hydroxamates, and citrate based poly-carboxylates) are agents selectively recognized for iron uptake. They can be reasonably coupled to antibacterial drugs. This strategy can overcome membrane-mediated resistances due to selective drug uptake.[23] Basilea (BAL30072) and Pfizer (MC-1) develop siderophore-coupled monobactams against multi-drug resistant gram-negative pathogens.[17]

Apart from those advancements, an essential issue that hinders antibacterial drug development is posed by dormant persister cells, which cannot be addressed with most of the marketed antibiotics and can lead to re-occurence of the infection after treatment. This problem can be approached by prodrugs that are selectively activated by specific enzymes inside the bacterial cell and that are then able to kill even non-replicating cells.[22] Isoniazide and ethionamide are examples of such prodrugs selective for a specific pathogen, in this case *M. tuberculosis*.[24] Identification of produg-like compounds is usually prevented by the common validation step of drug specificity. Thus, particular effort is needed to find these promising compounds in suitable screenings.[22]

Nevertheless, the possible limitations in finding antibiotics and the aforementioned strategies augmenting the versatility of existing antibiotics should not thwart efforts in the search for novel antibiotics. Ultimately, only a small number of targets is known for the thousands of natural antibiotics that were found in screening approaches (Figure 4). The most successful antibiotics address only three structures or pathways, namely the protein biosynthesis, the cell-wall biosynthesis and DNA gyrase or DNA topoisomerase. Therefore, the proportion of the exploited targets within the approximately 200 conserved essential proteins in bacteria is very small.[9, 22]

3.2.2   Anti-infective agents for antibacterial therapy

The need for antibacterial treatment options with reference to resistance emergence and spreading throughout clinically relevant pathogens clearly advances alternative approaches to classical drug development.

The role of the microbiome in resistance development and spreading, as well as the importance of its composition and integrity with regard to the general state of the immune system, diabetes, obesity and mental health urgently needs to be considered in drug development.[22, 25-28] In this respect, a species-specific approach is superior compared to broad-spectrum antibiotics. To achieve species specificity, several means can lead to the discovery of active agents. Basic research reveals novel information on bacteria, so that unique targets may be identified and used for rational drug design.[29] Furthermore, knowing the dynamics of infection and the details of pathophysiology involving bacterial and host interaction factors enables the development of anti-virulence drugs.[30] In this case, resistance emergence may not be as problematic as with the classical antibiotics because anti-virulence agents would not inhibit cell growth *in vitro* and therefore pose less selective pressure for resistant mutants.[15] This assumption, however, has not been formally proven yet. It is conceivable that decreased fitness of the bacteria in presence of the therapeutic agent is sufficient to drive resistance development, but this would still be restricted to the host environment where the targeted factor is essential for survival.[15, 22] Nevertheless, one major drawback is recognized for purely virulence targeted therapies. In these cases opsonization and phagocytic killing by the host immune system is indispensable for clearance of the bacteria. Therefore, virulence inhibitors would have only limited use in immune compromised individuals.[31]

The inhibition of virulence-associated factors and pathways (Figure 5) represents an innovative concept, which promises radically new mechanisms of action of antibacterial agents. A wide span of targets is summarized in this approach. It can be confined to those factors that are crucial for bacterial colonization and persistance in the host leading to pathogenicity, but which are not essential for basic metabolism *in vitro.*[15, 32] The effectors involved capacitate pathogenic bacteria to colonize, disseminate and adapt to various environments in the host as well as subvert host functions and overcome defense mechanisms.[33] Vaccine development has successfully exploited this section of bacterial targets already.[34]
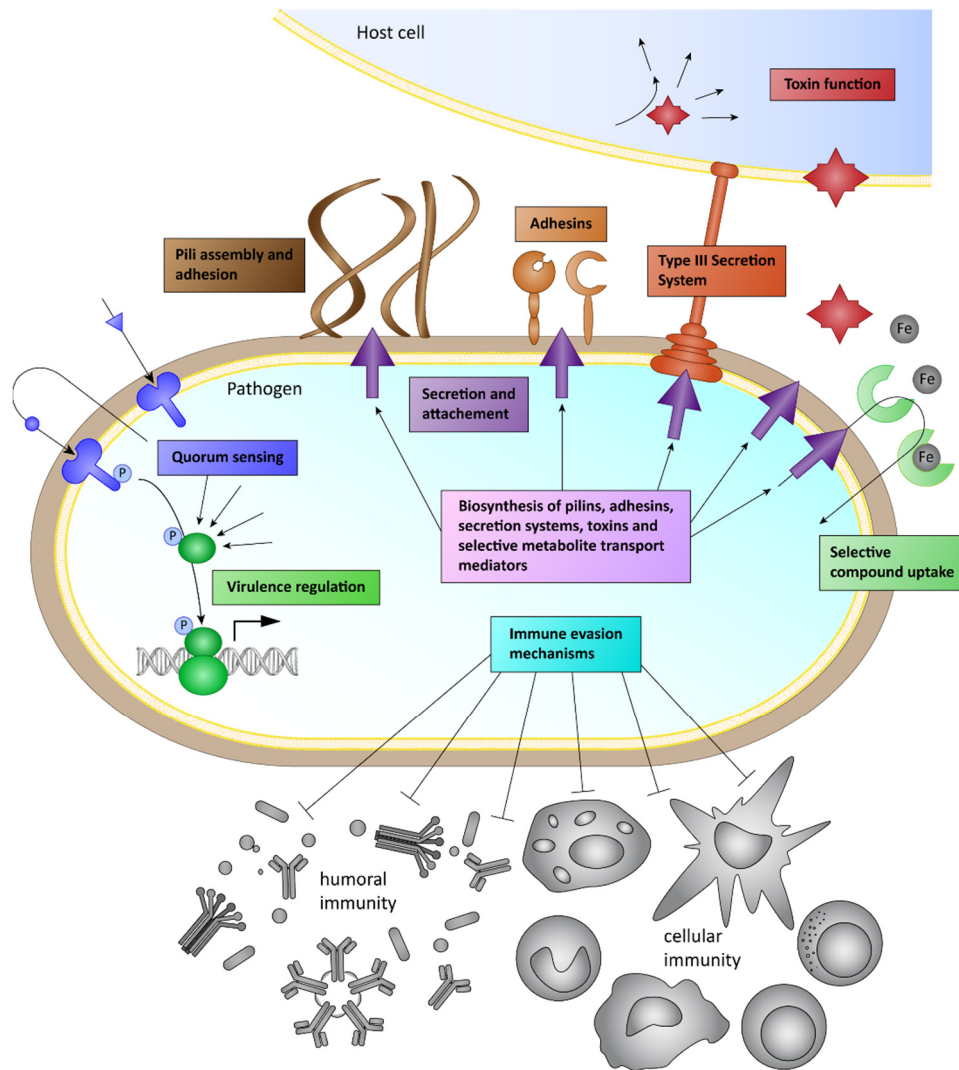
Figure 5: Bacterial virulence mechanisms

Bacterial virulence strategies are innovative targets for anti-infective drugs. Pathogenic bacteria differ in the mechanisms needed to establish an infection and survive in the host. Therefore, inhibition of the factors involved would lead to loss of virulence and help clearing the infection. Additional benefits are believed to arise from the species-specificity of the novel drugs as well as a reduced selection pressure for resistance development as the targets are not essential for *in vitro* survival.

Inhibition of adhesion and colonization has been experimentally achieved by interfering with pili formation and the type III secretion system of Gram-negative pathogens (*Chlamydia*, *E. coli*, *Pseudomonas*, *Salmonella*, *Shigella*, *Yersinia*) with which effectors are directly injected into host cells to enable colonization.[35, 36] Another possibility is to block the secretion of cell surface associated factors, which can be achieved via Sortase inhibition (chapter 3.3.4) or by targeting enzymes involved in their biosynthesis as has been done with siderophores. Blocking of the domain salicylation enzymes from *Mycobacterium tuberculosis* and *Yersinia pestis* led to growth inhibition under iron-limiting conditions.[37]

Quorum sensing describes a complex bacterial signaling network, which regulates adaptation to changes in cell density and environment. In particular, crucial pathogenic mechanisms like resistance to the innate immune system as well as formation of surface-associated multi-cellular bacterial

structures (biofilms) are regulated by quorum sensing. Therefore, factors essential and specific for this system are attractive targets for novel antibacterial drugs.[38]

Moreover, many pathogenic bacteria are able to secrete or deliver toxins in order to interfere with host cell functions and even lead to host cell death. It is obvious that inhibition of such processes by targeting bacterial or host factors would weaken the pathogen's survival in the host and also alleviate infection-specific symptoms.[39]

Finally, bacterial immune evasion mechanisms present valid targets for anti-infective development. Bacteria have evolved a plethora of possibilities to either hide from host defenses and escape or inhibit the host immune system. Blocking these abilities would thus promote infection clearance by the host. Immune evasion strategies are wide-ranging starting with inherent resistance to several effectors of the innate immunity such as the small peptide defensins or the complement system, based on the bacterial cell wall as first line of resistance.[15] Among many other strategies, adaptive host responses can be circumvented by variation of antigenic surface-exposed molecules. This is usually achieved either by switching between copies of associated genes or by highly variable regions in those molecules that are constantly changing.[40] Beyond these passive evasion strategies, bacteria can express factors that actively interfere with the host defense system. An example is the *Yersinia* outer protein H (YopH), which inhibits phosphorylation of B- and T-cell receptors leading to impaired adaptive immunity activation.[41]

Taken together, the strategy to target colonization, virulence and immune-evasion mechanisms of pathogenic bacteria is a valid route for antibacterial drug development. Certainly, the discovery of such anti-infectives demands profound knowledge of the pathophysiology to enable the establishment of valid screening and evaluation assays.[15] The inapplicability of long known methods and procedures, which were used for antibiotic discovery and clinical development, will change those rules for anti-bacterials.[32] In addition, anti-infective development will require next-generation sequencing or mass-spectrometry based diagnostic tools allowing for rapid identification of both the infecting bacterial species and resistances so that species-specific treatments are feasible in the future.[22]

3.2.3 Sources for novel drugs

Yet, there are more requirements apart from sophisticated identification of bacterial targets to efficiently discover promising antibacterial agents with drug-like features. Reliable platforms of compound libraries for (high throughput) screening as well as advanced *in silico* techniques for rational drug development need to be set up and provided for the diverse approaches described above. Despite the former stagnation in antibacterial development, there is still a lot of potential in natural product and synthetic libraries as well as the formerly unsuccessful rational, target-based drug discovery.[9]

Nearly all antibiotics on the market today were identified in natural compound screens. Natural products are especially recognized for yielding rare or novel modes-of-action with a variety of core structures. Therefore, to date untapped sources of compounds generated in secondary metabolism

of microbes and plants need to be exploited. To this end, innovative means, such as stress induction during microbe culturing to activate silent genes or accessing non-cultivable bacteria by genome mining, are made use of. To get the most value out of subsequent hight throughput screenings, efforts to dereplicate the natural compound libraries have to be made to efficiently identify novel compounds against the background of known antibiotic classes.[22, 42] Synthetic libraries might be improved by removing lytic, promiscuous and non-leadlike compounds and elucidation of compound characteristics needed to penetrate the bacterial envelope.[9, 22] For this purpose as well as for the rational based *in silico* screens, an increased research input from academia and industry is needed and should be expanded to meet the demand for novel antibacterial drugs.[17]

3.2.4 Assay development for drug identification

Lastly, screening assays need to be developed and validated for selected bacterial targets to reliably identify active compounds in large screening approaches or to verify the inhibitory activity of *in silico* identified compounds. In the first round of screening, all potentially specific inhibitors of a certain potency should be identified. Therefore, a thoroughly validated and robust test system is needed.[43] The importance of such assay validation for high throughput screening (HTS) applications is emphasized by the HTS-assay requirements set forth by the European Lead Factory[44], which is a project within the Innovative Medicine Initiative (IMI) of the European Union and the EFPIA (European Federation of Pharmaceutical Industries and Associations). These requirements were adapted for the screening assays employed in this work (chapters 6.1.2.2 and 6.2.3.2).

In short, the technology of the screening assay needs to be suitable for high throughput and small sample volumes e.g. in 96- or 384- well format. The reagents have to be of high quality to ensure accurate and reliable measurements. These measurements have to fulfill several quality criteria as well. Moreover, a reaction time of 4 hours should be implemented to enable the identification of slow binding or weak inhibitors[44] and the signal window for identification of inhibitory compounds needs to be suitably wide[45]. Finally, HTS specific demands such as DMSO tolerance and readout stability need to be assessed.[43]

3.3   *Staphylococcus aureus*

The Gram-positive faculatative anaerob *Staphylococcus aureus* is a coccoid bacterium that forms grape-like clusters. It can be a commensal on skin and the nasal mucosa but is also a major pathogen associated with purulent infections of various tissues including the skin and the respiratory tract. It was first identified in 1880 in a knee joint abscess[46] and four years later named according to the official system of nomenclature[47].

3.3.1   Epidemiology

Staphlococcus aureus can colonize humans as commensal. The most consistent area for isolation are the nares.[48] It has been shown that the bacteria may spread from the nares to other areas as local decolonization of the nares also led to decolonization of distinct areas.[49] Three *S. aureus* colonization patterns can be distinguished. About 20 % of average populations are persistent carriers colonized by one specific strain. 60 % are classified as intermittent carriers who can be colonized by different strains over time. The remaining 20 % of the population are non-carriers.[48] The persistent carrier pattern is most common in young children and can change between the age of 10 and 20.[50] It has been reported that persistent carriers may be protected from colonization and potential infection with other *S. aureus* strains. However, they may also be at particular risk during and after antibiotic treatment and surgical procedure.[51] Two more general risk factors for *S. aureus* infections are, firstly, repeated skin injections or catheter placing, which is the case in diabetes mellitus and dialysis patients as well as for intravenous drug addicts[52, 53], and, secondly, impaired immune status e.g. in HIV patients[54].

Methicillin-resistant *S. aureus* (MRSA) has been recognized as serious threat by the Centers for Disease Control and Prevention with 80 461 cases of invasive infections leading to 11 285 deaths in the United States in 2013. The infection rates are predicted to further increase without dedicated monitoring and preventive measures.[2] Europe presents a similar picture since MRSA causes about 171 000 healthcare-associated infections per year. This corresponds to 44 % of all healthcare-associated infections, 5 400 death cases and more than one million extra hospitalization days.[55] MRSA is not only a threat due to its nosocomial transmission route striking weakened individuals and causing complicated blood and wound infections but also due to increased mortality rates (180 %) compared to methicillin sensitive strains in all settings.[56] Therefore, increasing occurrence of community acquired MRSA infections is especially threatening. The simultaneous resistance to multiple additional antibiotics like vancomycin and the heightened virulence of the observed infecting strains culminate in devastating health outcomes underlining the urgent need for alternative therapeutic options.[57, 58]

3.3.2 Pathology

S. aureus can cause a wide spectrum of superficial and invasive diseases. The severity ranges from minor localized skin-infections to life-threatening conditions like the toxic shock syndrome, which is characterized by fever, rash, hypertension, and involvement of several organ systems (gastro-intestinal, renal, hepatic, central nervous system, mucous membranes, muscular, and hematologic).[59] Most frequent are skin and respiratory tract infections. Skin infections usually result from minor breaches and subsequent colonization. Previously commensal *S. aureus* can turn into the infectious agent. Otherwise, transmission can occur by skin-to-skin contact with an infected person or by contact with any kind of contaminated equipment.[60] *S. aureus* pneumonia is often nosocomially acquired and mostly affects patients with immune deficiencies or underlying infections.[61] Food poisoning can also be attributed to *S. aureus* contamination since strains may be capable of producing enterotoxins.[62]

The pathogen's ability to penetrate deep into the tissue and to cause bacteremia can lead to various severe diseases e.g. infective endocarditis, sepsis, necrotizing fasciitis and the toxic shock syndrome.[63] In all these cases, *S. aureus* evokes a massive inflammatory response but still evades the host defense system. It is also capable to resist antibiotic treatment to a certain extend even without any genetically encoded resistance genes and can thus lead to recurring infections after therapy termination.[59]

Acquisition of the staphylococcal cassette chromosome *mec* (SCC*mec*) and the encoded *mecA* gene results in methicillin-resistance of *S. aureus.* Healthcare-associated infections are usually caused by multidrug-resistant pathogens. These strains correspond to SSC*mec* types I, II and III, which usually are not involved in community acquired infections.[64] However, also community acquired infections display rising severity. In this aspect, distinct sequence types of SSC*mec* type IV have been described. The threat of severe infection is still low in Europe and community-aquired infections can reliably be treated, whereas difficult USA300 strains with multiple plasmid-encoded antibiotic resistances have been reported in the United States.[65]

3.3.3 Virulence factors

Apart from the spreading of resistances enabling *S. aureus* infections to arise as major threats in modern medicine settings, the pathogen is able to deploy a wide variety of virulence factors to colonize diverse sites in the host, manipulate and harm the host, and evade the immune system. These mechanisms are summarized in Figure 6 and described in-depth in the following chapters.
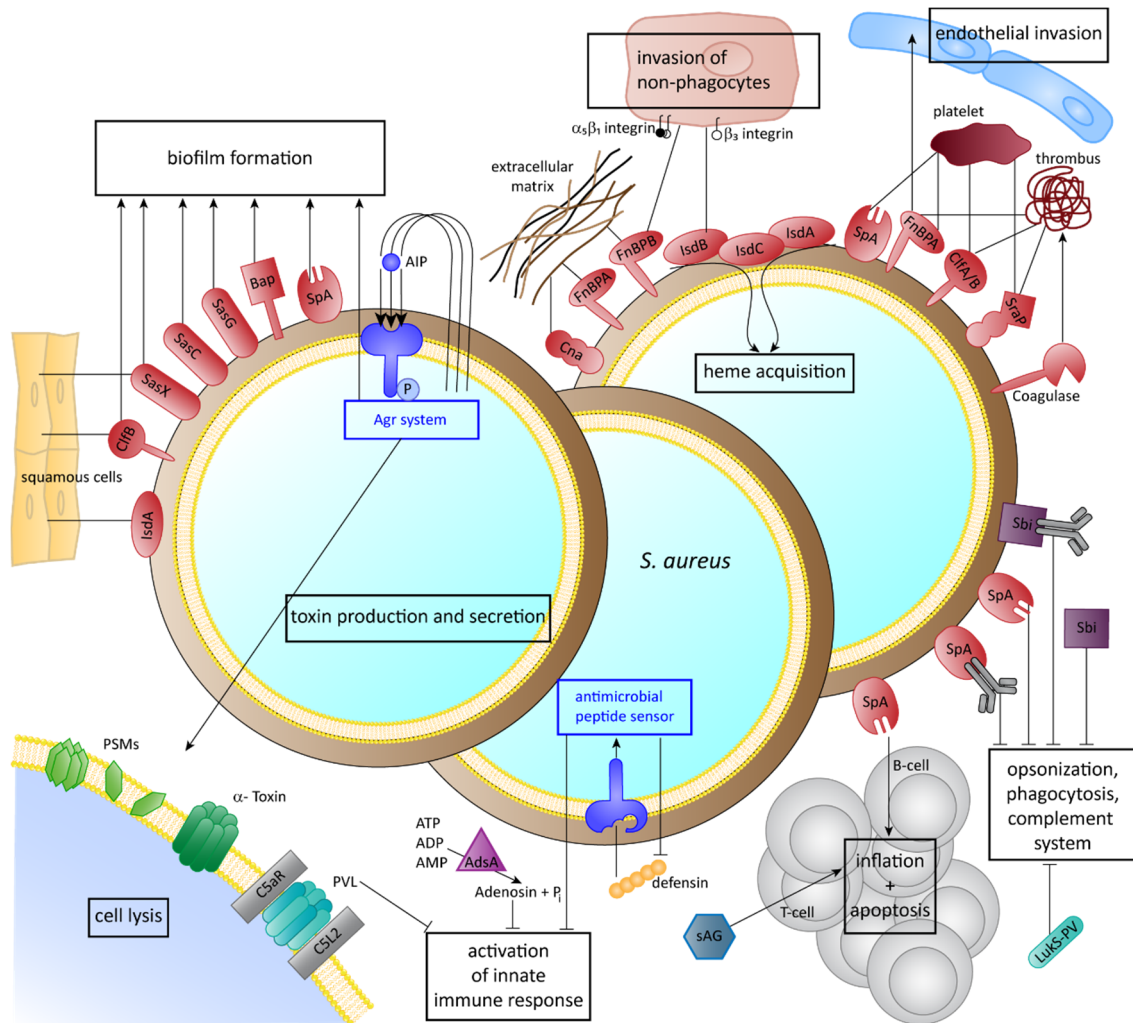
Figure 6: Virulence mechanisms of *S. aureus*

Staphylococcus aureus has developed a variety of factors allowing colonization, host injury and immune evasion to enable the pathogen to invade host tissues and avoid clearance while inducing massive inflammation. Mechanisms displayed in this graph are described in detail in chapters 3.3.3.1-3.3.3.3. Cell wall-anchored proteins depicted in red are linked to peptidoglycan precursor lipid II by Sortase A (chapter 3.3.4).

(Adapted in part from Foster, 2014[66] and Kim, 2012[67].)

3.3.3.1 Colonization and Invasion

S. aureus displays a wide variety of surface proteins. These are covalently attached to the bacterial cell-wall peptidoglycan and are crucially involved in commensal and pathogenic colonization.[66] Up to 24 cell wall-anchored proteins can be encoded in a single strain[68], whereas the expression pattern is also influenced by growth conditions like iron-limitation[69].

Nasal and epidermal colonization can be enabled by Clumping factor B (ClfB), the iron-regulated surface protein IsdA, and *S. aureus* surface protein X (SasX), which bind to squamous epithelial-cells.[70, 71] As mentioned above, a well-studied source of *S. aureus* infections are injection needles and catheters. In these cases, perforation of the skin barrier may enable entry of *S. aureus* colonizing the dermis.[52, 53] However, biofilm formation on indwelling medical devices plays a major role in systemic infections with *S. aureus*.[66] Biofilm formation is the pathogen's ability to manifest as multicellular

community and is mediated among others by the cell wall-anchored *S. aureus* surface proteins C, G, and X (SasC, SasG, and SasX)[72-74] as well as biofilm associated protein (Bap)[75], ClfB[76] and staphylococcal protein A (SpA)[77]. Moreover, *in vivo* virulence and growth depends on quorum sensing with the accessory gene regulator (Agr) system, also in the context of biofilms.[78] *S. aureus* releases a small autoinducing peptide (AIP), which leads to production and secretion of more AIP as well as a range of virulence factors, especially toxins.[79] At high cell densities, as can be found in biofilms, the Agr system runs in a positive feedback loop increasing the virulence of resident bacteria.[80]

After the skin barrier is overcome, *S. aureus* can bind to extracellular matrix via several factors, e.g. collagen adhesin (CNA)[81] and the well described fibronectin binding proteins FnBPA[82] and FnBPB[83]. The pathogen is also able to invade non-phagocytic cells via $\alpha_5\beta_1$ and β_3 integrins driven by FnBPB[84] and the cell wall-anchored protein IsdB[85]. IsdB, together with IsdA and IsdH, is also crucial for iron acquisition via haem uptake in the iron depleted host environment and thereby ensures successfull invasion and colonization of deep tissues.[86]

S. aureus can passively enter the blood stream after injection or surgical procedure but is also able to invade the endothelium depending on FnBPA.[87] Adherence to and colonization of thrombi and platelets aid survival in the blood stream and can ultimately lead to endocarditis, sepsis and toxic shock syndrome (TSS).[66] Several bacterial cell wall-anchored factors can be involved in this process, e.g. FnBPA[87], ClfB[88], and serine-rich adhesion for platelets factor (SraP)[89].

The variety of colonization and invasion associated factors inherent in a specific *S. aureus* strain and infection related events inducing their expression drive the nature of the infectious disease. However, the severity of the disease mainly depends on further virulence factors involved in host injury and immune evasion.[60]

3.3.3.2   Toxins

Many virulence factors described for *S. aureus* can be classified as toxins. They are secreted and able to directly interfere with the host, harming it and resulting in infection-associated pathology.[60]

Several phenol-soluble modulins (PSMs) have been identified in *S. aureus* isolates. They are small, amphiphatic peptides targeting host cell membranes non-specifically.[90] They are able to form pores or initiate membrane disintegration due to their detergent properties.[91] Thus, PSMs can lead to lysis of many cell types including blood cells eliciting systemic inflammatory responses.[92]

In the same way, *S. aureus* α-toxin is well known for its ability to form heptameric β-barrel pores in host cell membranes. Accordingly, these pores cause efflux of ions and are thereby lytic to red blood cells and leucocytes.[93] At high concentrations, this mechanism is non-specific, but also low concentrations result in pore formation in cells with distinct receptors. Unlike PSMs, α-toxin has a different mode-of-action depending on the interaction with the ADAM10 receptor.[94] This interaction leads to loss of epithelial barrier function due to cleavage of E-cadherin in adherence junctions.[95] Further β-barrel pore forming toxins have been described for *S. aureus*.[60] Among them, the bi-component toxin Panton-Valentine leukocidin (PVL), consisting of the proteins LukS-PV and LukF-PV, has been discussed in association with highly virulent, community-acquired MRSA.[96] Its host

receptors C5aR and C5L2 (both complement factor 5a receptors) explain its cytotoxic effect against neutrophils, monocytes and macrophages. The receptor is recognized by LukS-PV, which inhibits C5a-induced immune cell activation at sub-cytotoxic concentrations.[97]

Finally, enterotoxins are secreted by a small number of *Staphylococcus aureus* strains. They typically interfere with intestine function causing diarrhea and emesis in food poisoning.[62] In invasive *S. aureus* infections, they can act as superantigens triggering non-specific interaction of major histocompatibility complex II and the T-cell receptor resulting in massive T-cell activation and proliferation.[60] Superantigens can thus lead to cytokine release by the inflated T-cell population and induction of apoptosis, effects critical in the pathology of infective endocarditis and sepsis.[98, 99] Moreover, superantigens are especially associated with high mortality rates as they might induce the toxic shock syndrome (TSS).[59] A synergism of TSS toxins and Gram-negative associated lipopolysaccharide (LPS) with regard to TSS itself as well as myocardial and liver damage is discussed in the literature.[100, 101] It is proposed that liver tissue is severely impaired by TSS toxins whereby efficient detoxification of LPS absorbed from the intestine is hindered.[59, 102] The LPS may therefore enter the circulation resulting in systemic endotoxemia and multiple organ involvement.[103] The pro-inflammatory response to LPS is further increased by the ability of TSS toxins to up-regulate toll-like receptor 4 (TLR-4), which recognizes LPS and induces pro-inflammatory signaling.[104]

3.3.3.3 Immune evasion

Staphylococcus aureus deploys several strategies to evade the host immunity by hiding from the innate immune response, manipulating the adaptive immune response, and preventing its clearance from the bloodstream.[60, 105]

As a Gram-positive bacterium *S. aureus* can be recognized by the host's innate immune system on the basis of several pathogen associated molecular patterns (PAMPs), which are predominantly the cell wall components lipoteichoic acid, their leucocidin toxins, and components of the cell wall peptidoglycan.[106] The recognition of lipoteichoic acid is mediated by toll-like receptor 2 (TLR-2).[107] However, certain *S. aureus* strains are able to evade this host defense mechanism by secretion of the staphylococcal superantigen like protein SSL3. This protein is a highly potent antagonist of TLR-2 and can compete with several TLR-2 ligands. The cytokine production is thereby inhibited and inflammation and immune cell infiltration decreased.[108]

A long known capability of *S. aureus* is initiating blood coagulation, which is significantly involved in septic shock.[109] The cell wall-anchored enzyme coagulase reacts with prothrombin when exposed to blood plasma and forms the staphylothrombin complex. Thus, fibrinogen is converted to fibrin and the pathogen is coated in the blood clot in a ClfA and ClfB dependent manner.[66, 110] The pathogen can, therefore, prevent phagocytosis and hide from further immune effectors.[109] The coagulation pathway is pro-inflammatory and might contribute to systemic inflammation.[111]

Despite of eliciting systemic inflammatory responses in TSS and sepsis, *S. aureus* is also able to control inflammation for self-preservation. A prominent factor is adenosine synthase A (AdsA), which is covalently linked to the bacterial cell wall and catalyzes the hydrolysis of adenosine-phosphates to

adenosine.[112] Extracellular adenosine is a potent immune suppressor, usually associated with hypoxic stress, ROS exposure and cell lysis.[113] It is even thought to be the key signal to control overshooting inflammation.[67] Moreover, AdsA has been shown to enable *S. aureus* survival in neutrophil phagosomes.[114] Another specific mechanism to evade cellular effectors of the innate immunity is mediated by the virulence factor staphyloxanthin.[32] This yellow pigment helps to protect the pathogen from ROS produced by phagocytes and is crucially involved in resistance to host defenses.[115]

Antimicrobial peptides, defensins, are part of the host's innate immune response and are bactericidal at high concentrations.[116] *S. aureus* can sense these mostly cationic peptides with the so called antimicrobial peptide sensor (Aps), which is a three-component regulatory system. In response to defensins, the composition and net charge of cell wall components is altered reducing the pathogen's susceptibility.[117]

Moreover, several cell wall-anchored proteins involved in adhesion are also participating in immune evasion. The well-studied staphylococcal protein A (SpA) can interfere with many important immune factors.[106] It is able to bind the Fc region of immune globulin G (IgG) and thereby thwart recognition of underlying antigens, opsonization and the resulting phagocytosis.[118] Besides, SpA is able to bind von Willebrand factor and the complement protein C3, which increases the bacterial adhesion to platelets – an important virulence trait in infectious endocarditis.[119, 120] In addition to SpA, staphylococcal binder of immunoglobulin (Sbi) is a secreted protein of *S. aureus* with similar function. It may remain associated with the bacterial envelope and bind to Fc region of IgG. The free form of Sbi has been shown to block complement factor C3d and factor H, preventing their interaction with specific receptors.[121, 122] By inhibiting C3 signaling, the link between innate and adaptive immunity is significantly impaired.[67, 123]

Finally, SpA can stimulate B-cell proliferation[124] and thereby induce massive clonal expansion and subsequent cell death, thwarting efficient adaptive humoral responses[125]. The same is true for the cellular adaptive immunity as superantigen-mediated stimulation of T-cell proliferation, inflation, and apoptosis prevent host protection and memory formation.[85]

3.3.4 *Staphylococcus aureus* Sortase A

3.3.4.1 *Sortases*

Bacteria are generally classified on the anatomy of their cell envelope and specifically their peptidoglycan layer.[126] It is much thicker in Gram-positive than in Gram-negative bacteria, leading to distinct staining phenotypes.[127] Furthermore, Gram-positives possess only a cytoplasmic membrane and lack the LPS-rich outer membrane found in Gram-negatives.[128] The thick peptidoglycan layer protects the Gram-positive bacteria from osmotic lysis and constitutes an effective barrier against hydrolases or membrane targeted toxins.[126] The lack of an outer membrane implies direct secretion of signal-peptide bearing precursors to the extracellular space.[129] Hence, a specific mechanism has

evolved to anchor certain proteins to the peptidoglycan cell wall to enable their interaction with the environment like host tissue and immune cells.[130]

The first step for cell wall targeted proteins to reach their final destination is the secretion across the plasma membrane. This has been investigated in depth for *E. coli*. The so called Sec pathway comprises the SecYEG translocon channel in the plasma membrane[131], the cytoplasmic ATPase SecA[132] and further factors involved in release of the complex from the translocon[133]. The ribonucleoprotein SRP recognizes nascent precursor proteins and delivers the ribosome to the SecYEG translocon to enable co-translational secretion.[134] In the cytoplasm, further factors like chaperones and peptidyl-prolyl isomerase are involved in delivering the nascent protein in a secretion competent state.[135] Most Gram-positive bacteria are assumed to use this secretion pathway as they contain homologues of the involved factors.[136]
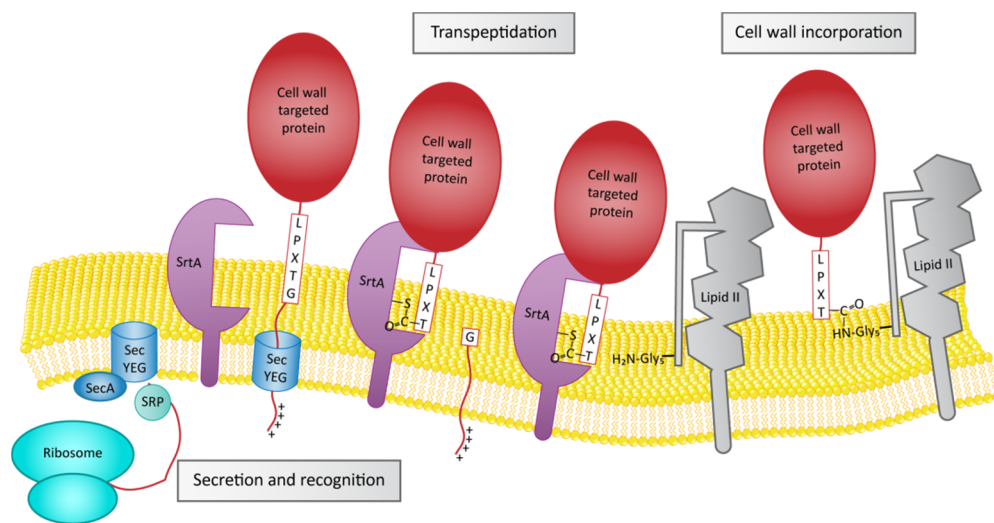
Figure 7: Sortase A covalently links sorting motif containing proteins to lipid II

Cell wall targeted proteins possess an N-terminal secretion signal that is recognized by SRP (signal recognition particle) and initiates translocation via the Sec pathway. The sorting signal consists of the recognition motif LPXTG, a hydrophobic span, and a C-terminal positively charged tail. With this, translocation is halted and the LPXTG motif is presented in perfect orientation to Sortase A. In the first step of the transpeptidation reaction, a thioester acyl-enzyme intermediate is formed, which is regenerated after transfer of the cell wall targeted protein to the Gly_5 branch of lipid II. Lipid II and the covalently attached protein are incorporated into the peptidoglycan cell wall. (Adapted from Schneewind, 2012[135].)

Crucial factors in protein surface display in Gram-positive bacteria are the sortases. They are membrane anchored transpeptidases that covalently link secreted proteins with a sorting signal to the bacterial cell wall.[137] The cell wall sorting signal consists of a specific amino acid sequence motif, a hydrophobic domain, and a positively charged C-terminus.[138] This is interpreted to stop Sec-dependent translocation and present the recognition motif in an appropriate distance to the plasma membrane to be recognized by the sortase.[129] The most common acceptor for sorted proteins is the cross-bridge portion of the cell wall building block lipid II. Those cross-bridges vary depending on the bacterial species, so that sortases have evolved to recognize their specific acceptor-substrate.[139]

Sortase A is present in almost all Gram-positive bacteria and recognizes proteins with C-terminal LPXTG motifs.[137] The scissile peptide bond is located between the threonyl and glycyl moiety.[140] The

nucleophilic attack of the active-site cysteine results in a thioester acyl-enzmye intermediate after release of the C-terminal remainder of the precursor protein.[141] It is resolved by nucleophilic attack of a free acceptor amino group. In the case of *S. aureus*, this acceptor is the N-terminal amine of the Gly$_5$ lipid II cross-bridge. Thus, sorted proteins are covalently attached to peptidoglycan building blocks, incorporated into the cell wall, and displayed on the bacterial surface.[142] The mechanism sequence is depicted in Figure 7.

Apart from the house-keeping Sortase A, Gram-positive bacteria may possess further sortases for specific purposes. Firstly, Sortase B is involved in anchoring of heme scavenging factors. In *S. aureus*, it is encoded on the iron-regulated surface determinant (*isd*) gene cluster.[143] It is capable of anchoring IsdC via its NPQTN sorting signal to peptidoglycan cross-bridges close to the plasma membrane.[144] This positioning is crucial for transfer of heme, which has been scavenged by IsdB and IsdA, to the IsdEF translocator to the cytoplasm as iron source.[135] Secondly, Sortase C is only found in spore-forming Gram-positives as it is needed for anchoring spore specific proteins with LPNTA sorting signals to the spore.[135] Thus, aerial dissemination of spores with highly hydrophobic surfaces is facilitated.[145] Finally, Sortase D is responsible for pili assembly in several Gram-positive bacteria including *Enterococcus* spp..[146] Pilin proteins are connected after cleavage of the sorting motif with the conserved lysine residue in the next pilin's YPKN pilin motif as acceptor.[135] In some species, the assembled pili can be attached to the peptidoglycan via Sortase A mediated transpeptidation.[147]

3.3.4.2   *S. aureus Sortase A catalytic activity and its role in virulence*

Sortase A from *S. aureus* (SaSrtA) has been investigated in detail. For *in vitro* studies the Δ1-59 recombinant protein has been widely used. It lacks an unstructured N-terminal segment, which contains the membrane anchor.[141] Its transpeptidase activity is characterized by a thioester acyl-enzyme intermediate.[141, 148] In SaSrtA, Cys184 is the active-site nucleophile and several mechanisms for its activation have been proposed.[149-151] In absence of an acceptor nucleophile, SaSrtA catalyzes the hydrolysis of the recognition peptide LPETG. However, the presence of diglycine or other glycine polymers stimulates the overall reaction about tenfold; this motif is the acceptor present in the pentaglycine branch of lipid II.[152, 153] The acceptor binding site can be segmented according to the binding amino acids nearest to the newly formed peptide bond (S1', S2',…). The N-terminal glycine residue of the acceptor peptide is imperative for binding in S1', the second glycine is preferred by the according acceptor binding site S2'. As glycine does not act as a transpeptidation acceptor, it is concluded that the amide bond between the first two acceptor amino acids is crucially involved in binding to the enzyme as well.[153]

The transpeptidation reaction follows a ping-pong bi-bi mechanism. Therefore, the reaction is characterized by two separate steps. First, the enzyme reacts with the sorting-motif peptide releasing the C-terminal part and forming a thioester acyl-enzyme intermediate. Second, the acceptor nucleophile may bind only to and react with this acyl-enzyme intermediate and lead to the formation of the final product.[153] Due to the perpetual competition with the hydrolysis reaction, the rate limiting steps of transpeptidation and hydrolysis were analyzed to ultimately understand the

enzyme mechanism at its site of action. It was found that in the transpeptidation reaction formation of the acyl-enzyme intermediate is rate-limiting, whereas the second step of the reaction is faster. In contrast, the second step of the reaction, e.g. hydrolysis of the acyl-enzyme intermediate, is rate limiting for the hydrolysis reaction. The overall physiological reaction mechanism is therefore described as ping-pong bi-bi with hydrolytic shunt.[148] Thus, wasteful escape of cell wall targeted proteins due to hydrolysis is reduced by the enzyme's kinetics and, additionally, by the close association of all necessary substrates and SaSrtA near the bacterial plasma membrane.[153]

Catalytic observations such as a high K_M-value for the LPXTG peptide, sensitivity to high and low pH levels, and participation of both Cys184 and His120 in the formation of the acyl-intermediate identified the reverse protonation mechanism for SaSrtA nucleophile activation. The active site residues Cys184 and His120 are reversely protonated in the active form of the enzyme, which comprises only a small fraction of SaSrtA. The thiolate group is the nucleophile attacking the carboxyl group of the peptide bond between Thr and Gly in sorting motifs. The resulting tetrahedral transient state is resolved by protonation of the C-terminal leaving group, which is accomplished by His120 activity as general acid, and the thioester acyl-enzyme intermediate is formed.[148]

However, not only active site residues are involved in the transpeptidation reaction. The β6/β7 loop near the active site has been described to be highly flexible in the absence of allosteric Ca^{2+} and, in this state, important residues for substrate recognition are removed from the active site.[154] Glu171 is involved in Ca^{2+} binding, which stimulates both transpeptidation and hydrolysis activity of SaSrtA. Therefore, correct positioning of the loop is supposedly important for the formation of the acyl-enzyme intermediate. During bacteremia, about 50 % of SrtA on the surface of *S. aureus* is estimated to be loaded with Ca^{2+}.[155] The β6/β7 loop has been recognized as major domain in sorting motif recognition due to sequence comparison of sortases and domain-swapping experiments underlining the effect of allosteric Ca^{2+}.[156] However, substrate binding itself immobilizes the β6/β7 loop and even initiates a short 3_{10} helix therein. NMR-structure analysis revealed the active site residue Arg197 to be involved in substrate binding in addition to several residues of the β6/β7 loop. These interactions reveal the sorting motif's Leu to be crucial for recognition but also explain the promiscuity for the residue between Pro and Thr.[157] The final reaction mechanism deduced is depicted in Figure 8.
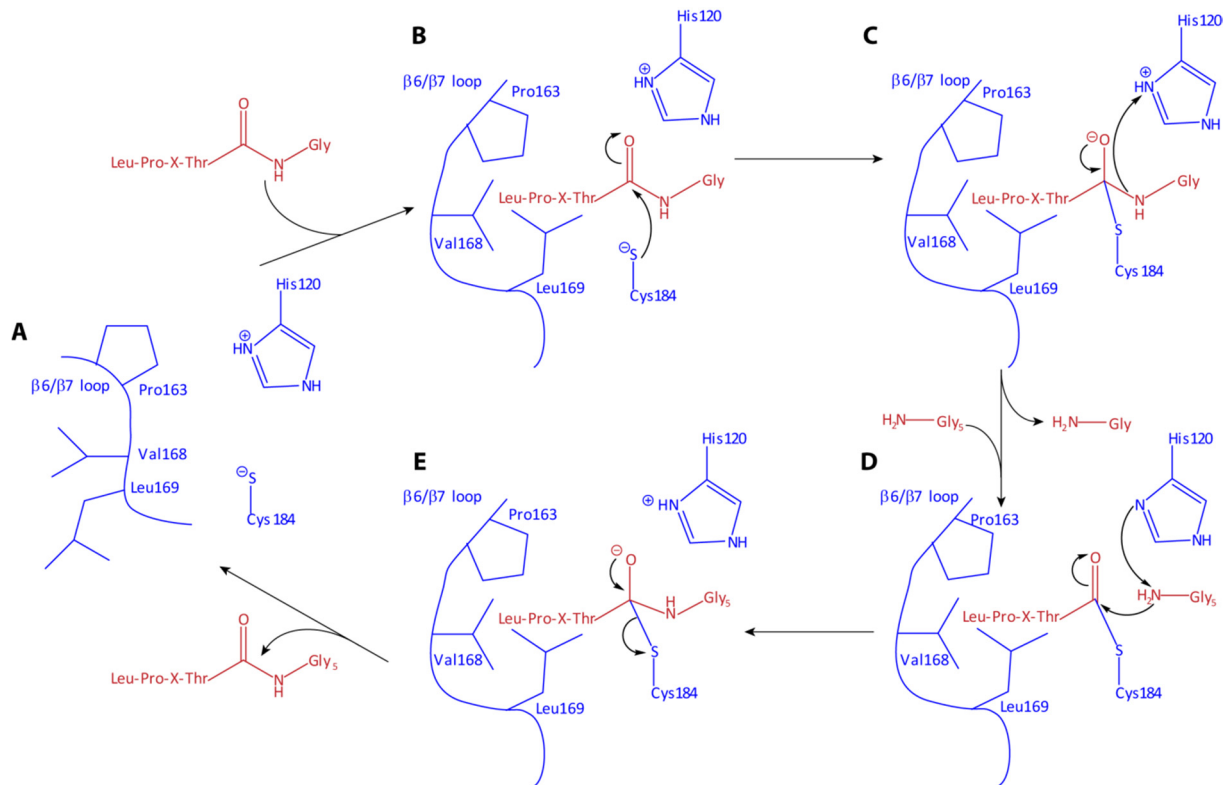
Figure 8: Reaction mechanism of SrtA catalyzed transpeptidation

Substrates of the transpeptidation reaction are shown in red; relevant parts of the SaSrtA are shown in blue. The corresponding amino-acid residues are indicated for the active site reverse protonation pair and residues of the β6/β7 loop involved in substrate binding and recognition.

(A) The nucleophilic thiol group of Cys184 is negatively charged in the active form of SaSrtA. The residues on the β6/β7 loop are not perfectly positioned for substrate binding. **(B)** After binding of the sorting signal motif LPXTG, positioning of the β6/β7 loop is initiated and the substrate's scissile peptide bond between Thr and Gly is attacked nucleophilically at the carbonyl group by the thiolate. **(C)** The tetrahedral transient state is resolved by His120 action as general acid for release of the C-terminal glycyl group. **(D)** The thioester acyl-enzyme intermediate is formed. The acceptor-substrate Gly$_5$ present in peptidoglycan branches binds to the acceptor binding site. The N-terminal amine of the acceptor is activated by His120 as general base for nucleophilic attack of the thioester bond. **(E)** The second tetrahedral transient state collapses assisted by His120 as general acid. The active site protonation state is regenerated and the β6/β7 loop is displaced after exit of the final transpeptidation product.

(Adapted from Suree, 2009[157].)

The catalytic activity enables the covalent linking of surface proteins to the bacterial cell wall *in vivo*. For Sortase A from *S. aureus*, several studies revealed its impact on virulence. SaSrtA knock-out strains manifested a hyper-spreading phenotype due to the lack of surface FnBPA, FnBPB, ClfA and ClfB imparing fibronectin binding[158] and biofilm formation[159]. Figure 6 (p. 24) displays virulence factors of *S. aureus*. Cell wall-anchored proteins sorted and covalently attached by SaSrtA are indicated in red. It is obvious that many important effectors in adhesion and invasion of host tissues, biofilm formation, and inhibition of opsonization and phagocytosis crucially depend on SaSrtA activity.[160] Indeed, surface display of adhesins is abolished in *srtA* deficient *S. aureus* mutants, leading to reduced virulence in experimental mouse infection and clearance in most of the animals.[161] Moreover, these mutants caused 70 % less mortality compared to wild type strains in another mouse infection experiment, and inhibition of SaSrtA activity during *S. aureus* infection could significantly decrease bacterial load.[162]

3.3.4.3   Sortase A – a role model anti-infective target

The previous chapters illustrated the strong link of Sortase A to the virulence of pathogenic *S. aureus*. The enzyme is present in almost all Gram-positive species with low G/C content and plays an important role in various pathogenic processes.[160] No human homologues are described so far. Thus, selective inhibition without host toxicity is likely feasible.[163]

About 20 % of sortase homologues are highly similar to SaSrtA and share the conserved active-site residues Cys184 and His120. They supposedly play a similar housekeeping role and are responsible for anchoring LPXTG containing proteins to peptidoglycan precursors.[164] Just as SaSrtA, they are not involved in bacterial growth or viability. Therefore, inhibitory agents are expected to have a reduced risk for resistance development and spreading. Additionally, as cell membrane proteins, sortases are conveniently accessible for inhibitor targeting. Consequently, not only SaSrtA but also the sortases of further *staphylococci, streptococci,* and *enterococci* are promising novel drug targets.[163] The availability of detailed data elucidating the biological role of SaSrtA and the involved molecular mechanisms, as described above, are a prerequisite to evaluate the target for pharmacological inhibition. Hence, Sortase A from *S. aureus* is established as ideal target for anti-infective drug development.[163]

It is not surprising that several efforts have already been made in the discovery of SaSrtA inhibitors. The first hit compounds were identified by different techniques. So far, high throughput screening (HTS) of natural and synthetic libraries and *in silico* screening have led to the identification of SaSrtA inhibitors, of which a few are also promising as anti-virulence drugs.[163]

The most obvious choice of starting points for sortase inhibitor discovery are substrate-derived peptides. Among others, replacement of the scissile bond with diazoketone or chloromethyl ketone groups created inhibitors that irreversibly alkylated the active-site cysteine.[165]

Several natural products were identified in screenings for SaSrtA inhibitory activity and fibronectin binding inhibition.[163] The most potent among them were the isoquinolone alkaloid berberine chloride with an IC_{50}-value of 8.7 µg/mL[166], isoaaptamin with 3.7 µg/mL[167], and (−)-discorhabdin Z with 2.2 µg/mL[168]. Moreover, a series of indole-type natural product analogues found dihydro-β-carboline with an IC_{50}-value of 25 µM and no effect on bacterial viability.[169]

In an *in silico* screening based approach, morpholinobenzoate derivatives were proposed as SaSrtA inhibitors.[170] The structure-activity relationship highlighted sterical requirements of sortase inhibitors. The most potent compound of the series had an IC_{50}-value of 58 µM.[171]

Screening of 1000 synthetic compounds identified diarylacrylonitriles as novel class of small molecule SaSrtA inhibitors.[172] (Z)-3-(2,5-dimethoxyphenyl)-2-(4-methoxyphenyl) acrylonitrile (DMMA) was developed as the most active compound with an IC_{50}-value of 9.2 µM. DMMA was characterized as competitive inhibitor and even validated in a mouse infection model, in which it increased the survival and decreased the pathogenicity.[162] However, the survival rates were lowest at the highest DMMA doses hinting at potential toxicity against the host.[163]

In another approach, a library of 135 625 small molecules was screened for SaSrtA inhibition and five active classes with a common core scaffold could be identified. Of these, the aryl (β-amino)ethyl

ketones were most active yielding IC$_{50}$-values of 47 µM and 15 µM against SaSrtA and even 4.8 µM and 5.6 µM against *Bacillus anthracis* Sortase A. These compounds act depending on sortase mediated β-elimination followed by Michael-like addition with the active-site thiol. Therefore, inhibition is non-competitive with irreversible covalent modification of the target.[173]

The most recent HTS screen with 30 000 compounds identified three further promising small molecule classes. The rhodanines, pyridazinones and pyrazolethiones achieved IC$_{50}$-values as low as 3.7 µM, 0.2 µM and 0.3 µM, respectively. The structure-activity relationship could be determined and revealed important characteristics of Sortase A inhibitors.[174] These compounds had no effect on bacterial viability indicating their potential as true anti-virulence candidates.[163]

In summary, several promising candidates for anti-virulence agents targeting the Sortase A from *S. aureus* have been identified. However, most of them are not sufficiently evaluated in comprehensive *in vitro* assays (e.g. biofilm formation, adhesion) and *in vivo* infection models (e.g. abscess formation, endocarditis). Therefore, not all described inhibitors are proven anti-virulence agents for *S. aureus*, yet.[163] In any case, the applicability of such drugs as alternative treatment options to antibiotics still has to be assessed on a general basis.[175] Nevertheless, the feasibility of SaSrtA inhibitor discovery and development is clearly displayed and encourages further efforts with distinct methods for hit identification. Tailored modeling approaches could be a fruitful addition to the already tried discovery approaches. Reasonable structural data for the apo-enzyme (1T2P[140], 1IJA[154]) and the enzyme bound to a covalently attached substrate analogue (2KID[157]) as well as endeavors to define a pharmacophore for SaSrtA based on the already identified inhibiotors[176] emphasize its feasibility.

3.4 *Helicobacter pylori*

The motile, microaerophilic and spiral shaped Gram-negative bacterium *Helicobacter pylori* is able to survive the acid environment in the stomach and actively reach the mucosa, thereby selectively colonizing and persisting lifelong in its unique niche. It was initially discovered by Warren and Marshall in 1983 in gastric biopsies and recognized as a major factor in the development of gastric and duodenal ulcers that can lead to cancer.[177] In 1994 *H. pylori* was ranked as Class I carcinogen by the World Health Organization since infected patients have a six-fold increased risk of gastric adenocarcinoma development compared to uninfected individuals.[178]

3.4.1 Epidemiology

It is assumed that *H.* pylori has been colonizing the human stomach for much longer than 60 000 years. This dates back to the time before humans left the African continent to colonize the rest of the world.[179] Coincident decrease of genetic diversity among *H. pylori* strains and humans with increasing distance to the common origin East Africa supports this presumption. Such long co-existence led to a profound adaptation of the bacterium to its host, which can be appreciated by considering its small genome size.[180] Likewise, there is a close correlation between molecular traits of colonizing *H. pylori* strains and the ethnicity of the patient, which can be explained by co-evolution.[181]

Infection with *H. pylori* supposedly occurs during early childhood via oral-oral or fecal-oral transmission from close relatives. This was concluded from genetic analysis of isolates from family members as well as from the lack of evidence for infection later in life.[182, 183]

The early transmission and the extreme adaptation of this pathogen to its host explain its exceptionally high prevalence of about 50 % in the human population worldwide. The infection is most prevalent in developing areas (up to 90 %) and decreases in westernized countries (20-30 %). This is attributed to advanced hygiene standards, reduced family size and improved socio-economic living conditions.[184]

However, only 10-20 % of infected individuals go beyond the non-symptomatic gastritis caused by *H. pylori* and develop gastric hyperacidity and peptic ulcers. These clinical symptoms can be treated by eradication of the causative pathogen with triple or quadruple therapies consisting of two antibiotics and a proton pump inhibitor, which can be combined with bismuth containing compounds.[185] Moreover, 0.1-4.0 % of infected patients develop gastric cancer[186], which is the fifth most common malignancy worldwide and the third most common cause of cancer death[187]. Understanding strain differences in *H. pylori* and patient's genetics leading to different outcomes is one focus of investigation and is needed for the development of advanced diagnostic tools, which can help the assessment of disease risks and treatment options. There are major indications justifying this field of research as the risk of clinical outcomes is not equal comparing distinct populations.[188] Rising resistance of *H. pylori* towards standard therapies particularly underlines the need for risk stratification and more targeted eradication approaches. The prevalence of antimicrobial resistance with up to 44.1 % for specific antibiotics especially decreases the efficacy of

first-line triple therapies.[189] Insufficient understanding of the complex interplay of bacterial and human genetics as well as environmental factors so far thwarted efforts in implementing regimens adapted to geographic patterns of resistance observations.[190] Therefore, the most advanced combination treatment options are more and more frequently chosen, which might lead to further resistance development in turn.[191] Another aspect is a compliance problem of current therapies, which is explained by drug side effects as well as the long durance of medication. Consequently, novel agents complementing and improving existing drug regimens or enabling novel treatment approaches are needed.[189, 192]

3.4.2 Pathology

Colonization with *H. pylori* induces histological gastritis in every patient by triggering neutrophil and mononucleated cell infiltration into the gastric mucosa.[193] As stated above, this remains asymptomatic for most individuals and the bacterium persists lifelong.

Yet, the chronic infection can provoke clinical pathology in up to 20 % of the cases. Depending on the precise site of infection, there are two main possibilities. In the case of an infection established in the antrum, an increased production of gastric acid may be induced. This leads to cellular damage in the adjacent duodenum, which can then be populated by gastric epithelial cells. This condition is described as gastric metaplasia, which can progress to duodenal ulcer under continuing inflammatory stimuli.[186, 194] In contrast, a colonization of the corpus can lead to atrophic gastritis based on induced inflammatory processes. Destruction of gastric glands leads to a tissue more resembling intestinal mucosa and which is, therefore, classified as intestinal metaplasia. It is recognized as an early step towards development of gastric adenocarcinoma.[194, 195] Moreover, mucosa-associated lymphoid tissue (MALT) lymphoma can be induced in the chronic *H. pylori* infection due to the constant stimulation of lymphocytes at the colonization site.[196] In any case, the influence of *H. pylori* on gastric carcinoma is especially eminent since more than 80 % of gastric cancers can be attributed to an infection.[197]Despite the risks indicated for this infection, it is not suggested to generally eradicate *H. pylori* positive patients. After all, 80 % will not develop any symptoms or complications and may even benefit from being colonized.[198] Based on the hygiene hypothesis, there are among others associations with reduced allergy and asthma occurrence[199], reduced susceptibility for tuberculosis[200], and reduced risk of esophageal cancer[201, 202]. Aforementioned advances in diagnostic tools may help to stratify patients according to their risk of *H. pylori* induced pathology and indicate treatment necessity. Additionally, a more targeted therapy of *H. pylori* infection would have further benefits like decreasing resistance development for the pathogen and the microbiome, and, in general, may save the patient's microbiota from unnecessary depletion and alteration.[198]

3.4.3 Virulence factors

Variability in clinical outcomes for *H. pylori* infected patients must in part be the consequence of differences in virulence characteristics of the specific infectious strain. Basic research revealed part of the plethora of bacterial factors enabling it to colonize and manipulate the host and achieve lifelong persistence in the gastric mucosa.[203] An overview is given in Figure 9.
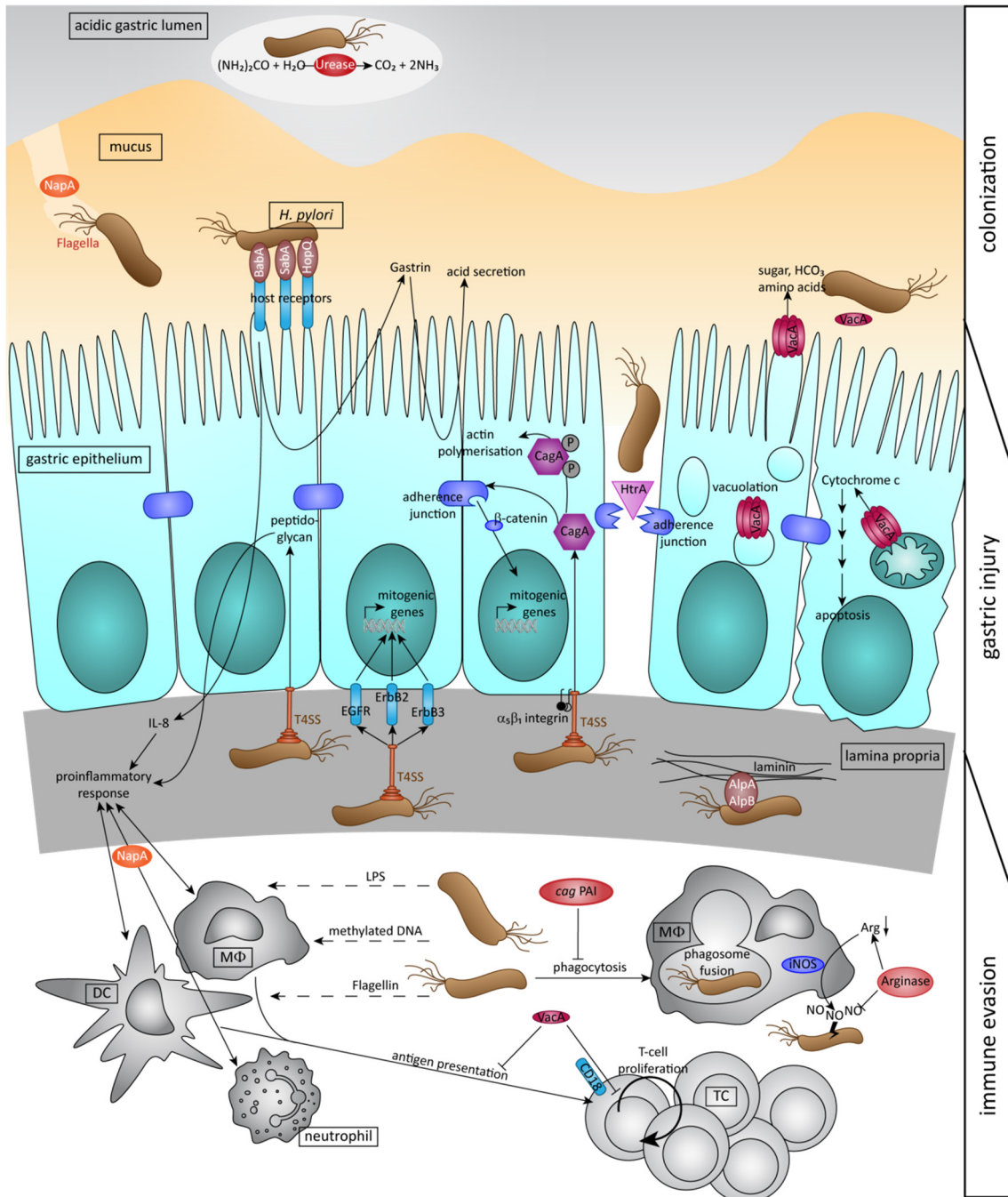
Figure 9: Virulence mechanisms of *H. pylori*

Helicobacter pylori possesses a variety of factors allowing colonization, gastric injury and immune evasion to finally enable the pathogen to persist in the gastric environment. Mechanisms displayed in this graph are described in detail in chapters 3.4.3.1 - 3.4.3.3. DC: dendritic cell, MΦ: macrophage, TC: T-cell.
(Adapted in part from Suerbaum, 2002[204] and Pachathundikandi, 2013[205].)

3.4.3.1   Crossing the mucus layer and binding to epithelial cells

Factors enabling colonization of *Helicobacter pylori's* distinct niche are focused on overcoming the acidic lumen and the mucus layer of the stomach as well as efficient adherence to the gastric epithelium.

In the acidic environment of the stomach, production of urease is induced, which can catalyze the hydrolysis of urea to carbon dioxide and ammonia.[206] This ability is based on the expression of nine genes.[207] The final product of this strategy, i.e. ammonia, is able to buffer the microenvironment of the bacterium to a neutral pH and it can additionally serve as nitrogen source for *H. pylori*.[206] As a first step, ammonia reacts with glutamate to form glutamine, which consumes ATP. Glutamine then serves as a nitrogen donor for further metabolites.[43]

The next barrier is the viscous mucus layer, which has to be actively crossed by the bacterium. For this purpose, *H. pylori* possesses a unipolar bundle of two to six-sheathed flagella.[208] Additionally, the direction of the movement is determined by chemotaxis. Involved are gradients of amino acids, mucin, urea, sodium bicarbonate and sodium chloride.[209] Again, urea and the urease play a part in this cooperative mechanism. In particular, the cytoplasmic generation of ammonium from urea may help to supply the proton motive force needed for flagella dependent movement.[210]

Binding to mucin correlates with the neutrophil-activating protein NapA and the bacterium from being transported too far towards the pyloric orifice before the colonization is established.[211] Moreover, this protein can degrade mucin and thereby lead to decreased viscosity near the bacterium, further facilitating its progression towards the epithelium.[212, 213]

Finally, adhesins are needed to mediate attachment to the epithelial cells and thereby prepare for colonization and persistent infection of the gastric epithelium, which undergoes constant cell renewal and is subjected to peristalsis of the digestive organ. The blood group binding antigen BabA can bind to its receptor Lewis[b].[214] This is the most extensively described interaction between the bacterium and its target cell. The expression of BabA is well conserved throughout *H. pylori* strains but varies in expression levels. In fact, BabA negative strains manifest lower colonization levels and cause less gastric injury.[215] Further adhesins such as SabA (sialic acid binding adhesion)[216] and HopQ (*Helicobacter* outer membrane protein Q)[217] modulate *H. pylori* binding to the gastric epithelium. This binding itself can cause gastric injury since it induces the secretion of the hormone gastrin, which stimulates acid production in the stomach. The severity of colonization correlates to overall strength of bacterial binding and was additionally shown to increase IL-8 secretion by the epithelial cells, which consequently leads to more pronounced inflammation and damage.[218]

3.4.3.2   Host manipulation

CagA (cytotoxin-associated gene A) represents the most intensely studied *H. pylori* virulence factor. It is an effector protein that is directly introduced into the host cell via the type IV secretion system (T4SS). Both are encoded on the *cag* pathogenicity island (*cag* PAI). The T4SS is a complex structure that interacts with integrin $\alpha_5\beta_1$ to enable injection of CagA into the target cell.[205] Additionally,

peptidoglycan is delivered to target cells triggering further pro-inflammatory responses and thereby promoting cancer development.[219, 220] However, the T4SS itself triggers mitogenic stimulation of target cells by interacting with EGFR, ErbB2 and ErbB3 of the epidermal growth factor receptor family.[205] Inside the gastric epithelial cell, CagA is partially phosphorylated at tyrosine residues in its EPIYA motifs by host kinases of the Src and Abl family.[203] This triggers alterations in the actin cytoskeleton resulting in the hummingbird phenotype of AGS cells (human gastric adenocarcinoma line), resembling an epithelial-to-mesenchymal transition.[221, 222] Furthermore, the integrity of tight junctions between epithelial cells is disrupted due to intercellular interaction of CagA with E-cadherin.[223] The resulting release of β-catenin from the junctional complexes induces mitogenic genes, which are associated with carcinogenesis.[224] Moreover, other factors encoded on the *cag* PAI are involved in virulence as well.

The relevance of CagA and the *cag* PAI in pathology induction is underlined by the occurrence of CagA producing and non-producing strains, whereas *cagA* positive strains are described with a higher risk for causing peptic ulcer or gastric cancer.[225] Moreover, several genetic variants of the corresponding gene and the *cag* PAI were identified and correlated with clinical risk. Especially, the difference between Western-type *cagA* and the more virulent East-Asian type *cagA* with distinct EPIYA motif types and numbers suggest its role in disease development.[226]

VacA (vacuolating cytotoxin A) is a secreted virulence factor of *H. pylori*, which exerts multiple cytotoxic effects on gastric epithelial cells.[227] The toxin can bind to host plasma membranes and trigger internalization. It is able to multimerize in host membranes forming anion-selective voltage-gated ion-channels. These lead to efflux of bicarbonate and organic anions as well as to vacuolation.[228] Furthermore, VacA can be targeted to the mitochondrial membrane. In this case, pore formation will lead to the release of cytochrome *c*, which induces apoptosis.[229] The loss of mucosal integrity might favor *H. pylori* growth due to the efflux of nutrients and additional neutralization of the gastric acid.[230] VacA is encoded in all *H. pylori* strains tested so far but not all strains can induce vacuolation. Actually, two regions in the *vacA* gene have been identified with allelic variation. In the sequence encoding the N-terminal signaling region, the *s* allele has been defined with the genotypes *s1* and *s2*. The *m* allele in the middle of the gene also has two described genotypes: *m1* and *m2*.[231] It has been shown that the s2 type of VacA is defective in vacuolation induction. In contrast, strains with *s1m1 vacA* have a strong activity and are also often *cagA* positive. In accorcance with this finding, *s1m1* strains are highly correlated with severe disease and they are classified as type I strains. Type II strains have only low vacuolating activity and are *cag* PAI negative.[232]

HtrA is a periplasmic chaperone of *H. pylori* that is important for its protein quality control and stress response.[233] It is a bifunctional protein since it also has serine protease activity. HtrA can be secreted to the environment and disrupt the intercellular adhesion of the gastric epithelial cells by cleaving the junctional protein E-cadherin.[234] The intercellular adherence junctions are essential for epithelial barrier function. In addition to efflux of nutrients into the gastric lumen, adherence junction disruption is necessary for the pathogen to cross the epithelium in a paracellular manner.[235, 236] *H. pylori* is then able to bind to laminin in the extracellular matrix of the lamina propria via AlpA and AlpB (adherence associated lipoproteins).[237] Lastly, the receptor for the T4SS, i.e. $\alpha_5\beta_1$ integrin, is

expressed on the basolateral site of epithelia.[238] Therefore, it can only be recognized after paracellular migration of *H. pylori* through the polarized epithelium allowing the CagA to be introduced into the epithelial cells.[205]

3.4.3.3   Immune evasion

The lifelong persistence of *Helicobacter pylori* in the human stomach suggests several mechanisms to evade the innate and adaptive immune responses activated since colonization.

Recognition of pathogen associated molecular patterns (PAMPs) is an important feature of the innate immune response. PAMPs are sensed via Toll-like receptors (TLRs) and related receptors of the pattern recognition family, which are for example expressed on cellular and intra-cellular membranes of antigen presenting cells (APCs). The signaling cascade typically leads to the secretion of pro-inflammatory cytokines like TNF-α, IL-1β and IL-8.[239] Lipopolysaccharide (LPS) present in bacterial membranes is described as one of the most effectively recognized PAMPs.[240] *H. pylori* does however produce an LPS variant with low immune-reactivity, which is assigned to the molecular mimicry of blood group saccharides similar to those expressed in the gastric mucosa.[241, 242] The corresponding receptor TLR-4 therefore does not play a major role in the defense reaction triggered by the pathogen. Additionally, *H. pylori* flagellin, which is sensed by TLR-5, is not efficiently recognized compared to *Salmonella typhimurium* flagella.[243] Furthermore, a PAMP, which is recognized by TLR-9, is defined as non-methylated CpG motifs in bacterial DNA.[244, 245] However, *H. pylori* shows strain-specific methylation patterns that evoke substantially reduced immune stimulatory effects.[246] Albeit, TLR polymorphisms can be correlated with an increased inflammatory response and thereby with a higher risk for gastric carcinoma.[247]

H. pylori colonization of the gastric epithelium induces local phagocyte infiltration and activation, in part as a result of NapA secretion[248, 249] and the inflammatory cytokines secreted by the gastric epithelium[250]. Yet, it can evade this defense mechanism by several means. Firstly, the production of nitric oxide, which is utilized as free radical to kill bacteria in macrophages, neutrophils and epithelial cells, can be alleviated by the *H. pylori* enzyme arginase.[251] Secondly, phagocytosis can be inhibited to a certain extend in a *cag* PAI dependent manner.[252] Finally, megasome formation via phagosome fusion can be induced by certain *H. pylori* strains after phagocytosis, which enables them to survive inside macrophages.[253]

Co-evolution of *H. pylori* with its human host also led to evasion mechanisms geared against the adaptive immune system. The aforementioned factor VacA is able to hinder efficient antigen presentation in dendritic cells and macrophages[254] as well as T-cell proliferation by targeting those cells via integrin β_2 (CD18)[255, 256]. Moreover, the *Helicobacter pylori* γ-glutamyl transpeptidase has been shown to inhibit T-cell proliferation as well.[257] This immune evasion factor elicits a wide variety of effects in *H. pylori* virulence and will be discussed in more detail in the following chapter.

3.4.4 *Helicobacter pylori* γ-glutamyl transpeptidase

3.4.4.1 *γ–Glutamyl transpeptidases*

The γ-glutamyl transpeptidases (gGT, EC 2.3.2.2) of the N-terminal nucleophilic hydrolase family are found in all kingdoms. They usually share more than 25 % similarity in amino acid sequence, suggesting a conserved function.[258] The cellular localization of these enzymes differs depending on the organism. In mammals, the enzyme is membrane-bound whereas plants can possess additional gGTs in apoplasts and vacuoles.[259] The bacterial enzymes are generally secreted, either to the periplasm or the extracellular space.[260]

As typical N-terminal nucleophilic hydrolase, gGTs are expressed as precursor proteins of about 60 kDa. They are post-translationally activated in an autocatalytic cleavage reaction leading to the formation of a small and a large subunit of about 20 kDa and 40 kDa, respectively.[261, 262] The nucleophilic N-terminal threonine and further amino acids of the active site are positioned to enable catalytic activity during this process.[263]

The transpeptidation reaction is characterized as a ping-pong bi-bi mechanism. This describes the independent reaction of enzyme with donor-substrate and enzyme with acceptor-substrate creating two independent reaction products (Figure 10).[264, 265] In the first step, γ-glutamyl transpeptidases catalyze the cleavage of a γ-glutamyl donor compound, which is often glutathione or its conjugates. The γ-glutamyl moiety is bound as an intermediate acyl to the enzyme's nucleophilic threonine. The remaining part of the donor-substrate is released. In a second step, the γ-glutamyl moiety is transferred to an acceptor, which can either be H_2O resulting in an overall hydrolysis reaction or amine groups of amino acids or peptides completing the transpeptidation reaction.[266] Resolving the acyl intermediate is the rate limiting step of the overall reaction.[267]
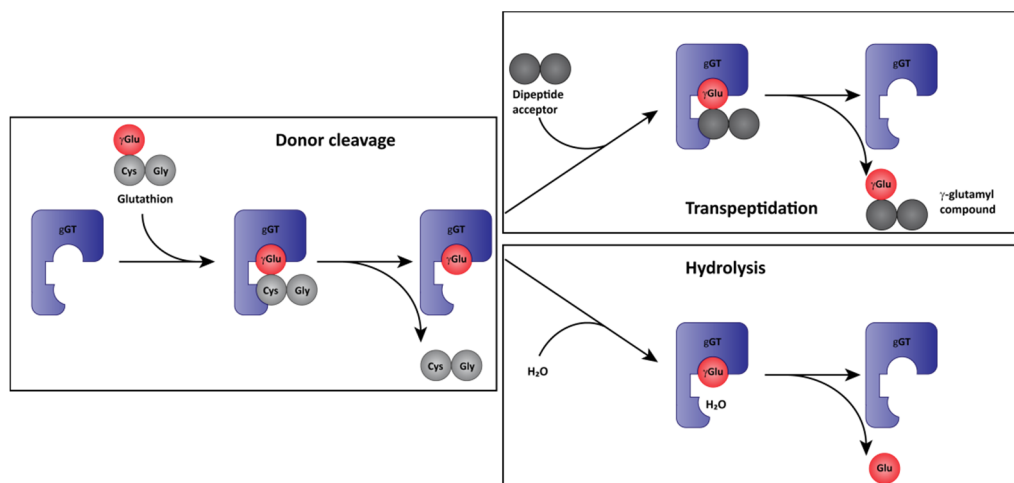
Figure 10: Scheme of γ-glutamyl transpeptidase transpeptidation and hydrolysis reaction

Firstly, the γ-glutamyl donor-substrate is cleaved and the intermediate acyl-enzyme and the remainder of the donor-substrate is formed. In the second step, the acyl-enzyme is resolved by transfer of the γ-glutamyl moiety to an acceptor-substrate (transpeptidation) or water (hydrolysis). The two separate steps with two substrates and two products define the catalytic mechanism as ping-pong bi-bi. (Adapted from Wickham, 2012[268])

The human gGT is predominantly expressed in ducts and glands for fluid secretion.[269] It is positioned on the apical sites of the epithelial cells and prevents excretion of glutathione.[270] Moreover, it is important for extracellular degradation of glutathione to release cysteine. Uptake of the local cystein is essential for intracellular glutathione homeostasis and thus for oxidative stress regulation.[271] Determination of gGT serum levels is used as diagnostic tool for detection of liver, biliary tract and pancreas disorders.[272] Aberrant expression of gGT was observed in several tumors; it led to elevated intracellular glutathione levels, and thereby increased detoxification of chemotherapeutics.[273] This resistance mechanism might be a therapeutic target itself with the purpose of increasing the tumor sensitivity towards standard therapies.[274]

Bacterial gGTs seem to have various and species specific functions. Poly γ-glutamate (PGA) can be surface associated and even the main building block of bacterial capsules.[275] Surface exposure of PGA enables escape from phagocytosis for *Staphylococcus epidermidis* and *Bacillus anthracis*.[276, 277] PGA itself and factors involved in synthesis and anchoring, such as the γ-glutamyl transpeptidase, are therefore bacterial virulence factors.[275] Bacterial gGTs are also involved in nitrogen and cystein metabolism, which are essential in challenging environments.[278, 279]

H. pylori gGT was found conserved and constitutively expressed in all isolated strains.[280] Multiple functions have been described for this enzyme especially in context of infection. Part of these functions has been confirmed to even be conserved in the *Helicobacter* genus.[281]

Autoprocessing and catalytic activity of the *H. pylori* enzyme have been studied in detail. Mature HPG presents itself as compact hetero-tetramer with two small and two large subunits. Site-directed mutagenesis revealed Thr380 to be critical for autoprocessing and enzymatic activity. Exchange to Ala prohibited both maturation and activity while T380S mutants were still capable of maturation and enzymatic catalysis, albeit with massively reduced rates. This implicated the importance of the added bulk in the threonine side chain for proper orientation of the nucleophile and other active site residues.[262] X-ray structure determination led to detailed insight into active site geometry. Autocatalytic activation does not only create the N-terminal Thr380 nucleophile but also exposes the substrate binding site, which would be covered in the unprocessed protein. The crystallographic data illustrates a considerable distance between the large subunit C-terminus and small subunit N-terminus indicating substantial conformational changes upon autoprocessing. Additionally, the role of the second conserved threonine, Thr398, could be elucidated. This residue is not involved in the autoprocessing reaction but influences the catalytic activity of the mature enzyme. Comparison of exchange mutants with Ala or Ser underlined the role of the γ-methyl group in optimal positioning of the hydroxyl group. Intermolecular activation of the nucleophilic Thr380 can thus be achieved in a threonine-threonine dyade including interaction of both side-chain hydroxyl groups and the N-terminal amine group. This reactive dyad enables nucleophilic attack at the γ-glutamyl peptide bond. The resulting transient state is stabilized by the backbone amides of Gly[472] and Gly[473] similar to serine protease oxyanion holes. The cleavage of the γ-glutamyl peptide bond is supported by the N-terminal amine as general acid. As a result, the tetrahedral transient state collapses and the remainder of the donor-substrate is released. The acyl enzyme intermediate is resolved by transferring the γ-glutamyl moiety to water or acceptor-substrate. Those are presumably activated by the Thr380 amino group

to enable the nucleophilic attack and regeneration of the enzyme's active site.[258] Figure 11 summarizes this process as an example of glutathione hydrolysis.
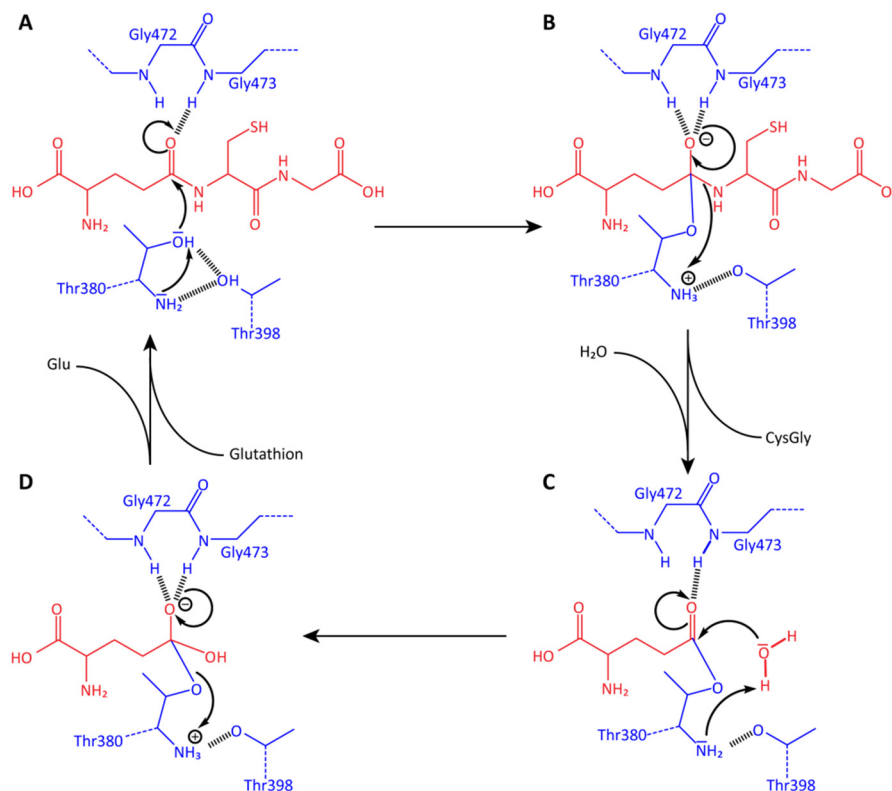

Figure 11: Reaction mechanism of glutathione hydrolysis catalyzed by HPG

Substrates of the glutathione hydrolysis reaction are shown in red, relevant parts of the HPG are shown in blue. The corresponding amino acid residues are indicated for the catalytic threonine-threonine dyade and the two glycines whose backbone amides serve to stabilize transient states of the reaction. **(A)** the nucleophilic hydroxyl group of the N-terminal Thr380 is activated by its own amine-group and the hydroxyl group of Thr398. It attacks carbonyl moiety of the γ-glutamyl peptide bond whereas the Thr380 amine group may act as general base. **(B)** the tetrahedral transient state is stabilized by Gly472 and Gly473 amide groups. It is resolved by cleavage of the γ-glutamyl peptide bond. Here, the amine group of Thr380 can act as general acid. The acyl-enzyme intermediate is formed. H$_2$O may be activated by the general base **(C)** to initiate the second tetrahedral transition state, which is again stabilized by the glycines' backbone amides **(D)**. Collapse of the transition state releases glutamate and regenerates the enzyme.
(Adapted from Boanca, 2006[258].)

3.4.4.2   *Helicobacter pylori γ-glutamyl transpeptidase in infection*

The role of the HPG in colonization, ulcer and cancer development as well as persistence has been described and in part elucidated in literature.[282] Apart from its role in nutrient supply, the functions exerted by the HPG can be divided into gastric injury, pro-carcinogenic stimulation and immune evasion. All these mechanisms create a complex and still incomplete picture of HPG and its relevance for clinical outcome.[283] However, it is appreciated that HPG is a typical virulence factor, which is not essential for *in vitro* growth of *H. pylori* but a premise for *in vivo* survival and persistence.[284] Figure 12 gives an overview of the HPG functions discussed in this chapter.
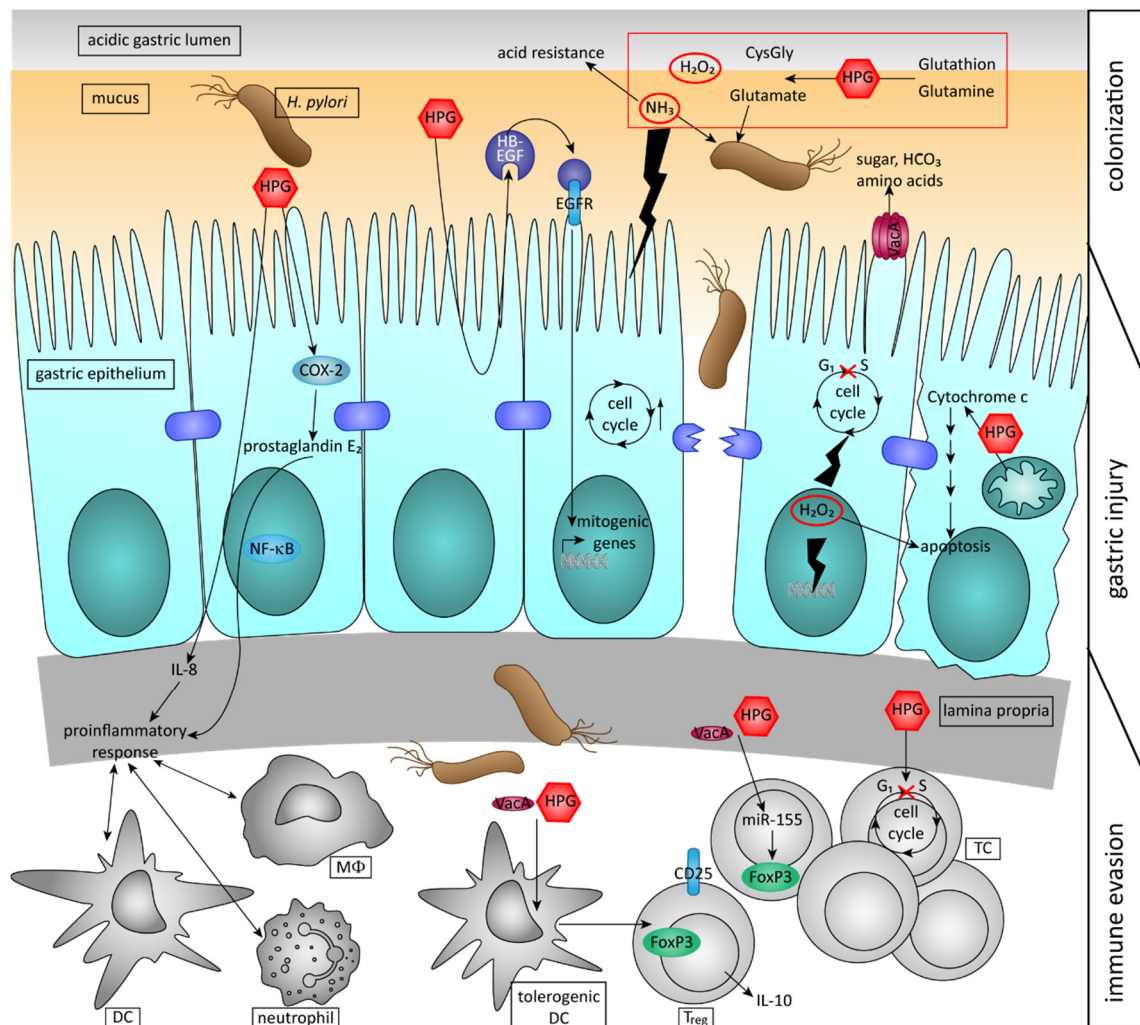
Figure 12: *H. pylori* γ-glutamyl transpeptidase is involved in various virulence mechanisms

Helicobacter pylori γ-glutamyl transpeptidase exerts a variety of functions in colonization, gastric injury and immune evasion to finally enable the pathogen to persist in the gastric environment. Mechanisms displayed in this graph are described in detail in chapter 3.4.4.2.
DC: dendritic cell, MΦ: macrophage, TC: T-cell.

The main physiological function of the HPG is degradation of extracellular glutathione and glutamine to provide glutamate, which can be taken up by *H. pylori* in a Na^+-dependent manner and, subsequently, be incorporated into the citric acid cycle as well as be used for intra-cellular glutamine synthesis.[285] Therefore, HPG creates a metabolic advantage for *H. pylori* during colonization and persistent infection. Moreover, HPG together with *H. pylori* arginase produce ammonia.[279] As mentioned above, ammonia serves as nitrogen source and buffers the acidic gastric environment but has also been reported to possess high toxicity towards human cells.[286] Another consequence of glutathione consumption is an alteration of the redox balance in gastric epithelial cells. This renders them more sensitive to reactive oxygen species (ROS) and the resulting DNA damage, cell cycle alterations, apoptosis and carcinogenesis.[283] HPG activity itself leads to the formation of H_2O_2 as a product of glutathione degradation.[287, 288] H_2O_2 is a ROS that is described to induce necrosis.[135] However, apoptosis induction has been observed in gastric epithelial cells *in vivo* and *in vitro* during *H. pylori* infection as well.[289-291] HPG was identified as one of the major factors involved in the resulting gastric injury. The observed dysregulation of the cell cycle by G1-S phase transition

inhibition[292] leads to apoptosis and can be an additional effect of H_2O_2 exposure.[288, 293] The HPG induced apoptosis is dependent on its enzymatic activity and occurs via the release of cytochrome c from the mitochondria[294]. Furthermore, HPG stimulates the inflammatory response at the site of infection. This is achieved by activation of NF-κB and the consequential release of IL-8.[295] IL-8 promotes recruitment of immune cells and maintenance of the chronic inflammation.[282] Moreover, cyclooxygenase-2 (COX-2) and its enzymatic product prostaglandin E_2 are reported to be up-regulated in a gastric cell line in the presence of HPG[296], presenting a further pro-inflammatory stimulus.[297] An inflammatory environment results in further gastric injury but also increases nutrient abundance for *H. pylori*. Therefore, it is not surprising that HPG was found to be essential for colonization *in vivo*.[284]

Peptic ulcer patient isolates of *H. pylori* were reported to have higher gGT activity compared to isolates from non-ulcer patients. This effect presented itself independent of other virulence genes (e.g. *cagA, vacA, babA*).[295] Epidermal growth factor receptor (EGFR) signaling is stimulated due to HPG mediated up-regulation of heparin-binding epidermal growth factor like growth factor (HB-EGF).[296] This leads to increased cell-survival and proliferation of the gastric epithelial cells as well as epithelial-mesenchymal transition.[298, 299] Therefore, HPG is indicated as important factor in gastric carcinoma development.[282] Beyond this mechanism, another more general role of the HPG in tumor genesis is discussed. As both apoptotic and survival promoting effects of HPG have been described, the balance between cell division and cell loss is disrupted.[300, 301] Taken together, with increased DNA damage, which might also be induced by HPG[295], the overall mutation rate increases leading to emergence of malignant, apoptosis-resistant cells.[300]

Finally, HPG can interact with host immune cells as it is a secreted factor and as *H. pylori* is able to disrupt the gastric epithelial barrier function.[234] Direct and indirect modulations of T-cell immunity have been described. HPG was identified to be the bacterial factor inducing G1 cell cycle arrest and proliferation inhibition in T-cells.[257, 302] Together with VacA, which also inhibits T-cell proliferation[106, 107], HPG leads to up-regulation of the micro-RNA miR-155, which was reported to be associated with B-cell lymphoma development[303], and Foxp3, the master regulator of regulatory T-cells[304]. The two bacterial factors also manipulate dendritic cells (DCs) to promote T-cell differentiation in the direction of regulatory T-cells. A so-called tolerogenic phenotype of DCs is induced and renders the DCs inefficient at mounting TH1 and TH17 polarized effector T-cell responses, which would have the potential of clearing the bacterial infection[305]. Instead, tolerogenic DCs initiate regulatory T-cell specific factors like the master regulator Foxp3, the anti-inflammatory cytokine IL-10 and the surface marker CD25 in naïve T-cells.[305] This manipulation of the host defense may contribute to persistence and immune evasion of *H. pylori*.[283]

3.4.4.3   *Helicobacter pylori γ-glutamyl transpeptidase as drug target*

The above described multiplicity of functions indicated for the enzymatically active HPG in colonization, virulence and persistence qualify this bacterial protein as target for anti-virulence therapy. Inhibition might lead to clearance of the infection as nutrient availability would be reduced

and immune reactivity could be enhanced. Furthermore, pathology associated functions including gastric injury and pro-carcinogenic interference with the gastric epithelium would be reduced leading to lower risk of severe disease. Even in context of the numerous described virulence factors of *H. pylori*, the overall contribution and cooperativety of the HPG is substantial and justifies efforts in drug discovery.

The HPG has been found constitutively expressed in all *H. pylori* isolates[280] and its functions are in part even conserved in the *Helicobacter* genus[281]. Therefore, HPG inhibitors would have a useful spectrum for treatment of *H. pylori* infections targeting all strains in the human population and quasispecies in an individual patient.[306, 307]

As gGT homologous enzymes have been found in all kingdoms, HPG must differ adequately from other gGTs to enable targeted inhibition. Sufficient differences to the human gGT are important since the human enzyme (HsgGT) is involved in many essential functions such as stabilizing the redox-balance, detoxification of a variety of compounds and preserving glutathione and cysteine levels. Therefore, inhibition of the human gGT potentially causes severe adverse-reactions and should be avoided. Fortunately, significant catalytic differences have been described for bacterial and non-bacterial gGTs as well as distinct variation in the substrate binding site comparing human and *H. pylori* gGT. In detail, the catalytic differences are oriented to efficiency of the transpeptidation reaction. The HsgGT is more than 100-fold more efficient at catalyzing transpeptidation reactions than HPG whereas their hydrolysis rates are comparable.[262] These discrepancies are most likely caused by distinct substrate binding site physicochemical geometries. Indeed, the glutamate binding sites are very similar but significant differences have been reported for the donor- and acceptor-substrate binding site. The binding site for the donor-substrate, in most cases glutathione, is rather shallow and non-polar for the HPG referencing to its promiscuity towards glutathione conjugates. These are presumably recognized by only weak binding contacts with the addition of the highly specific, secluded glutamate binding site. This substrate binding site is, however, also responsible for acceptor-substrate binding. In the human gGT, three Ala and one Ser residues present in the HPG binding site are replaced by His, Ser, Leu and Tyr. This results in a more polar and sterically constrained binding site for the human enzyme and may also explain the enhanced acceptor-substrate binding.[258] Furthermore, a flexible loop positioned above the active site contains a Tyr residue in bacterial gGTs. It has been proposed to shield the active site from solvent during catalysis and stabilizes the architecture of the active site. In eukaryotic gGTs, this Tyr is often substituted with Phe, which can also contribute to the differences in catalytic characteristics.[308]

Crystal-structure data of HPG (apo-enzyme: 2NQO[258], complex with glutamate: 2QM6[308], acivin-bound: 3FNM[309]), further bacterial gGTs (*E. coli*: 2DG5[260], *B. subtilis*: 2V36[310]) and HsgGT (4GDX[271]) are published and can be used to design specific compounds against the *H. pylori* enzyme. The substrate binding site of the bacterial gGT is distinct in several aspects, which can be exploited to achieve specificity. Also, specific targeting of the HPG against other bacterial gGTs seems feasible as there is surprisingly low identity with other bacterial gGT amino acid sequences e.g. between HPG and EcgGT 52.5 %.[282, 284]

4 Objective

Increasing antimicrobial resistance challenges modern medicine and endangers advanced therapeutic means for the treatment of premature infants, cancer and transplantation patients. In a striking contrast, a discovery void for novel antibiotics has been noted as no novel classes have been found since 1987. Therefore, infectious diseases are once again menacing conditions that call for novel treatment options and innovative drug-discovery approaches.

One possibility to meet the urgent need for anti-infective agents are virulence inhibitors, which preferably do not provoke rapid resistance development and are not affected by pre-existing resistances. These potential anti-infective drugs target bacterial mechanisms needed for colonization, virulence and immune evasion. Thus, they are expected to pose less risk for resistance development since these anti-virulence targets are not essential for bacterial viability and growth *in vitro* and would exert less selective pressure than classical antibiotics. Moreover, such targets involved in virulence of pathogenic bacteria are likely specific for the bacterial species and, thus, enable targeted therapy. Species-specific drugs would not only be able to treat resistant bacterial infections but also support controlling resistance development by saving advanced antibiotic regimens for most severe infectious conditions and by sparing the endogenous microbiota from selection processes. Therefore, the aim of this thesis was to apply drug-discovery approaches to two anti-virulence targets of relevant human pathogens.

Firstly, Sortase A from *S. aureus* is an exemplary anti-virulence target that plays a major role in infection establishment and virulence mechanisms by covalently linking protein factors involved in these processes to the bacterial cell wall. Consequently, inhibition of Sortase A will prohibit these factors from interactions with the host and substantially decrease *S. aureus* virulence. Sortase A function is however dispensable for *in vitro* growth and viability, which is a prerequisite for anti-infective drug-targets. An enzymatic high-throughput screening (HTS) assay, based on a fluorophore-quencher pair labeled peptide substrate, was to be established and validated. With this, a targeted approach of *in silico* modeling assisted drug-development and screening of natural compounds was to be performed. Inhibitors identified for the SaSrtA with these approaches were intended to be thoroughly tested for cross-reactivity with sortases from further gram-positive bacteria and physical binding needed to be proven with orthogonal assays to finally obtain suitable lead structures for drug development.

Secondly, specific inhibitor identification for the γ-glutamyl transpeptidase from *H. pylori* is of interest since this bacterial factor is involved in all virulence mechanisms neccessary to support livelong persistence of the pathogen in the human stomach, namely nutrient acquisition, gastric injury, pro-carcinogenic stimulation and immune evasion. Hence, drugs targeting this virulence factor will enable clearance of the infectious agent by the patient's immune system and simultaneously dampen the pathogen's detrimental impact on the gastric mucosa. For HPG, the enzymatic assay based on an artificial chromogenic substrate was to be optimized and validated for HTS application. Thus, it could be applied for inhibitor identification in a natural compound library and for evaluation of *in silico* designed inhibitors. Compounds exerting inhibitory activity against the HPG were intended

to be characterized for specificity with gGTs of human and bacterial origin. Moreover, orthogonal assays for determination of physical compound binding to the HPG, such as microscale thermophoresis, NMR-studies, and co-crystallization were envisaged to assess the compounds suitability as lead structures.

A complementing project aimed at preparing *H. pylori* candidate-proteins for in depth evaluation as therapeutic targets. These candidates have been identified via an optimized surface shaving approach (adapted from Grandi, 2006[311]) by Tobias Kruse (unpublished) for identification of bacterial surface-exposed proteins as novel drug targtets. These target proteins are currently prepared for patent protection. Therefore, the candidates can only be presented in a blinded form in this work. The candidate proteins were to be recombinantly produced to investigate *H. pylori* positive patients for serological reaction and to allow generation of murine antisera. These sera were used for verification of candidate-protein surface exposure. Furthermore, *H. pylori* knock-out mutants were intended to be generated to assess the candidates' relevance for *in vitro* growth and viability.

5 Materials and Methods

5.1 Materials

5.1.1 Chemicals and reagents

Ambion ®40 % (w/v) 19:1 Acrylamid : Bisacrylamid	Life Technologies (Carlsbad, US)
Anhydrotetracycline hydrochloride	Iba lifesciences (Göttingen, DE)
CellLytic™ B Cell Lysis Reagent	Sigma-Aldrich (Steinheim, DE)
Cholera toxin	Sigma-Aldrich (Steinheim, DE)
Invitrogen™ Ultra-Pure TEMED	Life Technologies (Carlsbad, US)
Pierce™ ECL Western Blotting Substrate	Pierce Biotechnology (Rockford, US)
Restore Plus Western Blot Stripping Buffer	Thermo Scientific (Waltham, US)
Roti®-Safe GelStain	Roth (Karlsruhe, DE)
TMB substrate reagent set	BioLegend (San Diego, US)

Kits

DNeasy Blood & Tissue Kit	Quiagen (Hilden, DE)
Pierce™ BCA Protein Assay Kit	Pierce Biotechnology (Rockford, US)
Pure Yield™ Plasmid Midiprep System	Promega (Madison, US)
Pure Yield™ Plasmid Miniprep System	Promega (Madison, US)
recomWell *Helicobacter* IgG	Mikrogen Diagnostik (München, DE)
Wizard® SV Gel and PCR Clean-Up System	Promega (Madison, US)

All chemicals not specifically mentioned were purchased from the following companies: AppliChem (Darmstadt, DE), Merck (Darmstadt, DE), Sigma-Aldrich (Steinheim, DE), Serva (Heidelberg, DE), Roth (Karlsruhe, DE).

5.1.2 Enzymes and Antibodies

USB® FideliTaq™ DNA Polymerase	Affymetrix, Inc (Cleveland, US)
Herculase II Fusion DNA Polymerase	Agilent (Santa Clara, US)
Q5® High-Fidelity DNA Polymerase 2x Mastermix	New England Biolabs (Ipswich, US)
GoTaq® Green Master Mix	Promega (Madison, US)
GoTaq® G2 Green Master Mix	Promega (Madison, US)
Gibson Assembly® Mastemix	New England Biolabs (Ipswich, US)
Restriction endonuclease DpnI	New England Biolabs (Ipswich, US)

Restriction endonuclease EcoRV	New England Biolabs (Ipswich, US)
Restriction endonuclease NdeI-HF	New England Biolabs (Ipswich, US)
Restriction endonuclease NotI-HF	New England Biolabs (Ipswich, US)
Restriction endonuclease XhoI-HF	New England Biolabs (Ipswich, US)
T4 DNA Ligase	New England Biolabs (Ispwich, US)
DNase I	AppliChem (Darmstadt, DE)
Lysozyme	Sigma-Aldrich (Steinheim, DE)
anti-His IgG1 (WB, 1:5000)	AbD Serotec (Kidlington, UK)
anti-mouse HRP (from goat) (WB, 1:5000 - 1:10000)	Dianova (Hamburg, DE)
anti-mouse HRP (from goat) (ELISA, 1:10000)	Abcam (Cambridge, UK)
anti-mouse IgG1 eFluor®660 (FC, 1:100)	eBioscience (San Diego, US)

5.1.3 Antibiotics

Antibiotic	Company	final concentration	
Ampicillin	Roth (Karlsruhe, DE)	100 mg/L	
Kanamycin	Roth (Karlsruhe, DE)	50 mg/L (100 mg/L for high density autoinduction cultures)	
Chloramphenicol	Roth (Karlsruhe, DE)	35 mg/L	
Vancomycin	Sigma-Aldrich (Steinheim, DE)	10 mg/L	
Helicobacter pylori selective supplement (dent)	Oxoid (Wesel, DE)	Vancomycin Trimethoprim Cefsulodin Amphotericin B	10 mg/L 5 mg/L 5 mg/L 5 mg/L

Table 1: Antibiotics used in this work

5.1.4 Media and Buffers

5.1.4.1 Media for E. coli culture

LB_0 medium	Peptone	1.0 % (w/v)
	Yeast extract	0.5 % (w/v)
	NaCl	0.5 % (w/v)

LB$_0$ agar plates	LB$_0$ medium	
	Agar	2.0 % (w/v)
TB$_0$ medium	Tryptone	1.2 % (w/v)
	Yeast extract	2.4 % (w/v)
	Glycerole	0.5 % (w/v)
	Potassium phosphate	89 mM
	Magnesium sulfate	2 mM
	pH (hydrochloric acid)	7.0
TB$_0$ medium (autoinduction)	TB$_0$ medium	
	Lactose	0.2 % (w/v)
SOC medium	Tryptone	2.0 % (w/v)
	Yeast extract	0.5 % (w/v)
	NaCl	0.5 % (w/v)
	MgSO$_4$	10 mM
	MgCl$_2$	10 mM
	Glucose	20 mM

5.1.4.2   Media for H. pylori culture

BHI-medium (Oxoid, Wesel, DE)	Brain infusion solids	1.25 % (w/v)
	Beef heart infusion solids	0.5 % (w/v)
	Proteose-peptone	1.0 % (w/v)
	Glucose	0.2 % (w/v)
	NaCl	0.5 % (w/v)
	Na$_2$HPO$_4$	0.25 % (w/v)
	pH (hydrochloric acid)	7.4
Brucella Medium (Oxoid, Wesel, DE)	Peptone	1 % (w/v)
	Lab-Lemco powder	0.5 % (w/v)
	Glucose	1 % (w/v)
	NaCl	0.5 % (w/v)
	pH (hydrochloric acid)	7.5
DMEM + F-12	(Gibco, Life Technologies (Carlsbad, US))	

WC plates (Oxoid, Wesel, DE)	Horse Blood	5.0 %
	Tryptone	1.0 % (w/v)
	Gelatin peptone	1.0 % (w/v)
	Yeast extract	0.5 % (w/v)
	Glucose	0.1 % (w/v)
	NaCl	0.5 % (w/v)
	L-Arginine	0.1 % (w/v)
	Sodium pyruvate	0.1 % (w/v)
	Menadione	0.00005 % (w/v)
	Hemin	0.0005 % (w/v)
	Agar	1.0 % (w/v)
	pH (hydrochloric acid)	7.1

5.1.4.3   Media for preparation of competent E. coli

TSS Medium	PEG3350	10 % (v/v)
	DMSO	5 % (v/v)
	$MgSO_4$	20 mM
	LB Medium	ad
	pH (hydrochloric acid)	6.5
Inoue Buffer	$MnCl_2$	55 mM
	$CaCl_2$	15 mM
	KCl	250 mM
	PIPES	10 mM
	pH (hydrochloric acid)	6.7

5.1.4.4   Buffers and solutions for DNA-methods

Tris acetate-EDTA (TAE) buffer	Tris	40 mM
	Acetic acid	20 mM
	EDTA	1 mM
	pH (acetic acid)	8.3

DNA loading dye (10×)	Tris-HCl	10 mM
	EDTA	1 mM
	Glycerole	50 % (v/v)
	Xylene cyanole	0.25 % (w/v)
	Bomphenol blue	0.25 % (w/v)

10×SLiCE Buffer	Tris	500 mM
	MgCl$_2$	100 mM
	ATP	10 mM
	DTT	10 mM
	pH (hydrochloric acid)	7.5

5.1.4.5   Buffers and solutions for protein analytic methods

4×SDS sample buffer	Tris	62.5 mM
	Dithiothreitol (DTT)	50 mM
	Sodium dodecyl sulfate (SDS)	2 % (w/v)
	Glycerole	10 % (v/v)
	Bromphenol blue	0.01 % (w/v)
	pH (hydrochloric acid)	6.8

SDS-PAGE buffer	Tris	25 mM
	Glycine	250mM
	SDS	0.1 % (w/v)
	pH (hydrochloric acid)	8,3

Stacking gel buffer	Tris	500 mM
	SDS	0.4 % (w/v)
	pH	6.8

Separating gel buffer	Tris	1.5 M
	SDS	0.4 % (w/v)
	pH (hydrochloric acid)	8.8

| 10 % APS solution | Ammonium persulfate (APS) | 10 % (w/v) |

Semi-dry blotting buffer	Tris Ultra	48 mM
	Glycine	39 mM
	Sodium dodecyl sulfate	0.04 % (w/v)
	Methanol	20 % (w/v)
	pH	not adjusted
TBS-T	Tris	5 mM
	NaCl	15 mM
	Tween-20	0.1 % (w/v)
	pH (hydrochloric acid)	7.5
Coomassie staining solution	Ethanol (for SDS-gels)	50 % (v/v)
	Methanol (for PVDF membranes)	50 % (v/v)
	Acetic acid	10 % (v/v)
	Coomassie Brillant Blue R-250	0.25 % (w/v)
Coomassie destaining solution	Methanol (for blotting membranes)	50 % (v/v)
	Acetic acid	10 % (v/v)

5.1.4.6   Buffers for protein purification

HisTrap Buffer A-HPG	Tris	100 mM
	NaCl	500mM
	pH (hydrochloric acid)	8.0
HisTrap Buffer B-HPG	Tris	100 mM
	NaCl	500 mM
	Imidazole	500 mM
	pH (hydrochloric acid)	8.0
HsgGT Resuspension Buffer	MgCl$_2$	80 mM
	NaOH	0.75 mM
HsgGT Extraction Buffer	Tris	100 mM
	Sodium dodecylcholat	2 % (w/v)
	PEG 6000	20 % (w/v)
	pH (hydrochloric acid)	8.5

AIX-Buffer A	Tris	50 mM
	Triton X-100	2 % (v/v)
	pH (hydrochloric acid)	7.5
AIX-Buffer B	Tris	50 mM
	NaCl	500 mM
	Triton X-100	2 % (v/v)
	pH (hydrochloric acid)	8.0
HisTrap Buffer A-SrtA	NaPO4	50 mM
	NaCl	500 mM
	pH (hydrochloric acid)	7.0
HisTrap Buffer B-SrtA	NaPO4	50 mM
	NaCl	500 mM
	Imidazole	500 mM
	pH (hydrochloric acid)	7.0
HisTrap Buffer A-HP-candidates	Tris	100 mM
	NaCl	500 mM
	pH (hydrochloric acid)	7.5
HisTrap Buffer B-HP-candidates	Tris	100 mM
	NaCl	500 mM
	Imidazole	500 mM
	pH (hydrochloric acid)	7.5
1×PBS	Na_2HPO_4	10 mM
	NaH_2PO_4	2 mM
	NaCl	137 mM
	KCl	2.7 mM
	pH (hydrochloric acid)	7.4
ArgPi	Arginine free base	330 mM
	pH (phosphoric acid)	7.4
Crystallization Buffer	Tris	5 mM
	NaCl	140 mM
	pH (hydrochloric acid)	8.0

MabSelect Buffer A	Na_2HPO_4	20 mM
	NaCl	140 mM
	pH (hydrochloric acid)	7.2
MabSelect Buffer B	Citric acid	100 mM
	pH	3.2
Elution Neutralization Buffer	Tris	2 M
	pH (hydrochloric acid)	8.0

5.1.4.7   Buffers for enzymatic assays

HPG-Assay-Buffer	Tris	100 mM
	pH (hydrochloric acid)	8.0
FRET-Assay Buffer	HEPES	20 mM
	$CaCl_2$	5 mM
	pH (hydrochloric acid)	7.5

5.1.5 Primers

All Oligonucleotides were synthesized at Eurofins MWG Operon (Ebersberg, DE) and delivered as salt free or HPSF or HPLC purified. They were dissolved in aqua ad injectibila to a final concentration of 100 µM. The working concentration of the primers was 10 µM.

Primer	Description	Sequence 5'→3'	T_m [°C]
CD_P1	*S. aureus* SrtA Δ1-25 His6 NdeI for	ctaaaacatatgcaccatcatcatcatcataaaccacatatcgataatt atcttcacg	59
CD_P2	*S. aureus* SrtA for pET30b XhoI rev	gttagactcgagttatttgacttctgtagctacaaagattttacg	61
CD_P27	HP1 for - Homology pSCask	ttttgtttaactttaagaaggagatatacatatgxxxxxx	60
CD_P28	HP1 rev - Homology pSCask	tcgaggcggccgcttaatgatgatgatgatggtgxxxxxx	59
CD_P29	HP2 for - Homology pSCask	ttttgtttaactttaagaaggagatatacatatgxxxxxx	61
CD_P30	HP2 rev - Homology pSCask	tcgaggcggccgcttaatgatgatgatgatggtgxxxxxx	61
CD_P31	HP3 for - Homology pSCask	ttttgtttaactttaagaaggagatatacatatgxxxxxx	62

CD_P32	HP3 rev - Homology pSCask	tcgaggcggccgcttaatgatgatgatgatggtxxxxxx	64
CD_P33	HP4 for - Homology pSCask	ttttgtttaactttaagaaggagatatacatatgxxxxxx	60
CD_P34	HP4 rev - Homology pSCask	tcgaggcggccgcttaatgatgatgatgatggtxxxxxx	62
CD_P35	HP5 for - Homology pSCask	ttttgtttaactttaagaaggagatatacatatgxxxxxx	61
CD_P36	HP5 rev - Homology pSCask	tcgaggcggccgcttaatgatgatgatgatggtxxxxxx	62
CD_P37	HP6 for - Homology pSCask	ttttgtttaactttaagaaggagatatacatatgxxxxxx	58
CD_P38	HP6 rev - Homology pSCask	tcgaggcggccgcttaatgatgatgatgatggtxxxxxx	60
CD_P39	HP7 for - Homology pSCask	ttttgtttaactttaagaaggagatatacatatgxxxxxx	58
CD_P40	HP7 rev - Homology pSCask	tcgaggcggccgcttaatgatgatgatgatggtxxxxxx	64
CD_P45	HP8 for - Homology pSCask	ttttgtttaactttaagaaggagatatacatatgxxxxxx	55
CD_P46	HP8 rev - Homology pSCask	tcgaggcggccgcttaatgatgatgatgatggtxxxxxx	62
CD_P51	G27 knock out w/ kana cassette HP7 up for	xxxxxx	57
CD_P52	G27 knock out w/ kana cassette HP7 down rev	xxxxxx	58
CD_P53	G27 knock out w/ kana cassette HP7 down for +CD_P87	ggaactaaggaggatattcatatgxxxxxx	57
CD_P54	G27 knock out w/ kana cassette HP7 up rev +CD_P88	cgaagcagctccagcctacacxxxxxx	58
CD_P56	G27 knock out w/ kana cassette HP5 up rev +CD_P88	cgaagcagctccagcctacacxxxxxx	59
CD_P57	G27 knock out w/ kana cassette HP1 down for +CD_P87	ggaactaaggaggatattcatatgxxxxxx	57
CD_P58	G27 knock out w/ kana cassette HP1 up rev +CD_P88	cgaagcagctccagcctacacxxxxxx	55
CD_P59	G27 knock out w/ kana cassette HP6 down for +CD_P87	ggaactaaggaggatattcatatgxxxxxx	57
CD_P60	G27 knock out w/ kana cassette HP6 up rev +CD_P88	cgaagcagctccagcctacacxxxxxx	59
CD_P61	G27 knock out w/ kana cassette HP1 down for +CD_P87	ggaactaaggaggatattcatatgxxxxxx	55
CD_P62	G27 knock out w/ kana cassette HP1 up rev +CD_P88	cgaagcagctccagcctacacxxxxxx	59

CD_P63	G27 knock out w/ kana cassette HP5 down rev	xxxxxx	59
CD_P64	G27 knock out w/ kana cassette HP5 up for	xxxxxx	59
CD_P67	G27 knock out w/ kana cassette HP1 up for	xxxxxx	58
CD_P68	G27 knock out w/ kana cassette HP1 down rev	xxxxxx	61
CD_P69	G27 knock out w/ kana cassette HP6 up for	xxxxxx	59
CD_P70	G27 knock out w/ kana cassette HP6 down rev	xxxxxx	58
CD_P71	G27 knock out w/ kana cassette HP5 down for +CD_P87	ggaactaaggaggatattcatatgxxxxxx	59
CD_P72	pET28b Gibson down	tgagatccggctgc	58
CD_P73	pET28b Gibson up	catatggctgccgc	58
CD_P75	opt HPG for pET28b Gibson rev	cctttcgggctttgttagcagccggatctcagaattctttacgcgggtc	58
CD_P76	opt HPG for pET28b Gibson for	cagcggcctggtgccgcgcggcagccatatggctagcgcttcttacccgcc	56
CD_P78	Sequencing opt HPG rev	cagaaccgtaagaagcg	58
CD_P79	Sequencing HPG upper boarder	gaagccagcgggtgag	64
CD_P80	Sequencing T7	taatacgactcactataggg	55
CD_P81	Sequencing T7 term	ctagttattgctcagcggt	59
CD_P82	Tet for	gagttattttaccactccct	56
CD_P83	Tet rev	cgcagtagcggtaaacg	61
CD_P84	Sequencing CMV for	cgcaaatgggcggtaggcgtg	73
CD_P85	Sequencing pCR3.1-BGHrev	tagaaggcacagtcgagg	61
CD_P87	for kana cassette from pKD4 rev	catatgaatatcctccttagttcc	58
CD_P88	kana cassette from pKD4 for	gtgtaggctggagctgcttcg	69
CD_P89	pPR Gibson up	catttgtatatctccttcttaaagttaaac	58
CD_P90	pPR HisTag Gibson down	caccatcatcatcatcattaataagcttg	62
CD_P91	*S. aureu*s SrtB Δ1-23 for + pPR up Homology	gtttaactttaagaaggagatatacaaatgxxxxxx	53
CD_P92	*S. aureus* SrtB rev + pPR down Homology	tcaagcttattaatgatgatgatgatggtgxxxxxx	54

CD_P95	*E. faecalis* SrtA Δ1-30 for + pPR up Homology	gtttaactttaagaaggagatatacaaatgxxxxxx	53
CD_P96	*E. faecalis* SrtA rev + pPR down Homology	tcaagcttattaatgatgatgatgatggtgxxxxxx	59
CD_P110	SP6	atttaggtgacactatag	49
CD_P113	Seq ko G27_HP5 for	xxxxxx	60
CD_P114	Seq ko G27_HP5 rev	xxxxxx	58
CD_P119	Seq ko G27_HP2 for	xxxxxx	60
CD_P120	Seq ko G27_HP2 rev	xxxxxx	60

Table 2: Primers used in this work

Restriction site, homology for SLiCE-/ Gibson-Reaction, second primer for PCR fusion.
T_m was calculated with http://tmcalculator.neb.com/#!/; for specific PCR-reactions the appropriate calculator was used to determine the annealing temperature.
Primer sequences for HP candidate proteins have been blinded to preserve intellectual property.

5.1.6   Strains

Organism	Strain	Genotype	Source
E. coli	DH5α	F⁻ endA1 glnV44 thi-1 recA1 relA1 gyrA96 deoR nupG Φ80d*lacZ*ΔM15 Δ(*lacZYA-argF*)U169, hsdR17(r_K^- m_K^+), λ⁻	Hanahan, 1983[312]
E. coli	DH10B™	F⁻ endA1 recA1 galE15 galK16 nupG rpsL ΔlacX74 Φ80lacZΔM15 araD139 Δ(ara,leu)7697 mcrA Δ(mrr-hsdRMS-mcrBC) λ⁻	Hanahan, 1983[312]
E. coli	PPY	DH10B with an optimized λ prophage Red recombinase	Zhang, 2012[313]
E. coli	BL21 (DE3)	F⁻ ompT gal dcm lon hsdSB(r_B^- m_B^-) λ(DE3)	Studier, 1986[314]
E. coli	Arctic Express (DE3)	F⁻ompT hsdS(r_B^- m_B^-) dcm⁺ Tet^r gal λ(DE3) endA Hte [cpn10cpn60 Gent^r]	Studier, 1986[314]
H. pylori	J99		Alm, 1999[315]
H. pylori	G27		Baltrus, 2009[316]
S. aureus	USA300		Diep, 2006[317]
E. faecalis	ATCC 47077		Schleifer, 1984[318]

Table 3: Strains used in this work

λ(DE3) = λ sBamHIo ΔEcoRI-B int::(lacI::PlacUV5::T7 gene1) i21 Δnin5

5.1.7 Plasmids

Plasmid	Description	Source
pET30b	Lactose induced T7 Transcription, MCS, His$_6$-Tag (C/N), S-Tag, Thrombin-site, Enterokinase-site, Kanamycin resistant	(NOVAGEN, Bad Soden, DE)
pET28b	Lactose induced T7 Transcription, MCS, His$_6$-Tag (C/N), T7-Tag, Thrombin-site, Kanamycin resistant	(NOVAGEN, Bad Soden, DE)
pKD4	Backbone used for amplification of Kanamycin-resistance cassette flanked by natural FRT-sites flanked, additional chloramphenicol resistance	(Coli genetic stock center, New Haven, US)[319]
pSCask HPG-h	based on pASK-IBA 17 plus: contains HPG-gene flanked by EcoRI sites for blunt end restriction (SLiCE compatible) with C-terminal His-Tag for gene products, inserted HPG - differentiates between fully and partly digested backbone, Ampicillin resistant	this work
pPR-IBA 1	Lactose induced T7 Transcription, MCS, Ampicillin resistance	Iba (Göttingen, DE)
pPRk	based on pPR-IBA backbone, Ampicillin switched to Kanamycin resistance, Lactose induced T7 transcription, MCS	cloned by Tobias Kruse
pGEM-T	T7 and SP6 promotors flanking MCS and a-peptide coding region of b-galactosidase (blue-white screening), Ampicillin resistant, linearized, T-overhangs for easy PCR cloning	Promega (Madison, US)
pPRk Δ1-26 oHPGh	sequence optimized *H. pylori* GT with C-terminally His$_6$ under lactose induced T7 transcription	cloned by Tobias Kruse
pET30b h-Δ1-20 Sa SrtA	lactose induced T7 transcription; gene product: N-terminally His$_6$-tagged *S. aureus* SrtA Δ1-20	this work
pPRk Δ1-23 Sa SrtB-h	lactose induced T7 transcription; gene product: C-terminally His$_6$-tagged *S. aureus* SrtB Δ1-23	this work
pPRk Δ1-30 Ef SrtA-h	lactose induced T7 transcription; gene product: C-terminally His$_6$-tagged *E. faecalis* SrtA Δ1-30	this work

pET30b Δ1-20 HP2-h	lactose induced T7 transcription; gene product: C-terminally His$_6$-tagged *H. pylori* HP2 Δ1-20	this work
pET30b Δ1-43 HP3-h	lactose induced T7 transcription; gene product: C-terminally His$_6$-tagged *H. pylori* HP3 Δ1-43	this work
pET30b Δ1-33 HP4-h	lactose induced T7 transcription; gene product: C-terminally His$_6$-tagged *H. pylori* HP4 Δ1-33	this work
pET30b Δ1-22 HP5-h	lactose induced T7 transcription; gene product: C-terminally His$_6$-tagged *H. pylori* HP5 Δ1-22	this work
pET30b HP6-h	lactose induced T7 transcription; gene product: C-terminally His$_6$-tagged *H. pylori* HP6	this work
pET30b HP8-h	lactose induced T7 transcription; gene product: C-terminally His$_6$-tagged *H. pylori* HP8	this work
pSCask Δ1-31 HP1-h	lactose induced T7 transcription; gene product: C-terminally His$_6$-tagged *H. pylori* HP1 Δ1-31	this work
pSCask Δ1-20 HP2-h	lactose induced T7 transcription; gene product: C-terminally His$_6$-tagged *H. pylori* HP2 Δ1-20	this work
pSCask Δ1-31 HP7-h	lactose induced T7 transcription; gene product: C-terminally His$_6$-tagged *H. pylori* HP7 Δ1-31	this work
pSCask HP8-h	lactose induced T7 transcription; gene product: C-terminally His$_6$-tagged *H. pylori* HP8	this work
pGEM-T ko HP1-3	for knock-out of the gene hp1 from *H. pylori* G27; Kanamycin cassette with gene flanking regions	this work
pGEM-T ko HP5-6	for knock-out of the gene hp5 from *H. pylori* G27; Kanamycin cassette with gene flanking regions	this work
pGEM-T ko HP6-2	for knock-out of the gene hp6 from *H. pylori* G27; Kanamycin cassette with gene flanking regions	this work

| pGEM-T ko HP7-2 | for knock-out of the gene hp7 from *H. pylori* G27; Kanamycin cassette with gene flanking regions | this work |

Table 4: Plasmids used or created in this work

5.1.8 Substrates and reference compounds

HPG-assay

L-γ-glutamyl-*p*-Nitroanilide	Sigma-Aldrich (Steinheim, DE)
Diglycine (D-Gly-D-Gly)	Sigma-Aldrich (Steinheim, DE)
D-γ-glutamyl-*p*-Nitroanilide	Bachem (Bubendorf, CH)
Acivicin	Sigma-Aldrich (Steinheim, DE)

Sortase A assay

Dabcyl-LPETG-Glu(EDANS)	Biomatik (Cambridge, CA)
	Caslo Lab (Lyngby, DK)
H-K(Dabcyl)VENPQTNAGTE(EDANS)-OH	AnaSpec (Fremont, US)
Pentaglycine (L-Gly$_5$)	Sigma-Aldrich (Steinheim, DE)
Dialanine (L-Ala-L-Ala)	Sigma-Aldrich (Steinheim, DE)
DMMA	kindly provided by Priaxon AG (München, DE)
(Z)-3-(2,5-dimethoxyphenyl)-2-(4-methoxyphenyl) acrylonitrile	
Rhodanine-1	ChemBridge
5-(3-bromo-2-hydroxy-5-nitrobenzylidene)-3-(2,4-dimethylphenyl)-	
2-thioxo-1,3-thiazolidin-4-one	
compound 2-17[174]	kindly provided by Prof. Clubb (UCLA)

5.1.9 DNA and Protein Standards

DNA-Standards

| 1kB DNA ladder | Promega (Madison, US) |
| 100bp DNA ladder | Promega (Madison, US) |

Protein Standards

peqGOLD Protein Marker IV	Peqlab (Erlangen DE)
peqGOLD Protein Marker V	Peqlab (Erlangen DE)
Precision Plus Protein™ Dual Color Standard	Bio-Rad (Hercules, US)

5.1.10 Instruments

Balances

Analytic scale	Kern & Sohn GmbH (Balingen, DE)
Precision scale	Kern & Sohn GmbH (Balingen, DE)

Centrifuges

Heraeus™ Biofuge™ Primo Centrifuge	Thermo Scientific (Waltham, US)
Heraeus™ Biofuge™ Primo R Zentrifuge	Thermo Scientific (Waltham, US)
Heraeus™ Megafuge™ 40R	Thermo Scientific (Waltham, US)
Sorvall™ RC 6+	Thermo Scientific (Waltham, US)
Tabletop centrifuge 5415D	Eppendorf (Hamburg, DE)

PCR-machines

Biometra T3000 Thermocycler	Analytik Jena (Überlingen, DE)

Electrophoresis equipment

Horizontal electrophoresis system	Bio-Rad (Hercules, US)
Novex® 4-20 % Tris-Glycine Mini Protein Gels	Life Technologies (Carlsbad, US)
Novex® Empty Gel Cassettes, mini, 1.0 mm	Life Technologies (Carlsbad, US)
PowerPac™ HC	Bio-Rad (Hercules, US)
Trans Blot® SD semi-dry transfer cell	Bio-Rad (Hercules, US)
XCell SureLock™ Mini-Cell Electrophoresis System	Life Technologies (Carlsbad, US)

Gel documentation

ChemoCam ECL Imager	Intas (Göttingen, DE)
Eagle Eye Gel Doc™	Bio-Rad (Hercules, US)
XcitaBlue™ Conversion Screen and Filter	Bio-Rad (Hercules, US)

Liquid chromatography

ÄKTA™ avant 25	GE Healthcare (Chalfont St. Giles, UK)
ÄKTA™ purifier	GE Healthcare (Chalfont St. Giles, UK)
HiLoad 16/600 Superdex 200 PG	GE Healthcare (Chalfont St. Giles, UK)
HiLoad 16/600 Superdex 75 PG	GE Healthcare (Chalfont St. Giles, UK)
HisTrap FF crude 1 mL	GE Healthcare (Chalfont St. Giles, UK)
HisTrap FF crude 5 mL	GE Healthcare (Chalfont St. Giles, UK)
MabSelect SuRe™ 1 mL	GE Healthcare (Chalfont St. Giles, UK)
Resource™ Q 1 mL	GE Healthcare (Chalfont St. Giles, UK)

Incubators

Celltron	Infors AG (Bottmingen, CH)
Forma™ Series II Water Jacket CO_2 Incubator	Thermo Scientific (Waltham, US)
Multitron Pro	Infors AG (Bottmingen, CH)

Spectrometers

Biophotometer	Eppendorf (Hamburg, DE)
Mithras LB 940 multimode microplate reader	Berthold Technologies (Bad Wildbad, DE)
NanoDrop 1000	Thermo Scientific (Waltham, US)
Sunrise™ microplate reader	Tecan (Männedorf, CH)

Additional equipment

CyAn™ ADP Analyzer	Beckman Coulter (Brea, US)
HERA freezer basic	Thermo Scientific (Waltham, US)
Ice flaker AF206	Scotsman (Ipswich, UK)
IKA® RH basic 2 magnetic stirrer	IKA (Staufen, DE)
inoLab® pH 720 pH-meter	WTW (Weilheim, DE)
Lambda® plus 8-channel pipette 50-300 µL	Corning (Kaiserslautern, DE)
Lambda® plus Single channel pipette 0.25-2µL	Corning (Kaiserslautern, DE)
Lambda® plus Single channel pipette 0.5-10µL	Corning (Kaiserslautern, DE)
Lambda® plus Single channel pipette 10-100µL	Corning (Kaiserslautern, DE)
Lambda® plus Single channel pipette 200-1000µL	Corning (Kaiserslautern, DE)
Lambda® plus Single channel pipette 20-200µL	Corning (Kaiserslautern, DE)
Lambda® plus Single channel pipette 2-20µL	Corning (Kaiserslautern, DE)
LSE™ Vortex Mixer	Corning (Kaiserslautern, DE)
Multipette® plus	Eppendorf (Hamburg, DE)
Multipette® Xstream	Eppendorf (Hamburg, DE)
Nalgene® Polysulfone Reusable Bottle Top Filter	Thermo Scientific (Waltham, US)
Thermomixer compact	Eppendorf (Hamburg, DE)
Tissue Grinder 7 mL	Wheaton (Millville, US)
Water bath WNB7	Mennert (Schwabach, DE)
Xplorer 8-channel pipette 15-300 µL	Eppendorf (Hamburg, DE)

5.1.11 Consumables

Assayplates and Lids	Kuhnle GmbH (Karlsruhe, DE)
Costar® black 96-well plates	Corning (Kaiserslautern, DE)
Falcon® 96-well tissue culture plate	BD (Heidelberg, DE)
Falcon® 14 mL sterile round bottom test tube	BD (Heidelberg, DE)
Test tube 1.5 mL	Zefa (Grasbrunn, DE)
Test tube 1.5 mL Safelock	Eppendorf (Hamburg, DE)
Test tube 2 mL Safelock	Eppendorf (Hamburg, DE)
Test tube 5 mL	Eppendorf (Hamburg, DE)
PCR-tube strips	Kisker (Steinfurt, DE)
Test tube 15 mL, conical	Greiner (Kremsmünster, AT)
Test tube 50 mL, conical	Greiner (Kremsmünster, AT)
Tips (1000 μL, 200 μL, 20 μL, 10 μL)	Zefa (Grasbrunn, DE)
TipOne Filter Tips (1000 μL, 200 μL, 20 μL, 10 μL)	Star Lab (Hamburg, DE)
Cryo-vials 1mL	Alpha laboratories (Eastleigh, UK)
Gas-chromatography vials, brown, 1.5 mL	Chromatographie Handel Müller (Fridolfing, DE)
Extra thick blot paper	Bio-Rad (Hercules, US)
Immobilon-P^{SQ} PVDF blotting membrane, 0.45 μm	Merck Millipore (Billerica, US)
Express Plus® membrane 0.22 μm	Merck Millipore (Billerica, US)
Express Plus® membrane 0.45 μm	Merck Millipore (Billerica, US)
Sample bags	Roth (Karlsruhe, DE)

5.1.12 Computer Software and Bioinformatic Tools

CLC Workbench	CLC BIO (Aarhus, DK)
GraphPad Prism	GraphPad Software (La Jolla, US)
ChemBioDraw Ultra 14.0	Perkin Elmer (Cambridge, US)
EndNote X6	Adept Scientific (Frankfurt, DE)
Microsoft Office	Microsoft (Redmond, US)
Unicorn™	GE Healthcare (Chalfont St. Giles, UK)
MicroWin	Berthold Technologies (Bad Wildbad, DE)
NanoDrop 1000 3.8.1	Thermo Scientific (Waltham, US)
Magellan	Tecan (Männedorf, CH)
http://tmcalculator.neb.com/#!/	New England Biolabs (Ipswich, US)
http://www.jcat.de/	Andreas Grote (TU Braunschweig, DE)
Adobe Illustrator CS3	Adobe Systems (San José, US)

5.2 Genetic Methods

5.2.1 Cultivation and Storage of *Escherichia coli*

E. coli was cultivated either on LB agar plates or in liquid LB or TB medium with suitable selection antibiotic.

For plasmid isolation, preparation of glycerol-stocks, or as pre-culture, *E. coli* was cultivated in LB-medium with selective antibiotic at 37°C in a shaker at 180-250 rpm. Medium volumes ranged from 5-250 mL according to the purpose of cultivation. Inoculants were taken from streaks on agar plates, previously prepared liquid LB cultures or from glycerol-stocks.

Streaks of *E. coli* on LB agar plates were incubated either at 37°C over-night or at room temperature for 2-3 days. Plates were kept at 4°C for up to 3 weeks.

TB-Medium with suitable antibiotic was used for large scale cultivation in the context of recombinant protein production. An over-night pre-culture in LB medium was used to inoculate 0.2-8 L of TB-medium. Matching the expression vector used, auto-induction with lactose was chosen or recombinant expression was induced with 200 µg/L AHT at OD_{600}=2-4. In both cases the cultures were incubated at 37°C and 200-250 rpm until OD_{600}=2-4 was reached. After that, the temperature was set to 15-37°C and 200-250 rpm depending on the protein to be expressed. Recombinant expression was allowed for further 16-48h; OD_{600} ranged from 10-21. The cultures were harvested by centrifugation for 20 min at 4000×g and 4°C. Bacterial cell pellets were transferred to sample bags and frozen at −20°C.

Glycerol-stocks served for long-term storage of *E. coli*. 1 mL of an over-night culture in LB medium (typically 5 mL) was pelletized for 5 min at 4000×g and resuspended in 0.5 mL LB medium without antibiotic. The cell suspension was mixed with 0.5 mL sterile glycerol in a cryo-tube and stored at −80°C.

5.2.2 Cultivation and Storage of *Helicobacter pylori*

Aliquots of *H. pylori* were prepared in BHI$_{dent}$ +20 % (v/v) FCS +20 % (v/v) glycerol and stored at −80°C.

The *H. pylori* wild type strains J99 and G27 were cultivated on WC$_{dent}$ agar plates for propagation. An aliquot was thawed swiftly, spread onto a plate and incubated for two days at 37°C in microaerophilic conditions and 10 % CO_2 for primary inoculation. After that, bacteria were transferred onto fresh WC$_{dent}$ agar in a dilution of 1:5 and incubated for another day to increase their vitality. Bacteria were scraped off the plates, washed in 1×PBS and resuspended in either BHI$_{dent}$ +20 % (v/v) FCS or 1×PBS for experiments. Cell concentrations were calculated from measured OD_{600} values with OD_{600}=1 corresponding to $2×10^8$ cells/mL.

For knock out strains the procedure was identical except for using WC$_{dent+Kan}$ plates at all steps.

To analyze *in vitro* growth of *H. pylori*, liquid culture was used. To this end, Brucella medium and DMEM+F12 (1:1) were supplemented with 10 % (v/v) FCS. In Brucella-medium, dent was used for selection whereas 10 mg/L Vancomycin were chosen for DMEM+F12. *H. pylori* was prepared according to the standard procedure described as above and used to inoculate the medium to a OD_{600} of 0.2. The experiments were performed in 5 mL culture volume in round bottom test tubes at 37 °C in microaerophilic conditions and 150 rpm.

5.2.3 Polymerase Chain Reaction

The Polymerase chain reaction (PCR)[320] was used in several settings to either amplify a gene or part of interest from genomic DNA or plasmids, linearize and amplify plasmids or ligate and amplify several DNA fragments.

Annealing temperature of the primers used was determined either in the CLC Workbench software or, for Q5® High-Fidelity DNA Polymerase, with the online tool http://tmcalculator.neb.com/#!/.

For amplifying target genes or linearizing and amplifying plasmid backbones, the PCR mixes and temperature cycles given in Table 5 and Table 6 were used. Annealing times were adjusted according to calculated temperatures. The elongation temperature for the USB® FideliTaq™ DNA Polymerase was 68°C and elongation time was adjusted to 1 min per 1 kB expected product length. Herculase II Fusion DNA Polymerase and Q5® High-Fidelity DNA Polymerase were used at 72°C and 30 sec per 1 kB expected product length.

Compound	Stock concentration	USB® FideliTaq™ DNA Polymerase	Herculase II Fusion DNA Polymerase	Q5® High-Fidelity DNA Polymerase
Template DNA	0.1-20 ng/µL	1-2 µL	1-2 µL	1-2 µL
Forward primer	10 µM	1.25 µL	1.25 µL	2.5 µL
Reverse Primer	10 µM	1.25 µL	1.25 µL	2.5 µL
Polymerase-Master Mix	2×	25 µL	25 µL	25 µL
ddH₂O		to 50 µL	to 50 µL	to 50 µL

Table 5: Components of a PCR reaction for target gene or linearized plasmid amplification

PCR step	Temperature	Time	
Initial Denaturation	95°C	2 min	
Denaturation	95°C	20 sec	
Annealing	variable	20 sec	35 cycles
Elongation	68/72°C	variable	
Final elongation	68/72°C	3-8 min	
Cooling	12°C	∞	

Table 6: Temperature profile for PCR amplification of target genes or linearized plasmids

Another setting for using PCR amplification was screening bacterial colonies after transformation with vectors. In this case primers specific for the backbone and/or for an insert were chosen to analyze product occurrence and product size. As PCR products were only produced for analysis, the GoTaq® Green Master Mix or the GoTaq® G2 Green Master Mix were used. These mixes already contain loading dye for agarose gel electrophoresis.

Usually 5-20 clones of a specific transformation were individually resuspended in 50 µL. The screening-master mix containing Polymerase Master Mix, primers and ddH$_2$O. The content of a single reaction is given in Table 7. The temperature program was standardized as given in Table 8.

Compound	Stock concentration	Volume
Resuspended bacterial colony	1 colony / 50 µL	2.5 µL
Forward primer	10 µM	0.5 µL
Reverse Primer	10 µM	0.5 µL
Polymerase-Master Mix	2×	7.5 µL
ddH$_2$O		4µL

Table 7: Components of a PCR reaction for bacterial colony screening

PCR step	Temperature	Time	
Initial denaturation	95°C	2 min	
Denaturation	95°C	20 sec	
Annealing	55°C	20 sec	35 cycles
Elongation	72°C	1 min	
Final elongation	72°C	8 min	
Cooling	12°C	∞	

Table 8: Temperature profile for PCR screening of bacterial colonies

A special set up was used to ligate DNA fragments with overlapping priming ends in a PCR reaction. In this case no primers were added, but equal amounts of each fragment were used to ensure low grade priming. Either Q5® High-Fidelity DNA Polymerase or, if 3'-T-extensions were needed, USB®

FideliTaq™ DNA Polymerase was used. The setup of a reaction is given in Table 9. The temperature program was according to Table 5, but 40 cycles were used for higher product yields.

Compound	Stock concentration	Volume
DNA fragment 1	100 ng/µL	1 µL
DNA fragment 2	100 ng/µL	1 µL
DNA fragment 2	100 ng/µL	1 µL
Polymerase-Master Mix	2×	25 µL
ddH$_2$O		to 50µL

Table 9: Components of a PCR driven ligation of DNA fragments

5.2.4 Agarose gel electrophoresis

Agarose gel electrophoresis was used for analysis or isolation of DNA. Depending on the expected sizes in a DNA sample, 0.8 % (w/v) (for large DNA fragments >5 kb, plasmids), 1 % (w/v) (for a wider range of DNA lengths to be analyzed) or 2 % (w/v) (for separation of short DNA fragments < 1 kB like PCR products) of agarose gels in 1×TAE were used. Roti®-Safe GelStain was added to the gels in a final concentration of 0.005 % (v/v) before casting them. Samples were prepared with DNA loading dye in a final concentration of 1× and loaded into suitably sized gel pockets. Electrophoresis was carried out in 1×TAE buffer for 40-60 min at 110 V. Bands were detected under at 365 nm.

5.2.5 Isolation of genomic DNA

Genomic DNA from bacteria was isolated with the DNeasy Blood & Tissue Kit according to the instruction manual for gram$^+$ or gram$^-$ bacteria. Isolated genomic DNA was stored at −20°C.

5.2.6 Isolation of plasmid DNA

Plasmid DNA was isolated from *E. coli* according to the instruction manual of the Pure Yield™ Plasmid Miniprep System or the Pure Yield™ Plasmid Midiprep System. Isolated plasmids were stored at −20°C.

5.2.7 Purification of DNA

DNA was purified from agarose gel slices, after PCR or other enzymatic transformations to exclude any interfering substances from further experiments. For this purpose the Wizard® SV Gel and PCR Clean-Up System was used according to the manufacturer's instructions. Purified DNA was stored at −20°C.

5.2.8 Determination of DNA concentration

DNA concentrations were determined spectrometrically at 260 nm using the NanoDrop and the software NanoDrop 1000 3.8.1. To assess DNA purity the ration of A_{260}/A_{280} was determined. For optimal results the ratio had to be 1.7 to 1.9, but larger variation was accepted for very low DNA concentrations.

5.2.9 Restriction digest of DNA

DNA was digested with restriction enzymes to prepare fragments for ligation or to analyze restriction patterns. The reaction mixture was assembled according to the instruction manuals of the enzymes in use. Reaction volumes varied from 10-100 µL depending on the purpose of the restriction digest. An overview is given in Table 10. The analytical digests were incubated at 37°C for 1-2 h. Inactivation of restriction enzymes was necessary if immediate processing of the product was not possible or not planned as often in the case of DpnI. Inactivation was performed according to the appropriate manual.

Compound	Final concentration	Typical Volume
DNA	100-2000 ng / reaction	variable
Buffer (10x)	1×	1-5 µL
Enzyme 1 (20 U/µL)	5-40 U / reaction	0.5-2 µL
(Enzyme 2)	(5-40 U / reaction)	0.5-2 µL
ddH$_2$O		to 10-100µL

Table 10: Scheme for restriction digests

5.2.10 Ligation of DNA fragments

Restriction digested and purified DNA fragments were joined with T4 DNA Ligase. The molar ratio of insert:vector was varied from 5:1 - 1:3. The amounts needed per DNA fragment were calculated with Formula 1. In general 100 ng of vector DNA were used per reaction. The reaction was assembled according to the instruction manual as given in Table 11. Afterwards, the reaction was incubated at room temperature for 3h or at 4°C over-night. A vector religation control was run for each experiment. Ligation products were directly transformed into *E. coli* or stored at −20°C.

$$\frac{\text{ng of vector} \times \text{kb size of insert}}{\text{kb size of vector}} \times \text{molar ratio of } \frac{\text{insert}}{\text{vector}} = \text{ng of insert}$$

Formula 1: Calculation of DNA fragment amounts for ligation reactions

Compound	Final concentration
Vector DNA	100 ng / reaction
Insert DNA	variable
T4 DNA Ligase Buffer (5x)	1×
T4 DNA Ligase	0.1-1 U
ddH$_2$O	to 10 µL

Table 11: Components of the T4-Ligase reaction

5.2.11 SLiCE-reaction of DNA fragments

DNA fragments were prepared with 35 bp homology arms for the SLiCE (seamless ligation cloning extract)-reaction[313] by PCR amplification with suitable primers. Vector backbones were linearized by restriction digestion to generate the envisioned homology arms. PCR-products were digested with DpnI to get rid of template plasmids if needed and purified with the Wizard® SV Gel and PCR Clean-Up System. The digestion product was subjected to agarose gel electrophoresis and the respective band was punched out to be cleaned up with the Wizard® SV Gel and PCR Clean-Up System.
The SLiCE-reaction exploits the recombination activity described for a lysate of the *E. coli* strain PPY. The lysate was prepared in CellLytic™ B Cell Lysis Reagent according to literature.[313]
The SLiCE-reaction mixture was set up according to Table 12 in the indicated order. A 1-10 fold molar excess of insert fragments for 100 ng of vector backbone was calculated with Formula 1. A reaction without added insert was set up to control for religation of the vector backbone. The reaction mixtures were incubated for 30-60 min at 37°C. SLiCE-reaction products were directly transformed into *E. coli* DH10B or stored at −20°C.

Compound	Final concentration
Vector DNA	100 ng / reaction
Insert DNA	variable
ddH$_2$O	to 10 µL
10× SLiCE Buffer	1×
PPY SLiCE extract	1 µL / reaction

Table 12: Components of the SLiCE reaction

5.2.12 Gibson assembly of DNA fragments

DNA fragments were prepared with 30 bp homology arms to be joined in the assembly reaction. Vector backbones were linearized and amplified with Primers generating blunt ended homology arms. Those were introduced to insert DNA fragments via PCR-primers during amplification. PCR products could be used without purification if DNA concentrations exceeded 300 ng/µL. In any case, DpnI restriction was conducted with the PCR-amplified vector backbone to eliminate any template

contamination. A 2-3 fold molar excess of insert fragments for 100 ng of vector backbone was calculated with Formula 1.

The DNA fragments were mixed and adjusted to 10 µL with ddH$_2$O on ice. 2.5 µL of this mixture was added to 2.5 µL Gibson Assembly® Master Mix (2×) in a PCR tube. The reaction was incubated in a thermocycler at 50°C for 15-30 min. The product was directly transformed into *E. coli* or stored at −20°C. The DpnI-digested, linearized vector backbone served as a control.

5.2.13 Sequencing of DNA

All produced plasmids, PCR-products for direct transformation and genomic mutants were verified by Sanger-sequencing[321]. For this purpose 750-1000 ng of the DNA product in 15 µL ddH$_2$O were sent to Eurofins MWG Operon (Ebersberg, DE). Standard sequencing primers were provided by the company or 3 µL of a specific primer (10µM) was added to the DNA product before shipping. Sequencing results were analyzed by alignment with the expected sequences in CLC Workbench.

5.2.14 Preparation of chemically competent *Escherichia coli*

TSS-Method[322]

Two 1 L flasks with 250 mL LB$_0$-medium were inoculated with an over-night culture of the *E. coli* strain of choice for a starting OD$_{600}$ of 0.1. A control culture without inoculation was also prepared to test for contaminations. The bacterial culture was grown at 37°C and 200 rpm until OD$_{600}$=0.4-0.5 was reached. The culture was cooled in an ice bath for 10 min before the bacteria were harvested in pre-chilled 50 mL tubes for 10 min at 2500×g and 4°C. The supernatant was removed completely and the pellets were resuspended in 50 mL of ice-cold TSS-Medium. The suspension was aliquoted into pre-chilled 1.5 mL tubes as needed and stored at −80°C after freezing in liquid N$_2$.

Inoue Method[323]

250 mL SOB-medium in a 2L flask were inoculated with an over-night culture of the *E. coli* strain of choice for a starting OD$_{600}$ of 0.1. A control culture without inoculation was also prepared to test for contaminations. The bacterial culture was grown at 37°C and 200 rpm until OD$_{600}$=0.50-0.55 was reached. The culture was cooled in an ice bath for 10 min before the bacteria were harvested in pre-chilled 50 mL tubes for 10 min at 2500×g and 4°C. The supernatant was removed completely and the pellets were resuspended by swirling in 80 mL ice-cold Inoue Buffer. The bacteria were harvested again under identical conditions and the supernatant was removed completely. The pellets were resuspended in 20 mL ice-cold Inoue Buffer by swirling. 1.5 mL DMSO was added and mixed in by swirling as well. The suspension was aliquoted into pre-chilled 1.5 mL tubes as needed and stored at −80°C after freezing in liquid N$_2$.

5.2.15 Transformation of chemically competent *Escherichia coli*

Chemically competent *E. coli* were thawed on ice and used as 50 µL aliquots in pre-chilled 1.5 mL tubes for each transformation. In case of ligation products, SLiCE reaction products or Gibson Assembly products 1µL and in case of retransforming verified plasmids 1 ng was added to the competent cells and mixed by snipping. The transformation setting was incubated as described in Table 13. Next, the cells were mixed with 950 µL SOC-Medium and incubated at 37°C and 850 rpm to recover. Finally 100 µL and 900 µL (pelletized at 4000×g for 5 min and resuspended in 100µL SOB medium) were streaked on LB agar plates with selective antibiotic.

Temperature	Time
on ice	10-30 min
42°C (water bath)	1 min
on ice	5 min

Table 13: Incubation scheme for transforming chemically competent *E. coli*

5.2.16 Natural transformation of *Helicobacter pylori*

H. pylori wild type cells were prepared as described in Chapter 5.2.2. The cells were scraped off one fully covered WC$_{dent}$ agar plate and resuspended in 1mL 1×PBS. The cells were harvested for 5 min at 4000×g at room temperature and resuspended in 100 µL BHI +20 % (v/v) FCS. 50 µL of the cell suspension was mixed with 1-10 µg of either PCR fragment or pGEM-T construct of the knock-out construct and then spotted onto WC$_{dent}$ agar plates (adapted from Noto, 2012[324]). The plates were incubated over-night at 37°C in microaerophilic conditions and 10 % CO_2. The cell spots were transferred to WC$_{dent+kan}$ agar plates and incubated until colonies could be identified.

5.3   Protein Chemistry and Analytical Methods

5.3.1   Recombinant production of Sortases

The Sortase A from *S. aureus* was produced as N-terminally His$_6$-tagged recombinant protein without the predicted signal sequence from pET30b h- Δ1-20 Sa SrtA. Sortase B from *S. aureus* and Sortase A from *E. faecalis* were recombinantly produced without the predicted signal sequences and with a C-terminal His$_6$-tag based on pPRk Δ 1-23 Sa SrtB-h and pPRk Δ1-30 Ef SrtA-h. The three vectors were designed to express the target proteins without any additional amino acids.

Clones of recombinant bacteria harboring one of the aforementioned vectors were screened for high expression levels to achieve adequate protein yields. To this end, 50-200 mL of an auto-induction expression culture was used. The recombinant proteins were expected to be soluble. Therefore, whole cell lysates were prepared in 1×SDS buffer and compared via SDS-PAGE.

The recombinant protein production from these constructs was performed with 1-2 L main culture (LB for SrtA from *S. aureus* with IPTG induction), which yielded 5-15 g of bacteria pellet. The pellets were resuspended in the tenfold volume of HisTrap Buffer A-SrtA. DNaseI (150 U/g bacterial pellet) and MgCl$_2$ (final concentration 5 mM) were added to facilitate cell disruption and exclude DNA from subsequent purification steps. 4-(2-Aminoethyl) benzenesulfonyl fluoride (AEBSF) was added in a final concentration of 1 mM to prevent host proteases from degrading the recombinant protein during the isolation process. The cell suspensions were passed through the high pressure homogenizer for three times at 800-1000 bar. Following this, the cell lysates were centrifuged for 20 min at 16000×g and 4°C to separate the soluble proteins from cell debris. The supernatants were filtered with 0.45 µM pore size. Subsequently, the purification was commenced with Ni-NTA affinity chromatography (HisTrap FF crude, 5 mL). The supernatants were loaded on the pre-equilibrated column and washed with 10 column volumes of HisTrap Buffer A-SrtA. The Sortases were eluted in a linear gradient from 0 M to 0.5 M imidazole (HisTrap Buffer B-SrtA). Collected fractions were analyzed on a SDS-gel for protein content. Selected fractions were pooled and dialyzed against FRET buffer. The isolated proteins were needed for enzymatic screening assays and if the purity was sufficient at this point, no further purification steps were run. If the purity was not satisfactory, the protein-sample was subjected to size-exclusion chromatography. 5-20 mg protein in 2-5 mL of FRET-Buffer were loaded on the column and eluted isocratically in the selected buffer. Afterwards, collected fractions were analyzed on SDS-gels for protein content and pooled and concentrated as needed for further use. All proteins were stored at −80°C after freezing in liquid N$_2$.

5.3.2 Recombinant production of the γ-glutamyl transpeptidases

Several recombinantly produced and subsequently purified proteins were already available in the laboratory and used for this work. In detail, the proteins yielded from pET30b_HpgGwt, pET30b_CjgGTwt and pET30b_EcgGTwt were produced and purified by Christian Bolz according tot the protocols described in his thesis[325].

Clones of recombinant bacteria harboring the vector pPRk_oHPGh were screened for high expression levels to achieve adequate yields in the production of this construct of the *H. pylori* γ-glutamyl transpeptidases. To this end, 50-200 mL of an auto-induction expression culture were used. The recombinant proteins were expected to be soluble. Therefore, whole cell lysates was prepared in 1×SDS buffer and compared via SDS-PAGE.

The recombinant production of the oHPGh from of this construct was realized with 1 L of bacterial culture, which yielded 18 g of protein pellet. All steps for cell disruption and protein purification were conducted at 4°C or on ice. The pellet was resuspended in 180 mL of HisTrap Buffer A-HPG. DNaseI (150 U/g bacterial pellet) and $MgCl_2$ (final concentration 5 mM) were added to facilitate cell disruption and exclude DNA from subsequent purification steps. 4-(2-Aminoethyl) benzenesulfonyl fluoride (AEBSF) was added in a final concentration of 1 mM to prevent host proteases from degrading the recombinant protein during the isolation process. The cell suspension was passed through the high pressure homogenizer for three times at 800-1000 bar. Subsequently, the cell lysate was centrifuged for 20 min at 16000×g and 4°C to separate the soluble proteins from cell debris. The supernatant was filtered with 0.45 µM pore size. The purification was commenced with Ni-NTA affinity chromatography (HisTrap FF crude, 5 mL). The supernatant was loaded on the pre-equilibrated column and washed with 10 column volumes of HisTrap Buffer A-HPG. The oHPGh was eluted with a linear gradient from 0 M to 0.5 M imidazole (HisTrap Buffer B-HPG) in 10 column volumes. Collected fractions were analyzed on a SDS-gel for protein content. Suitable fractions were pooled and dialyzed to either 1×PBS or Crystallization Buffer. Finally, the protein was polished via size exclusion chromatography (HiLoad 16/600 Superdex 200 PG). 10-20 mg of the protein in 2-5 mL buffer were loaded on the column and eluted isocratically in the selected buffer. The collected fractions were analyzed on a SDS-gel for protein content and purity, pooled and concentrated as needed for further use. The protein was stored at −80°C after freezing in liquid N_2 or directly used for crystallization.

5.3.3 Purification of human γ-glutamyl transpeptidase from HEP-G2 cells

The isolation and purification method was adapted from Selvaraj, 1985[326]. A pellet of HepG2 human hepatocellular carcinoma cells was kindly provided by Jeanny Probst. 2 g of the cells were resuspended in 8 mL ice-cold HsgGT Resuspension buffer and homogenized in the tissue grinder. The suspension was stirred for 2 h at 37°C afterwards cooled down rapidly on ice and centrifuged at 15000×g, 4°C for 30 min to pelletize membrane fragments. The pellet was resuspended in 8 mL HsgGT Extraction buffer with the tissue grinder and stirred for 1 h at 4°C. The suspension was again

pelletized as described above and the supernatant was dialyzed against 2 L of AIX Buffer A at 4°C for more than twelve hours.

The supernatant was loaded on the pre-equilibrated anion-exchange column (Resource Q, 1 mL) and washed with 10 column volumes of AIX Buffer A. Elution was realized with linear gradient from 0 M to 0.5 M NaCl (AIX Buffer B). Collected fractions were tested for gGT content with the gGT transpeptidation assay (5.4.1) and positive fractions were combined for further processing. In the next step papain was used to cleave the membrane anchor off the human gGT and thereby improving its solubility. For that, papain and L-cysteine were added to final concentrations of 0.4 mg/mL and 0.8 mg/mL, respectively, and the reaction was incubated at 37°C for 4 h. After that, the target protein was further purified via ammonium sulfate precipitation. 25 %, 50 % and 75 % of the precipitant was added and samples of supernatant and precipitate were analyzed in the gGT transpeptidation assay. The pellets at 50 % and 75 % ammonium sulfate contained most of the active protein. They were solubilized in SEC-buffer and loaded on the pre-equilibrated HiLoad Superdex75 for polishing. The protein was eluted isocratically in SEC-Buffer. Finally, the collected fractions were tested for gGT activity and pooled for further use. The protein was stored at −80°C after freezing in liquid N_2.

5.3.4 Protein A affinity chromatography of IgG from serum

For affinity purification of IgG from murine sera, the MabSelect SuRe™ 1 mL column was used. The serum samples were diluted in MabSelect Buffer A to a final volume of 10 mL and loaded onto the pre-equilibrated column. After washing with 10 CV MabSelect Buffer A, the antibodies were eluted with MabSelect Buffer B taking 1 mL fractions into 50 µL Elution Neutralization Buffer. The fractions were pooled according to the 280 nm absorbance chromatogram and dialyzed to 1×PBS. The sera were concentrated to approximately 2 mg/mL and stored at −20°C.

5.3.5 Recombinant production of *Helicobacter pylori* candidates

Genes of novel candidates were cloned into expression vectors for protein production and further analysis. Two approaches were chosen for this. The genes of the surface candidates were cloned without predicted signal sequences and terminal transmembrane regions, but no optimization concerning exclusion of predicted internal transmembrane regions was attempted. All genes were inserted into pET30b and pSCask for expression driven by the lac-operon or the tet-repressor system respectively.

Screening for clones with high protein expression was not conducted as many constructs were tested in parallel. The recombinant production of these constructs was realized with 0.2-1 L, which yielded 4-25 g of protein pellet. The pellets were resuspended in the tenfold volume of HisTrap Buffer A-HP-candidates. DNaseI (150 U/g bacterial pellet) and $MgCl_2$ (final concentration 5 mM) were added to facilitate cell disruption and exclude DNA from subsequent purification steps. 4-(2-Aminoethyl)benzenesulfonyl fluoride (AEBSF) was added in a final concentration of 1 mM to prevent host

proteases from degrading the recombinant protein during the isolation process. The cell suspensions were passed through the high pressure homogenizer for three times at 800-1100 bar. Following this, the cell lysates were centrifuged for 20 min at 16000×g and 4°C to separate the soluble proteins from cell debris. The supernatants were filtered with 0.45 µM pore size. Subsequently, the purification was commenced with Ni-NTA affinity chromatography (HisTrap FF crude, 5 mL). The supernatants were loaded on the pre-equilibrated column and washed with 4 column volumes of HisTrap Buffer A-HP-candidates + 10 % (v/v) HisTrap Buffer B-HP-candidates. The proteins were eluted with 0.5 M imidazole (HisTrap Buffer B-HP-candidates). Collected fractions were analyzed on SDS-gels for protein content. Positive fractions were pooled and dialyzed against ArgPi-Buffer for subsequent size-exclusion chromatography. 5-20 mg of the proteins in 2-5 mL of ArgPi buffer were loaded on the column and eluted isocratically in the selected buffer. Afterwards, collected fractions were analyzed on SDS-gels for protein content and pooled and concentrated as needed for further use. The proteins were stored at −80°C after freezing in liquid N_2.

5.3.6   Determination of protein concentration

The concentration of protein samples was either determined by measuring their absorbance at 280 nm or, for more accurate results and for protein mixtures, in a bicinchoninic acid (BCA) assay[327].
The absorbance at 280 nm was measured in the NanoDrop spectrometer. The theoretical molecular weight and molar extinction coefficient of the distinct protein was calculated in CLC workbench and entered into the software NanoDrop 1000 3.8.1 to obtain the concentration in mg/mL.
Alternatively, a BCA assay was used to determine low protein concentrations or if protein mixtures were to be quantified. The assay was performed with the Pierce™ BCA Protein Assay Kit according to the manufacturer's instructions in a microtiter plate to save protein sample and BSA standard for calibration. The protein sample was measured in several adequate dilutions to calculate its concentration based on the simultaneously measured calibration curve.

5.3.7   SDS polyacrylamide gel electrophoresis

SDS-PAGE was performed according to Laemmli, 1970[328].
Protein samples were mixed with 4×SDS sample buffer to a final concentration of 1×.
Gels with 10-15 pockets were prepared according to Table 14. They were run in SDS-PAGE buffer at 170 V until the dye frontline reached the bottom of the gel. The gels were stained in Coomassie staining solution for 15 min and destained with Coomassie destaining solution.
Alternatively, precast gradient gels were used according to the manufacturer's instructions.

Compound	Separation Gel (12 %)	Stacking gel (4 %)
H_2O	21.3 mL	10.3 mL
Separating gel buffer	12.0 mL	
Stacking gel buffer		4.0 mL
Acrylamide 40 % (w/v)	14.4 mL	1.6 mL
APS 10 % (v/v)	240 µL	80 µL
TEMED 1 % (v/v)	48 µL	16 µL

Table 14: Pipetting scheme for 8 SDS-gels

5.3.8 Western Blotting

Two sheets of suitably sized Whatman paper were soaked in Semi-Dry blotting buffer and placed onto the blotting machine. A piece of PVDF-membrane with a pore size of 0.45 µm was activated in methanol, rinsed with water and equilibrated in Semi-Dry blotting buffer. It was placed onto the Whatman paper while avoiding any air bubbles in between. The SDS-gel with the protein samples was also equilibrated in Semi-Dry blotting buffer and placed onto the membrane bewaring air bubbles. Two more sheets of soaked Whatman paper were placed on top and the whole set up was pressed on. The blotting process was run for 110 min at 2 mA per cm^2 (90 mA for a standard mini gel) at room temperature.

The blotted membranes were treated with several solutions to achieve recognition of desired protein or detection of specific antibodies. All incubation steps were performed with agitation in 50 mL tubes with 5 mL of the solutions or in cups with 10 mL of the solution. Firstly, membranes were blocked in TBS-T +5 % (w/v) skimmed milk powder for 1 h, then rinsed with TBS-T four times for 10 min. 5-10 mL of the primary serum was applied in the desired dilution in either TBS-T +1 % (w/v) skimmed milk powder or TBS-T +5 % (w/v) bovine serum albumin and incubated at room temperature for 1 h or at 4°C over-night. Again, the membrane was rinsed four times in TBS-T for 10 min. Lastly, the membrane was incubated in a dilution of the secondary horse-radish peroxidase (HRP) linked antibody in TBS-T +1 % (w/v) skimmed milk powder or TBS-T +5 % (w/v) bovine serum albumin for 1 h at room temperature. Before the detection reagent was applied, the membranes were rinsed with TBS-T four times for 10 min

The detection reagent Pierce ECL Western Blotting Substrate contains a chemoluminescent substrate that can be oxidized by the HRP. The reaction leads to the release of photons, which can be recorded. The included detection reagents 1 and 2 were mixed 1:1 as stated in the manual; 1 mL was prepared per membrane and pipetted onto it. Making sure that the membrane is evenly coated, the reagent was incubated for 1 min at room temperature. Excess reagent was removed with a piece of Whatman paper. The membrane was placed between two sheets of foil to prevent it from drying out. The signal was detected on a photographic film or in a CCD-imager for various periods of time, depending on the signal strength.

The antibodies were stripped from the blot with Restore Plus Western Blot Stripping Buffer, if sequential detection with distinct sera was needed. The process described above could then be repeated with another antibody combination.

The blots were finally stained with Coomassie staining solution for 15 min and destained in Coomassie destaining solution with visual surveillance if no further antibody detection was needed. This enabled monitoring the blot quality and correlating of WB signals and Coomassie stained protein bands.

5.3.9   Enzyme-linked immunosorbent assay

The enzyme-linked immunosorbent assay (ELISA[329]) was performed to detect protein specific antibodies in human patient sera or sera from immunized mice. The setup of an indirect ELISA was chosen for this purpose.

A 96-well cell culture plate was coated with 50 µL of recombinant proteins as antigen at a concentration of 2 µg/mL in 1×PBS by means of incubation over-night at 4°C.

The coating solution was removed and the wells were washed three times with 200µL 1×PBS. Blocking was achieved by incubating 200 µL/well 1×PBS +5 % (w/v) BSA for 2 h at room temperature. The coating solution was removed and the wells were washed twice with 200 µL 1×PBS.

The mouse and control sera were suitably diluted in 1×PBS +5 % (w/v) BSA and 100 µL of these dilutions were incubated for 2 h at room temperature in the corresponding wells. The serum dilutions were removed and the plate was washed four times with 1×PBS.

The detection of binding antibodies was achieved with horse-radish peroxidase (HRP) conjugated anti-human or anti-mouse antibodies. To this end the antibodies were diluted in 1×PBS +5 % (w/v) BSA and 100 µL were added to the appropriate wells.

The bound HPR-conjugate was detected by addition of the substrate 3,3′,5,5′-Tetramethylbenzidine (TMB), which was prepared and used according to the instruction manual. The oxidization reaction yields a blue-coloured diimine-product. The reaction is stopped with sulfuric acid to prevent saturation of the signal. As a consequence, the reaction product turns yellow and can be quantified at 450 nm with background correction at 570 nm.

5.3.10 Luminex® analysis of patient sera

The Luminex® assay was used to assess the antibody-reaction of multiple patient sera to multiple antigens. This multiplex assay is based on beads that are internally dyed with a distinct ratio of a red and infrared fluorophore allowing a distinct identification of 100 bead identities. The bead types were coated with the recombinant proteins separately and then mixed allow multiplexed analysis of a single serum sample with several antigens for binding antibodies. To this end bead mixtures were incubated with first patient sera and second detection antibody. The beads are detected and

identified via their dye ratio and the detection antibody is conjugated to another fluorescent dye and can thus be quantified.

These experiments were kindly performed by Dr. Stefanie Rimmele and Dr. Nicole Schneiderhan-Marra from the group of Dr. Thomas Joos at the NMI (Tübingen) according to their standards.

5.3.11 Flow cytometry analysis

Flow cytometry analysis was used to verify surface exposure of undescribed *H. pylori* candidate proteins. The method was adapted from the workflow for the gram-positive bacterium *S. aureus* as published by Grandi and coworkers in 2006[311].

Helicobacter pylori J99 or G27 wild type or knock-out mutant cells were prepared as described in chapter 5.2.2, scraped off the agar-plate and resuspended in 15 mL 1×PBS per plate. The OD_{600} was determined and the bacteria were harvested for 5 min at 4000 rpm. The pellet was resuspended in 1×PBS to an OD_{600} of 20. The suspension was split into two aliquots and treated with carboxyfluorescein diacetate succinimidyl ester (CFDA-SE, stock: 10 mM in DMSO) at a final concentration of 6 μM and equal volume of DMSO as a control. The tubes were wrapped in aluminum foil from now on to protect the dye from light. To allow the dye to cross to the bacterial cytoplasm, the aliquots were incubated at 37°C and 60 rpm for 20 min. The bacteria were washed in 1×PBS by harvesting as indicated above and resuspending. Blocking of any inherent antibody binding capacity of the *H. pylori* surface was achieved by incubating the bacteria in the set volume of heat inactivated FCS for 15 min at 37°C and 60 rpm. The bacteria were washed with 1×PBS with 0.5 % (v/v) BSA and set to an OD_{600} of approximately 0.5. The OD_{600} was measured for both aliquots and the cell concentration was calculated with the ratio of $2×10^8$ cells/mL at OD_{600}=1. Thus, 10^7 bacteria were distributed on a 96well round-bottom cell culture plate.

To stain the bacteria with the purified mouse sera those were diluted as desired in 1×PBS with 0.5 % (v/v) BSA. The bacteria were spun down in the plate for 5 min at 400 rpm and the supernatant was discarded completely by shaking out. Then the pellets were resuspended in 100 μL of the diluted sera and incubated for 30 min on ice. Non-binding antibodies were removed by washing two times with 200 μL 1×PBS with 0.5 % (v/v) BSA. For detection of the specific antibodies binding to the *H. pylori* surface, a secondary fluorescently labeled antibody against mouse-IgG (anti-mouse IgG1 eFluor®660) was used in a dilution of 1:100. The cells were incubated in 100 μL of that dilution for 30 min on ice. After washing two times with 200 μL 1×PBS with 0.5 % (v/v) BSA the cells were resuspended and fixed in 100 μL 1×PBS with 1 % (w/v) PFA and transferred to FACS-microtubes.

Measurement was performed at the CyAn™ ADP Analyzer.

5.4 Enzymatic assays for screening and compound validation

5.4.1 Transpeptidation assay for Sortases

The transpeptidation assay for sortases is based on the cleavage of a fluorophore-quencher labeled peptide[141]. The two dyes EDANS and Dabcyl are used for this purpose. As long as they are connected by the short peptide and therefore close to each other, the energy, absorbed by EDANS, is transferred to Dabcyl by Fluorescence Resonance Energy Transfer (FRET) and converted to vibrational and thermal energy. Hence, the donor-fluorophore EDANS does not efficiently emit light when being excited with light near its absorbance maximum of 336 nm. In this assay format, the peptide is the recognition sequence of the sortases to be investigated. The recognition sequence for the SrtA from *S. aureus* and *E. faecalis* is **LPETG**, and the recognition sequence for SrtB from *S. aureus* is VE**NPQTN**AGT. Enzymatic cleavage occurs as LPET$^\vee$G and NPQT$^\vee$N. The fluorescence of EDANS increases after cleavage of the peptide. A scheme is depicted in Figure 13. After substrate cleavage, the N-terminal fragment of the peptide remains covalently bound to the sortase's nucleophilic cysteine. It has to be transferred to an acceptor-substrate to regenerate the active enzyme. This acceptor is Gly$_5$ for the sortases from *S. aureus* and di-L-alanine for SrtA from *E. faecalis*.
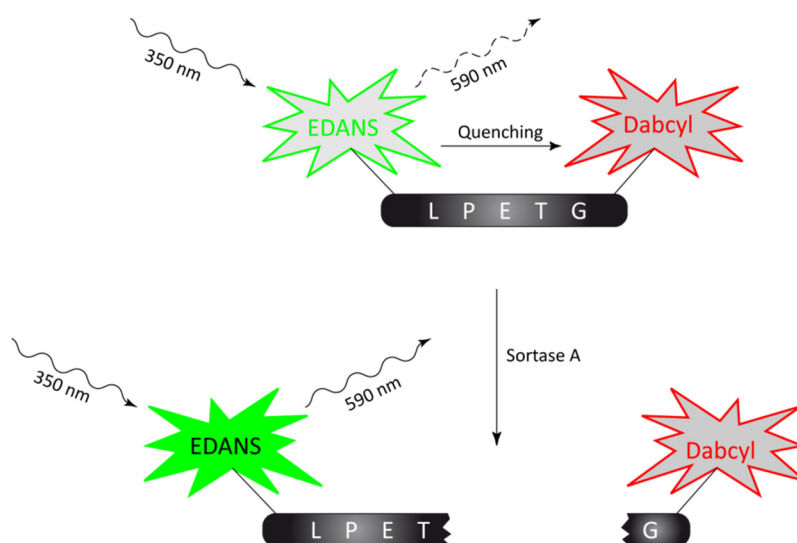
Figure 13: FRET-peptide cleavage for detection of Sortase A activity.

The peptide sequence LPETG is recognized by Sortase A and can be cleaved. Cleavage dislodges the quencher Dabcyl from the donor-flurophore EDANS and the emitted light can be detected

The conditions for SaSrtA activity assay were adapted from Surree, 2009[174]. In general, the assay was set up with 1 mM Gly$_5$, 100 µM Dabcyl-LPETG-(E)-EDANS and 2.5 µM SaSrtA. The substrates were prepared from 10 mM Dabcyl-LPETG-(E)-EDANS and 4 mM Gly$_5$ stock solutions in SrtA-Assay Buffer, which were stored at −20°C or at 4°C, respectively. Enzymes, prepared as described in 5.3.1, were diluted in SrtA-Assay Buffer. Table 15 depicts the composition of a single reaction with the standardized volumes and pipetting sequence. The reaction was run with a volume of 200 µL in 96-

well microtiter plates at 37°C in the plate reader for kinetic measurements or in the incubator, if only endpoint-fluorescence was to be recorded. The fluorescence was detected with an excitation-wavelength of 355 nm and an emission-wavelength of 590 nm.

Sortase B from *S. aureus* was used for specificity estimation of novel identified inhibitory compounds. The enzyme concentration was chosen to mimic the reaction of SaSrtA. To meet this prerequisite, 15 µM SaSrtB were used with its specific substrate.

Compound	Predilution	Volume	Final concentration
Gly$_5$ (4 mM)		50 µL	1 mM
SrtA-Assay Buffer		to 200 µL	
(Test compound (5-50 µM) / DMSO	variable	5-8 µL	variable)
SaSrtA	10 µM	50 µL	2.5 µM
Dabcyl-LPETG-(E)-EDANS (10 mM)	400 µM	50 µL	100 µM

Table 15: Pipetting scheme for the transpeptidation assay for sortases

The components of the reaction were set up in the given order from freshly prepared predilutions.

5.4.2 Transpeptidation assay for γ-glutamyl transpeptidases

This well established colorimetric assay relies on the donor-substrate LgGpNA for detecting transpeptidation activity of γ-glutamyl transpeptidases[264]. The amide-bond of the L-γ-glutamyl-moiety is attacked by the nucleophilic threonine of these enzymes and *p*-nitroanilide (pNA) is released. pNA can be quantified via its absorbance at 405 nm and its molar extinction coefficient of 8800 $M^{-1}cm^{-1}$. However, pNA can serve as acceptor for the L-γ-glutamyl moiety that remained covalently bound to the enzyme's threonine. The original donor-substrate LgGpNA is regenerated in this transpeptidation reaction. In case of the *H. pylori* enzyme, this transfer appears much more efficient than the hydrolysis reaction. Therefore, no absorbance increase could be measured. However, the first step of this reaction sequence can be monitored, if a more efficient acceptor-substrate is added. In this work, GlyGly is used for this purpose as it is a very efficient acceptor in the reaction with the gGT of *H. pylori*.[325] The reaction scheme is depicted in Figure 14.
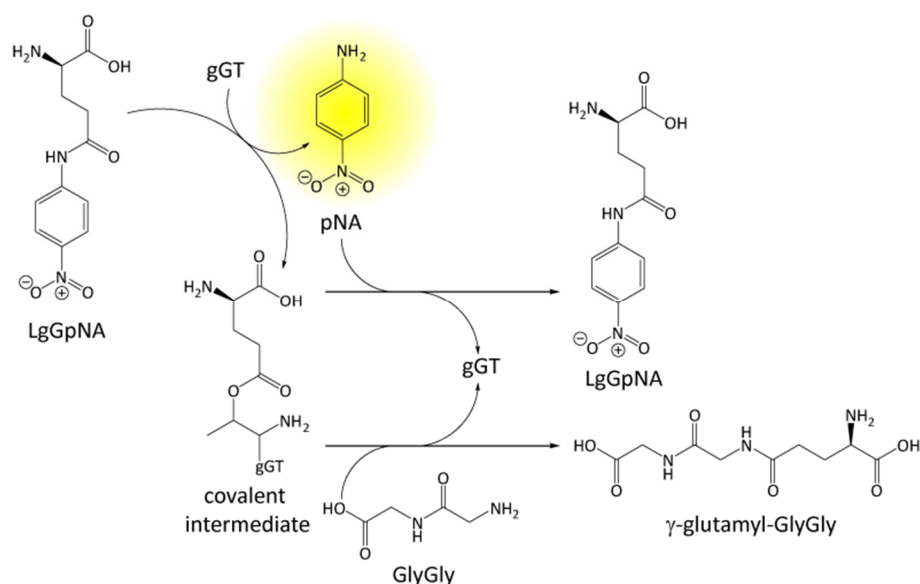
Figure 14: Transpeptidation assay with L-γ-glutamyl-*p*-nitroanilide for the detection of gGT activity

The γ-glutamyl moiety is removed from LgGpNA and pNA is released. If no efficient γ-glutamyl acceptor is present, LgGpNA is regenerated. To quantify the reaction, the acceptor-substrate GlyGly serves as acceptor and pNA can be measured at 405 nm.

Optimal pH and buffer system for this enzymatic reaction were already described for the gGT from *H. pylori*[325]. Other parameters, specifically the substrate and enzyme concentrations, were optimized for the envisioned screening assay in this work.

In general, the assay was set up with 20 mM GlyGly, 100 µM LgGpNA and 3 nM wtHPG or 500 pM oHPGh. The substrates were prepared from 5 mM LgGpNA and 100 mM GlyGly stock solutions in HPG-Assay Buffer, which were stored at −20°C or at 4°C respectively. Enzymes prepared as described in 5.3.2 were diluted in HPG-Assay Buffer. Table 16 depicts the composition of a single reaction with the standardized volumes and pipetting sequence. The reaction was run with a volume of 200 µL in 96-well microtiter plates at 37°C in the plate reader for kinetic measurements or in the incubator, if only endpoints were to be recorded. The absorbance of pNA was detected at 405 nm.

Compound	Predilution	Volume	Final concentration
Diglycine (100 mM)		40 µL	20 mM
HPG-Assay Buffer		to 200 µL	
(Test compound (50 µM) / DMSO	variable	8 µL	variable)
wtHPG / oHPGh	10-12 nM / 2 nM	50 µL	3 nM / 500 pM
L-γ-glutamyl-*p*-nitroanilide (5 mM)	400 µM	50 µL	100 µM

Table 16: Pipetting scheme for the transpeptidation assay for γ-glutamyl transpeptidases

The components of the reaction were set up in the given order from freshly prepared predilutions.

In compound screening approaches, reactions without enzyme addition were set up to measure the turbidity caused by the test compound to control for their solubility in the assay conditions.

The γ-glutamyl transpeptidases from other species were used for specificity estimation of novel identified inhibitory compounds. Their concentration was chosen to mimic the reaction of wtHPG /

oHPGh. Therefore, 8.0 nM CjgGT, 8.4 nM EcgGT and 0.075 µL/200 µL of HsgGT preparation were used.

5.4.3   Hydrolysis assay for γ-glutamyl transpeptidases

The hydrolysis-only assay for γ-glutamyl transpeptidases was used to distinguish between the transpeptidation activity (5.4.1) and the γ-glutamyl substrate cleavage as first step of the reaction[268]. Here, the donor-substrate is the stereo-isomer DgGpNA. As the D-γ-glutamyl moiety is not naturally occurring, it cannot be retransferred to *p*-nitroanilide. Therefore, hydrolysis of the covalent reaction intermediate is the only possibility to regenerate the enzyme. The reaction scheme is depicted in Figure 15.
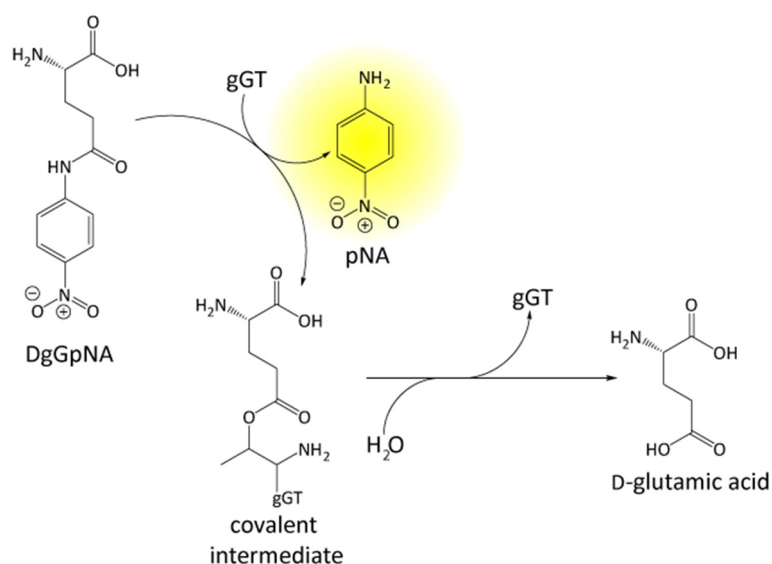
Figure 15: Hydrolysis assay for the detection of gGT activity

DgGpNA can be cleaved by gGT to release pNA. But the naturally not occurring D-γ-glutamyl moiety cannot be transferred back to regenerate the substrate. Only hydrolysis leads to regeneration of the active enzyme.

The reaction conditions were similar to the transpeptidation assay. In general, the assay was set up with 100 µM DgGpNA and 30 nM wtHPG. The substrate was prepared from 5 mM DgGpNA stock solution in HPG-Assay Buffer, which was stored at −20°C. Enzymes, prepared as described in 5.3.2, were diluted in HPG-Assay Buffer. The composition of a single reaction was achieved with the standardized volumes and pipetting sequence as given in Table 16, except for using D- instead of L-γ-glutamyl-*p*-nitroanilide, omitting GlyGly and using wtHPG in a final concentration of 30 nM. The reaction was run with a volume of 200 µL in 96-well microtiter plates at 37°C in the plate reader for kinetic measurements or in the incubator, if only endpoints were to be recorded. The absorbance of pNA was detected at 405 nm.

6 Results

6.1 *Staphylococcus aureus* Sortase A

6.1.1 Cloning and recombinant production of the Sortase constructs

The Sortase constructs used in this work were cloned without their predicted signal sequences, with His$_6$-tag for affinity purification, but without any other additional amino acids. Figure 16 depicts the expression vectors created for the Sortase project.
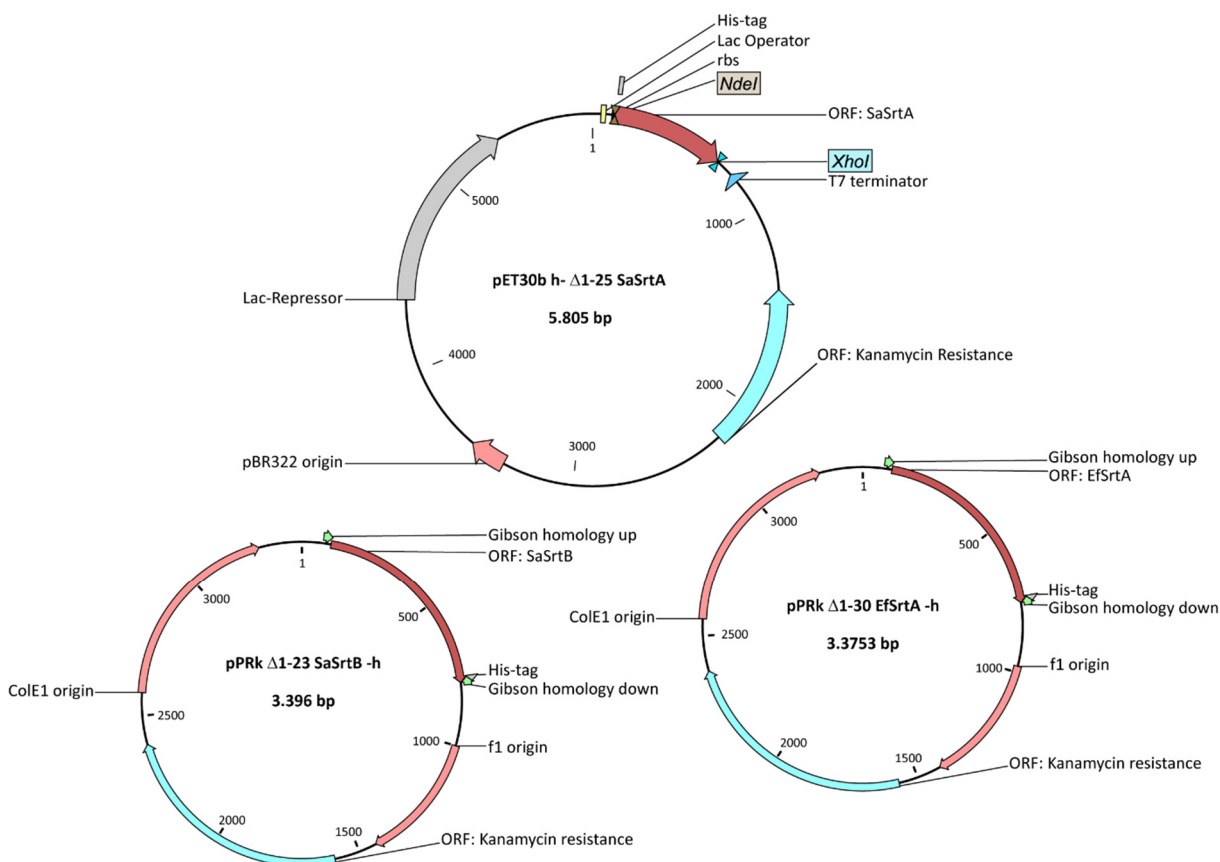
Figure 16: Plasmid maps for the Sortase constructs SaSrtA, SaSrtB and EfSrtA

The vectors for recombinant expression of SaSrtA, SaSrtB and EfSrtA are shown as plasmid maps indicating the open reading frames (ORFs) for the target proteins and the Kanymycin resistance. Features needed for cloning are indicated as restriction sites NdeI and XhoI for pET30b or homology arms for Gibson assembly in pPRk.

The Sortase A from *S. aureus* was cloned as construct SaSrtA. The gene sequence was PCR-amplified from genomic DNA (*S. aureus USA300*) with the primers CD_P1 and CD_P2 to enable seamless expression of the N-terminal His-tag and overhangs for restriction-ligation cloning into pET30b with the restriction sites NdeI and XhoI. PCR and classic cloning steps were realized according to the protocols given in chapters 5.2.3, 5.2.9 and 5.2.10.

Sortase B from *S. aureus* and Sortase A from *E. faecalis* were cloned as construct SaSrtB and EfSrtA, respectively. The genes were PCR-amplified from genomic DNA (*S. aureus* USA300 / *E. faecalis* ATCC 47077) with the primers CD_P91/92 and CD_P95/96 to generate seamless C-terminal His-tags and Gibson-homology overhangs for pPRk. PCR and Gibson cloning were performed as given in chapters 5.2.3 and 5.2.12.

The steps of protein production were performed as described in chapter 5.3.1. The recombinant proteins SaSrtA and SaSrtB from *S. aureus* had the desired purity already after HisTrap affinity chromatography. This can be assigned to the high expression level and the resulting overload of the affinity column.

SaSrtA was produced from 2 L expression culture (BL21 pET30b h- Δ1-25 SaSrtA). The chromatograms of the affinity purification and an SDS-PAGE of the final product are shown in Figure 17. The final yield was 70 mg.
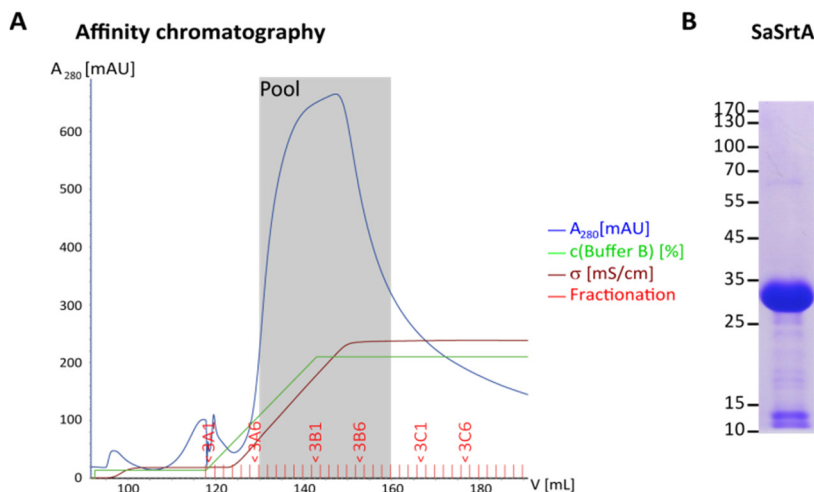
Figure 17: Purification of the construct SaSrtA

Graph **A** shows chromatograms recorded for the affinity-purification of a BL21 pET30b h- Δ1-25 SaSrtA lysate (HisTrap FF crude 5 mL). Fractions 3A7-3B9 were pooled and dialyzed to obtain the final product (5 μg) shown by the SDS-PAGE in **B**.

SaSrtB was purified from 0.8 L expression culture (BL21 pPRK Δ1-23 SaSrtB-h). Figure 18 depicts the chromatogram of the affinity purification and an SDS-PAGE of the final product. The final yield was 150 mg.
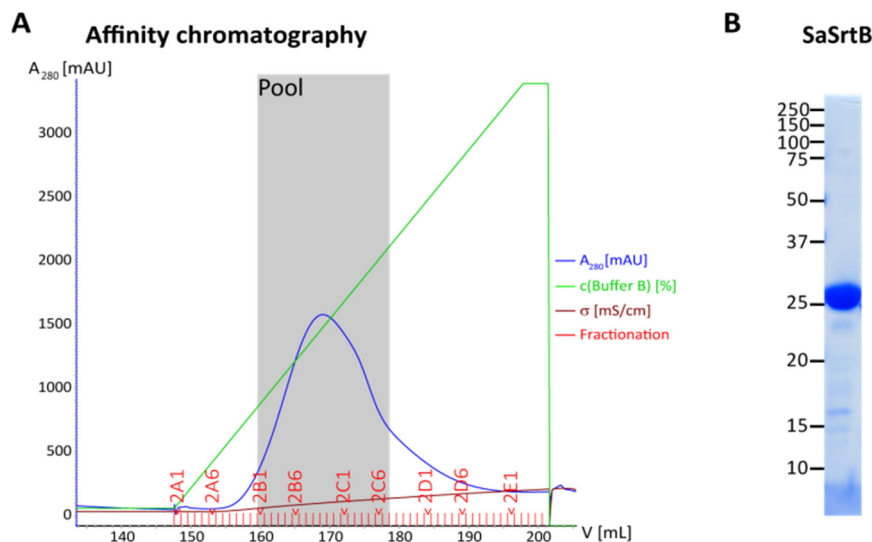
Figure 18: Purification of the construct SaSrtB

Graph **A** shows chromatograms recorded for the affinity-purification of a BL21 pPRK Δ1-23 SaSrtB-h lysate (HisTrap FF crude 5 mL). Fractions 2B1-2C7 were pooled and dialyzed to obtain the final product (5 μg) shown by the SDS-PAGE in **B**.

EfSrtA was purified from 0.8 L expression culture (BL21 pPRK Δ1-30 EfSrtA-h). The chromatograms illustrating the affinity purification and the size-exclusion chromatography as well as an SDS-PAGE of the final product are shown in Figure 19. It was not possible to obtain highly pure protein with the standard purification protocol. However, the recombinant EfSrtA should only be tested for transpeptidation activity and the purity was sufficient for this purpose. The final yield was 15 mg.
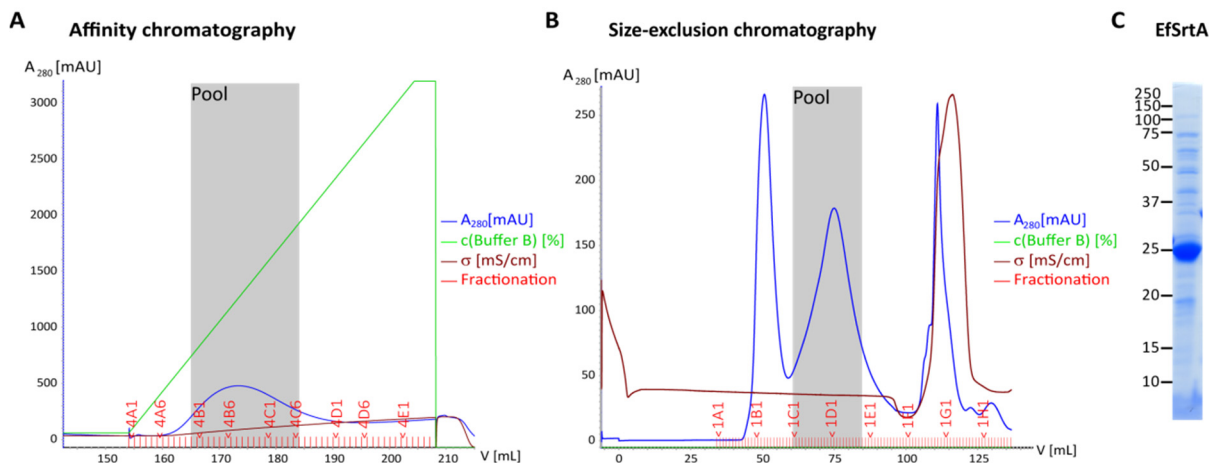
Figure 19: Purification of the construct EfSrtA

Graph **A** shows chromatograms recorded for the affinity-purification of a BL21 pPRK Δ1-23 SaSrtB-h lysate (HisTrap FF crude 5 mL) and graph **B** shows those for the subsequent size-exclusion chromatography (HiLoad 16/600 Superdex 200 PG) of the fractions 4A12-4C6 from the previous step. Fractions 1C1-1D10 were pooled and dialyzed to obtain the final product (5 μg) shown by the SDS-PAGE **C**.

6.1.2 Assay Development

6.1.2.1 *Activity of the recombinant Sortases*

In the case of SaSrtA, an enzyme-concentration of 2.5 µM was needed to provide continuous product formation for 4 h reaction time at 100 µM donor-substrate concentration. In contrast, 15 µM of SaSrtB had to be used to fulfill the same criteria. With EfSrtA, no activity could be observed at any sensible enzyme and substrate concentrations. The lipid II-crossbridge in *E. faecalis* is D-Ala-D-Ala and has been used in concentrations from 1 mM up to 125 mM. Thus, further optimization of assay conditions needed to be performed.

	SaSrtA
K_m	111.2 ± 8.3 µM
v_{max}	7077 ± 210 RFU/min
R^2	0.9917

	SaSrtB
K_m	35.9 ± 7.6 µM
v_{max}	7014 ± 398 RFU/min
R^2	0.9049
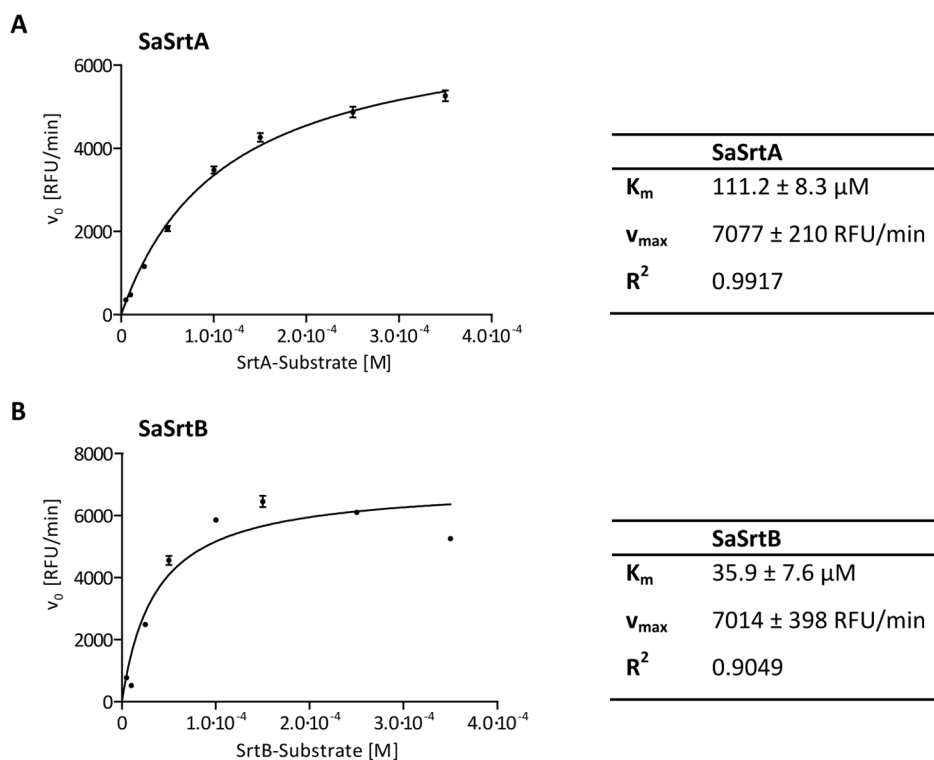
Figure 20: Michaelis-Menten kinetics of Sortase A and Sortase B from *S. aureus*

The initial reaction velocities of the constructs SaSrtA and SaSrtB were measured with varying concentration of the specific fluorophor-quencher labeled recognition peptides (n=3) at 1 mM Gly_5. The data was fitted in GraphPad Prism to obtain the asymptotic curve and the Michaelis-Menten parameters.

The above mentioned protein concentrations were used to determine the Michaelis-Menten kinetics of the enzymes (Figure 20). The K_M of Sortase A from *S. aureus* was published to be 141.19 ± 19 µM in a similar assay with 3 mM Gly_3.[153] With the assay conditions chosen in this work, the K_M for SaSrtA was determined to be 111.2 ± 8.3 µM at 1 mM Gly_5. The affinity for the specific peptide substrate is higher for SaSrtB (K_M =35.9 ± 7.6 µM). Both enzymes have comparable maximal velocities in the chosen setting but, as SaSrtB was used in a six-fold concentration compared to SaSrtA, the reaction catalyzed by a single enzyme is approximately six-fold lower. In both cases it was not possible to calculate the molar reaction velocity and therefore the k_{cat} because neither the quantum yield for

EDANS in the given buffer at the specific wavelengths (Q_f) nor the exact initial light intensity (I_0) was known to resolve the parametric equation given in Formula 2. Additionally, a profound inner filter effect of absorbing molecules for the excitation light by quenched EDANS as well as for the emission light by the quencher Dabcyl demands a calibration of the measurement with expensive custom synthesized single-dye fragments of the fluorescent substrate. However, for the ultimate objective of compound screening and IC$_{50}$-determination, relative activity assessment was sufficient as the inhibitory effect of different compounds were determined within the same experimental setting.

$$F = 2.3 \cdot Q_f \cdot I_0 \cdot \varepsilon \cdot c \cdot d$$

Formula 2: Calculation of the fluorescence intensity

F: fluorescence intensity, Q_f: quantum yield of the fluorophore, I_0: excitation light intensity, ε: absorbance coefficient of the fluorophore, c: concentration of the fluorophore, d: path length

In order to validate the activity of the recombinantly produced SaSrtA, the effect of known inhibitors was investigated. The inhibitors tested were DMMA ((Z)-3-(2,5-dimethoxyphenyl)-2-(4-methoxyphenyl) acrylonitrile) described by Oh, 2004 / 2006 / 2010[158, 162, 172] and kindly provided by Priaxon AG as well as two compounds published by Suree in 2009[174]. The inhibitor Rhodanine-1 (5-(3-bromo-2-hydroxy-5-nitrobenzylidene)-3-(2,4-dimethylphenyl)-2-thioxo-1,3-thiazolidin-4-one) was purchased and the inhibitor compound 2-17 was kindly provided by Prof. Clubb (UCLA). Figure 21 depicts these three compounds.

| DMMA | Rhodanine-1 | Compound 2-17 |
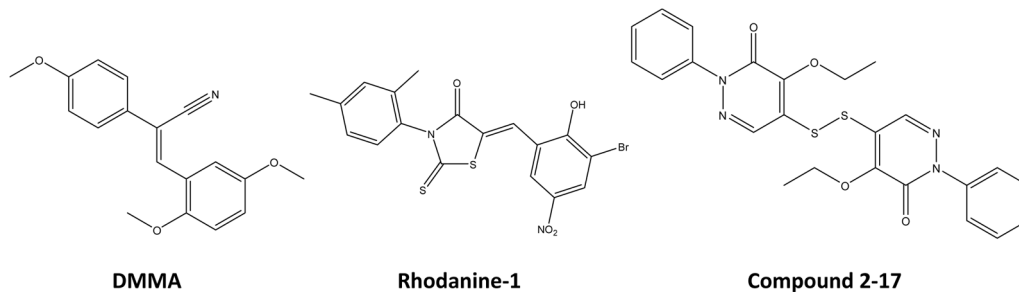
Figure 21: Published inhibitors tested in the SrtA transpeptidation assay

DMMA, Rhodanine-1 and compound 2-17 are published inhibitors for the Sortase A from *S. aureus* and were used for validation of the SaSrtA transpeptidation assay. Furthermore, Rhodanine-1 was applied as reference inhibitor in screening approaches.

The IC$_{50}$-values of these inhibitors were reported to be 9.24 ± 0,47 µM for DMMA, 3.7 ± 0.1 µM for Rhodanine-1, and 1.5 ± 0.4 µM for compound 2-17. The three inhibitors were tested in the standard setup of the SrtA transpeptidation assay in suitable concentration ranges. DMMA was tested in concentrations up to 1 mM, but no reliable effect could be measured. The compound was poorly soluble in the aqueous assay system, and the precipitation at higher concentrations led to increased background signals, which obscured any effect of the compound on the SaSrtA activity. The two other inhibitors could be measured in the IC$_{50}$ setup and showed clear inhibition of SaSrtA activity as depicted in Figure 22. Rhodanine-1 showed an IC$_{50}$-value of 16.28 ± 2.07 µM in this experiment, which was about five-fold higher than the published value. Due to limited supply of this compound, this phenomenon was not further investigated. For Compound 2-17 an IC$_{50}$-value of about 2.5 µM

could be determined. This was very close to the published data and therefore ascertains the assay setup as valid for identification of inhibitory compounds.
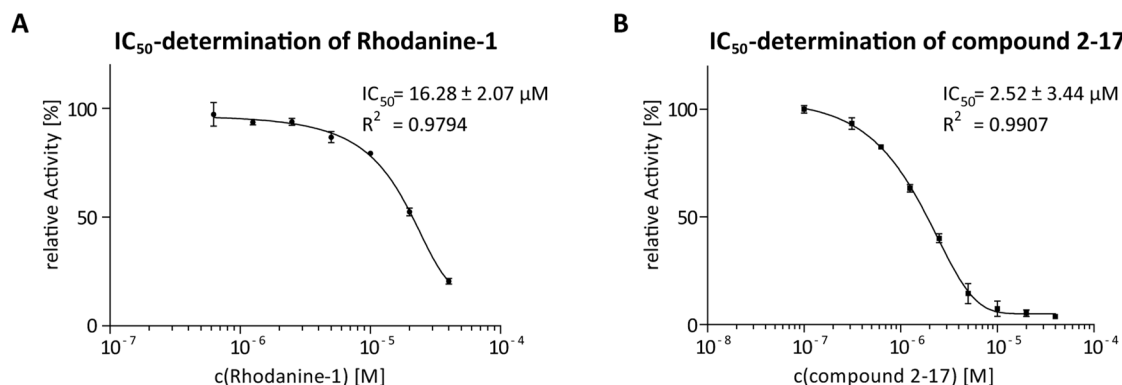
Figure 22: IC$_{50}$-determination of Rhodanine-1 and compound 2-17

The compounds were used in suitable concentration ranges to achieve the non-linear fit of the initial velocities measured (n=3). Graph **A** shows the data for Rhodanine-1 and **B** shows the data of compound 2-17. The sigmoidal fit for compound 2-17 was ambiguous despite obtaining a very good R^2. Therefore, the IC$_{50}$-value was obtained with a high deviation.

6.1.2.2   Assay Validation

Thorough validation of a screening assay is a prerequisite to reliably identify primary active compounds with suitable potency for further characterization, and no potential inhibitors should be missed in the first screening round. Therefore, criteria for HTS assays set forth by the European Lead Factory[44] have been adapted to the needs of the SaSrtA screening approach (Table 17).

The HTS assay requirements can be devided into four categories: suitability of the technology, reagent quality, measurement quality and HTS-specific demands.

The transpeptidation assay for sortases (chapter 5.4.1) is used for SaSrtA inhibitor identification in this work. It is suitable for small reaction volumes and is a homogenous assay of the mix-and-measure type. Rhodanine-1 is suitable as reference inhibitor in the screening approach and compound 2-17 confirmed the assay setup as valid.

Requirement	Criteria
Assay format	demonstrated in 96-well format
Homogenous assay	no wash steps required
Read out technology	mix-and-measure
Reference inhibitor	readily available
Protein purity	≥ 80 %
Protein stability	5 freeze-thaw cycles
Reagent stability	> 8 h
Reaction time	4 h
Endpoint measurement	correlation of endpoint measurement with initial reaction velocity
Signal / background ratio	> 3
Z' factor	> 0.6
Plate stability	CV < 10 %
DMSO tolerance	≥ 0.5 %
Readout stability	≥ 1 h

Table 17: Requirements for HTS screening assays

These requirements were adapted from the IMI screening project "European lead factory".[44]
CV: coefficient of variation

Further criteria were analyzed by suitable evalutation settings. Firstly, the quality and stability of the reagents used in the screening assay were assessed (Figure 23) to ensure accurate and reliable measurements. The enzyme SaSrtA was recombinantly expressed in *E. coli* BL21 (DE3) and purified to a final purity of >90 %. The stability of the protein was tested in multiple freeze-thaw cycles and the resulting enzymatic activity was compared to freshly prepared SaSrtA. The overall variability was 4.48 %. Thus, freeze-thaw cycles had no major effect on the enzymatic activity. Therefore, the recombinant enzyme is sufficiently stable for the screening assay. The FRET peptide substrate Dabcyl-LPETG-(E)-EDANS was prepared for the assay and incubated in various conditions to estimate its stability. The incubated substrates showed an overall reduced (–10 %) endpoint absorbance when compared to freshly prepared substrate. However, among the incubation conditions, no differences were observed, which was confirmed by a coefficient of variation (CV) of 2.51 % (calculated with Formula 3). Thus, incubation at different temperatures did not affect the assay performance. It is not clear whether using fresh substrate leads to higher endpoint absorbance in the assay or the observed shift, in endpoint absorbance between freshly prepared and incubated substrate, was due to differences in preparation. Overall, the substrate Dabcyl-LPETG-(E)-EDANS is sufficiently stable for screening applications.
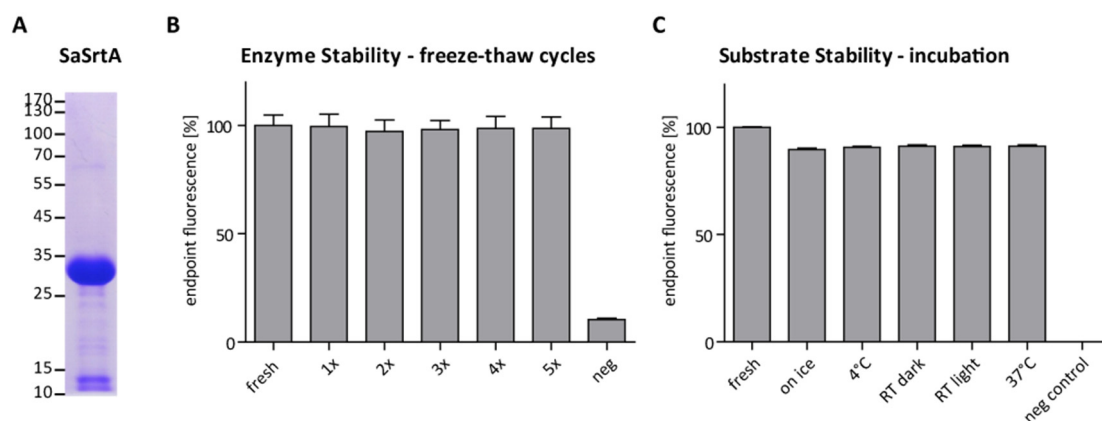
Figure 23: Quality and stability of reagents for the SrtA transpeptidation assay

The SDS-PAGE **A** illustrates the purity of the SaSrtA enzyme (10 μg). The band at 30 kDa corresponds to the N-terminally His$_6$-tagged protein. Graph **B** shows the stability of the enzyme SaSrtA. Aliquots were frozen and thawed for several cycles as indicated. The enzymatic activity was compared to freshly thawed enzyme (n=3×3). The coefficient of variability was 4.48 %. Graph **C** shows the stability of the substrate Dabcyl-LPETG-(E)-EDANS. The predilutions were incubated in the indicated conditions for 9 h before starting the assay (n=6×3). The difference to freshly prepared substrate was up to −10 %; the coefficient of variability among different incubation conditions was 2.51 %.

$$CV = \frac{\sigma}{\mu}$$

Formula 3: Calculation of the coefficient of variation

σ: standard deviation; μ: mean

Secondly, the quality of the measurement was determined for the SrtA transpeptidation assay as given in Figure 24. The screening setup has to guarantee identification of even slow binding and relatively weak inhibitors. This can be achieved by employing a total reaction time of four hours and end point measurement as kinetic measurements are not recommended for HTS assays.[44]

The fluorescence signal in the SaSrtA transpeptidation assay continuously increased within the envisioned reaction time of 4 h, which allows slow binding compounds altering the enzymatic activity to be identified. The readout signal of the screening assay was defined as endpoint fluorescence after 4 h incubation at 37°C, which correlated sufficiently with the initial reaction velocity measured in the plate-reader. The endpoint fluorescence intensity was rather more sensitive. Therefore, it could be used as relevant readout for any kinetic variations.
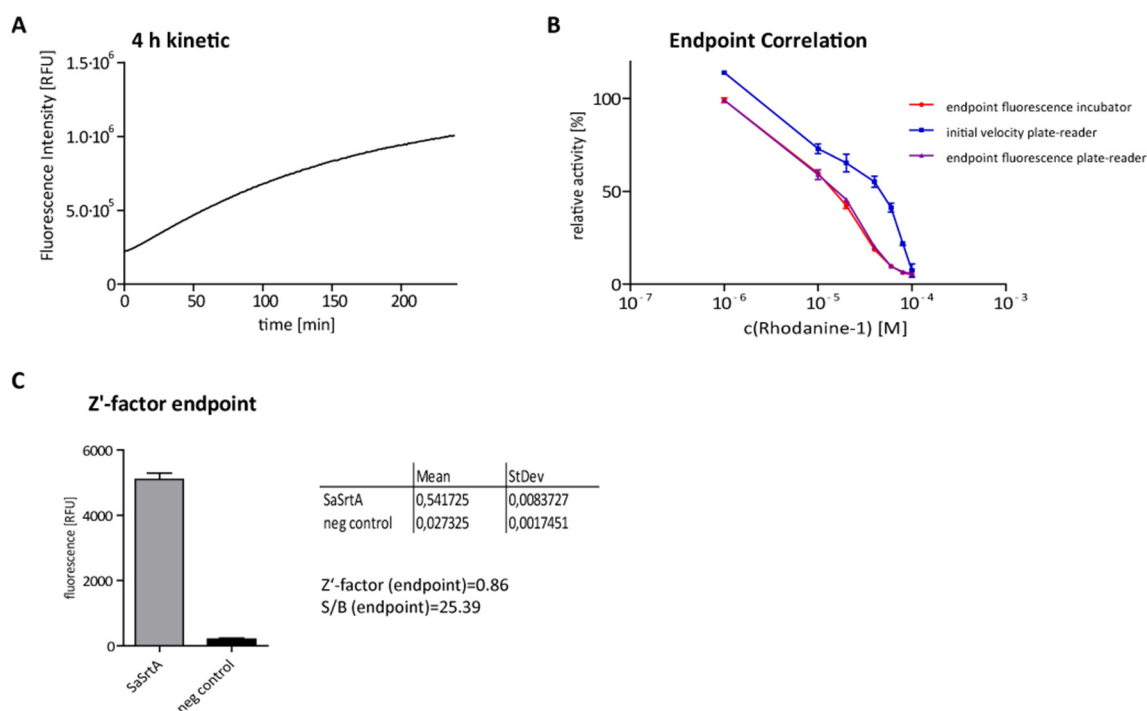
Figure 24: Quality of the SrtA transpeptidation assay measurement

Graph **A** plots the absorbance of a standard transpeptidation reaction with 2.5 µM SaSrtA against time (n=3). The fluorescence intensity increased for 4 h. In graph **B,** the readouts of the assay are compared (n=3). The standard assay was titrated with rhodanine-1 as model inhibitor. The endpoint fluorescence intensity after incubation in the incubator correlated with initial velocity measured in the plate-reader and the endpoint fluorescence measured in the plate-reader. The bar graph in **C** contrasts the endpoint fluorescence intensity (incubator) with and without (neg control) SaSrtA after 4 h incubation (n=24). The corresponding data is shown in the table of graph **C**. With these, the Z'-factor and signal/background ratio were calculated.

Furthermore, positive and negative control signal should define a suitable window for the detection of inhibitory compounds. Thus, the signal / background (S/B) ratio as well as the Z'-factor of the assay (Figure 24 C) had to be calculated with Formula 4 and Formula 5. The S/B ratio is a widely used quality criterion for measurements whereas the Z'-factor defines the screening window as ratio between the separation band and the signal dynamic range as specific parameter for HTS assays.[45] The Z'-factor of the SaSrtA screening assay was 0.86 and thus clearly above the required value of at least 0.6, which indicates an excellent screening assay. Also, the signal to background ratio of about 25 was much higher than the demanded ratio of 3. Taken together, the measurement quality for the SaSrtA transpeptidation assay was outstanding and empowered the implementation as screening assay.

$$\frac{S}{B} = \frac{positive\ control\ signal}{negative\ control\ signal}$$

Formula 4: Calculation of the signal / background ratio

$$Z' = 1 - \frac{3\sigma_{pos} + 3\sigma_{neg}}{|\mu_{pos} - \mu_{neg}|}$$

Formula 5: Calculation of the Z' factor for signal window determination

σ_{pos}: standard deviation of positive control signals; σ_{neg}: standard deviation of negative control signals; μ_{pos}: mean of positive control signals; μ_{neg}: mean of negative control signals

Figure 25 summarizes data collected to investigate the HTS-applicability of the SrtA transpeptidation assay. The robustness of the measurements can be assessed by evaluating the signal distribution on a plate with positive signals only. The coefficient of variability for the readout signal across the plate was 0.9 % and therefore well beneath the required maximum of 10 %. No systematic effects such as significant discrepancies between plate boarder and center could be identified.[43, 44] For ease of use the reaction could be terminated by addition of 10 % (v/v) acetic acid and the readout signal was stable for two hours. Furthermore, the assay tolerated up to 8 % of DMSO, which is the predominant solvent of screening compounds. With these findings, the SrtA transpeptidation assay was shown to be suitable for high throughput screening in the 96-well format.
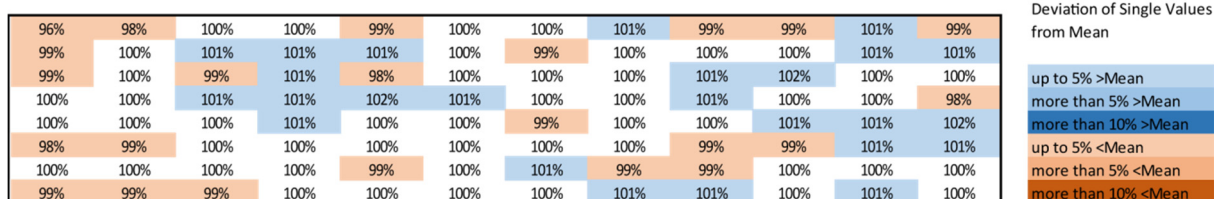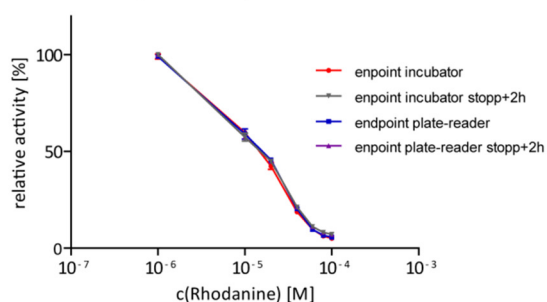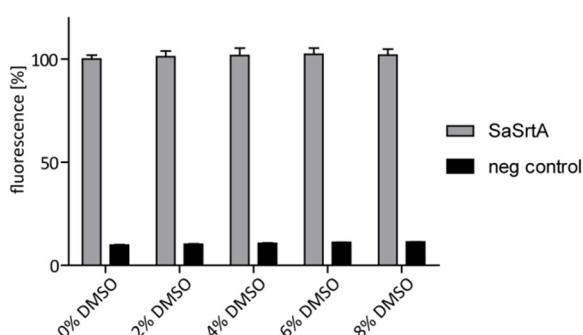
Figure 25: HTS-applicability of the SrtA transpeptidation assay

Figure **A** illustrates the signal distribution in the 96-well plate (n=3). The standard assay was incubated for 4 h and endpoint absorbance was measured. The single values are given relative to the overall mean of the plate. Graph **B** depicts the stability of the endpoint-absorbance signal after stopping the reaction with 10 % (v/v) acetic acid. The signals measured 2 h after reaction termination correlated exactly with endpoints after 4 h incubation. Graph **C** outlines the DMSO tolerance of the standard assay with up to 8 % (v/v) DMSO.

Novel inhibitory compounds were assessed for their specificity by determining their effect on the activity of Sortase B from *S. aureus* and Sortase A from *E. faecalis*. Figure 26 depicts Coomassie stained SDS-Gels of the purified Enzymes SaSrtB and EfSrtA. SaSrtB presented a purity of >90 % and EfSrtA presented a purity of >80 % after affinity and size-exclusion chromatography. It was possible to set up the transpeptidation assay with SaSrtB according to the assay with SaSrtA. However, the enzyme concentration had to be increased to 15 µM compared to 2.5 µM with SaSrtA. No activity of the recombinant EfSrtA could be observed with sensible enzyme and substrate concentrations.
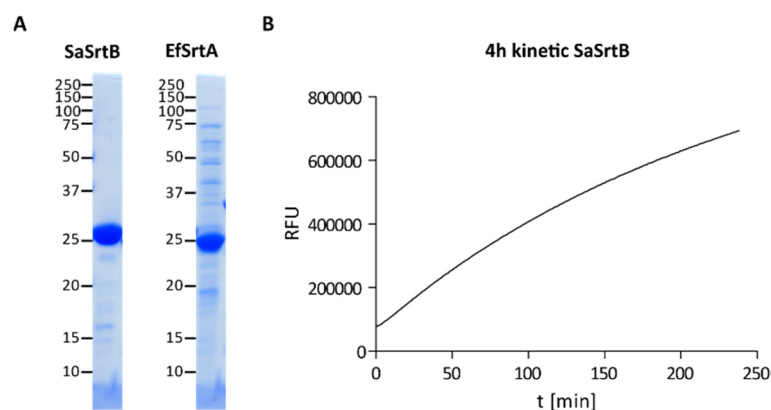
Figure 26: Sortases for Specificity testing

The SDS-PAGEs **A** show the purity of 5 µg of each SaSrtB and EfSrtA. The expected molecular weights of 27 and 25 kDa were confirmed for SaSrtB and EfSrtA, respectively. Graph **B** plots the fluorescence increase of the cleaved peptide product over time. 15 µM of SaSrtB and 100 µM of the specific substrate were used for product formation for 4 h reaction time.

6.1.3 Inhibitor identification

Several crystal structures for the apo-enzyme (1T2P[140], 1IJA[154]) and the enzyme bound to a covalently attached substrate analogue (2KID[157]) as well as known inhibitors of the *S. aureus* Sortase A like vinyl sulfones[330], diarylacrylonitriles[172], and pyridazinone and pyrazolethione analogues[174] enabled a targeted approach for the identification of novel inhibitory compounds. This was performed in a cooperation with Priaxon AG, who applied the published data to their PriaxPlore® technology (chapter 6.2.4). The tailored library of 61 compounds and a general screening library of 277 compounds (also kindly provided by Priaxon AG) were tested for inhibitory activity in a screening setup. Yet, this approach did not yield any hits for further characterization and development.

As an alternative approach for identifying SaSrtA inhibitors, the DZIF (Deutsches Zentrum für Infektionsforschung) natural compound library was screened for inhibitory activity against SaSrtA. This library was kindly provided by Prof. Dr. Rolf Müller and Dr. Jennifer Herrmann from the Helmholtz-Institut für Pharmazeutische Forschung Saarland (HIPS). It contains 259 isolated secondary metabolites from myxobacterial species, which are appreciated for their variety of core structures. Myxobacteria are Gram-negative δ-proteobacteria with rich secondary metabolisms generating polyketides, non-ribosomal peptides, terpenoids, phenyl-propanoids, and alkaloids. Another attractive feature of these myxobacterial compounds is their rare or novel modes-of-action, which have been described in anti-fungal, anti-bacterial and cytotoxic effects. The highly competitive habitat of myxobacteria in the soil, on decaying plant material, and the marine environment underlines their potential as producers of bioactive compounds. Therefore, myxobacterial com-pounds constitute attractive lead structures for drug discovery in the field of anti-infectives.[331, 332]

The data obtained from the library screen is illustrated in Figure 27. Three initial actives could be identified yielding a hit rate of 1.16 %. The three natural compounds N110, N145 and N150 inhibited the *S. aureus* Sortase A by 51.0 %, 41.7 % and 24. % at 25 µM, respectively. They were therefore suitably potent to verify their activity with IC_{50}-determination.
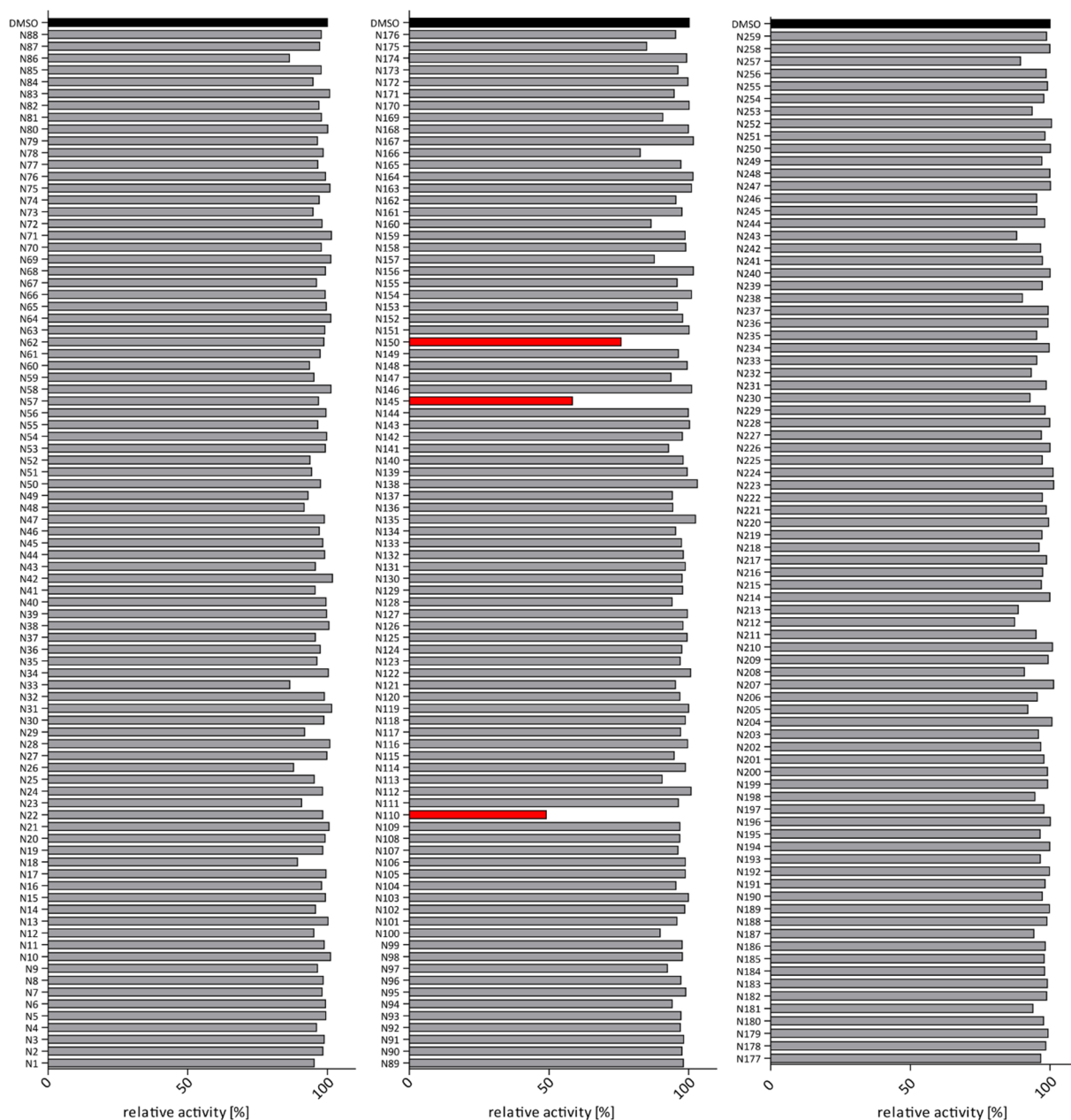
Figure 27: Screening of the DZIF natural compound library with the SaSrtA transpeptidation assay

Initial screening of the library compounds was realized in single measurements at 25 µM according to the validated screening assay. The endpoint fluorescence was normalized to DMSO treated controls (black bars). Primary actives are defined by activity inhibition >20 % and are indicated in red.

Two of the identified compounds are described in literature (Figure 28). Compound N150 is pyrronazol B (a chlorinated pyrrole-oxazole-pyrone) isolated from *Nannocystis pusilla*. The closely related compound pyrronazol A is recorded to have a mild anti-fungal activity (MIC= 33.3 µg/mL against *Mucor hiemalis*) but no effect on bacteria has been described so far.[333]

Compound N110 is hyaladion (S-methyl cyclohexadiene-dione) isolated from the myxobacterium *Hyalangium minutum*. Hyaladion is described to be active against mammalian cell lines and to exhibit anti-bacterial and anti-fungal activities. In this context a MIC of 0.85 µg/mL against methicillin-resistant *S. aureus* has been published.[334]

Compound N145 has not been described in literature yet.
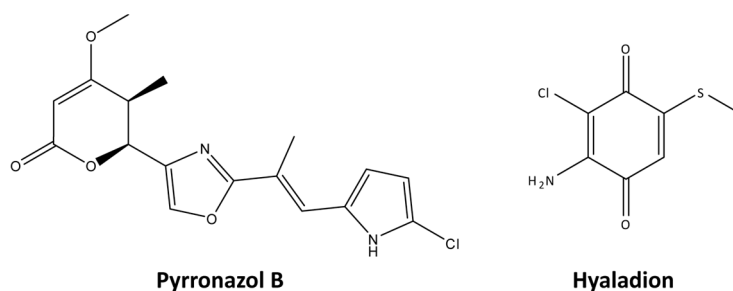
Figure 28: Structural formulas of two identified active compounds against SaSrtA

Pyrronazol B originates from Nannocystis pusilla.[333]
Hyaladion was isolated from Hyalangium minutum.[334]

Two of the three initial actives could be verified in IC$_{50}$-determination as shown in Figure 29. Pyrronazol B was not sufficiently active to deduce the IC$_{50}$-value from the measurements as only concentrations up to 100 µM could be tested due to limitations in supply. For Hyaladion and compound N145, the IC$_{50}$-values were estimated on the basis of the normalized data. Hyaladion inhibited the SaSrtA in the transpeptidation assay with an IC$_{50}$-value of about 80 µM whereas compound N145 was more potent with an IC$_{50}$-value of about 30 µM.
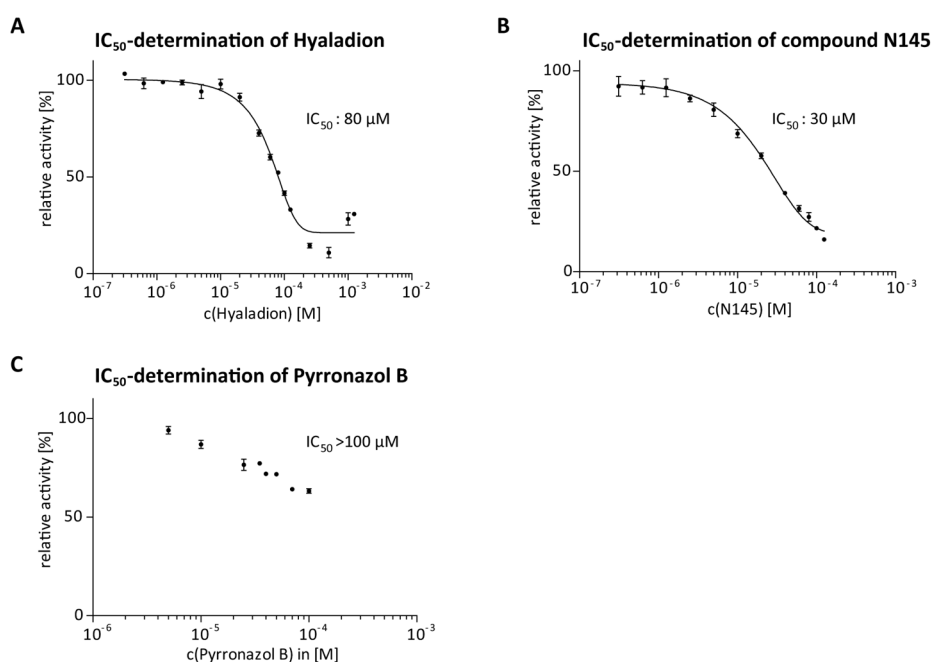
Figure 29: IC$_{50}$-determination of three natural compounds in the SrtA transpeptidation assay

The compounds were used in suitable concentration ranges to achieve the non-linear fit of the initial velocities measured (n=3). A wide range of concentrations had to be checked for **A** hyaladion and **B** compound N145 to obtain a sigmoidal curve. Yet, the fit was ambiguous so that IC$_{50}$-values were estimated on the basis of signal normalization to DMSO treated controls. For Pyrranazol B (**C**), the IC$_{50}$ was higher than 100 µM.

The next objective was to check the specificity of the validated hits with Sortase B from *S. aureus*. The IC$_{50}$-values for both Hyaladion and compound N145 were determined in the SaSrtB transpeptidation assay (Figure 30). The values obtained were very similar to those that were determined for the SaSrtA. As both enzymes use the pentaglycine moiety of the cell wall cross-

bridges as acceptor-substrates in the transpeptidation reaction, it was conceivable that both enzymes are inhibited to a similar extend by agents binding to the acceptor binding sites. This could be clarified in NMR-spectroscopy or crystallography based binding analysis.
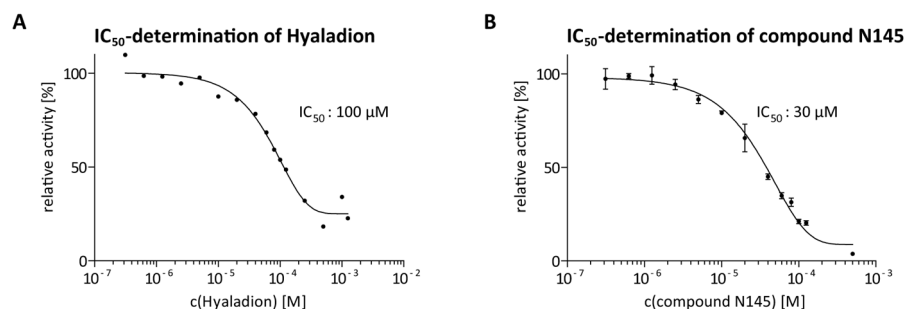
Figure 30: IC$_{50}$-determination of two natural compounds in the SrtB transpeptidation assay

The compounds were used in suitable concentration ranges to achieve the non-linear fit of the initial velocities measured (hyaladion: n=1; compound N145 n=3). A wide range of concentrations had to be checked for **A** hyaladion and **B** compound N145 to obtain a sigmoidal curve. Yet, the fit was ambiguous, so that IC$_{50}$-values were estimated on the basis of signal normalization to DMSO treated controls.

However, as both Hyaladion and compound N145 had a dark red appearance as dilutions in DMSO, they could potentially interfere with the fluorescence signal due to additional inner filter effects in the reaction mixture. Thus, it was also possible that the observed 'inhibitory' effect is independent of enzymatic activity and rather an artifact of the fluorescence based assay. The absorbance spectrum of compound N145 shown in Figure 31 A indicates possible interactions with light in the whole visible spectrum. Therefore, the direct effect on the fluorescence signal was determined for the two natural compounds. To this end, the standard SaSrtA transpeptidation assay was run for 4 h and the final fluorescence intensity was measured. Then, the natural compounds were added in suitable dilutions to assess the effect on the fluorescence signal. Addition of both compounds led to a decreased fluorescence signal due to the inner filter effect of absorbing molecules in the reaction mixture (Figure 31 B).
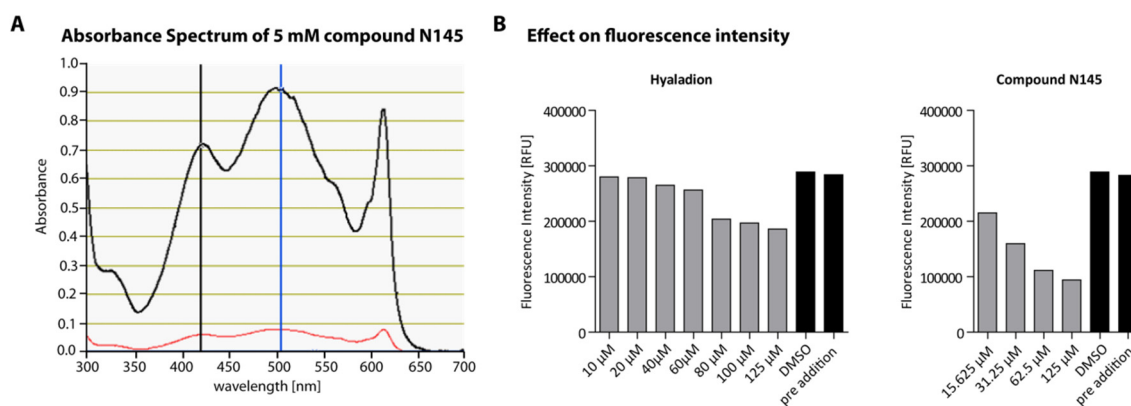
Figure 31: Interference of natural compounds with fluorescence signal

The absorbance spectrum of compound N145 (**A**) indicates potential interference of the compound with signals in the VIS-spectrum. The black line plots the absorbance at 1 mm path length; the red line plots the measurement at 0.1 mm path length. The two natural compounds were added at the reaction endpoint to assess the effect in the SaSrtA transpeptidation assay (**B**) (n=1, DMSO: n=5, pre addition: n=16).

In conclusion, the two identified hits Hyaladion and compound N145 were reducing the readout signal in the SaSrtA and SaSrtB transpeptidation assay. Detailed analysis revealed, however, that this 'inhibitory activity' can be explained by an inner filter effect and thus most likely turns out to be an artifact of the fluorescence measurement. Therefore, the project was not advanced on the basis of these compounds.

Nevertheless, the assay is well suited for inhibitor identification since it met all set criteria and was able to reproduce data published with known inhibitors. Thus, further screening and development approaches to detect promising Sortase A inhibitors as anti-virulence agents will be supported by this work in the future.

6.2 *Helicobacter pylori* γ-glutamyl transpeptidase

6.2.1 Recombinant production of the γ-glutamyl transpeptidase from *H. pylori*

Two constructs of the *H. pylori* γ-glutamyl transpeptidase for recombinant protein production were used for the standard gGT transpeptidation activity assay.

The first was the *H. pylori* gGT expressed from the vector pQETri_wtHPG harboring the Δ1-26 truncated gGT gene of the strain ATCC 700392. Cloning and protein production were performed by Dr. Christian Bolz[325]. The protein sequence is given in Figure 32. Apart from the His$_6$-tag and the large and small subunits of the *H. pylori* γ-glutamyl transpeptidase, it also contained a few amino acids between His$_6$-tag and the coding sequence of the HPG encoded by the vector backbone. This construct is used for various experiments in the lab.

The second construct, which was also used for the crystal-structure determination, was based on the pPRk-oHPGh vector. The gene sequence from the strain ATCC 700392 was codon optimized for expression in *E. coli* with the free online tool JCat[335]. The sequence was synthesized as GeneArt® Strings™ DNA fragment (Life Technologies (Carlsbad, US)) and cloned for seamless expression of the Δ1-26 C-terminally His-tagged recombinant protein. The protein sequence is given in Figure 32.
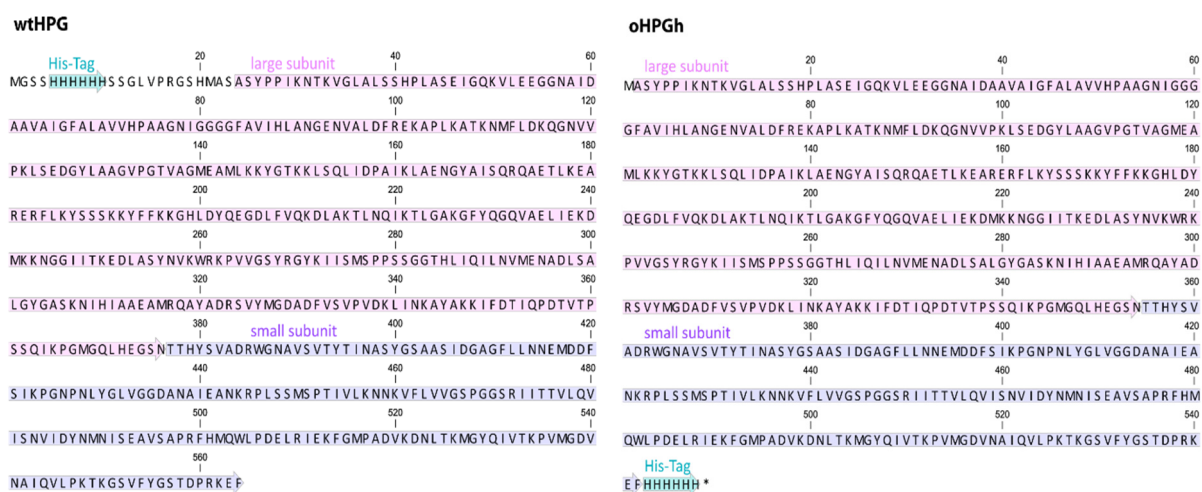
Figure 32: Amino acid sequences of the *H. pylori* gGT constructs used in this work

Both constructs contain the large and the small subunit of the *H. pylori* gGT as well as the His$_6$-tag for purification. The wtHPG is N-terminally tagged and also contains additional amino acids encoded by the vector backbone. The oHPGh is C-terminally tagged and does not contain any additional amino acids.

The process of production of oHPGh was established as described in chapter 5.3.2. Figure 33 shows the purification process via HisTrap and size-exclusion chromatography as well as an SDS-PAGE of the final product. The final yield was 100 mg.
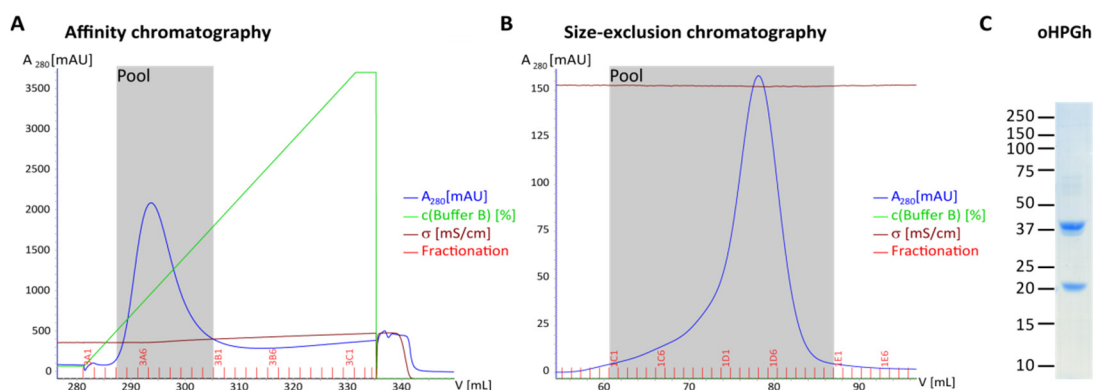
Figure 33: Purification of the construct oHPGh

Graph **A** shows chromatograms recorded for the affinity-purification of a BL21 pPRk Δ1-26 oHPG-h lysate (HisTrap FF crude 5 mL) and graph **B** depicts those for the subsequent size-exclusion chromatography (HiLoad 16/600 Superdex 200 PG) of the fractions 3A4-3A12 of the previous step. Fractions 1C1-1D10 were pooled and dialyzed to obtain the final product (2.5 µg) shown by the SDS-PAGE in **C**. The bands at 40 kDa and 20 kDa correspond to the large and small subunit of the oHPGh, respectively.

6.2.2 Crystal Structure

For obtaining *H. pylori* γ-glutamyl transpeptidase devoid of additional amino acids to be used for crystallization experiments, recombinant protein was produced from pPRk-oHPGh. The novel construct was expressed in BL21 according to standard procedure and purified via HisTrap® and size-exclusion chromatography. Crystallization, X-ray data collection and analysis were performed by Dr. Grzegorz Popowicz at the Institute of Structural Biology, Helmholtz Center München (Group of Prof. Sattler).

The protein was crystallized using the vapor diffusion sitting drop method. Crystals were obtained within several days in a crystallization solution containing 0.2 M ammonium acetate, 25 % (w/v) PEG3350, 0.1 M Tris at pH 8.5. The crystals were frozen for analysis after washing in mother liquor supplemented with 20 % (v/v) glycerol. Several datasets were measured with the ID23-2 microfocus beamline at the ESRF synchrotron (Grenoble, FR). The data has been processed by XDS software and scaled in XSCALE.[336] Molecular replacement was achieved using the published structure 2NQO[258] with the Molrep software[337] of the CCP4 suite[338]. Subsequently, the model was refined by iterative cycles of maximum likelihood refinement using Refmac5[339] and model rebuilding using COOT[340].
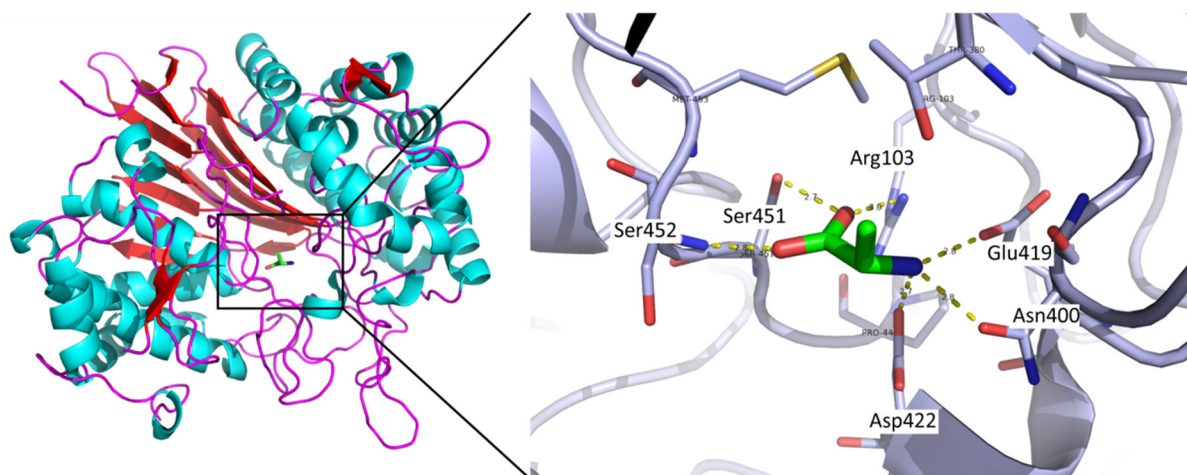
Figure 34: Apo-structure of the novel recombinant construct oHPGh

The overall topology of the novel γ-glutamyl transpeptidase construct from *H. pylori* is identical to the published apo-structure 2NQO. The ligand coordinated by defined active site residues was identified to be alanine.

Figure 34 displays the overall structure determined for the novel construct oHPGh as well as a detailed view of the enzyme's active site with a small ligand. Identification of this ligand as alanine was achieved due to the outstanding resolution of 1.2 Å. It was present in published HPG structures as well but it could not be annotated before (2NQO[258]). In our structural data, we could identify several interactions of the resident alanine with the oHPGh active site residues. Alanine coordinates to Ser451, Ser452 and Arg103 via its carboxy moiety and to Asp422, Glu419 and Asn400 via its amino moiety. Table 18 summarizes the diffraction data and refinement statistics for the crystallography of oHPGh. The overall topology as well as the concrete amino acid sidechain positioning of the oHPGh X-ray analysis is identical to the published apo-structure (2NQO: Boanca, 2007[258]). This information supports the use of this recombinant protein in the screening and evaluation of novel inhibitory compounds.

Diffraction	
space group	P2$_1$
cell constants	a=63.44 Å
	b=95.78 Å
	c=91.53 Å
	β=105.8°
wavelength	1.0 Å
resolution range[a]	90-1.2 Å (1.2-1.23 Å)
all reflections	1205046
unique reflections	71396
completeness[a]	99.7 % (99.3 %)
I/σ(I)[a]	9.43 (1.3)
redundancy	3.7

Refinement	
resolution	90-1.2 Å
used reflections	412695
R-factor	0.16
R_{free}	0.18
average B-factor	17.9 Å²
RMS bond	0.02 Å
RMS bond angles	2.4°

Table 18: X-ray data collection and refinement statistics for the structure of oHPGh

[a] The values indicated in parentheses correspond to the last resolution shell.

6.2.3 Assay Development

6.2.3.1 *Activity of gGT constructs*

In the case of oHPGh, an enzyme concentration of 500 pM was sufficient to provide continuous product formation for 4 h assay reaction with 100 µM LgGpNA. In contrast, 3 nM of the wtHPG protein were less active but still sufficient for 4 h product formation at 100 µM LgGpNA (also see Figure 38).

These enzyme concentrations were used to determine the Michaelis-Menten kinetics of the constructs and control for batch to batch variation. Figure 35 presents the data and non-linear fit used to determine the Michaelis-Menten parameters stated. The K_M of wtHPG corresponded well with the previously determined value of 9.8 ± 1.5 µM whereas the k_{cat} of the protein batch used in this work was more than threefold lower (500 ± 13 min^{-1}) compared to the published k_{cat} of 1740 ± 50 min^{-1}.[325] The novel construct oHPGh had a lower affinity for the donor-substrate LgGpNA (K_M = 34.8 ± 3.1 µM) but catalyzed the reaction twelvefold faster than the wtHPG.

	oHPGh	wtHPG
K_M	34.8 ± 3.1 µM	9.4 ± 1.5 µM
v_{max}	3.3 ± 0.1 µM/min	1.5 ± 0.0 µM/min
k_{cat}	6000 ± 180 min^{-1}	500 ± 13 min^{-1}
R^2	0.965	0.807
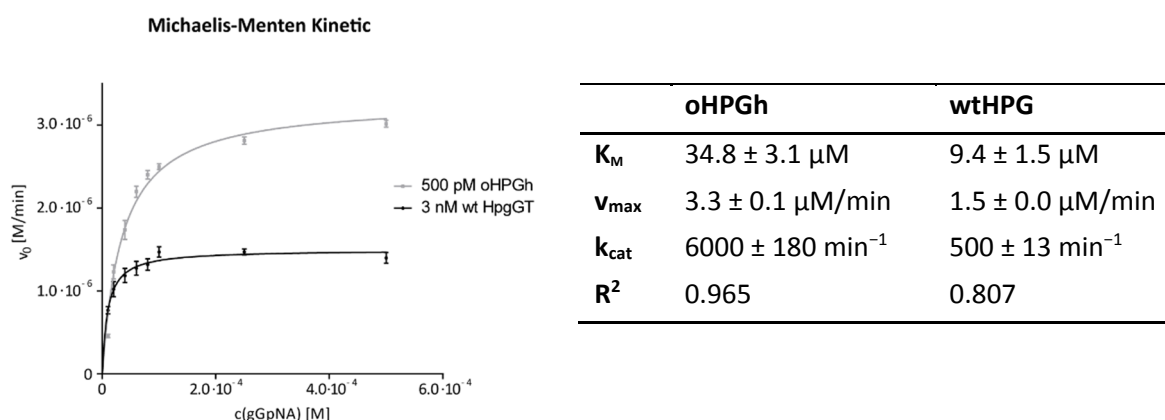
Figure 35: Michaelis-Menten kinetic of *H. pylori* gGT constructs

The initial reaction velocities of the constructs oHPGh and wtHPG were measured with varying concentration of LgGpNA (n=3). The data was fitted in GraphPad Prism to obtain the Michaelis-Menten asymptotic curve (hill function) and parameters.

Comparability of the assays with either construct was proven by analyzing IC_{50}-determinations of identified inhibitory compounds utilizing both recombinant proteins. Figure 36 shows the corresponding measurement with compound #13 (described in chapter 6.2.4). The determined IC_{50}-values were comparable and the non-linear fit of the data was excellent in both cases. Therefore, results obtained with both recombinant forms of the HPG were presumed to be interchangeable.
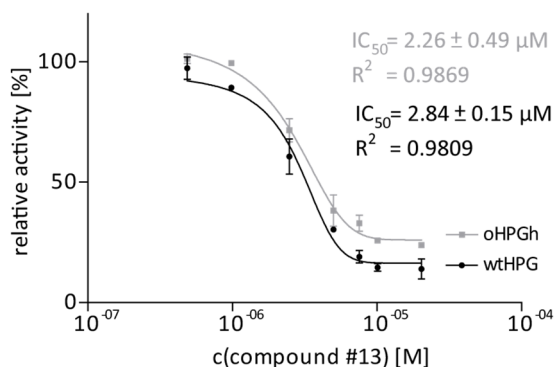
Figure 36: Comparison of the HPG-construct via IC_{50}-determination

The initial reaction velocities of transpeptidation reaction of the two HPG constructs were measured with varying concentration of compound #13 (n=3). The data was fitted in GraphPad Prism to obtain the sigmoidal dose-response.

The activity of the HPG and the validity of the assay setup was further investigated by the described inhibitory effect of the compound Acivicin ((2*S*)-Amino[(5*S*)-3-chloro-4,5-dihydro-1,2-oxazol-5-yl]ethanoic acid)[325, 341]. In the thesis of Dr. Christian Bolz, an IC_{50}-value of 51.5 ± 1.1 nM was described for the wtHPG, which was fiftyfold lower than the IC_{50}-value determined as shown in Figure 37. The assay setup was, however, distinct from the standard assay in this work especially with regard to a tenfold lower donor-substrate concentration and pre-incubation of enzyme and inhibitor. Therefore IC_{50}-values were not comparable. Nevertheless, Acivicin yielded a good dose response and was used as control inhibitor in the screening approach described in chapter 6.2.4.
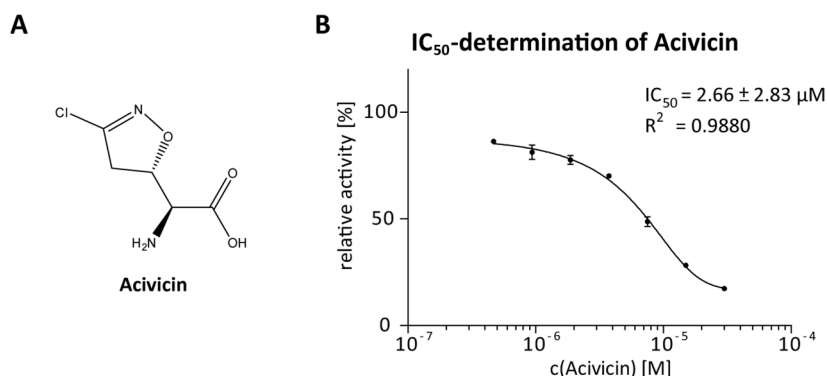
Figure 37: IC_{50}-determination of Acivicin

A shows the chemical structure of Acivicin and graph **B** shows the data for the IC_{50}-determination of Acivicin. The compound was used in a suitable concentration range to achieve the non-linear fit of the initial velocities measured (n=3). The sigmoidal fit was ambiguous despite obtaining a very good R^2. Therefore, the IC_{50}-value was obtained with a high deviation.

6.2.3.2   Assay Validation

The HPG screening assay was established according to HTS-assay requirements set forth by the European Lead Factory[44] (described in detail in chapter 6.1.2.2). Thorough validation of a screening assay is a prerequisite to reliably identify primary active compounds with suitable potency for further characterization.

Firstly, the quality and stability of the reagents used in the screening assay (5.4.2) were assessed (Figure 38). The enzyme oHPGh was recombinantly expressed in *E. coli* BL21 (DE3) and purified to a final purity of >90 %. The stability of the protein was tested by subjecting it to multiple freeze-thaw cycles and comparison of the resulting enzymatic activities. The freeze-thaw cycles had no major effect on the enzymatic activity; the overall variability was 1.69 %. Therefore, the recombinant enzyme is sufficiently stable for the screening assay. Furthermore, the chromogenic substrate LgGpNA was prepared for the assay and incubated in various conditions to estimate its stability. The incubated substrates showed an overall reduced (−15 %) endpoint absorbance compared to freshly prepared substrate. However, between the incubation conditions, no differences were identified (CV=1.29 %, Formula 3). Thus, the tested incubation-conditions did not affect the assay performance. It is not clear wheter freshly prepared substrate leads to higher endpoint absorbance in the assay or the preparation was distinct from those before incubation. Overall, the substrate LgGpNA is sufficiently stable for screening applications.
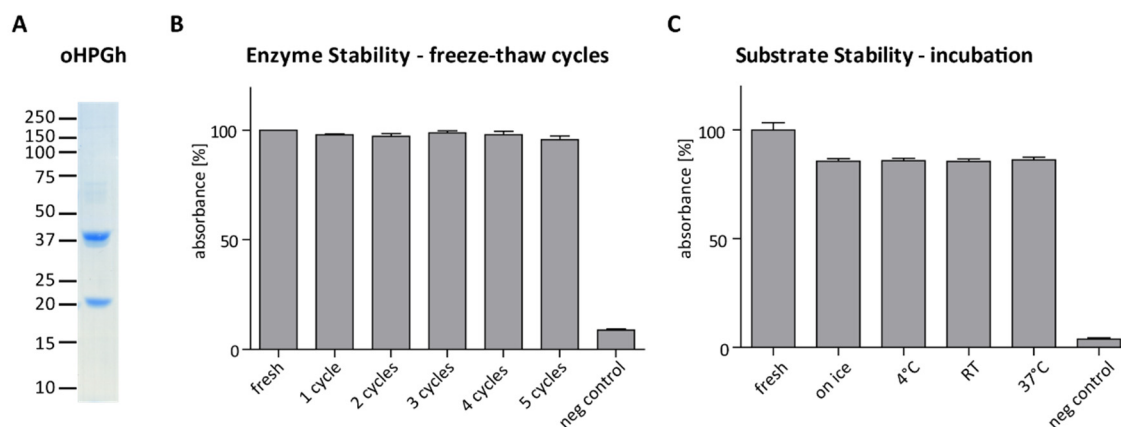
Figure 38: Quality and stability of reagents for the gGT transpeptidation assay

The SDS-PAGE **A** illustrates the purity of the oHPGh enzyme. 2.5 µg of the protein were loaded on the gel. The bands at 40 kDa and 20 kDa correspond to the large and small subunit of the gGT, respectively. Graph **B** shows the stability of the enzyme oHPGh. Aliquots were frozen and thawed for several cycles as indicated. The enzymatic activity was compared to once thawed enzyme (n=3×3). The coefficient of variability was 1.69 %. Graph **C** shows the stability of the substrate LgGpNA. The predilutions were incubated at the indicated temperatures for 9 h before starting the assay (n=12×3). The difference to freshly prepared substrate was up to −15 %. The coefficient of variability among the incubation conditions was 1.29 %.

Secondly, the quality of the measurement was determined for the gGT transpeptidation assay as given in Figure 39. The absorbance signal steadily increased within the assay reaction time of 4 h. Thus, slow binding compounds that alter the enzymatic activity could still be identified. The readout signal of the screening assay was the endpoint absorbance after 4 h incubation at 37°C, which

correlated with the initial reaction velocity measured in the plate-reader. Therefore, the endpoint absorbance could be used as relevant readout for kinetic variations. Furthermore, the Z'-factor of the assay of 0.94 (Formula 5) was clearly above 0.6 and near the maximum of 1.0, which indicates an excellent screening assay. Also, the signal to background ratio of nearly 20 (Formula 4) was much higher than the demanded ratio of 3. Taken together, the measurement quality for the gGT transpeptidation assay was outstanding and empowered the implementation as screening assay.
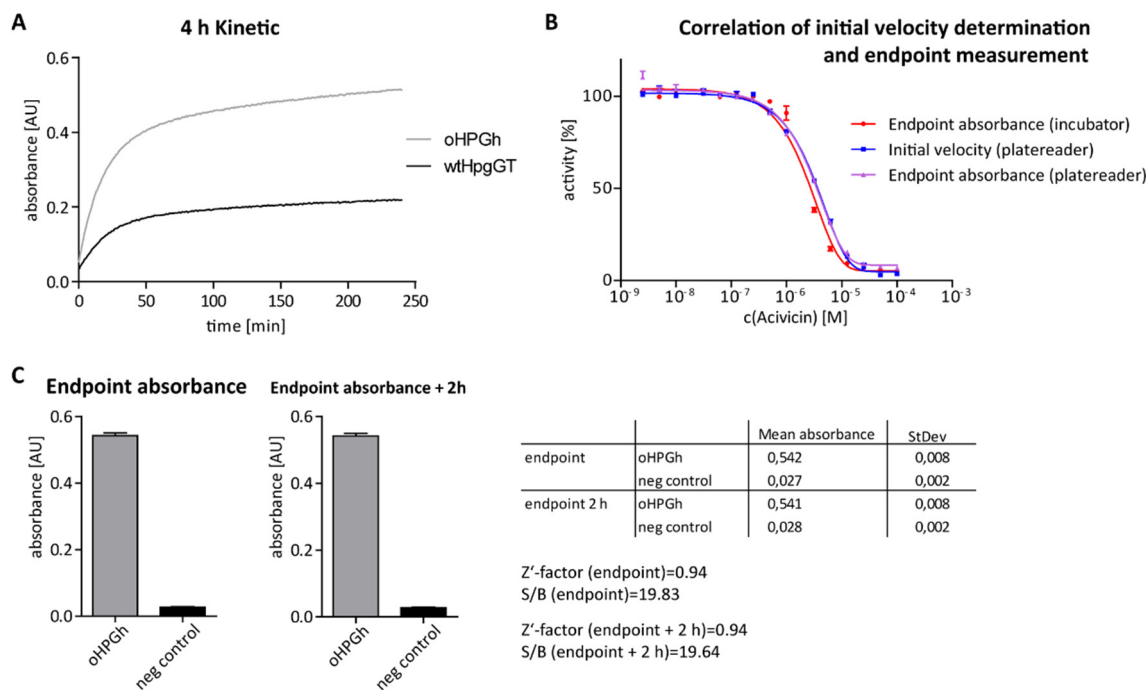
Figure 39: Quality of the gGT transpeptidation assay measurement

Graph **A** plots the absorbance at 405 nm of a standard transpeptidation reaction with 500 pM oHPGh and 3 nM wtHPG against time (n=52). The product absorbance increased for 4 h. Three readouts of the assay are compared in Graph **B** (n=3). The standard assay with 500 pM oHPGh was titrated with acivicin as reference inhibitor. The screening readout, endpoint absorbance after incubation in the incubator, correlated well with initial velocity measured in the plate-reader and the endpoint absorbance measured in the plate-reader. The two bar-graphs **C** contrast the endpoint absorbance (incubator) with and without (neg control) 500 pM oHPGh after 4 h incubation and after terminating the reaction with 10 % (v/v) acetic acid after 4 h and additional 2 h incubation (n=48). The corresponding data is shown in the table of graph **C**. End-point absorbances of assay with and without oHPGh were used to calculate the S/B ratio and the Z'-factor.

Figure 40 summarizes data collected to investigate the HTS applicability of the gGT transpeptidation assay. The coefficient of variability for the readout signal across the plate was 2.42 % and therefore well beneath the required maximum of 10 %. However, it has to be noted that measurements in wells at the boarder of the plate tended to yield slightly reduced values. The reaction could efficiently be terminated with 10 % (v/v) acetic acid and the readout signal was stable for 2 hours (also see Figure 39 C). Furthermore, the assay tolerated up to 8 % of DMSO, which is the predominant solvent of screening compounds. With these findings, it can be stated that the gGT transpeptidation assay can be used for high throughput screening in the 96-well format.

A **Plate Stability**

99%	96%	99%	96%	99%	97%	98%	97%	97%	93%	98%	92%
95%	100%	100%	100%	101%	99%	100%	100%	99%	100%	100%	96%
96%	103%	100%	101%	101%	101%	100%	102%	100%	103%	103%	98%
95%	102%	100%	103%	103%	103%	102%	102%	103%	104%	102%	97%
98%	101%	99%	103%	99%	103%	102%	103%	103%	101%	101%	99%
99%	104%	98%	97%	102%	99%	102%	102%	101%	101%	103%	97%
99%	102%	100%	98%	102%	97%	100%	101%	102%	101%	99%	97%
100%	101%	101%	102%	98%	100%	99%	102%	100%	101%	99%	101%

Deviation of Single Values from Mean

- up to 5% >Mean
- more than 5% >Mean
- more than 10% >Mean
- up to 5% <Mean
- more than 5% <Mean
- more than 10% <Mean

B **Signal stability**

endpoint absorbance 4 h incubation

99%	96%	97%	97%	100%	97%
99%	102%	100%	96%	100%	100%
98%	101%	100%	100%	100%	102%
99%	100%	102%	101%	101%	103%
100%	99%	100%	102%	102%	101%
101%	99%	99%	99%	102%	100%
102%	100%	102%	101%	101%	102%
99%	101%	100%	100%	98%	100%

endpoint absorbance 2 h after Stopp

99%	97%	97%	97%	100%	97%
98%	101%	100%	97%	99%	100%
98%	101%	100%	100%	100%	102%
99%	100%	102%	101%	101%	103%
100%	99%	100%	102%	101%	101%
100%	99%	99%	99%	102%	100%
101%	100%	101%	101%	100%	101%
99%	101%	100%	100%	98%	100%

C **DMSO tolerance**
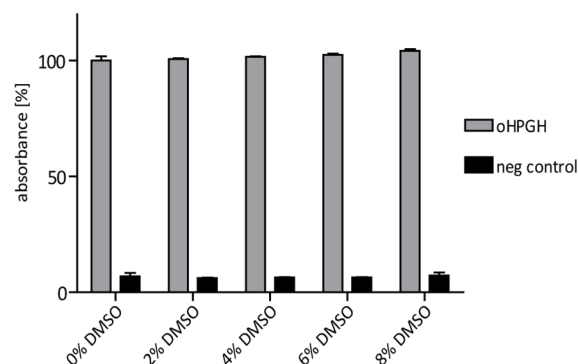
Figure 40: HTS-applicability of the gGT transpeptidation assay

Figure **A** illustrates the signal distribution in the 96-well plate (n=3). The standard assay with 500 pM oHPGh was incubated for 4 h and endpoint absorbance was measured. The single values are given relative to the overall mean of the plate. Figure **B** depicts the stability of the endpoint absorbance signal after stopping the reaction with 10 % (v/v) acetic acid. The signals measured 2 h after reaction termination are indicated relative to the mean before the termination. Graph **C** outlines the DMSO tolerance of the standard assay with up to 8 % (v/v) DMSO.

Specificity tests of novel inhibitory compounds were performed with the enzymes CjgGT, EcgGT and HsgGT. The two bacterial gGTs were kindly provided by Dr. Christian Bolz[325]. Concentrations needed for the assay format were optimized with regard to the 4 h increase of absorbance. HsgGT was prepared from HepG2 cells. The final product was highly active in the gGT transpeptidation assay but the concentration was too low to be determined. Therefore, the volume of preparation needed per reaction was determined. 800 pM CjgGT, 8.4 nM EcgGT and 0.0075 µL HsgGT preparation per reaction met the set criteria (Figure 41).
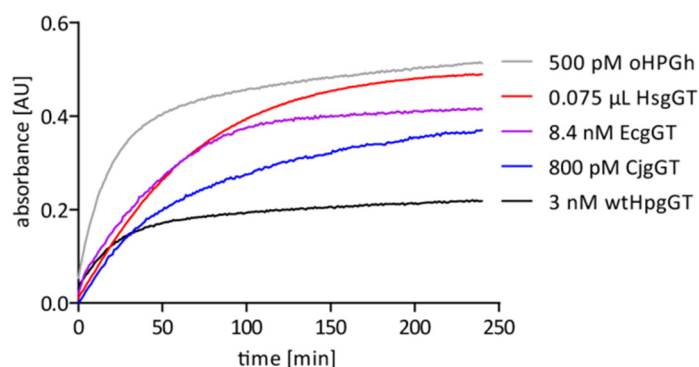
Figure 41: 4 h kinetics of gGTs used for specificity estimation

The graph shows the absorbance increase of the standard transpeptidation setting with the enzymes used for specificity estimation against time (oHPGh and wtHPG: n=52; HsgGT, EcgGT, and CjgGT: n=3). The absorbance of the reaction product increases for 4 h.

The hydrolysis assay for the γ-glutamyl transpeptidase was established to investigate interactions of identified inhibitory compounds with the enzyme. In this assay, only compounds that interact with the γ-glutamyl donor-substrate binding site or the γ-glutamyl binding site can reduce the enzymatic activity. In accordance with the transpeptidation assay, the substrate DgGpNA was used in a final concentration of 100 µM and the enzyme concentration was adjusted for product formation over a reaction time of 4 h. 30 nM of wtHPG were needed to fulfill these criteria. The Michaelis-Menten kinetic was determined as given in Figure 42. The turnover number k_{cat} is more than tenfold reduced compared to the transpeptidation assay.

	30 nM wtHPG
K_M	17.39 ± 3.26 µM
v_{max}	1.13 ± 0.03 µM/min
k_{cat}	38 ± 1 min^{-1}
R^2	0.9291
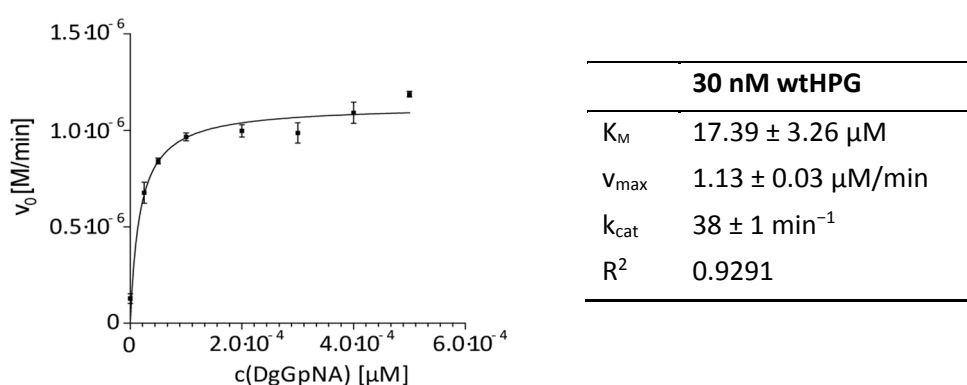
Figure 42: Michaelis-Menten kinetic for the gGT hydrolysis assay

The initial reaction velocities wtHPG were measured with varying concentration of DgGpNA (n=3). The data were fitted in GraphPad Prism to obtain the Michaelis-Menten curve and parameters.

6.2.4 Inhibitor identification

In contrast to the SaSrtA screening approach, the DZIF natural compound library did not yield any active compounds for the HPG. Thus, the crystal structure of the HPG was used to identify compounds that bind to its active site *in silico*. However, known inhibitory compounds were needed as a starting point to efficiently model a variety of new promising scaffolds using the PriaxPlore® technology. This approach uses a chemical space of compounds that is defined by either products of the company's specific multi-component reaction (MCR) or compounds from vendors and PubChem resulting in more than 200 Mio compounds in total. This chemical space is then searched for 2D connectivity similarity and 3D geometric shape similarity to previously known inhibitors as well as 3D inverse shape similarity with the target site of the enzyme. A combined similarity score is defined for each compound and a ranked list of hits is deduced (performed by Priaxon AG).

Literature search revealed ten derivatives of an inhibitory scaffold (Figure 43) published in context of the human gGT[342]. Those were synthesized by Priaxon and tested for their inhibitory effect on the *H. pylori* enzyme. An overview is presented in Table 19. The compounds were tested in three concentrations (1 mM, 100 µM and 10 µM) but the overall inhibition of the wtHPG was low, so that only 1 mM compound concentration was considered when comparing the effects. In general, there was a tendency that compounds with good inhibition of the human enzyme were less effective for the wtHPG and vice versa. This indicated that inhibitors specific for one of the enzymes can be

developed. Strikingly, compound #10 inhibited the wtHPG best of all compounds tested (86.9 % reduction of enzymatic activity) while no effect on the human enzyme was reported. Therefore, this structure was chosen as starting point for the development of tailored inhibitors for the *H. pylori* gGT.

	R1	R2	R3	app. K_i [µM][342] for the human gGT	inhibition [%] of wtHPG at 1 mM
#1	-Cl	-Cl		28.7 ± 1.0	no inhibition
#2		-Cl		43.3 ± 1.6	9.2
#3		-OCH$_3$		73.8 ± 2.5	22.1
#4	-Cl			75.9 ± 1.7	no inhibition
#5	-NO$_2$	-Cl		74.3 ± 6.9	54.9
#6				99.7 ± 3.1	74.6
#7	-NO$_2$	-OCH$_3$		114 ± 8.4	86.8
#8	-OCH$_3$	-OCH$_3$		226 ± 12.7	31.2
#9	-OCH$_3$	-OCH$_3$	-OCH$_3$	1115 ± 100	43.5
#10	-NHCOCH$_3$	-OCH$_3$		no inhibition	86.9

Table 19: Inhibition of wtHPG by compounds designed against human gGT[342]

The compounds were tested in a 15 min kinetic measurement with the wtHPG. The effect was calculated from the initial velocity normalized to the DMSO treated control (n=3).
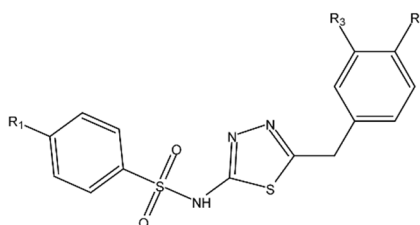
Figure 43: Core structure of human gGT inhibitor series[342]

The *in silico* screening was performed by Priaxon. In detail, this included the aforementioned PriaxPlore® search technology as well as subsequent selection of the most promising compounds on the basis of *in silico* docking and molecular modeling studies. Finally, synthesis of the selected compounds was performed with the specific multi-component reaction at Priaxon AG. A tailored library of 102 compounds was developed and analyzed in the screening assay described in chapter 6.2.3.2. Another general library of 277 compounds was provided to supplement the search for inhibitors in the context of the *H. pylori* gGT.

The screening results are summarized in Table 20. The selected screening conditions led to the identification of compounds that had a much higher inhibitory potential in comparison to the series of inhibitors for the human gGT. Specifically, 60 µM, 30 µM and 15 µM of the screening compounds were used in the assay. Initial actives were defined to have more than 20 % reduction of enzymatic activity at 60 µM compound concentration. They were confirmed in triplicate measurements. To

control for compound absorbance, absorbance of compounds has been determined without enzyme addition. Thus, insolubility could be detected for many of the identified actives at higher concentrations.

	Tailored library	General library
number of compounds tested	102	277
number of initial actives	47	44
confirmed actives	34	41
≥ 90 % inhibition (60 µM)	10	4
80-90 % inhibition (60 µM)	8	4
60-80 % inhibition (60 µM)	5	19
40-60 % inhibition (60 µM)	3	7
20-40 inhibition (60 µM)	8	7
rate of confirmed actives in library	33.33 %	14.80 %

Table 20: Screening of a tailored and a general library with *H. pylori* gGT

Initial screening of the library compounds was performed in single measurements at 60 µM, 30 µM and 15 µM. Data from three experiments were normalized to DMSO treated controls and averaged to confirm the identified actives. They were categorized into five groups after background subtraction.

The rate of confirmed actives was more than twofold higher in the tailored library compared to the general library. Additionally, more highly effective compounds were identified in the tailored library (17.6 % compared to 2.9 % of compounds with more than 80 % inhibition). Therefore, the tailored approach of developing inhibitors for the gGT form *H. pylori* is superior to a random compound screening and yields more promising compound structures for further development.

	inhibition [%] at 60 µM	IC_{50} [µM]	R^2 of nonlinear regression
#11	75.78	>60	
#12	94.80	>60	
#13	89.73	2.43 ± 0.32	0.9910
#14	78.23	10.46 ± 9.70	0.9873
#15	86.54	34.16 ± 0.90	0.9822
#16	93.49	13.91 ± 1.24	0.9738
#17	89.41	21.79 ± 1.70	0.9639
#18	90.14	>60	
#19	93.64	4.53 ± 0.31	0.9695
#20	81.47	8.12 ± 2.60	0.9845
#21	95.21	2.75 ± 0.19	0.9846

Table 21: IC_{50}-values of confirmed actives for scaffold selection

The IC_{50}-values were determined using suitable ranges of compound concentrations for fitting the data with sigmoidal dose-response non-linear regression (GraphPad Prism, n=3).

Eleven compounds were prioritized on the basis of their initial potency, the conclusiveness of the *in silico* model, and their physico-chemical properties. Their IC$_{50}$-values were determined to enable the final ranking (Table 21). The range of compound concentrations to be measured was estimated on the basis of the concentration dependency analyzed in screening and primary active confirmation (60 µM, 30 µM and 15 µM). The data from three reactions was normalized to DMSO treated controls and averaged. The values were fitted with non-linear regression for a sigmoidal dose-response with variable slope in GraphPad Prism. For three of the chosen compounds, it was not possible to determine the IC$_{50}$-value as they were not sufficiently water-soluble to measure higher concentrations as needed.

The determined IC$_{50}$-values allowed the identification of the two most promising scaffolds A and B from the corresponding compounds #13 and #21. Analysis of these data is depicted in Figure 44.

In the next step, these scaffolds were subjected to ample derivatization to ultimately determine the structure-activity relationship (SAR), which is needed to increase the potency of the rationally designed compounds and enable hit-to-lead transition.
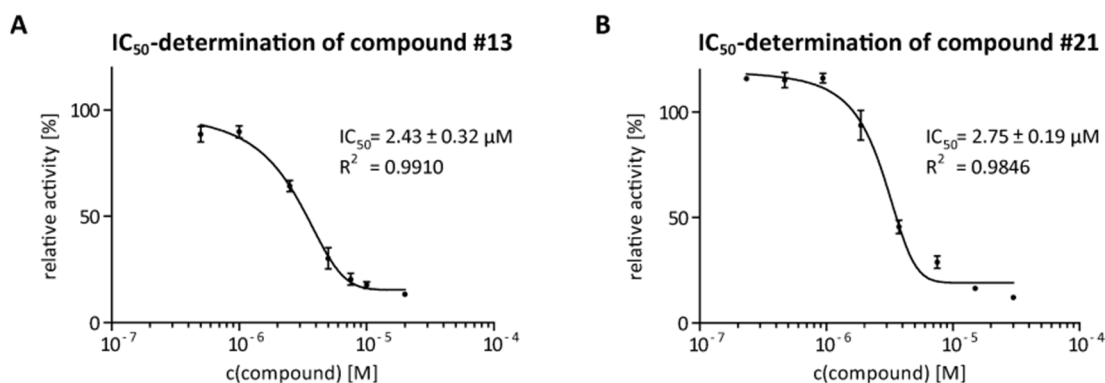
Figure 44: IC$_{50}$-determination of the two most promising scaffolds against HPG activity

The compounds were used in suitable concentration ranges to achieve the non-linear fit of the initial velocities measured (n=3). In the case of compound #21, the apparent maximal velocity of the reaction did not match the DMSO-treated control. This is due to precipitation of the compound, which confounded the measurement. Nevertheless, the measurement was well reproducible and the fit of the data was good, so that it could be used for ranking of this compound.

23 derivatives with scaffold B were produced and assayed for their inhibition of the *H. pylori* gGT. Although SAR-determination seemed feasible, development of this scaffold was not persued due to marked instability of these compounds.

Therefore, scaffold A was prioritized for optimization. Three derivatives of this scaffold had been included already in the tailored library where compounds #13 and #14 were highly active (Table 21) while a third compound was less active in screening assay and triplicate verification of primary actives (24.2 % reduction of enzymatic activity at 60 µM compound concentration) and did not qualify for IC$_{50}$-determination. This preliminary SAR analysis thus provided a valid starting point for hit development. In summary, 40 derivatives with scaffold A were produced after intensive molecular modeling and selection of compounds to validate the deduced SAR modeling data. As *in silico* modeling proposed that compounds based on scaffold A most likely bind to the acceptor-substrate site of the *H. pylori* enzyme, it was also tried to additionally address the γ-glutamyl binding channel

by further addition of substituents to the scaffold. However, these compounds had no inhibitory effect in the assay and will not be discussed in the SAR-determination.

	R1	R2	IC$_{50}$ [µM] (R^2)	inhibition [%] at 60 µM compound		
				CjgGT	EcgGT	HsgGT
#13			2.43 ± 0.32 (0.9910)	55.92	21.98	inactive
#14			10.46 ± 9.72 (0.9873)	87.74	n.d.	26.81
#22			8.34 ± 0.30 (0.9667)	86.36	inactive	inactive
#23			inactive	n.d.	n.d.	n.d.
#24			inactive	n.d.	n.d.	n.d.
#25			3.30 ± 0.20 (0.9714)	85.52	inactive	inactive
#26			19.12 ± 1.35 (0.9899)	91.61	inactive	5.40
#27			5.26 ± 0.31 (0.9669)	2.60	5.35	inactive
#28			3.40 ± 0.31 (0.9854)	94.98	61.54	inactive
#29			inactive	15.19	inactive	inactive
#30			inactive	n.d.	n.d.	n.d.
#31			inactive	n.d.	n.d.	n.d.
#32			inactive	2.60	5.36	inactive
#33			inactive	n.d.	n.d.	n.d.
#34			7.55 ± 0.94 (0.8764)	54.83	42.09	inactive
#35			2.64 ± 0.17 (0.9563)	76.51	1.06	inactive
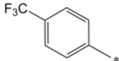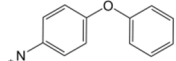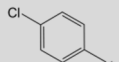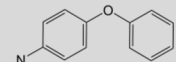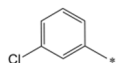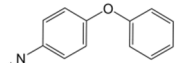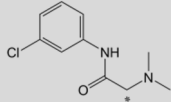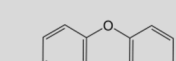
	R1	R2	IC$_{50}$ [µM]	*C. jejuni*	*E. coli*	*H. sapiens*
#36	F$_3$C-phenyl	*N*-phenoxyphenyl	4.82 ± 0.36 (0.9933)	inactive	inactive	inactive
#37	Cl-phenyl	*N*-phenoxyphenyl	2.70 ± 0.81 (0.9920)	82.23	inactive	34.97
#38	Cl-phenyl	*N*-phenoxyphenyl	1.28 ± 0.15 (0.9830)	83.79	inactive	30.01
#39	Cl-phenyl amide	*N*-phenoxyphenyl	1.10 ± 0.09 (0.9394)	78.70	62.95	35.44

Table 22: *H. pylori* gGT inhibtion of the scaffold A series

The IC$_{50}$-values were determined using suitable ranges of compound concentrations for fitting the data with sigmoidal dose-response non-linear regression in GraphPad Prism (n=3). Inactive compounds exhibited no inhibition at 60 µM concentration in the transpeptidation assay.

The specificity of the compounds' effects was assessed by determining their gGT activity reduction at 60 µM concentration for the enzymes of *C. jejuni*, *E. coli* and *H. sapiens* (n=3, n.d.: not determined).

Table 22 gives an overview of the data produced for the determination of the SAR for scaffold A. The selection of the compounds shown exemplifies the identification of the most potent inhibitor of the *H. pylori* gGT series identified in this work.

As mentioned above, compounds #13 and #14 from the tailored library already share the prioritized scaffold A. They differ in both substituents R1 and R2.

For compound #13, R2 is a *p*-phenoxyphenyl group, and for compound #14, it is a *p*-chlorophenyl group, both are coupled to the scaffold via a nitrogen atom. When exchanging R2 of #14 with the respective one of #13, the IC$_{50}$-value decreases from 10.64 µM to 8.34 µM (compound #22). This indicates that both residues occurring in compound #13 are more effective than those of #14.

When exchanging R2 of compound #13 to a methyl ether or hydroxyl moiety (#23 and #24) the inhibitory effect was lost. This clearly states that R2 is significantly involved in target binding. Limited changes of the *p*-phenoxyphenyl group such as adding an *o*-chloro moiety to the phenoxy group, using a *m*-phenoxyphenyl group or adding a methylene moiety between phenyl ring and nitrogen atom or phenyl ring and ether bond (compounds #25-28) neither abrogated the inhibitory effect nor rendered the compounds more effective. More pronounced changes of R2 as in #29-32 lead to inactive compounds, which can be explained in different ways. Firstly, the *p*-phenoxyphenyl group may be best suited to bind to the corresponding region of the target enzyme, or secondly, the *in silico* model may not be ideal and cannot identify better substituents to address the *H. pylori* gGT. Thirdly, only those compounds that could be prepared by the specific MCR were synthesized at Priaxon and could be analyzed for SAR-determination. As a consequence, further optimization was focused on R1.

Substituent R1 of compound #13 is a *p*-methoxyphenyl group whereas it is a phenyl group for compound #14. As stated above, the effects of these two substituents are directly compared by analyzing compound #22 and #13. The *p*-methoxyphenyl group leads to increased inhibition of the *H. pylori* gGT. The positioning of the methoxy group seems to be important because *o*-methoxyphenyl as substituent R1 rendered compound #33 inactive. The *p*-methoxyphenyl group was extended by coupling it via an amide bond to a tertiary carbon atom that is bound to an additional

morpholine ring via its amine moiety. This yielded compound #34, which was active with an IC_{50}-value of 7.55 μM. Since *in silico* data proposed that it was advantageous to add the amide bond to the *p*-methoxyphenyl, the aforementioned morpholine ring was exchanged with a dimethyl-amine group in compound #35 (R1 = (*N*-(*p*-methoxyphenyl)-2-(dimethylamino)acetamide)). This compound had an IC_{50}-value of 2.64 μM and was therefore as active as compound #13.

A further attempt was to modify the R1 phenyl ring and substitute the methoxy group for a trifluoromethyl group or a chloro moiety. Compounds #36 and #37 both inhibited the HPG with the latter being virtually as active as compound #13 (IC_{50}= 2.70 μM). The chloro group was also tested in *meta*-position on the phenyl substituent of compound #38. Unlike with the methoxy substituted version, this compound was more active than the originally identified compound #13 with an IC_{50}-value of 1.28 μM. Since the rational design proposed the amide bond for the R1 substituent and the additional dimethylamine group, compound #39 combined this finding with the *m*-chlorophenyl group, which yielded the highest activity of the series (IC_{50}=1.10 μM; R1 = (*N*-(*m*-chlorophenyl)-2-(dimethylamino)acetamide)).

Taken together, scaffold A was most active with a *p*-phenoxyphenyl group as substituent R2, which can convey non-covalent interaction via π-stacking and hydrogen-bonding with suitable spatial and steric constitution. Substituent R1 yielded the highest inhibitory effect on the *H. pylori* gGT as an amide coupled *m*-chlorophenyl group with the additional dimethylamine moiety, which together potentially mediate halogen bonding, hydrogen bonding, dipole-dipole interaction, π-stacking and hydrophobic interaction with suitable spatial and steric constitution.

The next requirement was to assess the specificity of the active compounds in the series, allowing a more educated prioritization to be done. Hence, the effect of these compounds on the gGTs from *C. jejuni*, *E. coli* and *H. sapiens* was assayed. The conditions were set up according to the screening assay for the gGT form *H. pylori* (chapter 6.2.3.2, Figure 41). Again, the effect was validated on the basis of gGT activity inhibition at 60 μM compound concentration (Table 22).

Most of the compounds tested had a marked inhibitory effect on the gGT from *C. jejuni*, which was expected due to its close phylogenetic relation to *H. pylori*. The inhibition of *E. coli* gGT was varying, and seemed to mostly depend on the substituent R2 when comparing those compounds with the methoxyphenyl group as R1. For example, compound #13 and #28 inhibited the EcgGT but compound #26 and #27 were not or only slightly inhibitory. Hence, minor changes of the R2 phenoxyphenyl group influenced the compound's effect on EcgGT. Nevertheless, R1 could also drive the compounds' specificity for the *E. coli* enzyme as can be deduced by comparing compound #35 and #39. These two compounds only differ in the phenyl substituent being a *p*-methoxy moiety or an *m*-chloro moiety, which rendered the compound virtually inactive or the most active against EcgGT in this series, respectively.

Most important is, however, the compounds' selectivities against the human gGT. Most compounds of this series did not inhibit the HsgGT. Yet, compounds #37-39, which share a chloro-moiety on their R1 phenyl ring, were inhibitory with 30-35 % HsgGT transpeptidation activity reduction at 60 μM concentration. Unfortunately, these compounds include those that were most active against the

H. pylori gGT. Including compound #39 being active also against the *E. coli* enzyme, compound #35 with R1 being the extended methoxyphenyl group was therefore preferable and chosen for hit-to-lead development.

In order to prepare for further hit-to-lead development of the identified hit compounds #13 and #35 the physical binding of these compounds to the target enzyme had to be proven. Furthermore, the *in silico* model of compound binding had to be confirmed with the corresponding crystal structures.

As a first test to investigate the proposed binding of the compounds to the acceptor binding sites, selected compounds were assayed in the γ-glutamyl transpeptidase hydrolysis-only assay. If the compounds bind to the enzyme as proposed, no inhibition of the hydrolysis activity was expected as the substrate of the reaction acts via the donor-binding site only. Taking into consideration that the tenfold concentration of wtHPG was needed in the hydrolysis assay compared to the transpeptidation assay, it is striking that compound #34, which is very similar to #35, inhibited the hydrolysis by >90 % at 60 μM (transpeptidation assay: 80 % inhibition at 60 μM). Still, compound binding to the acceptor binding site could not be excluded on the basis of results from the hydrolysis assay as an induced fit mechanism could also affect the donor and glutamyl binding sites. With this finding, it was of utmost importance to analyze the physical binding of the compounds to the *H. pylori* gGT. The exact binding mode had to be illuminated to enable further compound optimization.

Table 23 lists measured solubilities of three prioritized compounds that were already indicated to have limited solubility in the turbidity measurements. For analysis of compound binding and crystallization, the solubility needs to be at least ten times higher than the corresponding IC_{50}-value but is preferably higher than 100 μM. Only the solubility of compound #13 is ten times higher than the determined IC_{50}-value but this proved to be insufficient as well. For compound #25 and #38, solubilities were clearly below the needed level.

	IC_{50} [μM]	solubitlity [μM]
#13	**2.43** ± 0.32	28
#25	**3.30** ± 0.20	13
#38	**2.64** ± 0.17	0.18

Table 23: Solubility of selected compounds

The solubility of selected compounds in 1×PBS was determined at Proteros biostructures GmbH. It needs to be at least ten times higher than the determined IC_{50}-value but is preferably at above 100 μM to be reliably analyzed in binding and crystallographic experiments.

In order to verify the physical binding of the compounds, two approaches were tried. Firstly, NMR studies were performed to identify induced shifts of binding compounds (in collaboration with Dr. Grzegorz Popowicz, Helmholtz Zentrum München). This was not possible due to insufficient solubility of the compounds (Table 23).

Secondly, binding was analyzed with microscale thermophoresis (MST) at the NMI in Tübingen (in collaboration with Anne Mehnert and Dr. Nicole Schneiderhan-Marra, Group of Dr. Thomas Joos).

For this analysis, detergent had to be added in concentrations above its critical micellar concentrations to prevent protein aggregation in the sample capillary tube. However, the detergent also led to reduced compound availability as these were dissolved in the micellar phase, which was confirmed in the standard gGT transpeptidation assay with detergent addition. Therefore, interaction could not be measured via MST either.

In order to obtain structural data of compound binding, two approaches were attempted. Firstly, soaking of existing wtHPG crystals was tried at Proteros Biostructures GmbH. Secondly, co-crystallization of two *H. pylori* gGT constructs with the prioritized compounds was attempted by Dr. Grzegorz Popowicz (Helmholtz Zentrum München). Both of these approaches failed due to the limited solubility of the compounds.

In conclusion, it was possible to identify novel inhibitory compounds for the *H. pylori* γ-glutamyl transpeptidase with the established transpeptidation screening assay. The tailored strategy demonstrated to be superior to a general library screening approach due to a higher frequency of potent verified actives. It was possible to identify promising scaffolds for compound development. The potency of derivatives of scaffold A was tractable and yielded a convincing SAR. Taken together with the specificity profile, a subclass of compounds could be prioritized to advance hit-to-lead development. Unfortunately, the solubility of the selected compounds was insufficient to prove direct binding of the compounds to the HPG and for obtaining information on the precise mode-of-action. Without these essential pieces of information, a rational non-clinical development of these hit compounds into lead candidates for *in vivo* ADMET studies was not yet feasible and the project was therefore put on hold.

Input from complementary approaches such as fragment-based drug discovery could help to define the pharmacophore of the HPG, and thereby also suggest the binding modes of the inhibitors described in this work. Detailed knowledge of the interaction between HPG and inhibitory compounds would facilitate the optimization of currently adverse characteristics, i.e. the limited water solubility, and could thus revive this project.

6.3 Validation of novel HP candidate proteins as therapeutic targets

Both targets for novel anti-infectives focussed on in chapters 6.1 and 6.2 are characterized by the fact that they are conveniently accessible for inhibition. Sortase A is an enzyme found in the cytoplasmic membrane of many Gram-positive bacteria[137], whereas HPG is targeted to the periplasm but can also be found in supernatants of *H. pylori*[257, 302]. Drugs addressing targets in the bacterial cytoplasm have to fulfill a narrow profile of physicochemical demands to enter the cell. Additionally, they are prone to be depleted from their target site due to efficient bacterial efflux systems. Therefore, inhibitory agents that are not required to enter the bacterial cytoplasm have an increased chance of fulfilling their intended purpose.[163]

Consequently, identification and characterization of novel surface exposed bacterial proteins is a valid approach for anti-infective target discovery. Several cutting-edge techniques qualify to obtain such new information. Indeed, genome and proteome based methods are ever more applied to the field of target discovery yielding a plethora of information, which needs to be validated with regard to biological relevance in infection and suitability for drug development. [29, 343, 344] Here, surface-exposed protein candidates had been identified in a *H. pylori* surface shaving approach (adapted from Grandi, 2006[311]) by Tobias Kruse (unpublished).

In this work, eight novel *H. pylori* target candidates identified with this optimized method were prepared for in-depth validation. Cloning and protein production were successfully performed. Antisera were generated to examine the proposed surface exposure in a flow cytometry based experiment. The recombinant proteins were also used to analyze characterized human sera for antibody responses, allowing first conclusions regarding their antigenicity and patient exposure during infection. Moreover, kock-out mutants gave first information on weather or not these novel proteins are essential for *in vitro* growth and viability.

6.3.1 Cloning and recombinant production

The amino-acid sequences of the novel target proteins were analyzed *in silico* to be able to exclude signal peptides and terminal transmembrane regions from the recombinant proteins. The selected gene regions were amplified as described in chapter 5.2.3 from *H. pylori J99* with overhangs allowing cloning of the C-terminal His$_6$-tagged constructs. To this end, primers CD_P29-40 and 45/46 were utilized to generate the plasmids pET30b HPx-h and pSCask HPx-h. The cloning strategy was adapted to apply to all target candidates allowing classical restriction cloning for pET30b constructs (chapters 5.2.9 and 5.2.10) and SLiCE cloning for pSCask constructs (chapter 5.2.11). A scheme of the obtained vectors is given in Figure 45.
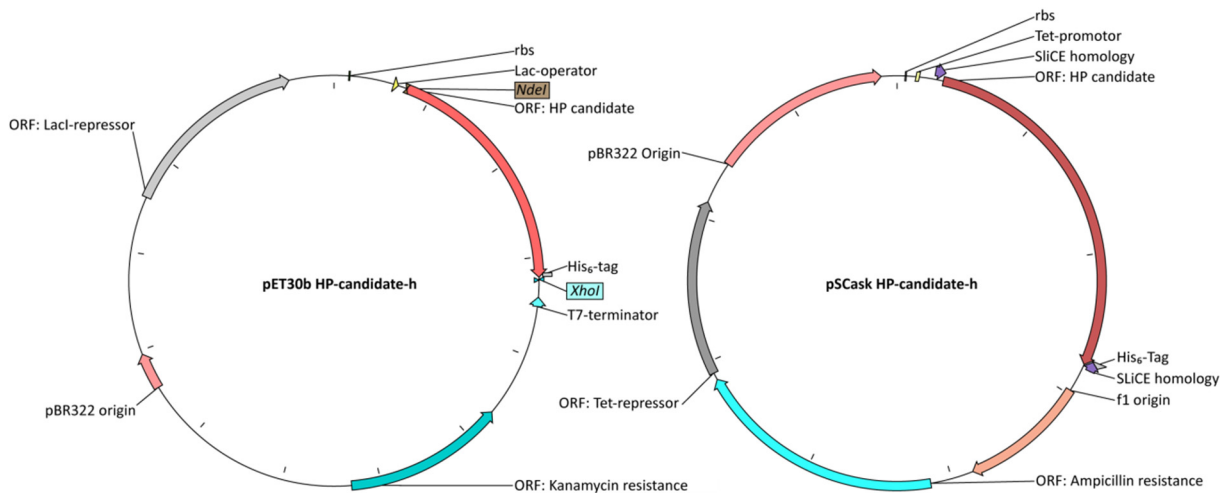
Figure 45: Plasmid maps for HP-candidate constructs

The vectors for recombinant expression of the HP candidates are shown as plasmid maps indicating the open reading frames (ORFs) for the target proteins, the selection resistance, and regulatory elements. The restriction sites NdeI and XhoI for the pET30b constructs and homology arms for SLiCE cloning in the pSCask constructs are indicated.

The process of protein production was performed as described in chapter 5.3.5. The results are summarized in Table 24. The chromatograms of the affinity purification, size exclusion chromatography and SDS-PAGEs of the final products are shown in Figure 46.

Expression vector	Culture volume	Yield (standard procedure)
pET30b Δ1-20 HP2-h*	1,5 L	10.7 mg
pET30b Δ1-43 HP3-h	200 mL	9.8 mg
pET30b Δ1-33 HP4-h	2 L	5.1 mg
pET30b Δ1-22 HP5-h	200 mL	2.2 mg
pET30b HP8-h	200 mL	9.9 mg
pSCask Δ1-31 HP1-h	800 mL	14.0 mg
pSCask Δ1-31 HP7-h	2 L	1.9 mg
pSCask HP8-h	200 mL	9.2 mg

Table 24: Expression and purification of *H. pylori* candidates

*produced by Tobias Kruse

HP1   Affinity purification (pSCask)
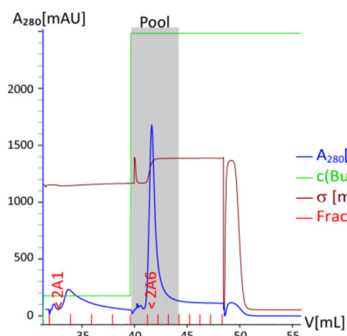
Size-exclusion chromatography (S200)
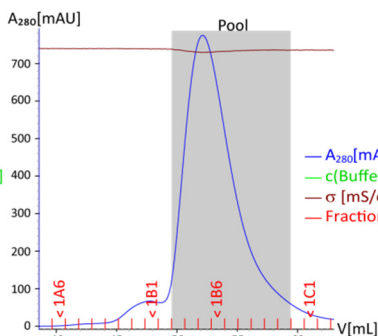
HP1 (M_w = 33.9 kDa)
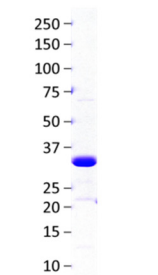
HP3   Affinity purification (pET30b)
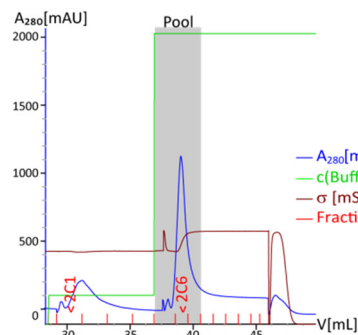
Size-exclusion chromatography (S75)
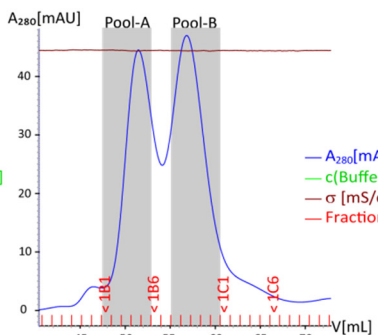
HP3 (M_w = 26.6 kDa)
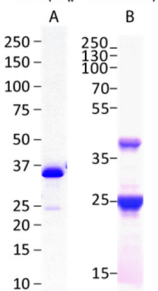
HP4   Affinity purification (pET30b)
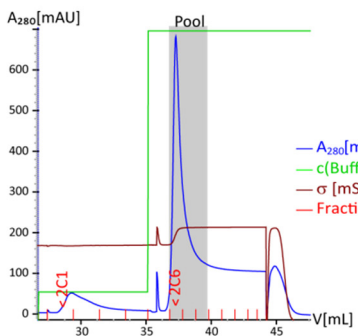
Size-exclusion chromatography (S200)
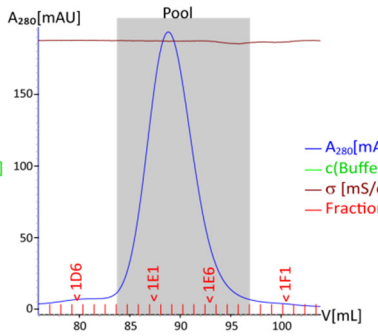
HP4 (M_w = 19.3 kDa)
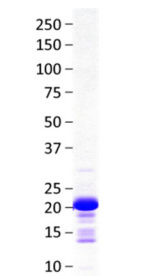
HP5   Affinity purification (pET30b)
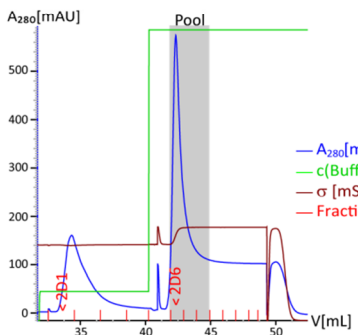
Size-exclusion chromatography (S75)
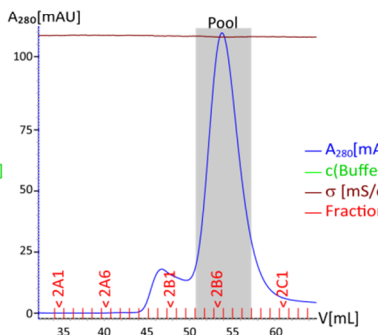
HP4 (M_w = 31.2 kDa)
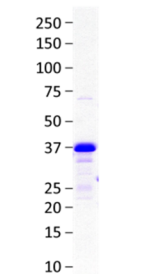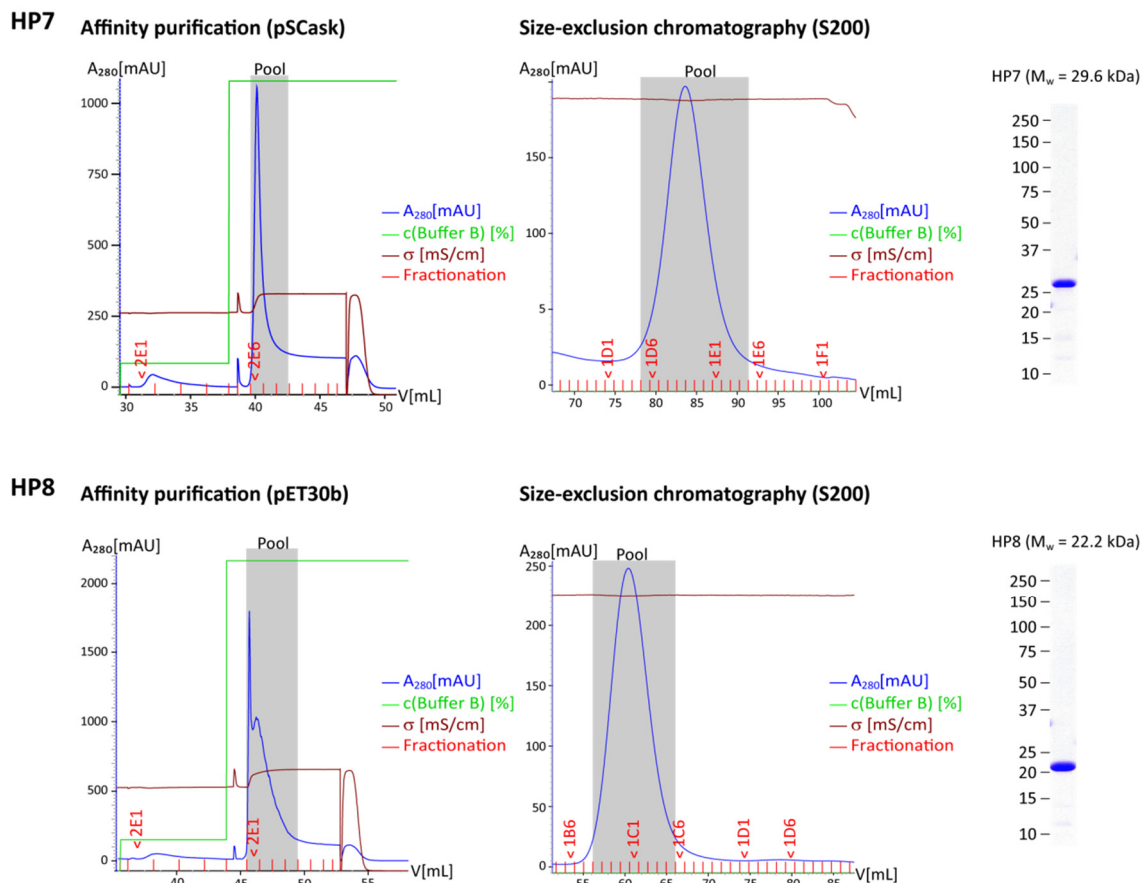
Figure 46: Purification of the recombinant HP candidates

The purification processes are presented for the recombinantly produced HP candidate-proteins HP1, HP3, HP4, HP5, HP7 and HP8. The recombinant proteins were expressed in *E. coli* BL21 with either pET30b or pSCask expression constructs. All proteins were affinity purified (HisTrap FF crude 1 mL / 5 mL) and the enriched fractions (indicated in gray) were subjected to size-exclusion chromatography (HiLoad 16/600 Superdex 75 PG or 200 PG). The final products (5 µg) are shown on the SDS-PAGEs.

The recombinantly produced HP candidates HP1, HP4, HP5, HP7 and HP8 were obtained with satisfactory purity (> 90 %) and presented the expected apparent molecular weights in SDS-PAGE analysis. Strikingly, HP3 was found to exist with two distinct forms of about 25 kDa and 36 kDa in denaturing SDS-PAGE whereas the predicted size was 26.6 kDa. Therefore, the larger form was unexpected and a gel-slice was analyzed via mass spectrometry for protein identity (TopLab; Martinsried, DE). The peptide mass fingerprint of the trypsin digested protein unambiguously (p<0.05) determined the protein to be HP3. Therefore, this protein batch was used for further investigations.

The recombinant protein HP2 was kindly produced by Tobias Kruse according to the standard purification procedure. The final product is shown on the SDS-PAGE in Figure 47 A. Several impurities could be detected. However, the protein was used for subsequent experiments to be able to perform them in parallel with all other recombinant HP candidates.

Unfortunately, HP6 could not be produced with the standard procedure. A convincing elution peak was obtained in affinity purification, but neither major peak in size-exclusion chromatography nor clear enrichment of a protein with expected size in SDS-PAGE was observed (Figure 47 B). Therefore,

this protein was excluded from further experiments, since a characterization of the multiple peaks of size-exclusion chromatography was not suitable for the scope of this approach.
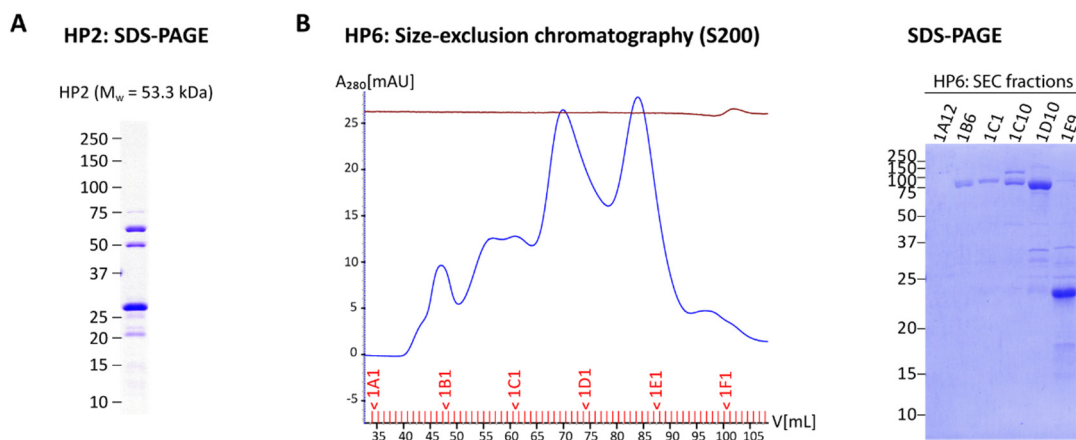
Figure 47: Recombinant production of HP2 and HP6

A HP2 was produced according to standard procedure by Tobias Kruse. The final product (5 µg) still included major impurities. **B** The size-exclusion chromatography and the corresponding SDS-Gel (HiLoad 16/600 Superdex 200 PG) revealed a widespread mixture of proteins in the affinity enriched fraction of HP6 produced from *E. coli* BL21 pET30b HP6-h.

Taken together, seven out of eight undescribed *H. pylori* proteins were cloned, produced and purified. The proteins showed no noticeable precipitation in the selected ArgPi-Buffer and serve as basis for further investigations.

6.3.2 Examination of HP candidate-protein surface-exposure

The surface exposure of the HP candidate-proteins needed to be tested. To this end, a flow cytometry based approach was chosen in which the selected proteins should be detected by labeling *H. pylori* with antibodies against the protein candidates. Therefore, antisera were generated in female BALB/c mice by Dr. Florian Anderl and Tobias Kruse. Immunization and boosts after 7, 14 and 21 days were performed with 30 µg of purified antigen and 10 µg cholera toxin as adjuvant. On day 28, the mice were sacrificed and serum was prepared. The mouse immunized with HP1 died during the experiment. However, coherence with the immunization seemed unlikely since it could be repeated without side effect later. Antiserum dilutions were tested in an ELISA (chapter 5.3.9). Figure 48 shows the dilution-dependent detection of the antigens by the generated murine sera (HP1 not included), whereas a cholera toxin (CT) control serum as well as the secondary detection antibody control with blocking reagent only yielded low ELISA signals. Thus, the sera could be used for detection of surface antigens on *H. pylori*.
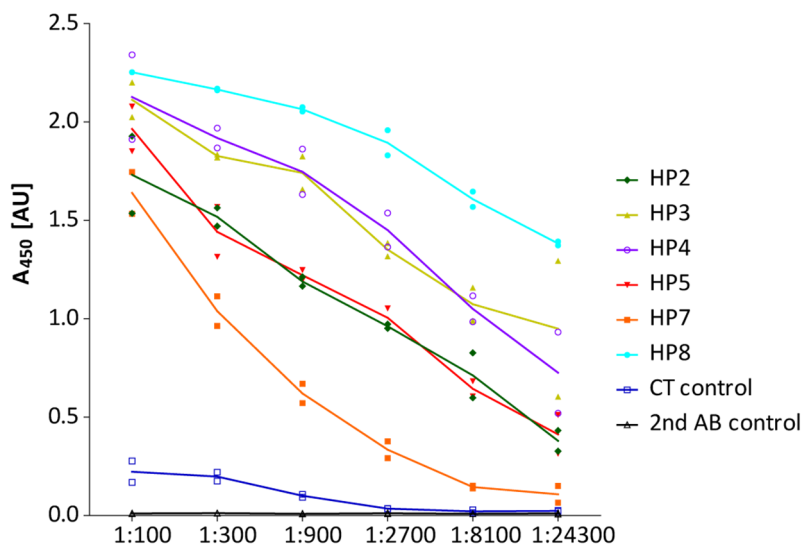
Figure 48: ELISA with generated mouse sera against HP candidates

The purified HP candidate-proteins were coated as antigens onto 96-well plates. Blocking was achieved with 5 % bovine serum albumin (BSA) in 1×PBS. A duplicate serial dilution of mouse sera against the HP candidates was set up in 5 % BSA in 1×PBS. For detection of bound antibodies, anti-mouse IgG serum conjugated with horse-radish peroxidase (HRP) was used in a 1:10000 dilution. HRP activity was detected with TMB reagent and read at 450 nm (corrected at 570 nm) after stopping the enzymatic reaction with 1 M H_2SO_4. The graph plots the recorded absorbance and indicates a dilution dependent ELISA signal for the murine sera.

To obtain purified and concentrated antibody solutions for the flow-cytometry experiment, mouse sera were subjected to protein A affinity chromatography (chapter 5.3.4).

Labeling of *H. pylori* with CFDA-SE (Carboxyfluorescein diacetate succinimidyl ester) and the purified sera was performed as described in chapter 5.3.11. The dye CFDA-SE enters the bacterial cells via diffusion and is cleaved by intracellular esterases, yielding CFSE, which is an efficient fluorophore that reacts with intracellular amines preventing its release from the cells. This additional staining of *H. pylori* was included to identify the bacteria with more reliability than relying on forward- and sideward-scatter characteristics. Purified sera against two known *H. pylori* antigens, HPG and the surface exposed protein HpaA[345], were titrated to estimate starting antibody concentrations for the HP-candidate investigation. Concentrations ranging from 0.4 µg/mL to 40 µg/mL were tested. Binding antibodies were detected with anti-mouse IgG1 conjugated with the fluorescent dye eFluor® 660. Figure 49 illustrates the gating strategy to identify eFluor® 660 positive cells in CFSE stained bacteria as well as the obtained staining frequencies. The staining result of an anti-CT serum served as control. For both HPG and HpaA, the frequency of labeled bacteria was antibody-concentration dependent. HPG was weakly recognized even though it is localized in the periplasm. Therefore, it might be useful for comparison of surface-exposed and intracellular antigen staining.
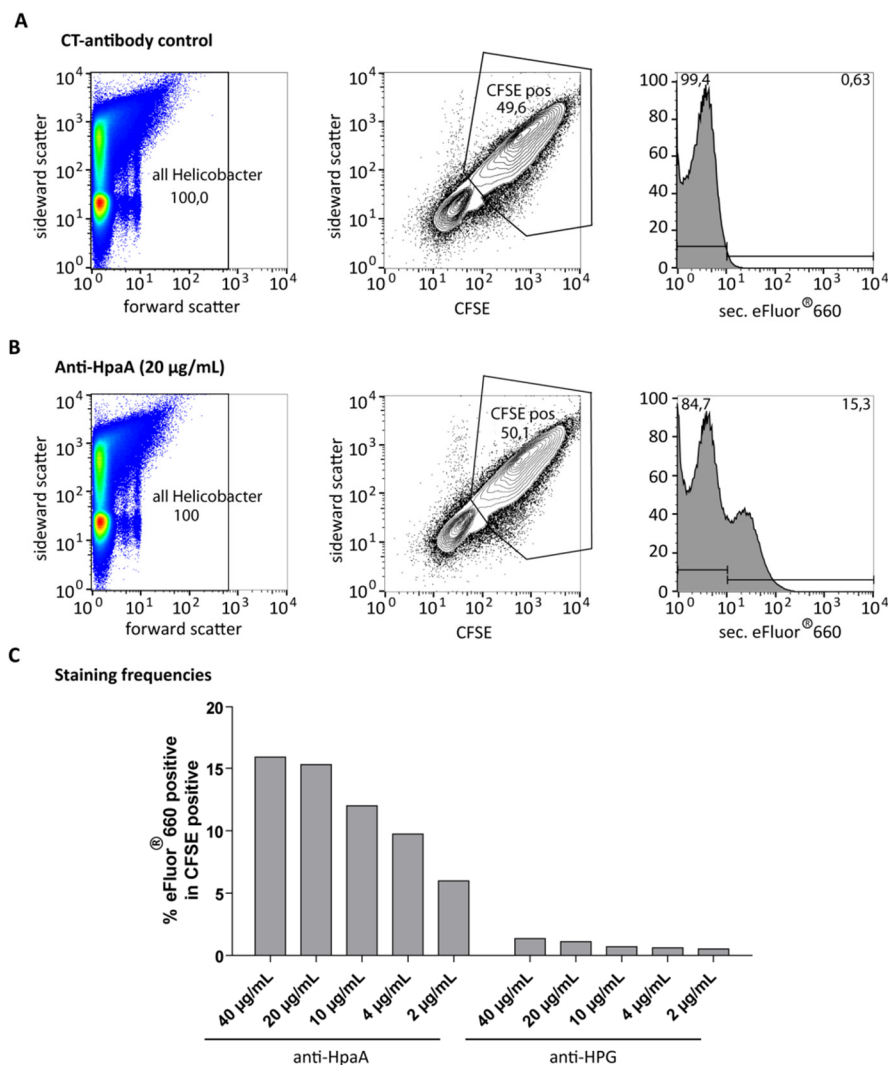
Figure 49: Titration of purified sera for labeling of *H. pylori*

CFSE stained wild type *H. pylori* J99 was labeled with varying concentrations of purified murine antibodies against the periplasmatic protein HPG and the outer membrane protein HpaA. **A/B** All particles displayed in the forward- and sideward-scatter dot plot (left) were used to identify the CFSE positive *H. pylori* (middle). **A** To quantify the eFluor® 660 positive cells, the bacteria treated with CT-control serum were used to define a cut-off intensity (right). **B** Cells with higher eFluor® 660 intensities than this defined cut-off were assumed to be positively stained for HpaA (right) and HPG, respectively. **C** The frequency of eFluor® 660 positive cells is plotted for the two antigens and is found to be dependent on the concentration of the purified murine sera.

Clearly, an antibody concentration of 20 µg/mL was sufficient for detecting the antigen HpaA on the surface of *H. pylori*. Figure 50 and Figure 51 display the *H. pylori* J99 staining frequencies obtained with purified murine sera against HP candidates and HPG as well as the established surface exposed *H. pylori* proteins HpaA and HopQ[346]. The staining with serum obtained from mice immunized with cholera toxin only has been used as negative control to determine staining of the tested antigens. In accordance to the HpaA titration-experiment, purified sera were used in a concentration of 20 µg/mL, even though antibody affinities and protein quantity on the surface of *H. pylori* might divert dramatically for the HP candidates. However, limited supply of the murine antisera justified a precluded individual titration experiments for each HP candidate.
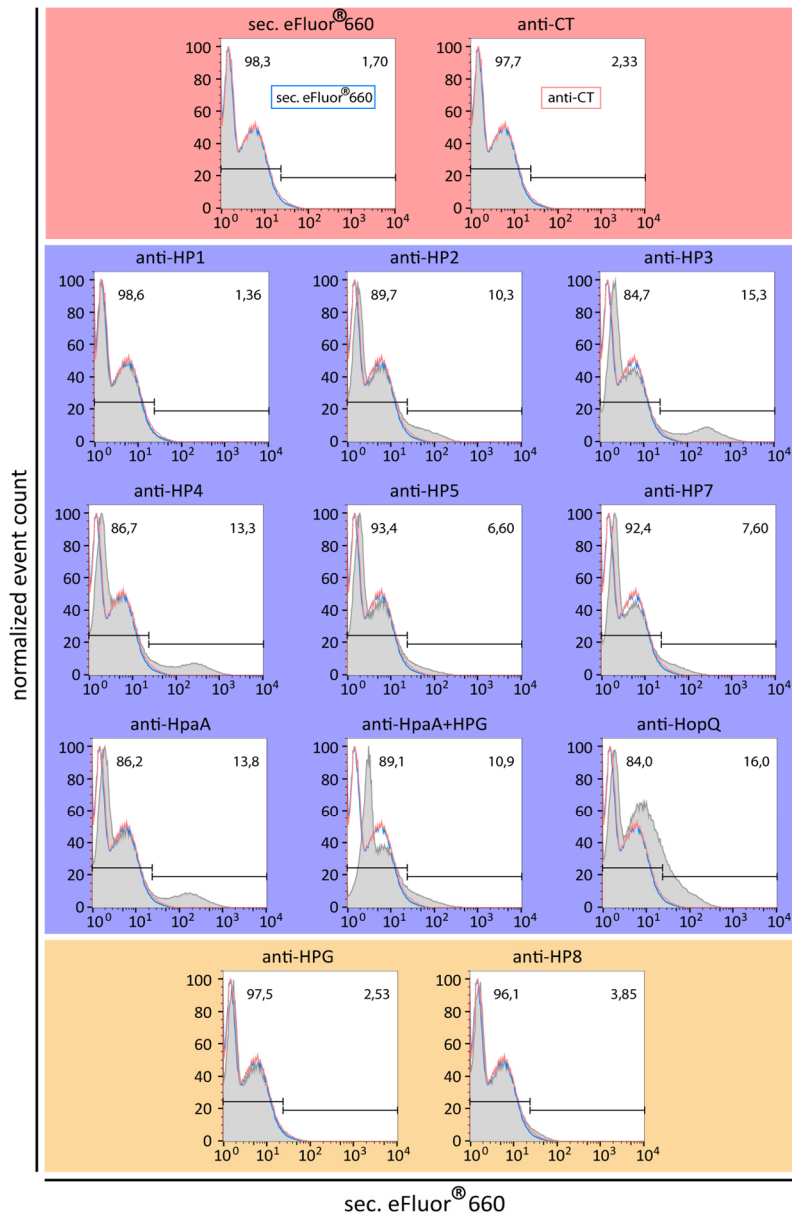
Figure 50: Antibody staining and flow-cytometry analysis of *H. pylori* J99

CFSE stained *H. pylori* J99 was labeled with purified murine antibodies against HP candidate-proteins and with antibodies purified from control sera (20 µ/mL). Additionally, CT control serum was applied. The raw data of the flow-cytometry experiment with 20 µg/mL murine antibodies are displayed as histograms of eFluor® 660 intensity in CFSE positive cells. Graphs with blue background refer to stainings with murine antibodies against predicted or known surface proteins. Stainings against known intracellular proteins are indicated in orange and stainings with antibodies from control sera are indicated in pink. Every histogram also shows the curves for the secondary antibody control (blue) and the staining with the CT control serum (red).

Figure 51: Staining frequencies and MFI of *H. pylori* J99

CFSE stained *H. pylori* J99 was labeled with purified murine antibodies against HP candidate proteins and with antibodies purified from control sera (20 µg/mL). Antibody binding was detected with eFluor® 660 conjugated anti-mouse IgG1. The frequencies of eFluor® 660 positive cells within the CFSE labeled population is given in the graph **A**. The red line indicates the background of CT-staining. Graph **B** shows the mean fluorescence intensities (MFIs) of eFluor® 660 in CFSE positive cells. The CT-control was substracted from all other staining conditions. Colors were used according to the presentation of histograms in Figure 50. Blue: (predicted) surface-exposed protein, orange: intracellular proteins, pink: control stainings.

Figure 50 displays histograms of eFluor® 660 staining intensities within the CFSE positive population. The CT-control staining differs only marginally from the secondary-antibody control. Several staining outcomes have been observed with the murine sera against HP candidate-proteins and with control sera. Anti-HpaA serum stained a population of bacteria that is clearly distinguishable from the CT-control, whereas a shift of the whole population can be observed for anti-HopQ. These varying outcomes of *H. pylori* staining and flow cytometry analysis need to be carefully considered in the evaluation of HP-candidate stainings.

The bar graphs depicting the staining frequencies and the mean fluorescence-intensities (Figure 51) demonstrate the staining of surface exposed proteins. With the exception of HP1 and HPG, all antigens were detected with staining frequencies higher than the CT-control. The proposed surface proteins HP2-5 and HP7 yielded higher staining frequencies than the periplasmatic protein HPG and the cytoplasmatic protein HP8. Among the candidates, HP3 and HP4 were stained with the highest frequencies and displayed distinct populations of stained bacteria. These frequencies were comparable to the results for HpaA (+HPG) and HopQ. HP1 could not be stained with its specific antiserum. It is, however, not clear if this is caused by a lack of expression of the protein, no surface exposure, or a non-reacting antiserum. HP8 was reported to be localized in the cytoplasm. The staining frequency was higher than that of HPG but lower than the other stained surface antigens. Therefore, the flow cytometry based validation of these proteins as surface exposed or intracellular according to the used staining protocol for *H. pylori* J99 is not entirely convincing and further experimental evidence is needed.
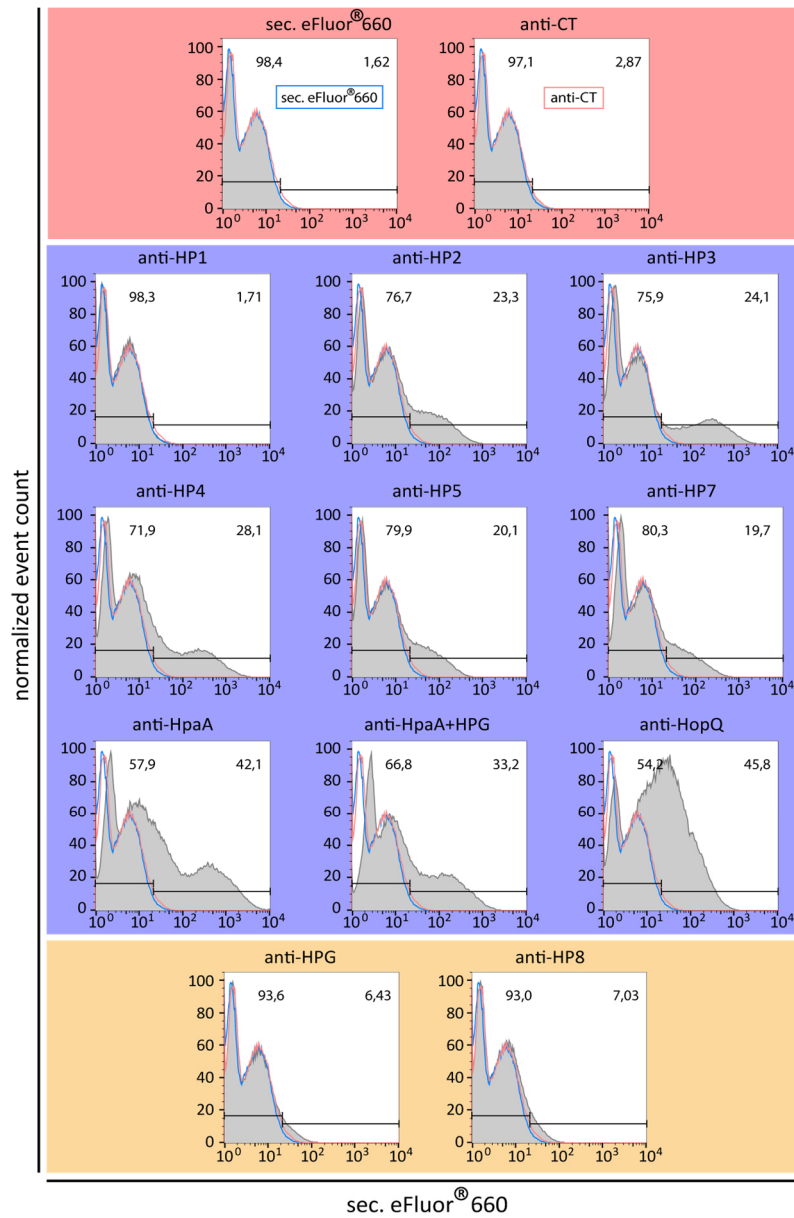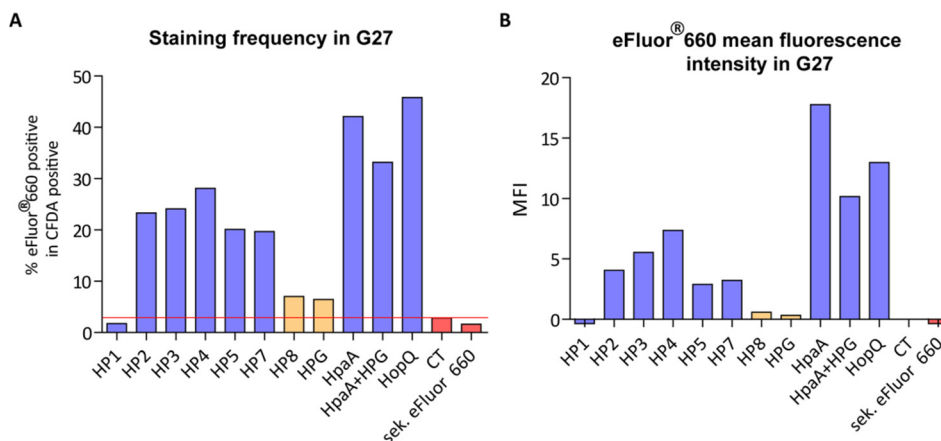
Figure 52: Antibody staining and flow-cytometry analysis of _H. pylori_ G27

CFSE stained _H. pylori_ G27 was labeled with purified murine antibodies against HP candidate-proteins and with antibodies purified from control sera (20 µ/mL). Additionally, CT control serum was applied. The raw data of the flow-cytometry experiment with 20 µg/mL murine antibodies are displayed as histograms of eFluor® 660 intensity in CFSE positive cells. Graphs with blue background refer to stainings with murine antibodies against predicted or known surface proteins. Stainings against known intracellular proteins are indicated in orange and stainings with antibodies from control sera are indicated in pink. Every histogram also shows the curves for the secondary antibody control (blue) and the staining with the CT control serum (red).

Figure 53: Staining frequencies and MFI of *H. pylori* G27

CFSE stained *H. pylori* G27 was labeled with purified murine antibodies against HP candidate proteins and with antibodies purified from control sera (20 µg/mL). Antibody binding was detected with eFluor® 660 conjugated anti-mouse IgG1. The frequencies of eFluor® 660 positive cells within the CFSE labeled population is given in the graph **A**. The red line indicates the background of CT-staining. Graph **B** shows the mean fluorescence intensities (MFIs) of eFluor® 660 in CFSE positive cells. The MFI of the CT-control was substracted from all other staining conditions. Colors were used according to the presentation of histograms in Figure 52. Blue: (predicted) surface-exposed protein, orange: intracellular proteins, pink: control stainings.

Additionally, wild type *H. pylori* G27 was stained in an equivalent setup. The obtained staining frequencies are displayed in Figure 53. In general, the frequencies of bacteria stained with murine sera against surface-exposed proteins are higher for G27 than for the strain J99. Stainings for HP2, HP3, HP5 and HP7 achieved identification of positive populations (Figure 52). For anti-HP4 and the control antisera against HpaA and HpaA+HPG, a shift of the whole population in combination with a more brightly stained population could be observed. HopQ staining resulted in a shift of the whole population as has already been observed for the strain J99. HP1 is not recognized by its specific antiserum in this experiment either. The staining frequencies and MFIs obtained with the test sera (anti-HpaA, anti-HpaA+HPG and anti-HopQ) were conciderably higher than those for the HP candidates. Nevertheless, the general profile of the HP candidate staining frequencies is comparable for both strains. Staining of the intracellular protein HP8 yielded frequencies similar to staining of HPG. Therefore, the increased staining efficiency observed for *H. pylori* G27, allows preliminary distinction between surface exposed and intracellular proteins.

Taken together, flow-cytometry based analysis of *Helicobacter pylori* surface antigens has been shown feasible using sera against known surface-exposed proteins as well as predicted candidate proteins. This was possible with *H. pylori* J99, which was used in the cloning of the HP candidate expression constructs, and with the strain G27 yielding similar patterns of staining frequencies. The sample preparation still has to be optimized to obtain meaningful results.

6.3.3 Hp knock outs of candidate genes

Helicobacter pylori knock-out mutants of the HP candidate-genes were prepared to investigate the effect on bacterial growth and survival *in vitro* and *in vivo*. Candidates influencing bacterial growth and viability *in vitro* cannot be classified as potential anti-virulence targets in the strict sense. Only HP-candidate knock-out mutants that display similar growth rate in comparison to the wild type strain *in vitro* would further be evaluated in cell culture based and *in vivo* settings to investigate their role in infection.

To create knock-out mutants for validation, five HP candidates were selected due to their potential suitability as drug targets based on sequence analysis. Among others features, predicted secretion or membrane targeting was taken into consideration. Thus, HP1, HP2, HP5, HP6 and HP7 were chosen. The PCR based cloning strategy (chapter 5.2.3) is illustrated in Figure 54.
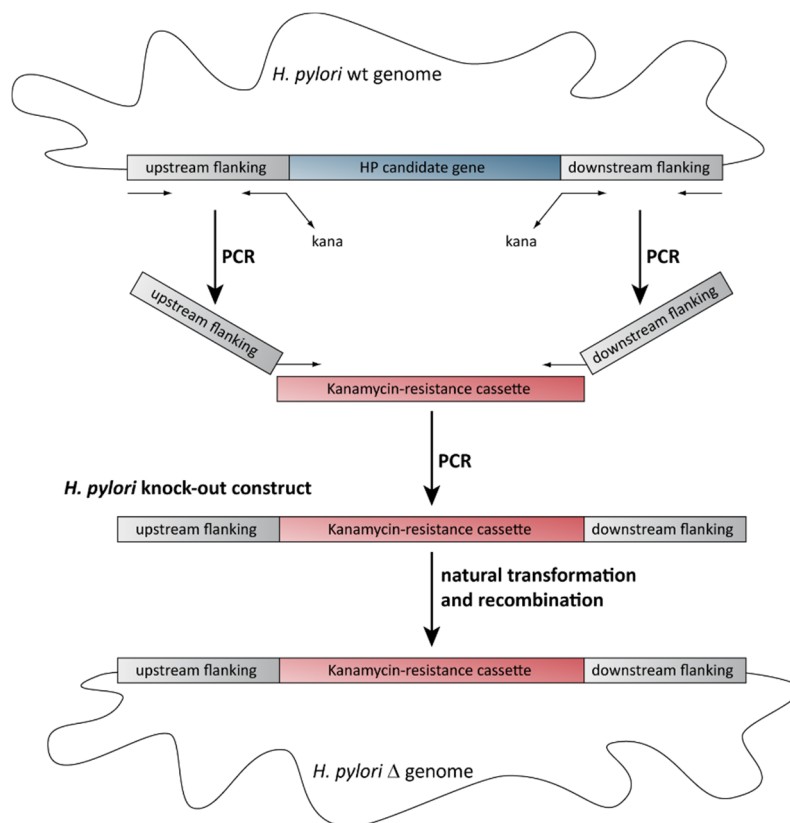
Figure 54: *H. pylori* candidate knock-out strategy

300 bp flanking sequences of the target gene were amplified with overhangs that allowed PCR-ligation with the Kanamycin-resistance cassette. The obtained *H. pylori* knock-out construct was used for natural transformation of the strain G27 yielding Kanamycin-resistant mutant strains.
(Adapted from Derbise, 2003[347])

To finally allow exchange of the target gene with the Kanamycin-resistance cassette by natural recombination, 300 bp up- and downstream flanking regions were amplified via PCR from *H. pylori* G27 genomic DNA with the primers CD_P51-54, 56-64 and 67-71. Upstream-reverse and downstream-forward primers were designed to create extensions acting as primers for the Kanamycin-resistance cassette to enable PCR-mediated ligation of the fragments. For this purpose,

the Kanamycin-resistance cassette was amplified via PCR with the primers CD_P87/88 from the plasmid pKD4. The PCR fragments of the *H. pylori* knock-out constructs could be used directly for natural transformation of the strain G27. However, the constructs were also inserted into pGEM-T vectors to allow production of large construct quantity.

The PCR and pGEM-T knock-out constructs of HP2, HP5, HP6 and HP7 were obtained with this strategy and they were used for natural transformation of *H. pylori* G27 (chapter 5.2.16). HP2 and HP5 knock-outs were successfully generated with 1-10 µg of knock-out construct (PCR fragment and pGEM-T) for natural transformation. HP6 and HP7 knock-out constructs did not yield any Kanamycin-resistant clones at any condition tried. This implies an essential role of the targeted genes in bacterial growth or viability. However, further experiments with independent knock-out constructs and a complementation strategy are needed to prove this assumption.

Two mutant strains of each HP2 and HP5 were verified via sequencing (Primers CD_P113/114 and CD_P119/120). In all four strains, the target genes could not be identified in their locus whereas the boarders of the Kanamycin-resistance cassettes were found. Figure 55 shows the sequencing result for *H. pylori* G27 ΔHP5e as a representative result.
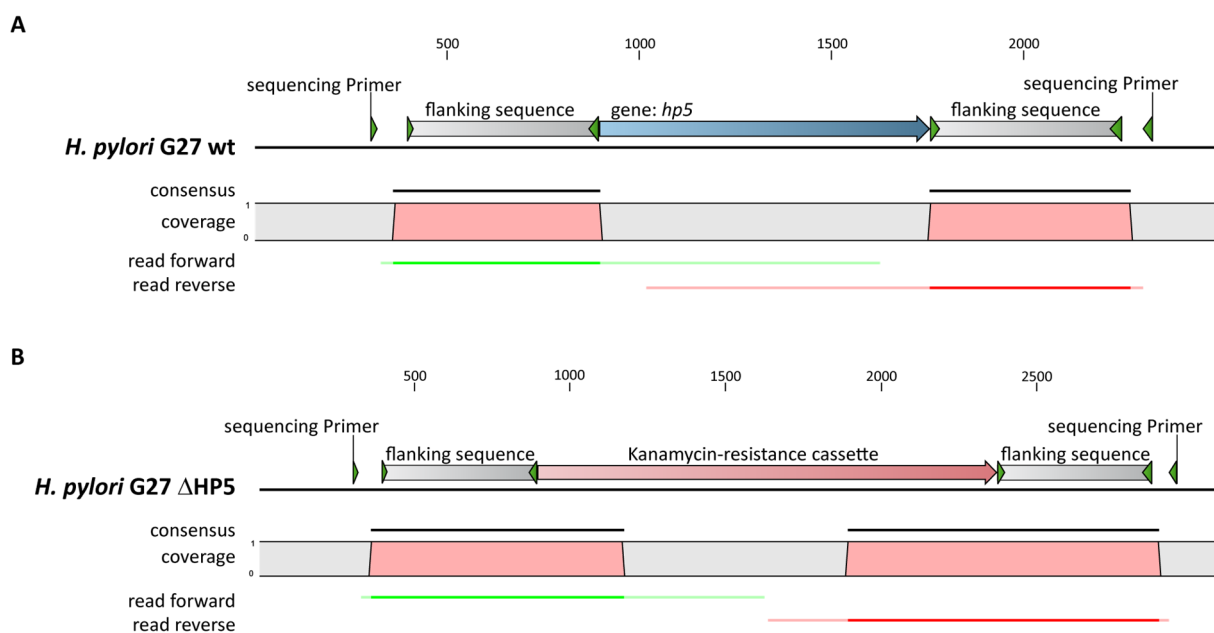
Figure 55: Sequencing of the target locus in *H. pylori* G27 ΔHP5e

Sequencing primer PCR product from G27 ΔHP5e genomic DNA was sent for sequencing at Eurofins MWG Operon (Ebersberg, DE). The obtained reads were aligned with the target locus in G27 wt and G27 ΔHP5 in CLC Workbench. The consensus stretch clearly illustrates the absence of the gene *hp5*. Instead, the Kanamycin-resistance cassette could be identified between the flanking sequences.

To verify the absence of the target genes in the knock-out strains, WB analysis was performed. Lysates of the wild-type strain and two knock-out strains as well as a sample of the recombinant protein of the corresponding HP candidate were separated via SDS-PAGE, blotted onto PVDF membranes and tested with the previously described murine anti-sera. The recombinant proteins and their impurities elicited strong WB signal. For both HP candidates, weak bands were recognized in the wild-type–strain lysate whereas no signal could be detected in the knock-out strains (Figure

56). This verified the absence of the target protein in the knock-out strains, which were subsequently used for *in vitro* and *in vivo* experiments.
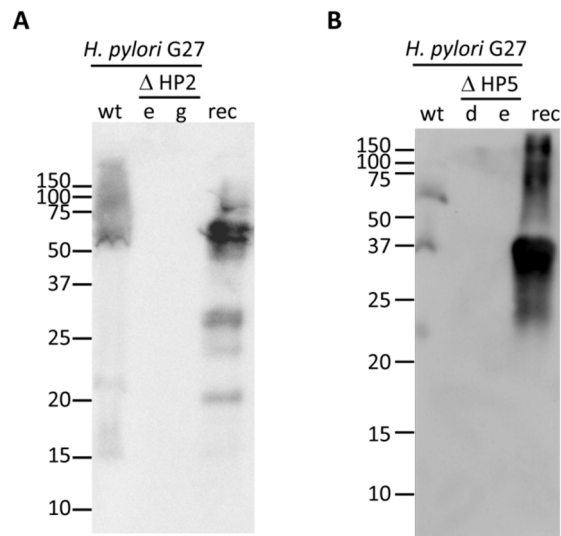

Figure 56: Western-Blot analysis of HP-candidate knock-out strains

5 µL of lysate preparation (pellet of 1 mL bacterial solution at OD_{600}=5 in 200 µL 1×SDS buffer) and 5 µg of the recombinantly produced *H. pylori* proteins HP2 or HP5 (rec) were separated via SDS-PAGE and blotted onto PVDF-membranes, which were subsequently blocked with 5 % (w/v) skimmed milk powder in TBS-T. Murine antisera were used in a 1:200 dilution in 1 % (w/v) skimmed milk powder in TBS-T and detected with 1:5000 diluted HRP-conjugated anti-mouse IgG. **A, B** Both HP candidates could be detected in the wt lysate but not in the knock-out strains.

A first investigation of *in vitro* growth was performed for the *H. pylori* strains G27 ΔHP2e/g and G27 ΔHP5d/e in comparison to wt G27. The strains were grown in two liquid media: Brucella with dent supplement and 10 % FCS, and DMEM + F-12 (1:1) with Vancomycin and 10 % FCS. The optical density at 600 nm (OD_{600}) was measured twice per day. Figure 57 shows the growth curves obtained for the *H. pylori* strains. In both media, knock-out strains of HP5 behaved similar to the wild-type strain whereas HP2 knock-out mutants display a significant growth deficiency. This correlates well with published data on HP2 involvement in *H. pylori* antimicrobial resistance as efflux-pump component. Addition of dent supplement and Vancomycin to the media used in this experiment, might thus be less well tolerated by HP2 knock-out mutants. Comparing these results to growth curves obtained without addition of antibiotics could elucidate the effect of antibiotic presence on the growth of the HP2 knock-out mutants.
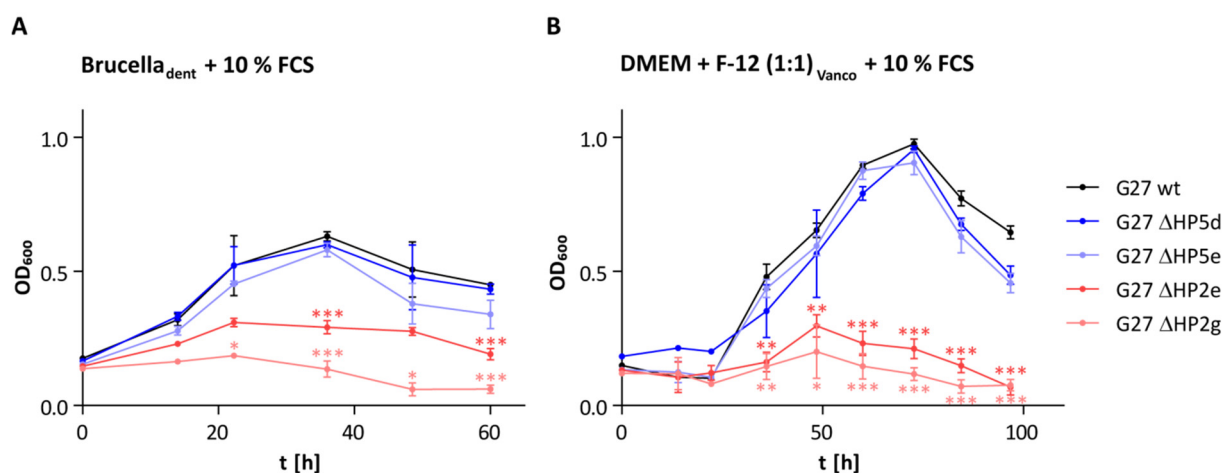
Figure 57: HP-candidate knock-out effect on *H. pylori* growth

5 mL of liquid medium were inoculated with standardly prepared *H. pylori* to an initial OD_{600} of 0.2. The cultures were incubated at 37°C in microaerophilic conditions and 10 % CO_2, 150 rpm. **A** The OD_{600} of the *H. pylori* strains, growing in Brucella$_{dent}$ medium supplemented with 10 % (v/v) FCS, is plotted against time. HP5 knock-out mutants behave similar to the wt strain. HP2 knock-out mutants display a growth deficiency. **B** The OD_{600} of the *H. pylori* strains, growing in DMEM + F-12 supplemented with 10 mg/L Vancomycin and 10 % (v/v) FCS, is plotted against time. HP5 knock-out mutants behave similar to the wt strain. In comparison with Brucella$_{dent}$ medium, a growth lag of about 24 hours was observed. HP2 knock-out mutants exhibit a significant growth deficiency. (Statistical analysis was performed in GraphPad Prism with the unpaired t-test. Significance levels -, *: $p<0.05$, **: $p \leq 0.01$, ***: $p<0.0005$)

Taking into consideration that HP2 is involved in antimicrobial resistance, both HP5 and HP2 might be suitable drug targets for *H. pylori* therapy. Obviously, further *in vitro* and *in vivo* evaluation is needed to draw a final conclusion. Nevertheless, the suggested surface exposure of these two candidates as well as the availability of antisera and confirmed knock-out strains lay a strong foundation for future work.

6.3.4 Analysis of candidates with characterized human patient sera

Another application for potentially surface-exposed bacterial proteins is their use as antigens in serological test assays for infection diagnostics for the corresponding pathogen. First tests have been performed to assess the *Helicobacter pylori* candidates' extend of recognition in *H. pylori* positive patients. The sera used in this work had been characterized before by Luca Formichella with regard to their serologic reactivity toward 16 other *H. pylori* antigens (secreted, surface-exposed and cytoplasmatic). Furthermore, *H. pylori* status of the patients had been proved by histological analysis of correspondig stomach biopsies.

Crucial information for analysis of patient sera with *H. pylori* antigens is the conservation of the proteins across differen strains. To investigate this conservation, Reference Clusters at UniProt (http://www.uniprot.org/) were evaluated for each HP candidate-protein. In the case of HP2, 4, 7 and 8, homologous proteins (90 % homology) were present in 96 % of sequenced strains. HP1 had homologues in 94 % and HP5 in 89 % of sequenced strains. The conservation of HP3 was lower but still reached 96 % for a homology level of 50 %. Thus, most patients should have been exposed to

strains encoding the HP-candidates. However, no data is available stating the expression levels of the HP-candidate proteins.
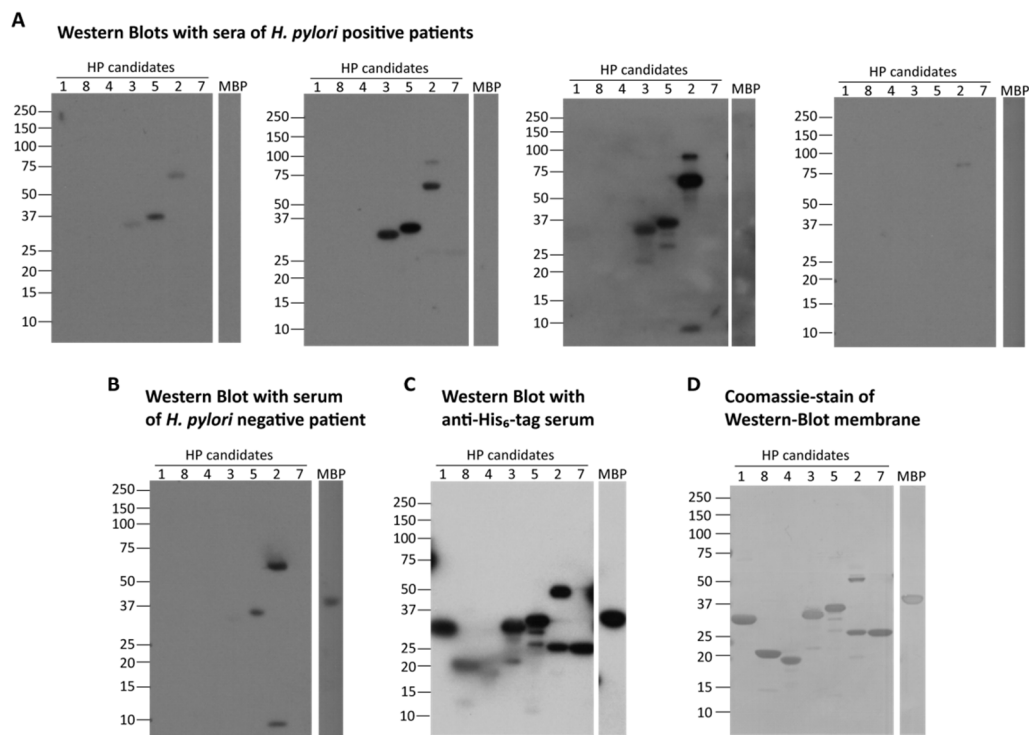

Figure 58: Western-Blot analysis of patient sera

5 µg of the recombinantly produced *H. pylori* proteins and His$_6$-tagged MBP were separated via SDS-PAGE and blotted onto PVDF membranes, which were subsequently blocked with 5 % (w/v) skimmed milk powder in TBS-T. **A, B** Patient sera were used in a 1:100 dilution and detected with 1:500 diluted HRP-conjugated anti-human IgG (recomWell *Helicobacter* IgG). **C** The His$_6$-tag of the HP candidate-proteins was detected with 1:5000 diluted anti-His$_6$ IgG and anti-mouse HRP conjugated IgG in a 1:10000 dilution. **D** The membranes were finally stained with Coomassie to verify the protein bands and enable correlation with the detected Western-Blot signals (staining of second positive serum WB).

Human patient sera were analyzed in two approaches. In the first attempt to investigate the HP candidates as potential serological marker proteins, the recombinant proteins were separated via SDS-PAGE, blotted onto PVDF-membranes and subjected to Western Blot analysis with four sera from *H. pylori* positive individuals and one negative serum. As control, maltose-binding protein (MBP) with His$_6$-tag was included in all tests. Subsequently, all proteins were detected with His$_6$-tag specific antiserum and the membranes were stained with Coomassie to compare protein bands with Western-Blot signals. Figure 58 shows the signals detected in this experiment. Unfortunately, no conclusive observations could be made with the chosen sera in WB analysis. On the one hand, only a few proteins (HP2, HP3 and HP5) were recognized by sera from *H. pylori* positive patients. Especially, the low purity protein HP2 was recognized with high intensity. However, it is hard to differentiate between impurities and target-protein recognition since only the two bands also visible in the Coomassie-staining are recognized with His$_6$-tag specific antiserum but signals at disparate molecular weights are detected with patient sera. On the other hand, a reaction of the negative patient serum with HP5, HP2 and even maltose-binding protein hinders sensible interpretation of the detected WB signals. Therefore, this analysis suggests HP3 as sole antigen useful for serology. However, variable

recognition of antigens between multiple *H. pylori* positive human sera is generally known. Thus, HP1, 4, 7 and 8, which are well conserved among *H. pylori* strains, might still be recognized by different patient sera.

To test a larger collection of patient sera, the recombinant proteins were used in a multiplexed approach for serum characterization. The Luminex® assay (chapter 5.3.10) was performed by Dr. Stefanie Rimmele and Dr. Nicole Schneiderhan-Marra from the group of Dr. Thomas Joos at the NMI (Tübingen) according to their standard protocol. With this technique, the sera were applied to a mixture of discriminable beads that were coated with native HP candidate-proteins. This is a substantial distinction compared to denatured and reduced proteins in the WB. This difference might influence the availability of antigenic sites and lead to disparate outcomes of the techniques. Characterized patient sera (40 *H. pylori* positive, 40 *H. pylori* negative) were employed to investigate the extend of recognition of the HP candidate-proteins.

Figure 59: Cross table for classification of assay outcomes

Assay outcomes of positive and negative characterized sera are classified according to this table.

$$Sensitivity = \frac{true\ positives}{true\ positives+\ false\ negative}$$

Formula 6: Sensitivity of diagnostic tests

$$Specificity = \frac{true\ negatives}{true\ negatives+false\ positives}$$

Formula 7: Specificity of diagnostic tests

For serologic validation of novel antigens with characterized sera, the test outcome for each antigen-antiserum comination is divided into four groups (Figure 59). True positives and true negatives are reacting as expected according to the known *H. pylori* status of the patient sera. False positives are positively detected samples within the collection of negative sera and false negatives are negative outcomes found within positive sera. For determining the sensitivity with which a specific antigen is detected, the frequency of true positive identification in the collection of positive sera is considered

(Formula 6). The specificity is defined by the frequency of true negative identification in the collection of negative sera (Formula 7). In the Luminex® assay, median fluorescence intensity (MFI) for the secondary antibody on the beads was determined for each human patient serum. Figure 60 depicts the recorded MFIs of 80 measured sera. For a preliminary analysis of the antigenicity of the HP candidates in patients, a cut-off was determined to detect *H. pylori* positive sera in this setup. The cut-off was calculated according to Formula 8. Sera yielding an MFI higher than the cut-off are classified as positive.

$$\text{cut-off} = \mu_{neg} + 3 \cdot \sigma_{neg}$$

Formula 8: Calculation of the cut-off in the Luminex® assay

μ_{neg}: mean MFI of negative patient sera
σ_{neg}: standard deviation of the MFI recorded for negative patient sera

A

Fluorescence signals detected for HP candidates in the Luminex® assay
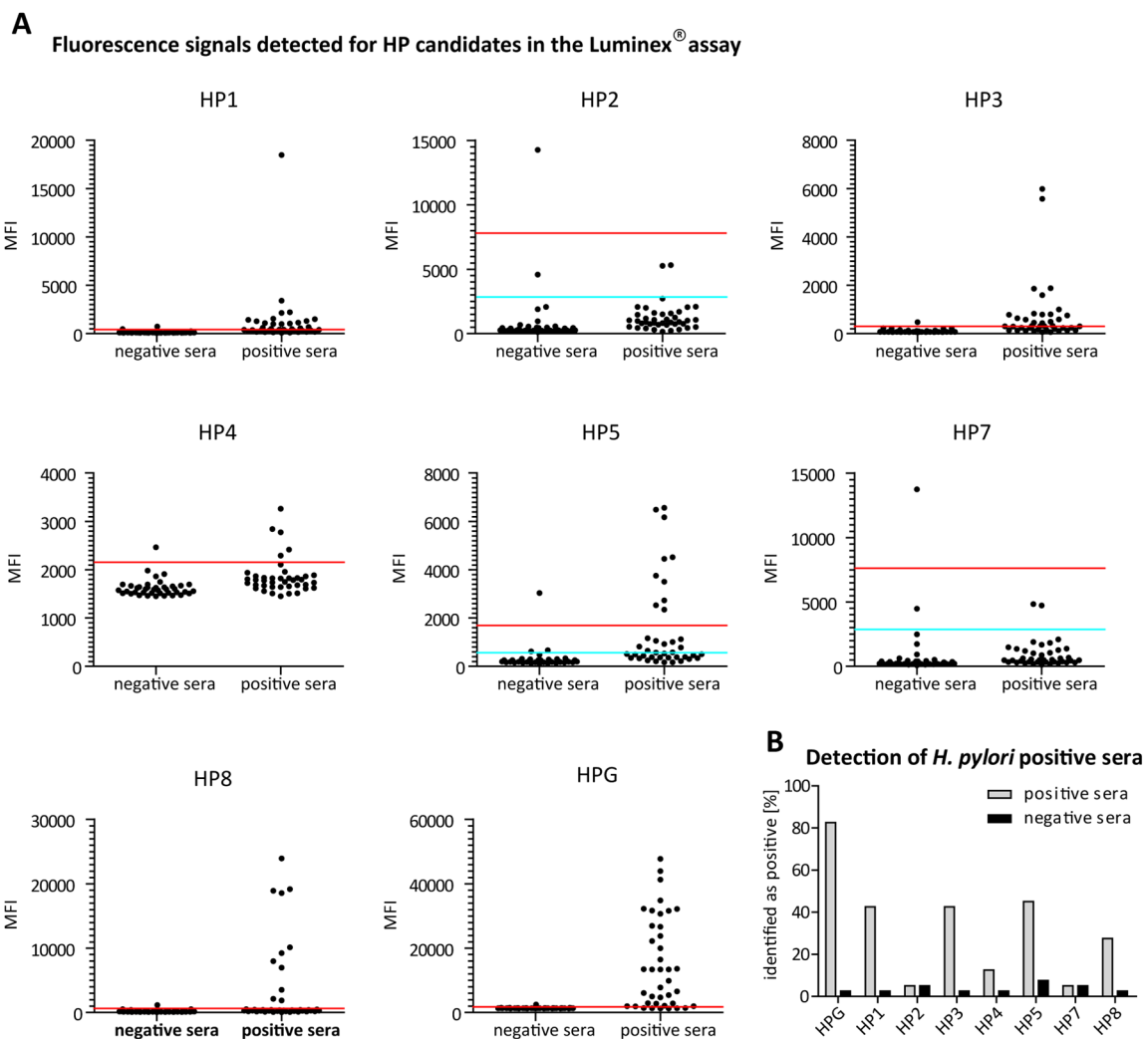
Figure 60: Luminex® based analysis of patient sera

The recombinant HP candidate-proteins and HPG were coated onto Luminex® beads and tested against each fourty H. pylori positive and negative human patient sera (characterized by Luca Formichella, dilution 1:400). A The obtained mean fluorescence intensities (MFIs) for each serum are plotted for the HP candidates. The red lines indicate the cut-off levels for definition of responders and the blue lines were calculated excluding one outlier. B The rate of responder identification in positive and negative sera is summarized to facilitate the comparison of the tested H. pylori proteins.

The known antigen HPG was coated onto beads and included in the experiment for comparison. The raw data of the experiment is displayed in Figure 60 and calculated sensitivities and specificities are summarized in Table 25. For HPG, 82.5 % of true positives were found with the Luminex® assay. HP1 and HP3 identified 42.5 % samples with MFIs above the cut-off as true positives. However, the median fluorescence intensity obtained with these two HP candidates (<7000) was much lower compared to HPG (up to 50000). This trend to lower MFIs is consistent for all HP candidates tested with human sera and suggests a lower antigenicity of these proteins. A lower antigenicity could be caused by low exposure of the patient's immune system to HP candidate-proteins but may also be an intrinsic feature depending on their amino-acid sequences. HP8 (27.5 % true positives), HP5 (25 % true positives) and HP4 (12.5 % true positives) showed lower recognition rates than HP1 and HP3. In contrast, HP2 and HP7 detected no true positives at all. However, high MFI outliers in the tested *H. pylori* negative patient sera of HP2 and HP7 shifted the cut-off and hampered analysis of the data collected with positive patient sera. Therefore, outliers were excluded from cut-off calculation to better compare the single antigens. This was performed for HP5 as well since it substantially influenced the sensitivity outcome. The resulting specificities were still very high for all antigens. Further steps for their evaluation should allow lower specificities and thus yield better sensitivities to enable identification of patients carrying distinct *H. pylori* strains. For general infection diagnostics, the antigens may be combined to obtain higher specificity. However, such exploratory investigation of the data should rely on higher sample numbers in the future.

HP candidate	Sensitivity	Specificity
HP1	42.5 %	97.5 %
HP2	5.0 %	95.0 %
HP3	42.5 %	97.5 %
HP4	12.5 %	97.5 %
HP5	45.0 %	92.5 %
HP7	5.0 %	95.0 %
HP8	27.5 %	97.5 %
HPG	82.5 %	97.5 %

Table 25: HP candidate sensitivity and specificity as antigens in Luminex® serologic testing

The sensitivity and specificity for HP candidates were calculated according to Formula 6 and Formula 7.

Data to determine the antigenicity of HP candidate-proteins are preliminary but hint at lower responses compared to the known *Helicobacter* antigen HPG. HP3 was recognized by *H. pylori* positive and not by negative patient sera in both WB and Luminex® approaches. HP5 was recognized by positive patient sera with both techniques; however, a WB signal was detected with a negative serum as well. HP1 and HP8 only reacted with positive patient sera in the Luminex® assay but not in the WB. The low purity recombinant protein HP2 showed unspecific signals in WB but was only weakly recognized in the Luminex® assay. HP7 did not react with patient sera in the WB and was only weakly recognized in the Luminex® assay. In conclusion, a variety of outcomes in WB and Luminex® based analysis of the HP candidates was found.

7 Discussion

In this work, screening assays for two relevant anti-virulence targets were set up and validated. The assays fulfilled standard requirements and are, therefore, prepared for further application in inhibitor discovery. They were used in two screening approaches and, subsequently, for characterization of identified inhibitors.

Furthermore, drug target candidates from *H. pylori*, which were identified with surface shaving, were analyzed for surface exposure, antigenicity and knock-out effect. These data prepared the candidates for thorough biological analysis.

7.1 Potential of *S. aureus* Sortase A inhibitor development

A fluorophore-quencher pair based transpeptidation assay for Sortase A from *Staphylococcus aureus* was implemented for inhibitor identification and characterization. The detailed assay validation underlined the suitability and quality of the assay. All criteria requested by the European Lead Factory[44] were fulfilled and proved the outstanding quality of the assay.

Synthetic compounds designed for the SaSrtA as well as a natural compound library were screened for inhibitory activity. Unfortunately, no valid inhibitors could be identified. Albeit, replication of the published IC_{50}-value for the compound 2-17[174] confirmed the feasibility of inhibitor discovery with the chosen setup. Both screening approaches provided experience with the SaSrtA transpeptidation assay that will be of value in future projects. An important issue proved to be fluorescence artifacts caused by test compounds. Two primary actives that were found in the natural compound library and even yielded encouraging IC_{50}-values, could be shown to decrease the fluorescence signal of the assay independent of SaSrtA activity. Since compounds themselves may be fluorogenic, or could absorb excitation or emission light and thereby influence the overall signal by an inner filter effect, appropriate controls have to be included in future screening processes.

To extend the platform for SaSrtA inhibitor identification, additional counter-screening assays need to be established to be able to investigate the specificity of inhibitors for SaSrtA or to identify further applications of active compounds against other relevant pathogenic bacteria. The SaSrtB is especially interesting, since it shares the acceptor substrate with SaSrtA but recognizes a different sorting signal in the transpeptidation reaction. Thus, specificity can only be achieved by addressing the donor-peptide binding-site. The transpeptidation assay for SaSrtB is established for compound characterization in 4 h kinetic measurements. To fully validate the SaSrtB assay, however, further studies are still needed. The stability of the reagents has to be investigated via freeze-thaw-cycle and incubation experiments as has been shown for the SaSrtA transpeptidation assay. Another possible readout for the protein stability that can easily be implemented is the thermal shift assay (TSA). For TSA analysis, the proteins are prepared in various buffers suitable for storage and for the activity assay and mixed with an unspecific protein binding fluorescent dye that displays increased fluorescence intensity in hydrophobic environments. The protein and the dye are heated and the

fluorescence-intensity increase, caused by hydrophobic protein patches exposed during unfolding, is detected. For each buffer condition tested, a melting curve is obtained. The deduced melting temperatures are a measure for the protein stability in a given buffer, which can thus be optimized.[348] This technique can also be used later for compound binding analysis during inhibitor development and will thus serve as an orthogonal screeing assay.[349] Furthermore, aspects of measurement quality such as signal/background ratio and Z'-factor need to be addressed for SaSrtB to define the signal window that can be used for identification of compound effects.

Additionally, sortases from different pathogenic species (e.g. *Streptococcus pneumoniae* and *Bacillus anthracis*) need to be included in the panel. An important aspect of the specificity approach is avoiding side effects especially with regard to the human microbiota. *Lactobacilli*, for example, are a substantial part of the human urinary, digestive and genital tracts and help prevent pathogenic colonization. Their attachment to mucosa and epithelium has been shown to be at least in part dependent on sortase activity.[350] Therefore, unfavorable influence on the human microbiome can be provoked by application of unspecific sortase inhibitors and should be avoided.

The Sortase A from *Enterococcus faecalis* has already been produced and purified in this work for its application in a specificity counter-screen. However, even at high enzyme as well as donor- and acceptor-substrate concentrations, no enzymatic activity could be observed. Additionally, the purity of the *E. faecalis* SrtA needs to be increased to allow meaningful concentration adjustments in the assay. The experience with this tenacious enzyme stresses the need of adjusting assay conditions for all enzymes in the counter-screen panel to achieve optimal enzymatic activity in all cases.

Particular consideration is also needed when choosing the acceptor-substrates since the lipid II cross-bridges vary between Gram-positive strains. In the case of *E. faecalis*, this cross bridge is D-Ala-D-Ala and has been used in concentrations from 1 mM up to 125 mM in the *in vitro* transpeptidation assay without yielding enzymatic activity. In contrast, the activities of sortases from *S. aureus* were observed at 1 mM acceptor-substrate Gly_5. Obviously, major optimization is needed in the assay composition for diverse sortases.

Furthermore, it has to be taken into account that sortases are slow acting enzymes *in vitro*. In the *S. aureus* Sortase A *in vitro* transpeptidation assay a k_{cat} of 0.0016 s^{-1} has been described.[153] This is a 100-fold lower reaction rate than the one described for lysozyme (0.15 s^{-1}), which is recognized as very slow acting enzyme.[351] As membrane proteins, sortases are perfectly positioned to recognize co-translationally secreted proteins, which are unfolded and thereby have an easily accessible recognition peptide. Such high local concentrations of both enzyme and substrates might explain high K_M-values and low turnover numbers of sortases in homogenous *in vitro* assays. Consequently, reagents have to be used at high concentrations in the assays. This is a potential problem for the identification of inhibitors that might be needed at equally high concentrations as well. Thus, supply and water solubility of test compounds can dramatically restrict screening application. Therefore, enzymatic sortase-assays have to be thoroughly validated for sensitivity. In this work, the transpeptidation assay for SaSrtA was shown to be sufficiently sensitive yielding IC_{50}-values in the lower micromolar range with reference inhibitors (2.5 µM for compound 2-17).

Despite the two inconclusive inhibitor discovery approaches applied in this work, sortases are eminent anti-virulence targets that call for continuing inhibitor development attempts. Therefore, further compound library screens should be made use of to identify novel inhibitory agents. The availability of crystallographic[140] and NMR-spectroscopy data[157] of SaSrtA as well as a variety of described inhibitors[163] enable targeted approaches. Moreover, fragment based inhibitor development has so far not been tried with sortases and would benefit from previous work while generating further fundamental knowledge of the active site geometry and pharmacophore constitution.[352]

Fragment based drug design (FBDD) exploits libraries of lead-like fragments with an optimal ratio of molecular weight (complexity) and expected binding sites.[353] The fragment size usually lies between 150 and 300 Da. This implicates high hit probability with low binding affinities to target proteins.[354] Therefore, highly sensitive assays are needed to detect fragment binding. Suitable technologies are among others NMR (nuclear magnetic resonance) spectroscopy, SPR (surface plasmon resonance), TSA (thermal shift assay), high-concentration enzymatic assays, and X-ray crystallography.[352] The most sensitive method is NMR-spectroscopy measurement of the tested fragments with addition of target proteins. However, binding fragments identified in any of the mentioned assays need to be validated with an orthogonal method, which most often is X-ray crystallography.[355] Such structural data facilitates the development of lead structures. After all, binding fragments have affinities in the higher micromolar or lower millimolar range. Thus, they are not suitable as lead structures themselves but can be developed into compounds with higher affinities.[356]

This development can be based on one of three approaches. Firstly, if several fragments that bind to distinct target site positions are found, they may be connected by suitable linkers to achieve additive affinity. Structural data obtained earlier can help in this process. Secondly, fragment growing can be applied on starting fragments that are characterized by several crucial interactions with the target site. These interactions should be preserved and expanded to achieve higher binding affinities adequate for lead compounds. Lastly, structural data on fragment binding in overlapping target sites can allow merging of fragments while conserving the specific interactions.[352]

One major advantage of FBDD is the small scope of initial screening effort in comparison to high throughput screening (HTS) approaches. In theory, a diverse library of 1000 fragments can yield similar information as HTS libraries with one million compounds.[354] Consequently, FBDD is an attractive method for drug discovery, which can also be realized in purely academic settings. Additionally, FBDD is a valuable complementation of HTS and *in silico* approaches since the combined knowledge of compound and fragment binding may reveal possibilities of substitutions or extensions on a rational basis.[352]

In the context of SaSrtA, FBDD is a valid approach to either develop novel lead compounds or generate detailed information on the target protein and suitable chemical moieties to address the active site. Thus, published data on SaSrtA inhibitors and experience with meaningful assays for analysis of binding compounds set a promisingly firm basis for the application of FBDD.

Importantly, discovery of SaSrtA inhibitory agents should be accompanied by biological readouts, such as *S. aureus* fibronectin binding, as early as possible. Thus, relevant compounds can be selected

from the beginning and the development process will be accelerated. In contrast, many sortase inhibitors described in literature lack comprehensive *in vitro* analysis and are therefore not yet considered to be potential anti-virulence agents, which is an important priority in such discovery programs.[163]

SaSrtA inhibitors will have the potential of treating many *S. aureus* infection conditions. However, their applicability would be restricted to slow advancing infectious diseases since their anti-virulence action will be too slow to fight fast disease progression as e.g. is the case for sepsis. Nevertheless, therapies addressing specific infection patterns are of substantial importance since they would prevent other advanced drug regimens from being used in this setting. Thus, drugs targeting SaSrtA will help reserve other therapies for most severe indications and support advances in restricting antimicrobial-resistance development.

7.2   Potential of *H. pylori* gGT inhibitor development

For the γ-glutamyl transpeptidase from *Helicobacter pylori* (HPG), a colorimetric transpeptidation assay was setup for compound screening. The assay is based on the artificial donor-substrate γ-glutamyl *p*-nitroanilide and the acceptor-substrate diglycine. With the new construct oHPGh, a markedly reduced enzyme concentration (500 pM) could be used in the assay, rendering it very sensitive for inhibitor identification. The screening assay could be presented with outstanding quality since it fulfilled all criteria demanded by the European Lead Factory[44].

A high-resolution crystal structure was obtained for oHPGh. In contrast, the published crystallographic data (2NQ0[258]) was obtained from a recombinant construct in the vector pET28b with an N-terminal His_6-tag and additional vector amino acids. Although a thrombin cleavage site was included in this amino acid stretch, it was not used to remove dispensable residues before crystallization. Electron density found in the active site of HPG could not be annotated in the published data. However, the crystal structure presented in this work resolved this molecule to be alanine bound by specific active site resiedues. The established crystallization procedure for oHPGh will facilitate future co-crystallization with potential inhibitors.

The natural compound library screen yielded no hits in this assay. However, the targeted approach with tailored library screening in cooperation with Priaxon AG was successful. Crystal-structure data[258] and evaluation of inhibitors designed for the human γ-glutamyl transpeptidase[342] provided the starting point for the proprietary PriaxPlore® technology, which yielded 102 compounds for the HPG-targeted library. This tailored library yielded a hit rate of 33.33 % whereas a general screening library of 277 compounds contained 14.80 % less active confirmed hits, underlining the superiority of the tailored approach.

From the tailored library, eleven confirmed actives were prioritized on the basis of potency, physico-chemical properties and *in silico* data. Determination of the IC_{50}-values identified the two most promising scaffolds. Due to instabilities observed for scaffold B, structure-activity–relationship studies were only performed with scaffold A. Forty rationally designed derivatives were synthesized and assayed for their inhibitory activity. Additionally, their effect on three further γ-glutamyl transpeptidases was tested (HsgGT, EcgGT, CjgGT). With these data, the tractability of the scaffold's inhibitory effect was proved for two substituents R1 and R2. The substituent with the highest inhibitory effect in R2 was a nitrogen-linked *p*-phenoxyphenyl group. For R1, several compounds were obtained with low IC_{50}-values (compounds #34-39). Due to inhibitory effects against the human enzyme, the most active compounds were not prioritized for subsequent development and compound #35 was chosen for the next optimization steps. Here, R1 is a *N*-(*p*-methoxyphenyl)-2-(dimethylamino)acetamide, which is coupled via the acetamide α-carbon atom to scaffold A.

However, data proving the physical binding of the compound to the target enzyme were needed to justify efforts in hit-to-lead development. Unfortunately, neither dynamic measurements via NMR spectroscopy or MST, nor crystallographic analysis of compound binding was possible due to insufficient solubility of the compounds.

Nevertheless, the convincing SAR, which has been found for the compounds in the HPG transpeptidation assay, demonstrated the eminent capability of targeted, *in silico* modeling assisted drug discovery for HPG. Yet, structural data on compound binding is indispensable for further modeling approaches. In order to successfully utilize the inhibitory compounds described in this work, supportive information on compound binding generated with different methods will be needed.

The HPG features several characteristics that can impede inhibitor identification and development. The donor-/acceptor–substrate binding site is shallow and mostly non-polar in HPG enabling its promiscuity towards substrates. The specific recognition of donor-substrates is mediated by a defined γ-glutamyl binding pocket. However, this binding pocket cannot be easily addressed in a specific manner since it is very similar to the human γ-glutamyl transpeptidase, which should not be affected by novel HPG targeted drugs. On the contrary, the donor-/acceptor–substrate binding site should be exploited since it constitutes the most pronounced differences between the target sites of human and *H. pylori* γ-glutamyl transpeptidase. For all that, the physico-chemical characteristics of the HPG are not promising for inhibitor targeting.

Thus, complementary techniques are needed to generate novel input for the HPG targeted drug development. Fragment based drug development (FBDD, chapter 7.1) can create such new information about target site and properties of binding molecules. FBDD is especially valued for addressing so called "undruggable" targets.[357] The small, low complexity fragments applied in FBDD are able to explore unique binding sites and help define the pharmacophore of a protein target.[358] Therefore, soluble fragments that may be identified for HPG can elucidate binding strategies in the inconvenient target site and help understand small molecule features needed for HPG drug development. Experience with crystallization of the oHPGh recombinant protein will help in structural analysis of identified fragments and compounds. Optimally, a correlation of binding fragments and SAR-results for the investigated substituents in this work can be deduced. This would allow conclusions about the binding modes of the corresponding compounds and may justify further efforts in developing those into leads with higher solubility and potency.

The challenge will also be to achieve target specificity and spare the human enzyme and other bacterial gGTs to prevent adverse reactions. The availability of the counter-screening assays for physical analysis of compounds as well as the structural data on these enzymes (*E. coli*:2DG5[260], *B. subtilis*: 2V36[310], *H. sapiens*; 4GDX[271]) will support the targeted development of such HPG inhibitors. However, these counterscreening assays should be validated according to the HPG transpeptidation assay to obtain the most reliable readouts.

Furthermore, orthogonal binding assays should be established and pre-tests in the transpeptidation assay with detergent addition, which e.g. is needed for microscale thermophoresis (MST), should be run to assess the feasibility of these setups. Such a step could save time, recombinant enzyme and compounds from unpromising evaluation methods. With regard to the orthogonal assays, the need for a valid reference inhibitor to set up meaningful test systems is evident. The only reference compounds available (Acivicin, Azaserein, DON)[341, 359] are covalently binding, irreversible inhibitors. To achieve specificity of novel HPG inhibitors, covalently binding compounds are not suitable since

they usually are inherently reactive and might therefore easiliy crossreact with other gGTs. Therefore, binding characteristics of novel targeted compounds will differ dramatically from that of the available inhibitors. Orthogonal binding assays (e.g. MST) have to be performed with a variety of novel inhibitors, found in enzymatic screening assays or whose binding to the HPG has been proven by other physical methods such as crystallography, to be able to evaluate those for compound characterization.

The discovery and development of promising HPG inhibitors would address the rise in *H. pylori* antimicrobial resistance worldwide. As a universally and constitutively expressed virulence-factor, HPG is a suitable target in all settings regarding geographical patterns of resistance and infection severity. HPG is involved in colonization, gastric injury, pro-carcinogenic stimulation and immune-evasion mechanisms. Inhibitors would therefore dampen gastric injury by counteracting apoptosis induction and inflammation as well as hinder EGFR-signaling, which promotes epithelial-mesenchymal transition and cell proliferation. Furthermore, inhibition of immune-evasion mechanisms might enable the patient's immune system to successfully fight the bacterial infection. However, this will only be effective in immune competent individuals. The need for combination of HPG inhibitory drugs with established or novel regimens will have to be considered to obtain the most efficient therapy.

7.3 Evaluation of novel *H. pylori* drug targets

Novel target candidates selected via *H. pylori* surface shaving (performed by Tobias Kruse, unpublished) were recombinantly produced and first experiments addressing their suitability as therapeutic targets were performed. This approach expands the drug discovery approaches for the targets Sortase A from *S. aureus* and γ-glutamyl transpeptidase from *H. pylori*, which are not localized in the bacterial cytoplasm and are therefore far easier to address with inhibitory agents. Thus, novel targets for anti-virulence drug development are preferably surface exposed.[163]

Seven proposedly surface-exposed proteins from *H. pylori* (HP candidates) were recombinantly produced to satisfying purity with the exception of HP2, which displayed several additional bands in SDS-PAGE. For this protein the expression conditions need to be optimized to increase the overall yield and further purification steps have to be tested to finally obtain HP2 with sufficient purity.

Also the candidate HP3 showed two bands of different apparent molecular weight at 25 kDa and 37 kDa, respectively. Peptide mass-spectrometry analysis identified the larger, unexpected band at 37 kDa to be HP3. However, this approach did not provide any information on missing or additional fragments in this protein. Since this higher molecoular-weight form was identified in reductive, denaturing SDS-PAGE analysis, a covalent alteration of HP3 is most likely. Therefore, this HP3 isoform needs to be analyzed in more detail with respect to its molecular composition, if HP3 is prioritized as target candidate in the future. A suitable method would be MALDI analysis since it allows investigation of the intact protein.

The candidate-protein HP6 manifested as multiple bands in SDS-PAGE analysis and multiple peaks in size-exclusion chromatography. The most prominent bands at 23 kDa and 75 kDa do not match the expected size of 59 kDa. This unexpected appearance of HP6 might be a feature of the protein itself or an artifact due to exclusion of the *in silico* predicted signal peptide and the recombinant expression system. As a consequence of this phenomenon, HP6 was excluded from further experiments.

The seven successfully purified proteins were used to generate murine antisera, which were tested in an ELISA experiment. The antisera yielded concentration dependent ELISA signals with their specific antigens, whereas no unspecific reaction of secondary antibody or cholera-toxin control serum was observed. The murine sera were purified and used to stain and analyze two strains of *H. pylori*, i.e. J99 and G27, in a flow-cytometry based experiment. For comparison, known *H. pylori* antigens were used to validate this experimental approach. The surface proteins HpaA and HopQ as well as the periplasmic protein HPG were probed on the bacterial surface with specific antisera. Distinct staining of HpaA was achieved with antibody-concentrations ranging from 2 µg/mL to 40 µg/mL. HPG staining was very weak with the same amounts of antibody and not distinguishable from CT-control serum staining in the strain J99. Based on the titration experiment with HpaA-specific antiserum, an antibody-concentration of 20 µg/mL was used for a first investigation of the HP candidates since a limited amount of antiserum was produced. Nevertheless, it has to be taken into consideration that antibody affinities and protein quantity on the bacterial surface are not comparable. Therefore, all antisera need to be titrated to achieve optimal staining results for analysis.

The protein HP8 was *in silico* predicted to be localized in the cytoplasm. Indeed, staining frequencies achieved with its specific antiserum were lower than for HpaA and HopQ and comparable to HPG in the strain G27. The remaining HP candidate-proteins were predicted to be surface exposed. However, antiserum generated with HP1 (production not in parallel with the other candidates) yielded no staining of *H. pylori*. This antiserum has not been tested in an ELISA yet, and therefore needs to be further characterized to help interpreting the finding in the flow-cytometry experiment. Nevertheless, the remaining predicted surface-exposed candidate-proteins HP2-HP5 and HP7 could be surface stained on *H. pylori*. For evaluation, the staining frequencies based on the CT-control serum as well as the mean fluorescence intensities (MFIs) for the secondary antibody anti-mouse IgG1 eFluor® 660 within the CFSE positive population were quantified. HpaA, HP3 and HP4 showed the most pronounced eFluor® 660 positive populations in J99. In G27, all predicted surface-exposed HP candidate-specific antisera yielded staining of a distinct positive population with frequencies of about 20 %. Additionally, for HopQ, HpaA and HP4, a shift of the whole population could be observed, which is best reflected in the MFI.

One major aspect impeding unambiguous identification of *H. pylori* cells in flow cytometry is their small size and low fluorescence intensities after staining. As a consequence, unspecific particles and bacterial cell debris are found at a similar size. Furthermore, CFDA-SE, activated in the bacterial cytoplasm, reacts as CFSE with free amine-groups, thus labeling intracellular regions of membrane proteins as well. Cell destruction occurring during subsequent steps or formation of outer membrane vesicles will therefore generate CFSE-positive membrane fractions, which may cause a background signal since measurements needed to be performed at highest detector sensitivity. This issue needs to be addressed by optimizing the staining procedure and possibly including a centrifugation step enriching whole bacteria.

Another reason explaining the fact that not all bacteria were positively stained for surface-proteins could be varying morphologic phenotypes of *H. pylori* in the experiment. The preparation of *H. pylori* for this experiment typically yielded 50 % coccoid and 50 % spiral-shaped bacteria. In a stable isotope labeling approach, it has been shown by quantitative mass spectrometry that several outer membrane proteins are up-regulated in the coccoid state of the bacteria whereas other proteins, which are e.g. involved in chemotaxis and cell division are down-regulated.[360] Furthermore, subdivision of these two morphological states based on their cultivability and infectivity has been proposed and indicates even more distinguishable phenotypes of *H. pylori*.[361] These findings might explain disparate labeling intensities and frequencies of mixed morphological states of *H. pylori*. Therefore, coccoid and spiral-shaped bacteria should be separated for analysis or enriched with suitable culture conditions during preparation to elucidate the effect of morphology on staining frequency and intensity.

Finally, antibody-concentrations need to be titrated for all HP candidates to ensure optimal staining results. However, this will consume large amounts of murine serum, which was generated only in limiting amounts. Nevertheless, the basic staining of the HP candidate-proteins on the surface of *H. pylori* mixed morphologic phenotypes reveals HP2-HP5 and HP7 surface-exposure and justifies further efforts in their validation as novel surface-exposed therapeutic targets.

Finally, knock-out mutants have been created for the HP candidates HP2 and HP5. The selected knock-out strategy based on natural transformation and recombination of *H. pylori* G27 allowed positive selection of knock-out clones with Kanamycin. However, this strategy did not yield any clones for HP1, HP6 and HP7 knock-outs. This may be a first hint at essential functions of these proteins in the chosen culturing conditions. However, to achieve a clear statement for these three HP candidates, the strategy needs to be repeated with diverse knock-out constructs and plasmid-based complementation.

HP2 and HP5 knock-out mutants were successfully established and two clones each were chosen for affirmation. Firstly, genomic DNA was prepared and PCR-fragments covering the insertion of the Kanamycin-resistance cassette were sent for sequencing to investigate the target locus. All four strains did not contain the original target gene, but the Kanamycin cassette could be identified between the flanking regions selected for recombination driven knock-out. Secondly, lysates of wild-type and knock-out mutant strains were subjected to SDS-PAGE and WB-analysis with the specific murine sera. Weak bands of HP2 and HP5, respectively, could be identified in the wild-type lysates whereas no WB signals could be detected in the knock-out mutant lysates. This confirmed the absence of the HP candidate proteins from the knock-out strains and justified further experiments with these strains.

For a first estimation of knock-out effects, the *in vitro* growth of wild-type and knock-out strains of HP2 and HP5 were compared. Two media were chosen for liquid culture of *H. pylori*. Brucella-medium is widely used for *in vitro* cultivation of *H. pylori* and F-12 has also been described for this purpose. In combination with DMEM, the latter medium resembles conditons in co-culture with eukaryotic cell lines and its influence on growth was of interest for future application of the knock-out mutants. The growth was monitored until the optical density declined. Principal differences were noted for G27 wt growth in the two media since it was delayed in DMEM+F-12, but higher optical densities were achieved. Nevertheless, both knock-out mutant clones for HP5 behaved similar to the wild-type strain. Therefore, HP5 is not essential for *in vitro* growth, which is a hallmark as anti-infective target. Strikingly, HP2 knock-outs had a significant growth defect in both media. According to literature, HP2 is a component of a bacterial efflux pump and knock-outs can, therefore, impair the inherent antimicrobial resistance of *H. pylori*. Consequently, the supplementation of the media with *H. pylori* selective agents (dent, Vancomycin) can be the cause of this observation. Thus, *in vitro* growth analysis needs to be repeated without addition of antibiotics to the medium to prove this assumption and exclude a polar effect of the knock-out mutation on downstream gene expression being responsible for the growth deficiency. Even though not a classical anti-virulence target, HP2 might still be a suitable for therapeutic interference since blocking its function could enable antibiotic treatment that would otherwise be ineffective.

Another aspect that is important to be investigated for novel drug target candidates, especially for those implicated as anti-virulence targets, is their applicability as antigen for serological diagnostic testing. All HP candidate-proteins were expressed in the strain J99 and are well conserved within

sequenced strains (90 % homology level in ≥89 % of strains) with the exception of HP3 (50 % homology level in 96 % of strains). However, it is unclear, if the candidates are expressed in all these strains. The possibility of heterogeneity of a specific drug target for the human pathogen *H. pylori* justifies their validation as diagnostic tool to identify *H. pylori* infected individuals and eventually even stratify patients according to their disease risk in order to subject them to appropriate therapy. As predicted surface exposed proteins, HP candidates are likely to be recognized by the human immune system and provoke specific antibody responses.

Serological diagnostics are a valuable approach for infection diagnosis and further patient stratification, since they are non-invasive and rapid. The HP candidates were evaluated as diagnostic antigens via Western Blot and in the multiplexed Luminex® assay at the NMI (Tübingen).

The WB approach was performed with four sera from *H.* pylori positive patients and with one negative serum. Three positive sera reacted with HP2, 3 and 5 whereas one did only weakly react with HP2. It has to be taken into consideration that HP2 was not sufficiently purified and several impurities could be observed. WB signals were detected for bands that did not correspond to the predicted molecular weight of HP2 and which also did not react with His-tag specific antibody. Therefore, these reactions are most likely caused by contaminations from the *E. coli* expression strain. Consequently, these experiments should be repeated with HP2 that has been purified to a sufficient degree. Furthermore, the negative patient serum yielded WB signals with HP2 and HP5 as well and even reacted with the control protein maltose-binding protein. Nevertheless, it has to be taken into consideration that five patient sera are not representative for serologic analysis. A high variability of serum reactivity is known in *H. pylori* serology. Hence, analysis with a larger collection of patient sera is needed to evaluate the HP candidates as antigens for WB.

With the Luninex® approach, it was possible to test each 40 positive and negative characterized human patient sera reactivity with native HP candidate-proteins. A cut-off level for distinction between positive and negative outcome was defined as the mean response for the negative sera plus three times the standard deviation. For HP2, HP5, and HP7, outliers were excluded from cut-off calculation. With this, overall high specificities of 92.5 % to 97.5 % were achieved. In contrast, the sensitivity was variable for the HP candidates. The highest sensitivities were found for HP5 with 45.0 % followed by HP1 and HP3 with 42.5 %. Taken together, these results imply low to medium antigenicity of the HP candidates in patients. Such outcomes may be the result of minor patient exposure due to low expression levels in infecting *H. pylori* or it might be an intrinsic characteristic of the amino-acid sequences of the HP candidates.

The outcomes of HP1 and HP3 reactivity with patient serum can be compared in WB and Luminex® analysis. Both were recognized in the Luminex® assay with 42.5 % specificity. However, only HP3 reacted with three out of four positive patient sera in the WB whereas HP1 did not react at all. These different outcomes can arise from distinct features of the methods, i.e. denatured proteins application in the WB and native protein application in the Luminex® assay. These conformations of the candidate proteins can differ substantially in the availability of antigenic sites and, therefore, present discrepant reactivities in the selected analyses.

147

Additionally, no direct correlation of serologic testing and flow-cytometry based analysis of HP candidate surface-exposure could be found except for HP3, which reacted with positive patient serum in both serologic approaches and yielded a considerable staining frequency of 24.1 % for the *H. pylori* strain G27. However, the interpretation of flow-cytometry data allows for variable expression of the HP candidate-proteins comparing morphologic states of *H. pylori*. In the human infection setting, even more variability is to be expected than in culturing conditions due to differences in patient genetics and microbiota composition. Furthermore, high genetic variation of *H. pylori* exposes each patient to its own composition of *Helicobacter* strains.[306, 307] Consequently, antigen exposure and recognition is highly variable between infected individuals. Nevertheless, evaluation of serologic tools with the HP candidates as antigens can contribute to the fundamental knowledge about these proteins in the infection setting. Therefore, larger patient cohorts should be tested for reactivity with these antigens to set a solid basis for their possible application in combination with other Hp antigens in serologic test assays.

In summary, studies performed to identify novel *H. pylori* protein candidates for in depth evaluation as therapeutic targets yielded recombinant proteins, specific murine antisera and knock-out strains for future investigations. Furthermore, the results obtained from flow-cytometry experiments indicated HP2-HP5 and HP7 as surface-exposed proteins, which could be easily targeted by therapeutic agents. The knock-out experiments identified HP5 as non-essential for *in vitro* growth, and HP2 involvement in antimicrobial resistance was indicated. Moreover, a small fraction of human sera, tested in WB and Luminex® assay, reacted with several of the HP candidates suggesting their recognition by the patient's immune system.

In the next steps, biological function of the HP candidates has to be addressed *in vitro* and *in vivo*. The availability of recombinant protein will facilitate the investigation of direct effects on suitable gastric cell lines as well as therapeutic vaccination studies. Infection experiments with wild-type and knock-out strains will be of particular interest. However, G27 is not suitable for mouse infection experiments. Therefore, knock outs have to be conferred to SS1 or PMSS1 strains.

The data collected for the HP candidates in this work suggest the power of the methods used for their identification as surface-exposed proteins and potential therapeutic targets. Accordingly, they are valid tools for candidate identification of further pathogenic bacteria. Such approaches of target discovery are an important piece of the puzzle in the search for novel anti-virulence therapeutics to combat rising resistances observed in infectious diseases worldwide.

8 Registers

8.1 Abbreviations

×g	times Earth's gravitational force
°C	degree Celsius
Abl	Abelson murine leukemia viral oncogene homolog
ADAM10	A Disintegrin And Metalloproteinase 10
AdsA	adenosine synthase A
Agr	accessory gene regulator
AHT	anhydrotetracyline
AIP	autoinducing peptide
AIX	anion exschange chromatography
AlpA/B	adherence associated lipoprotein A/B
Amp	Ampicillin
APC	antigen presenting cell
APS	ammonium persulfate
Aps	antimicrobial peptide sensor
ArgPi	arginine phosphate
ATCC	American Type Culture Collection
ATP	adenosine triphosphate
BabA	blood group binding antigen (*H. pylori*)
Bap	biofilm associated protein (*S. aureus*)
BCA	bicinchoninic acid
BHI	brain-heart infusion
bp	base pairs
BSA	bovine serum albumin
C. jejuni	*Campylobacter jejuni*
C5aR	complement factor 5a receptor
CagA	cytotoxin-associated gene A (*H. pylori*)
*cag*PAI	cytotoxin-associated gene pathogenicity island (*H. pylori*)
CD25	cluster of differentiation 25
CFDA-SE	carboxyfluorescein diacetate succinimidyl ester
CjgGT	recombinant gGT from *C. jejuni*
ClfB	clumping factor B (*S. aureus*)

CNA	collagen adhesion (*S. aureus*)
COX-2	cyclooxygenase 2
CT	cholera toxon
CV	coefficient of variability
DC	dendritic cell
ddH2O	double distilled water
DgGpNA	D-γ-glutamyl-*p*-nitroanilide
DMEM	Dulbeccos modified eagle medium
DMMA	(Z)-3-(2,5-dimethoxyphenyl)-2-(4-methoxyphenyl) acrylonitrile
DMSO	dimethylsulfoxid
DNA	deoxyribonucleic acid
DTT	dithiotreitol
E. coli	*Eschericia coli*
E. faecalis	*Enterococcus faecalis*
EcgGT	recombinant gGT from *E. coli*
ECL	enhanced chemoluminescence
EDANS	(5-((2-Aminoethyl)amino)naphthalene-1-sulfonic acid)
EDTA	ethylenediaminetetraacetic acid
EfSrtA	recombinant SrtA from *E. faecalis* (expressed from pPRk Δ1-30 Ef SrtA-h)
EGFR	epidermal growth-factor receptor
ELISA	enzyme-linked immunosorbent assay
ErbB2/3	avian erythroblastic leukemia viral oncogene homolog 2/3
ESBL	extended spectrum β-lactamase
ESFR	European Synchrotron Radiation Facility
FBDD	fragment based drug discovery
FCS	fetal calf serum
FnBPA/B	fibronectin binding protein A/B (*S. aureus*)
Foxp3	forkhead-box protein 3
FRET	Förster resonance energy transfer
gGT	γ-glutamyl transpeptidase
Gly$_5$	pentaglycine
GlyGly	diglycine
H. pylori	*Helicobacter pylori*
H. sapiens	*Homo sapiens*
HEPES	4-(2-hydroxyethyl)-1-piperazineethanesulfonic acid

HP candidate	*H. plyori* target candidate identified via surface shaving
HP1-8	HP candidate 1-8
HPG	gGT from *H. pylori*
HPLC	high performance liquid chromatography
HPR	horse-radish peroxidase
HPSF	high purity salt free
HRP	horseradish peroxidase
HsgGT	human gGT, purified from Hep G2 cells
HtrA	high temperature requirement factor A (*H. pylori*)
HTS	high-throughput screening
IC_{50}	inhibitor concentration at 50 % activity inhibition
IgG	immune globulin G
IL	interleukin
isd	iron regulated surface determinant (*S. aureus*)
IsdA/B/H	iron regulated surface determinant protein A/B/H (*S. aureus*)
Kan	Kanamycin
kB	kilo bases
k_{cat}	reaction rate constant
kDa	kilo Dalton
K_M	Michaelis constant
LB	Luria Bertani
LgGpNA	L-γ-glutamyl-*p*-nitroanilide
LPS	lipopolysaccharide
MALDI	matrix assisted laser desorption / ionisiation
MBP	maltose-binding protein
MFI	mean / median fluorescence intensity
mH2O	Millipore sterile filtered water
MIC	minimum inhibitory concentration
MRSA	methicillin resistant *S. aureus*
MST	microscale thermophoresis
n	number of replicates
NapA	neutrophil-activating protein (*Helicobacter pylori*)
NMR	nuclear magnetic resonance
OD_{600}	optical density at 600 nm
oHPGh	recombinant protein (expressed from pPRk oHPGh)

PAGE	polyacrylamide gel electrophoresis
PAMP	pathogen associated molecular pattern
PBS	phosphate buffered saline
PCR	polymerase chain reaction
PEG	polyethylen glycol
PFA	*p*-formaldehyde
PGA	poly γ-glutamate
PIPES	piperazine-N,N′-bis(2-ethanesulfonic acid)
pNA	*p*-nitroanilide
PSM	phenol-soluble modulin (*S. aureus*)
PVDF	polyvinylidene difluoride
PVL	Panton-Valentine leucocidin (*S. aureus*)
R^2	coefficient of variation
ROS	reactive oxygen species
rpm	revoultions per minute
S. aureus	Staphylococcus aureus
S/B ratio	signal/background ratio
SabA	sialic acid binding adhesion (*H. pylori*)
SAR	structure-activity relationship
SasC/G/X	*S. aureus* surface protein X
SaSrtA	recombinant SrtA from *S. aureus* (expressed from
	pET30b h- Δ1-20 Sa SrtA)
SaSrtB	recombinant SrtB from *S. aureus* (expressed from pPRk Δ 1-23 Sa SrtB-h)
Sbi	staphylococcal binder of immunoglobulin
SDS	sodiumdodecylsulfate
SLiCE	seamless ligation cloning extract
SOC	super optimal broth with catabolite repression
Spa	*S. aureus* protein A
SPR	surface plasmon resonance
SraP	serine-rich adhesion for platelets factor
Src	avian sarcoma (Schmidt-Ruppin A-2) viral oncogene homolog
SRP	signal recognition particle
SrtA	Sortase A
SrtB	Sortase B
SSL	staphylococcal superantigen like protein

T4SS	type IV secretion system
TAE	Tris-Acetate-EDTA
TB	terrific broth
TBS	Tris-buffered saline
TEMED	*N,N,N',N'*-tetramethylethylenediamine
TLR	toll-like receptore
T_m	melting temperature (oligonucleotides)
TMB	3,3',5,5'-Tetramethylbenzidine
TNF	tumor necrosis factor
Tris	Tris (hydroxymethyl-) aminomethane
TSA	thermal shift assay
TSS	toxic shock syndrom
TSS-Buffer	transformation and storage solution
TSS-Method	transformation and storage solution method
US$	US-dollar
v/v	volume per volume
v_0	initial reaction velocity
VacA	vacuolating cytotoxin A (*H. pylori*)
v_{max}	maximal reaction velocity
w/v	weight per volume
WB	Western Blot
WC	Wilkins Chalgren
wt	wild type
wtHPG	recombinant gGT from *H. pylori*

8.2   List of Figures

8.3   List of Tables

8.4 List of formulas

8.5 Bibliography

1.   Gell, P.G., *The restless tide: The persistent challenge of the microbial world by Richard M. Krause, National Foundation for Infectious Diseases, 1981.* . Immunol Today, 1983. **4**(7): p. 200.

2.   Centers for Disease Control and Prevention, *Antibiotic Resistance Threats in the United States, 2013*. 2013: US Department of Health and Human Services

3.   O'Neill, J., *Antimicrobial Resistance: Tackling a crisis for the health and wealth of nations*. 2014, AMR Review paper: http://amr-review.org/.

4.   Boucher, H.W., et al., *Bad Bugs, No Drugs: No ESKAPE! An Update from the Infectious Diseases Society of America.* Clinical Infectious Diseases, 2009. **48**(1): p. 1-12.

5.   Infectious Diseases Society of America, et al., *Combating antimicrobial resistance: policy recommendations to save lives.* Clin Infect Dis, 2011. **52** (Suppl 5): p. S397-428.

6.   Emori, T.G., et al., *National nosocomial infections surveillance system (NNIS): description of surveillance methods.* Am J Infect Control, 1991. **19**(1): p. 19-35.

7.   Martinez, J.L. and F. Baquero, *Mutation frequencies and antibiotic resistance.* Antimicrob Agents Chemother, 2000. **44**(7): p. 1771-7.

8.   Bryan, L.E., *Two forms of antimicrobial resistance: bacterial persistence and positive function resistance.* J Antimicrob Chemother, 1989. **23**(6): p. 817-20.

9.   Silver, L.L., *Challenges of antibacterial discovery.* Clin Microbiol Rev, 2011. **24**(1): p. 71-109.

10.   Courvalin, P., *Predictable and unpredictable evolution of antibiotic resistance.* J Intern Med, 2008. **264**(1): p. 4-16.

11.   Livermore, D.M., *Current epidemiology and growing resistance of gram-negative pathogens.* Korean J Intern Med, 2012. **27**(2): p. 128-42.

12.   Dzidic, S. and V. Bedekovic, *Horizontal gene transfer-emerging multidrug resistance in hospital bacteria.* Acta Pharmacol Sin, 2003. **24**(6): p. 519-26.

13.   Walsh, C., *Where will new antibiotics come from?* Nat Rev Microbiol, 2003. **1**(1): p. 65-70.

14.   Nugent, R., Back, E., Beith, A., *The Raice Against Drug Resistance*. 2010, Center for Global Development.

15.   Escaich, S., *Antivirulence as a new antibacterial approach for chemotherapy.* Current Opinion in Chemical Biology, 2008. **12**(4): p. 400-408.

16.   Becker, D., et al., *Robust Salmonella metabolism limits possibilities for new antimicrobials.* Nature, 2006. **440**(7082): p. 303-7.

17.   Coates, A.R.M., G. Halls, and Y. Hu, *Novel classes of antibiotics or more of the same?* British Journal of Pharmacology, 2011. **163**(1): p. 184-194.

18.   Crowley, P.J., *Compositions containing amoxycillin trihydrate and potassium clavulanate*. 1978, Beecham Group Limited: United Kingdom.

19.   Reading, C. and M. Cole, *Clavulanic Acid: a Beta-Lactamase-Inhibiting Beta-Lactam from Streptomyces clavuligerus.* Antimicrobial Agents and Chemotherapy, 1977. **11**(5): p. 852-857.

20. Lagacé-Wiens, P.R.S., et al., *Activity of NXL104 in Combination with β-Lactams against Genetically Characterized Escherichia coli and Klebsiella pneumoniae Isolates Producing Class A Extended-Spectrum β-Lactamases and Class C β-Lactamases.* Antimicrobial Agents and Chemotherapy, 2011. **55**(5): p. 2434-2437.

21. Zhanel, G., et al., *Ceftazidime-Avibactam: a Novel Cephalosporin/β-lactamase Inhibitor Combination.* Drugs, 2013. **73**(2): p. 159-177.

22. Lewis, K., *Platforms for antibiotic discovery.* Nat Rev Drug Discov, 2013. **12**(5): p. 371-387.

23. Mollmann, U., et al., *Siderophores as drug delivery agents: application of the "Trojan Horse" strategy.* Biometals, 2009. **22**(4): p. 615-24.

24. Banerjee, A., et al., *inhA, a gene encoding a target for isoniazid and ethionamide in Mycobacterium tuberculosis.* Science, 1994. **263**(5144): p. 227-30.

25. Kau, A.L., et al., *Human nutrition, the gut microbiome and the immune system.* Nature, 2011. **474**(7351): p. 327-36.

26. Larsen, N., et al., *Gut microbiota in human adults with type 2 diabetes differs from non-diabetic adults.* PLoS One, 2010. **5**(2): p. e9085.

27. Turnbaugh, P.J., et al., *A core gut microbiome in obese and lean twins.* Nature, 2009. **457**(7228): p. 480-4.

28. Neufeld, K.M., et al., *Reduced anxiety-like behavior and central neurochemical change in germ-free mice.* Neurogastroenterol Motil, 2011. **23**(3): p. 255-64, e119.

29. Freiberg, C. and H. Brotz-Oesterhelt, *Functional genomics in antibacterial drug discovery.* Drug Discov Today, 2005. **10**(13): p. 927-35.

30. Kurz, C.L. and J.J. Ewbank, *Infection in a dish: high-throughput analyses of bacterial pathogenesis.* Curr Opin Microbiol, 2007. **10**(1): p. 10-6.

31. Maresso, A.W. and O. Schneewind, *Sortase as a target of anti-infective therapy.* Pharmacol Rev, 2008. **60**(1): p. 128-41.

32. Escaich, S., *Novel agents to inhibit microbial virulence and pathogenicity.* Expert Opin Ther Pat, 2010. **20**(10): p. 1401-18.

33. Sasakawa, C. and J. Hacker, *Host-microbe interaction: bacteria.* Current Opinion in Microbiology, 2006. **9**(1): p. 1-4.

34. Gotz, F., *Staphylococci in colonization and disease: prospective targets for drugs and vaccines.* Curr Opin Microbiol, 2004. **7**(5): p. 477-87.

35. Berg, V., et al., *Design, synthesis and evaluation of peptidomimetics based on substituted bicyclic 2-pyridones-targeting virulence of uropathogenic E. coli.* Bioorg Med Chem, 2006. **14**(22): p. 7563-81.

36. Galan, J.E. and H. Wolf-Watz, *Protein delivery into eukaryotic cells by type III secretion machines.* Nature, 2006. **444**(7119): p. 567-73.

37. Ferreras, J.A., et al., *Small-molecule inhibition of siderophore biosynthesis in Mycobacterium tuberculosis and Yersinia pestis.* Nat Chem Biol, 2005. **1**(1): p. 29-32.

38. Kong, K.F., C. Vuong, and M. Otto, *Staphylococcus quorum sensing in biofilm formation and infection.* Int J Med Microbiol, 2006. **296**(2-3): p. 133-9.

39. Clatworthy, A.E., E. Pierson, and D.T. Hung, *Targeting virulence: a new paradigm for antimicrobial therapy.* Nat Chem Biol, 2007. **3**(9): p. 541-8.

40. Finlay, B.B. and G. McFadden, *Anti-Immunology: Evasion of the Host Immune System by Bacterial and Viral Pathogens.* Cell, 2006. **124**(4): p. 767-782.

41. Hornef, M.W., et al., *Bacterial strategies for overcoming host innate and adaptive immune responses.* Nat Immunol, 2002. **3**(11): p. 1033-40.

42. Genilloud, O., *The re-emerging role of microbial natural products in antibiotic discovery.* Antonie Van Leeuwenhoek, 2014. **106**(1): p. 173-88.

43. Iversen PW, B.B., Chen YF, et al, *HTS Assay Validation*, in *Assay Guidance Manual (Internet)*, C.N. Sittampalam GS, Nelson H, et al., Editor. 2012, Available from: www.ncbi.nlm.nih.gov/books/NBK83783/: Bethesda (MD): Eli Lilly & Company and the National Center for Advancing Translational Sciences.

44. *Screening requirements*. Available from: https://www.europeanleadfactory.eu/proposals/biological-assays/screening-requirements/.

45. Zhang, J.H., *A Simple Statistical Parameter for Use in Evaluation and Validation of High Throughput Screening Assays.* Journal of Biomolecular Screening, 1999. **4**(2): p. 67-73.

46. Ogston, A., *"On Abscesses".* Review of Infectious Diseases, 1984. **6**(1): p. 122-128.

47. Rosenbach, A.J., *Mikro-Organismen bei den Wund-Infektions-Krankheiten des Menschen.* Wiesbaden, J.F. Bergmann, 1884: p. 18.

48. Williams, R.E.O., *Healthy carriage of Staphylococcus aureus: its prevalence and importance.* Bacteriological Reviews, 1963. **27**(1): p. 56-71.

49. Reagan, D.R., et al., *Elimination of coincident Staphylococcus aureus nasal and hand carriage with intranasal application of mupirocin calcium ointment.* Ann Intern Med, 1991. **114**(2): p. 101-6.

50. Armstrong-Esther, C.A., *Carriage patterns of Staphylococcus aureus in a healthy non-hospital population of adults and children.* Ann Hum Biol, 1976. **3**(3): p. 221-7.

51. Noble, W.C., et al., *Some aspects of nasal carriage of staphylococci.* Journal of Clinical Pathology, 1964. **17**(1): p. 79-83.

52. Nouwen, J., et al., *Staphylococcus aureus carriage patterns and the risk of infections associated with continuous peritoneal dialysis.* J Clin Microbiol, 2006. **44**(6): p. 2233-6.

53. Tashakori, M., et al., *Staphylococcus aureus nasal carriage and patterns of antibiotic resistance in bacterial isolates from patients and staff in a dialysis center of southeast Iran.* Iran J Microbiol, 2014. **6**(2): p. 79-83.

54. Kluytmans, J., A. van Belkum, and H. Verbrugh, *Nasal carriage of Staphylococcus aureus: epidemiology, underlying mechanisms, and associated risks.* Clinical Microbiology Reviews, 1997. **10**(3): p. 505-520.

55. Gould, I.M., et al., *New insights into meticillin-resistant Staphylococcus aureus (MRSA) pathogenesis, treatment and resistance.* International Journal of Antimicrobial Agents. **39**(2): p. 96-104.

56. de Kraker, M.E., et al., *Clinical impact of antimicrobial resistance in European hospitals: excess mortality and length of hospital stay related to methicillin-resistant Staphylococcus aureus bloodstream infections.* Antimicrob Agents Chemother, 2011. **55**(4): p. 1598-605.

57.   Gardete, S. and A. Tomasz, *Mechanisms of vancomycin resistance in Staphylococcus aureus.* The Journal of Clinical Investigation, 2014. **124**(7): p. 2836-2840.

58.   Uhlemann, A.-C., et al., *Evolution of community- and healthcare-associated methicillin-resistant Staphylococcus aureus().* Infection, genetics and evolution : journal of molecular epidemiology and evolutionary genetics in infectious diseases, 2014. **21**: p. 563-574.

59.   Kulhankova, K., J. King, and W. Salgado-Pabón, *Staphylococcal toxic shock syndrome: superantigen-mediated enhancement of endotoxin shock and adaptive immune suppression.* Immunologic Research, 2014. **59**(1-3): p. 182-187.

60.   Otto, M., *Staphylococcus aureus toxins.* Current opinion in microbiology, 2014. **0**: p. 32-37.

61.   Francis, J.S., et al., *Severe community-onset pneumonia in healthy adults caused by methicillin-resistant Staphylococcus aureus carrying the Panton-Valentine leukocidin genes.* Clin Infect Dis, 2005. **40**(1): p. 100-7.

62.   Hennekinne, J.A., M.L. De Buyser, and S. Dragacci, *Staphylococcus aureus and its food poisoning toxins: characterization and outbreak investigation.* FEMS Microbiol Rev, 2012. **36**(4): p. 815-36.

63.   Perbet, S., et al., *Multifocal community-acquired necrotizing fasciitis caused by a Panton-Valentine leukocidin-producing methicillin-sensitive Staphylococcus aureus.* Infection, 2010. **38**(3): p. 223-5.

64.   International Working Group on the Classification of Staphylococcal Cassette Chromosome, E., *Classification of staphylococcal cassette chromosome mec (SCCmec): guidelines for reporting novel SCCmec elements.* Antimicrob Agents Chemother, 2009. **53**(12): p. 4961-7.

65.   McDougal, L.K., et al., *Emergence of Resistance among USA300 Methicillin-Resistant Staphylococcus aureus Isolates Causing Invasive Disease in the United States.* Antimicrobial Agents and Chemotherapy, 2010. **54**(9): p. 3804-3811.

66.   Foster, T.J., et al., *Adhesion, invasion and evasion: the many functions of the surface proteins of Staphylococcus aureus.* Nat Rev Micro, 2014. **12**(1): p. 49-62.

67.   Kim, H.K., et al., *Recurrent infections and immune evasion strategies of Staphylococcus aureus.* Current Opinion in Microbiology, 2012. **15**(1): p. 92-99.

68.   McCarthy, A.J. and J.A. Lindsay, *Genetic variation in Staphylococcus aureus surface and immune evasion genes is lineage associated: implications for vaccine design and host-pathogen interactions.* BMC Microbiol, 2010. **10**: p. 173.

69.   Hammer, N.D. and E.P. Skaar, *Molecular mechanisms of Staphylococcus aureus iron acquisition.* Annu Rev Microbiol, 2011. **65**: p. 129-47.

70.   Mulcahy, M.E., et al., *Nasal Colonisation by <italic>Staphylococcus aureus</italic> Depends upon Clumping Factor B Binding to the Squamous Epithelial Cell Envelope Protein Loricrin.* PLoS Pathog, 2012. **8**(12): p. e1003092.

71.   Clarke, S.R., et al., *Identification of in vivo-expressed antigens of Staphylococcus aureus and their use in vaccinations for protection against nasal carriage.* J Infect Dis, 2006. **193**(8): p. 1098-108.

72.   Schroeder, K., et al., *Molecular characterization of a novel Staphylococcus aureus surface protein (SasC) involved in cell aggregation and biofilm accumulation.* PLoS One, 2009. **4**(10): p. e7567.

73.   Corrigan, R.M., et al., *The role of Staphylococcus aureus surface protein SasG in adherence and biofilm formation.* Microbiology, 2007. **153**(Pt 8): p. 2435-46.

74.   Li, M., et al., *MRSA epidemic linked to a quickly spreading colonization and virulence determinant.* Nat Med, 2012. **18**(5): p. 816-819.

75.   Cucarella, C., et al., *Bap, a Staphylococcus aureus surface protein involved in biofilm formation.* J Bacteriol, 2001. **183**(9): p. 2888-96.

76.   Abraham, N.M. and K.K. Jefferson, *Staphylococcus aureus clumping factor B mediates biofilm formation in the absence of calcium.* Microbiology, 2012. **158**(Pt 6): p. 1504-12.

77.   Merino, N., et al., *Protein A-mediated multicellular behavior in Staphylococcus aureus.* J Bacteriol, 2009. **191**(3): p. 832-43.

78.   Pollitt, E.J.G., et al., *Cooperation, Quorum Sensing, and Evolution of Virulence in Staphylococcus aureus.* Infection and Immunity, 2014. **82**(3): p. 1045-1051.

79.   Novick, R.P., *Autoinduction and signal transduction in the regulation of staphylococcal virulence.* Mol Microbiol, 2003. **48**(6): p. 1429-49.

80.   Carnes, E.C., et al., *Confinement-induced quorum sensing of individual Staphylococcus aureus bacteria.* Nat Chem Biol, 2010. **6**(1): p. 41-5.

81.   Zong, Y., et al., *A 'Collagen Hug' model for Staphylococcus aureus CNA binding to collagen.* EMBO J, 2005. **24**(24): p. 4224-36.

82.   Keane, F.M., et al., *Fibrinogen and elastin bind to the same region within the A domain of fibronectin binding protein A, an MSCRAMM of Staphylococcus aureus.* Mol Microbiol, 2007. **63**(3): p. 711-23.

83.   Peacock, S.J., et al., *Bacterial fibronectin-binding proteins and endothelial cell surface fibronectin mediate adherence of Staphylococcus aureus to resting human endothelial cells.* Microbiology, 1999. **145 (Pt 12)**: p. 3477-86.

84.   Sinha, B., et al., *Heterologously expressed Staphylococcus aureus fibronectin-binding proteins are sufficient for invasion of host cells.* Infect Immun, 2000. **68**(12): p. 6871-8.

85.   Zapotoczna, M., et al., *Iron-regulated surface determinant B (IsdB) promotes Staphylococcus aureus adherence to and internalization by non-phagocytic human cells.* Cell Microbiol, 2013. **15**(6): p. 1026-41.

86.   Grigg, J.C., et al., *Structural biology of heme binding in the Staphylococcus aureus Isd system.* J Inorg Biochem, 2010. **104**(3): p. 341-8.

87.   Que, Y.-A., et al., *Fibrinogen and fibronectin binding cooperate for valve infection and invasion in Staphylococcus aureus experimental endocarditis.* The Journal of Experimental Medicine, 2005. **201**(10): p. 1627-1635.

88.   Entenza, J.M., et al., *Contribution of clumping factor B to pathogenesis of experimental endocarditis due to Staphylococcus aureus.* Infect Immun, 2000. **68**(9): p. 5443-6.

89.   Siboo, I.R., H.F. Chambers, and P.M. Sullam, *Role of SraP, a Serine-Rich Surface Protein of Staphylococcus aureus, in binding to human platelets.* Infect Immun, 2005. **73**(4): p. 2273-80.

90.   Rautenberg, M., et al., *Neutrophil responses to staphylococcal pathogens and commensals via the formyl peptide receptor 2 relates to phenol-soluble modulin release and virulence.* FASEB J, 2011. **25**(4): p. 1254-63.

91. Talbot, J.C., et al., *Dynamics and orientation of amphipathic peptides in solution and bound to membranes: a steady-state and time-resolved fluorescence study of staphylococcal delta-toxin and its synthetic analogues.* Eur Biophys J, 2001. **30**(2): p. 147-61.

92. Peschel, A. and M. Otto, *Phenol-soluble modulins and staphylococcal infection.* Nat Rev Micro, 2013. **11**(10): p. 667-673.

93. Valeva, A., et al., *Transmembrane beta-barrel of staphylococcal alpha-toxin forms in sensitive but not in resistant cells.* Proc Natl Acad Sci U S A, 1997. **94**(21): p. 11607-11.

94. Inoshima, I., et al., *A Staphylococcus aureus pore-forming toxin subverts the activity of ADAM10 to cause lethal infection in mice.* Nat Med, 2011. **17**(10): p. 1310-4.

95. Wilke, G.A. and J. Bubeck Wardenburg, *Role of a disintegrin and metalloprotease 10 in Staphylococcus aureus alpha-hemolysin-mediated cellular injury.* Proc Natl Acad Sci U S A, 2010. **107**(30): p. 13473-8.

96. Vandenesch, F., et al., *Community-Acquired Methicillin-Resistant Staphylococcus aureus Carrying Panton-Valentine Leukocidin Genes: Worldwide Emergence.* Emerging Infectious Diseases, 2003. **9**(8): p. 978-984.

97. Spaan, András N., et al., *The Staphylococcal Toxin Panton-Valentine Leukocidin Targets Human C5a Receptors.* Cell Host & Microbe, 2013. **13**(5): p. 584-594.

98. Lin, C.F., et al., *Different types of cell death induced by enterotoxins.* Toxins (Basel), 2010. **2**(8): p. 2158-76.

99. Salgado-Pabon, W., et al., *Superantigens are critical for Staphylococcus aureus Infective endocarditis, sepsis, and acute kidney injury.* MBio, 2013. **4**(4).

100. Schlievert, P.M., et al., *Identification and characterization of an exotoxin from Staphylococcus aureus associated with toxic-shock syndrome.* J Infect Dis, 1981. **143**(4): p. 509-16.

101. Schlievert, P.M., *Enhancement of host susceptibility to lethal endotoxin shock by staphylococcal pyrogenic exotoxin type C.* Infect Immun, 1982. **36**(1): p. 123-8.

102. Canonico, P.G. and M.J. Van Zwieten, *Swelling of mitochondria from rabbit liver induced by staphylococcal enterotoxin B.* J Infect Dis, 1971. **124**(4): p. 372-8.

103. Stone, R.L. and P.M. Schlievert, *Evidence for the involvement of endotoxin in toxic shock syndrome.* J Infect Dis, 1987. **155**(4): p. 682-9.

104. Rossi, R.J., et al., *Staphylococcal enterotoxins condition cells of the innate immune system for Toll-like receptor 4 stimulation.* Int Immunol, 2004. **16**(12): p. 1751-60.

105. Nizet, V., *Understanding how leading bacterial pathogens subvert innate immunity to reveal novel therapeutic targets.* Journal of Allergy and Clinical Immunology. **120**(1): p. 13-22.

106. Zecconi, A. and F. Scali, *Staphylococcus aureus virulence factors in evasion from innate immune defenses in human and animal diseases.* Immunology Letters, 2013. **150**(1–2): p. 12-22.

107. Schroder, N.W., et al., *Lipoteichoic acid (LTA) of Streptococcus pneumoniae and Staphylococcus aureus activates immune cells via Toll-like receptor (TLR)-2, lipopolysaccharide-binding protein (LBP), and CD14, whereas TLR-4 and MD-2 are not involved.* J Biol Chem, 2003. **278**(18): p. 15587-94.

108. Bardoel, B.W., et al., *Evasion of Toll-like receptor 2 activation by staphylococcal superantigen-like protein 3.* J Mol Med (Berl), 2012. **90**(10): p. 1109-20.

109. Powers, M.E. and J.B. Wardenburg, *Igniting the Fire: Staphylococcus aureus Virulence Factors in the Pathogenesis of Sepsis.* PLoS Pathogens, 2014. **10**(2): p. e1003871.

110. Panizzi, P., et al., *Fibrinogen substrate recognition by staphylocoagulase.(pro)thrombin complexes.* J Biol Chem, 2006. **281**(2): p. 1179-87.

111. Schouten, M., et al., *Inflammation, endothelium, and coagulation in sepsis.* J Leukoc Biol, 2008. **83**(3): p. 536-45.

112. Thammavongsa, V., et al., *Staphylococcus aureus synthesizes adenosine to escape host immune responses.* J Exp Med, 2009. **206**(11): p. 2417-27.

113. Thiel, M., C.C. Caldwell, and M.V. Sitkovsky, *The critical role of adenosine A2A receptors in downregulation of inflammation and immunity in the pathogenesis of infectious diseases.* Microbes Infect, 2003. **5**(6): p. 515-26.

114. Voyich, J.M., et al., *Insights into Mechanisms Used by Staphylococcus aureus to Avoid Destruction by Human Neutrophils.* The Journal of Immunology, 2005. **175**(6): p. 3907-3919.

115. Liu, C.I., et al., *A cholesterol biosynthesis inhibitor blocks Staphylococcus aureus virulence.* Science, 2008. **319**(5868): p. 1391-4.

116. Jenssen, H., P. Hamill, and R.E. Hancock, *Peptide antimicrobial agents.* Clin Microbiol Rev, 2006. **19**(3): p. 491-511.

117. Li, M., et al., *The antimicrobial peptide-sensing system aps of Staphylococcus aureus.* Mol Microbiol, 2007. **66**(5): p. 1136-47.

118. Lindmark, R., K. Thoren-Tolling, and J. Sjoquist, *Binding of immunoglobulins to protein A and immunoglobulin levels in mammalian sera.* J Immunol Methods, 1983. **62**(1): p. 1-13.

119. Hartleib, J., et al., *Protein A is the von Willebrand factor binding protein onStaphylococcus aureus*. Vol. 96. 2000. 2149-2156.

120. Sullam, P.M., et al., *Diminished platelet binding in vitro by Staphylococcus aureus is associated with reduced virulence in a rabbit model of infective endocarditis.* Infect Immun, 1996. **64**(12): p. 4915-21.

121. Smith, E.J., et al., *The Sbi Protein Is a Multifunctional Immune Evasion Factor of Staphylococcus aureus.* Infection and Immunity, 2011. **79**(9): p. 3801-3809.

122. Gomez, M.I., et al., *Staphylococcus aureus protein A activates TNFR1 signaling through conserved IgG binding domains.* J Biol Chem, 2006. **281**(29): p. 20190-6.

123. Toapanta, F.R. and T.M. Ross, *Complement-mediated activation of the adaptive immune responses: role of C3d in linking the innate and adaptive immunity.* Immunol Res, 2006. **36**(1-3): p. 197-210.

124. Forsgren, A., A. Svedjelund, and H. Wigzell, *Lymphocyte stimulation by protein A of Staphylococcus aureus.* Eur J Immunol, 1976. **6**(3): p. 207-13.

125. Goodyear, C.S. and G.J. Silverman, *Staphylococcal toxin induced preferential and prolonged in vivo deletion of innate-like B lymphocytes.* Proc Natl Acad Sci U S A, 2004. **101**(31): p. 11392-7.

126. Shockman, G.D. and J.F. Barrett, *Structure, function, and assembly of cell walls of gram-positive bacteria.* Annu Rev Microbiol, 1983. **37**: p. 501-27.

127. Gram, H.C., *Über die isolierte Färbung der Schizomyceten in Schnitt- und Trockenpräparaten.* Fortschritte der Medizin, 1884. **2**: p. 185-89.

128. Duong, F., et al., *Biogenesis of the gram-negative bacterial envelope.* Cell, 1997. **91**(5): p. 567-73.

129. Schneewind, O., P. Model, and V.A. Fischetti, *Sorting of protein A to the staphylococcal cell wall.* Cell, 1992. **70**(2): p. 267-81.

130. Navarre, W.W. and O. Schneewind, *Surface proteins of gram-positive bacteria and mechanisms of their targeting to the cell wall envelope.* Microbiol Mol Biol Rev, 1999. **63**(1): p. 174-229.

131. Gorlich, D. and T.A. Rapoport, *Protein translocation into proteoliposomes reconstituted from purified components of the endoplasmic reticulum membrane.* Cell, 1993. **75**(4): p. 615-30.

132. Economou, A., et al., *SecA membrane cycling at SecYEG is driven by distinct ATP binding and hydrolysis events and is regulated by SecD and SecF.* Cell, 1995. **83**(7): p. 1171-81.

133. Duong, F. and W. Wickner, *The SecDFyajC domain of preprotein translocase controls preprotein movement by regulating SecA membrane cycling.* EMBO J, 1997. **16**(16): p. 4871-9.

134. Halic, M., et al., *Following the signal sequence from ribosomal tunnel exit to signal recognition particle.* Nature, 2006. **444**(7118): p. 507-11.

135. Schneewind, O. and D.M. Missiakas, *Protein secretion and surface display in Gram-positive bacteria.* Philos Trans R Soc Lond B Biol Sci, 2012. **367**(1592): p. 1123-39.

136. Sibbald, M.J., et al., *Mapping the pathways to staphylococcal pathogenesis by comparative secretomics.* Microbiol Mol Biol Rev, 2006. **70**(3): p. 755-88.

137. Mazmanian, S.K., et al., *Staphylococcus aureus sortase, an enzyme that anchors surface proteins to the cell wall.* Science, 1999. **285**(5428): p. 760-3.

138. Fischetti, V.A., V. Pancholi, and O. Schneewind, *Conservation of a hexapeptide sequence in the anchor region of surface proteins from gram-positive cocci.* Mol Microbiol, 1990. **4**(9): p. 1603-5.

139. Dhar, G., K.F. Faull, and O. Schneewind, *Anchor structure of cell wall surface proteins in Listeria monocytogenes.* Biochemistry, 2000. **39**(13): p. 3725-33.

140. Zong, Y., et al., *Crystal structures of Staphylococcus aureus sortase A and its substrate complex.* J Biol Chem, 2004. **279**(30): p. 31383-9.

141. Ton-That, H., et al., *Purification and characterization of sortase, the transpeptidase that cleaves surface proteins of Staphylococcus aureus at the LPXTG motif.* Proc Natl Acad Sci U S A, 1999. **96**(22): p. 12424-9.

142. Marraffini, L.A., A.C. Dedent, and O. Schneewind, *Sortases and the art of anchoring proteins to the envelopes of gram-positive bacteria.* Microbiol Mol Biol Rev, 2006. **70**(1): p. 192-221.

143. Mazmanian, S.K., et al., *Passage of heme-iron across the envelope of Staphylococcus aureus.* Science, 2003. **299**(5608): p. 906-9.

144. Mazmanian, S.K., et al., *An iron-regulated sortase anchors a class of surface protein during Staphylococcus aureus pathogenesis.* Proc Natl Acad Sci U S A, 2002. **99**(4): p. 2293-8.

145. Elliot, M.A., et al., *The chaplins: a family of hydrophobic cell-surface proteins involved in aerial mycelium formation in Streptomyces coelicolor.* Genes Dev, 2003. **17**(14): p. 1727-40.

146. Nallapareddy, S.R., et al., *Endocarditis and biofilm-associated pili of Enterococcus faecalis.* J Clin Invest, 2006. **116**(10): p. 2799-807.

147. Oh, S.Y., J.M. Budzik, and O. Schneewind, *Sortases make pili from three ingredients.* Proc Natl Acad Sci U S A, 2008. **105**(37): p. 13703-4.

148. Frankel, B.A., et al., *Staphylococcus aureus sortase transpeptidase SrtA: insight into the kinetic mechanism and evidence for a reverse protonation catalytic mechanism.* Biochemistry, 2005. **44**(33): p. 11188-200.

149. Ton-That, H., et al., *Anchoring of surface proteins to the cell wall of Staphylococcus aureus. Cysteine 184 and histidine 120 of sortase form a thiolate-imidazolium ion pair for catalysis.* J Biol Chem, 2002. **277**(9): p. 7447-52.

150. Dessen, A., *A new catalytic dyad regulates anchoring of molecules to the Gram-positive cell wall by sortases.* Structure, 2004. **12**(1): p. 6-7.

151. Marraffini, L.A., et al., *Anchoring of surface proteins to the cell wall of Staphylococcus aureus. A conserved arginine residue is required for efficient catalysis of sortase A.* J Biol Chem, 2004. **279**(36): p. 37763-70.

152. Ton-That, H., et al., *Anchoring of surface proteins to the cell wall of Staphylococcus aureus. Sortase catalyzed in vitro transpeptidation reaction using LPXTG peptide and NH(2)-Gly(3) substrates.* J Biol Chem, 2000. **275**(13): p. 9876-81.

153. Huang, X., et al., *Kinetic mechanism of Staphylococcus aureus sortase SrtA.* Biochemistry, 2003. **42**(38): p. 11307-15.

154. Ilangovan, U., et al., *Structure of sortase, the transpeptidase that anchors proteins to the cell wall of Staphylococcus aureus.* Proc Natl Acad Sci U S A, 2001. **98**(11): p. 6056-61.

155. Naik, M.T., et al., *Staphylococcus aureus Sortase A transpeptidase. Calcium promotes sorting signal binding by altering the mobility and structure of an active site loop.* J Biol Chem, 2006. **281**(3): p. 1817-26.

156. Bentley, M.L., et al., *Engineering the substrate specificity of Staphylococcus aureus Sortase A. The beta6/beta7 loop from SrtB confers NPQTN recognition to SrtA.* J Biol Chem, 2007. **282**(9): p. 6571-81.

157. Suree, N., et al., *The structure of the Staphylococcus aureus sortase-substrate complex reveals how the universally conserved LPXTG sorting signal is recognized.* J Biol Chem, 2009. **284**(36): p. 24465-77.

158. Oh, K.B., et al., *Inhibition of sortase-mediated Staphylococcus aureus adhesion to fibronectin via fibronectin-binding protein by sortase inhibitors.* Appl Microbiol Biotechnol, 2006. **70**(1): p. 102-6.

159. Tsompanidou, E., et al., *The Sortase A Substrates FnbpA, FnbpB, ClfA and ClfB Antagonize Colony Spreading of Staphylococcus aureus.* PLoS One, 2012. **7**(9): p. e44646.

160. Paterson, G.K. and T.J. Mitchell, *The biology of Gram-positive sortase enzymes.* Trends Microbiol, 2004. **12**(2): p. 89-95.

161. Mazmanian, S.K., et al., *Staphylococcus aureus sortase mutants defective in the display of surface proteins and in the pathogenesis of animal infections.* Proc Natl Acad Sci U S A, 2000. **97**(10): p. 5510-5.

162. Oh, K.B., et al., *Therapeutic effect of (Z)-3-(2,5-dimethoxyphenyl)-2-(4-methoxyphenyl) acrylonitrile (DMMA) against Staphylococcus aureus infection in a murine model.* Biochem Biophys Res Commun, 2010. **396**(2): p. 440-4.

163. Cascioferro, S., M. Totsika, and D. Schillaci, *Sortase A: an ideal target for anti-virulence drug development.* Microb Pathog, 2014. **77**: p. 105-12.

164. Comfort, D. and R.T. Clubb, *A comparative genome analysis identifies distinct sorting pathways in gram-positive bacteria.* Infect Immun, 2004. **72**(5): p. 2710-22.

165. Scott, C.J., et al., *Irreversible inhibition of the bacterial cysteine protease-transpeptidase sortase (SrtA) by substrate-derived affinity labels.* Biochem J, 2002. **366**(Pt 3): p. 953-8.

166. Kim, S.H., et al., *Inhibition of the bacterial surface protein anchoring transpeptidase sortase by isoquinoline alkaloids.* Biosci Biotechnol Biochem, 2004. **68**(2): p. 421-4.

167. Jang, K.H., et al., *Aaptamines as sortase A inhibitors from the tropical sponge Aaptos aaptos.* Bioorg Med Chem Lett, 2007. **17**(19): p. 5366-9.

168. Jeon, J.E., et al., *Discorhabdins from the Korean marine sponge Sceptrella sp.* J Nat Prod, 2010. **73**(2): p. 258-62.

169. Lee, Y.J., et al., *Synthetic analogs of indole-containing natural products as inhibitors of sortase A and isocitrate lyase.* Bioorg Med Chem Lett, 2010. **20**(23): p. 6882-5.

170. Chenna, B.C., et al., *Identification of novel inhibitors of bacterial surface enzyme Staphylococcus aureus Sortase A.* Bioorg Med Chem Lett, 2008. **18**(1): p. 380-5.

171. Chenna, B.C., et al., *Synthesis and structure activity relationship studies of novel Staphylococcus aureus Sortase A inhibitors.* Eur J Med Chem, 2010. **45**(9): p. 3752-61.

172. Oh, K.B., et al., *Discovery of diarylacrylonitriles as a novel series of small molecule sortase A inhibitors.* J Med Chem, 2004. **47**(10): p. 2418-21.

173. Maresso, A.W., et al., *Activation of inhibitors by sortase triggers irreversible modification of the active site.* J Biol Chem, 2007. **282**(32): p. 23129-39.

174. Suree, N., et al., *Discovery and structure-activity relationship analysis of Staphylococcus aureus sortase A inhibitors.* Bioorg Med Chem, 2009. **17**(20): p. 7174-85.

175. Fitzgerald-Hughes, D., M. Devocelle, and H. Humphreys, *Beyond conventional antibiotics for the future treatment of methicillin-resistant Staphylococcus aureus infections: two novel alternatives.* FEMS Immunol Med Microbiol, 2012. **65**(3): p. 399-412.

176. Uddin, R., M.U. Lodhi, and Z. Ul-Haq, *Combined pharmacophore and 3D-QSAR study on a series of Staphylococcus aureus Sortase A inhibitors.* Chem Biol Drug Des, 2012. **80**(2): p. 300-14.

177. Marshall, B.J. and J.R. Warren, *Unidentified curved bacilli in the stomach of patients with gastritis and peptic ulceration.* Lancet, 1984. **1**(8390): p. 1311-5.

178. ORGANIZATION, W.H., *Schistosomes, Liver Flukes and Helicobacter Pylori.* IARC Monographs on the Evaluation of Carcinogenic Risks to Humans, 1994. **61**(ISBN 92 832 12614).

179. Moodley, Y., et al., *Age of the Association between Helicobacter pylori and Man.* PLoS Pathogens, 2012. **8**(5): p. e1002693.

180. Atherton, J.C. and M.J. Blaser, *Coadaptation of Helicobacter pylori and humans: ancient history, modern implications.* J Clin Invest, 2009. **119**(9): p. 2475-87.

181. Linz, B., et al., *An African origin for the intimate association between humans and Helicobacter pylori.* Nature, 2007. **445**(7130): p. 915-8.

182. Drumm, B., et al., *Intrafamilial clustering of Helicobacter pylori infection.* N Engl J Med, 1990. **322**(6): p. 359-63.

183. Taylor, D.N. and M.J. Blaser, *The epidemiology of Helicobacter pylori infection.* Epidemiol Rev, 1991. **13**: p. 42-59.

184. Kauser, F., et al., *The cag pathogenicity island of Helicobacter pylori is disrupted in the majority of patient isolates from different human populations.* J Clin Microbiol, 2004. **42**(11): p. 5302-8.

185. Urgesi, R., R. Cianci, and M.E. Riccioni, *Update on triple therapy for eradication of Helicobacter pylori: current status of the art.* Clinical and Experimental Gastroenterology, 2012. **5**: p. 151-157.

186. Megraud, F. and H. Lamouliatte, *Helicobacter pylori and duodenal ulcer. Evidence suggesting causation.* Dig Dis Sci, 1992. **37**(5): p. 769-72.

187. Ferlay, J., et al., *Cancer incidence and mortality worldwide: sources, methods and major patterns in GLOBOCAN 2012.* Int J Cancer, 2015. **136**(5): p. E359-86.

188. Zhang, X., et al., *Analysis of the association of interleukin-17 gene polymorphisms with gastric cancer risk and interaction with Helicobacter pylori infection in a Chinese population.* Tumor Biology, 2014. **35**(2): p. 1575-1580.

189. Yang, J.-C., C.-W. Lu, and C.-J. Lin, *Treatment of Helicobacter pylori infection: Current status and future concepts.* World Journal of Gastroenterology : WJG, 2014. **20**(18): p. 5283-5293.

190. Ierardi, E., et al., *How antibiotic resistances could change Helicobacter pylori treatment: A matter of geography?* World Journal of Gastroenterology : WJG, 2013. **19**(45): p. 8168-8180.

191. Papastergiou, V., S.D. Georgopoulos, and S. Karatapanis, *Treatment of Helicobacter pylori infection: Past, present and future.* World Journal of Gastrointestinal Pathophysiology, 2014. **5**(4): p. 392-399.

192. Anderl, F. and M. Gerhard, *Helicobacter pylori vaccination: Is there a path to protection?* World Journal of Gastroenterology : WJG, 2014. **20**(34): p. 11939-11949.

193. Fiocca, R., et al., *Epithelial cytotoxicity, immune responses, and inflammatory components of Helicobacter pylori gastritis.* Scand J Gastroenterol Suppl, 1994. **205**: p. 11-21.

194. Carrick, J., et al., *Campylobacter pylori, duodenal ulcer, and gastric metaplasia: possible role of functional heterotopic tissue in ulcerogenesis.* Gut, 1989. **30**(6): p. 790-7.

195. Ernst, P.B. and B.D. Gold, *The disease spectrum of Helicobacter pylori: the immunopathogenesis of gastroduodenal ulcer and gastric cancer.* Annu Rev Microbiol, 2000. **54**: p. 615-40.

196. Fischbach, W., *Gastric MALT lymphoma – Update on diagnosis and treatment.* Best Practice & Research Clinical Gastroenterology. **28**(6): p. 1069-1077.

197. Crew, K.D. and A.I. Neugut, *Epidemiology of gastric cancer.* World J Gastroenterol, 2006. **12**(3): p. 354-62.

198. Lin, D. and B. Koskella, *Friend and foe: factors influencing the movement of the bacterium Helicobacter pylori along the parasitism–mutualism continuum.* Evolutionary Applications, 2015. **8**(1): p. 9-22.

199. Chen, Y. and M.J. Blaser, *Inverse associations of Helicobacter pylori with asthma and allergy.* Arch Intern Med, 2007. **167**(8): p. 821-7.

200. Perry, S., et al., *Infection with Helicobacter pylori is associated with protection against tuberculosis.* PLoS One, 2010. **5**(1): p. e8804.

201. Whiteman, D.C., et al., *Association of Helicobacter pylori infection with reduced risk for esophageal cancer is independent of environmental and genetic modifiers.* Gastroenterology, 2010. **139**(1): p. 73-83; quiz e11-2.

202. Xie, F.J., et al., *Helicobacter pylori infection and esophageal cancer risk: an updated meta-analysis.* World J Gastroenterol, 2013. **19**(36): p. 6098-107.

203. Yamaoka, Y., *Mechanisms of disease: Helicobacter pylori virulence factors.* Nat Rev Gastroenterol Hepatol, 2010. **7**(11): p. 629-41.

204. Suerbaum, S. and P. Michetti, *Helicobacter pylori infection.* N Engl J Med, 2002. **347**(15): p. 1175-86.

205. Pachathundikandi, S.K., N. Tegtmeyer, and S. Backert, *Signal transduction of Helicobacter pylori during interaction with host cell protein receptors of epithelial and immune cells.* Gut Microbes, 2013. **4**(6): p. 454-74.

206. Weeks, D.L., et al., *A H+-Gated Urea Channel: The Link Between Helicobacter pylori Urease and Gastric Colonization.* Science, 2000. **287**(5452): p. 482-485.

207. Cussac, V., R.L. Ferrero, and A. Labigne, *Expression of Helicobacter pylori urease genes in Escherichia coli grown under nitrogen-limiting conditions.* J Bacteriol, 1992. **174**(8): p. 2466-73.

208. Suerbaum, S., *The complex flagella of gastric Helicobacter species.* Trends Microbiol, 1995. **3**(5): p. 168-70; discussion 170-1.

209. Valenzuela, M., O. Cerda, and H. Toledo, *Overview on chemotaxis and acid resistance in Helicobacter pylori.* Biol Res, 2003. **36**(3-4): p. 429-36.

210. Nakamura, H., et al., *Urease plays an important role in the chemotactic motility of Helicobacter pylori in a viscous environment.* Infect Immun, 1998. **66**(10): p. 4832-7.

211. Namavar, F., et al., *Neutrophil-activating protein mediates adhesion of Helicobacter pylori to sulfated carbohydrates on high-molecular-weight salivary mucin.* Infect Immun, 1998. **66**(2): p. 444-7.

212. Slomiany, B.L., et al., *Campylobacter pyloridis degrades mucin and undermines gastric mucosal integrity.* Biochem Biophys Res Commun, 1987. **144**(1): p. 307-14.

213. Talebi Bezmin Abadi, A., *Novel Idea: Virulence-Based Therapy Against Helicobacter pylori Infection (Smart Therapy).* Frontiers in Medicine, 2014. **1**: p. 18.

214. Boren, T., et al., *Attachment of Helicobacter pylori to human gastric epithelium mediated by blood group antigens.* Science, 1993. **262**(5141): p. 1892-5.

215. Gerhard, M., et al., *Clinical relevance of the Helicobacter pylori gene for blood-group antigen-binding adhesin.* Proc Natl Acad Sci U S A, 1999. **96**(22): p. 12778-83.

216. Odenbreit, S., *Adherence properties of Helicobacter pylori: Impact on pathogenesis and adaptation to the host.* International Journal of Medical Microbiology, 2005. **295**(5): p. 317-324.

217. Loh, J.T., et al., *Helicobacter pylori HopQ outer membrane protein attenuates bacterial adherence to gastric epithelial cells.* FEMS Microbiol Lett, 2008. **289**(1): p. 53-8.

218. Oleastro, M. and A. Menard, *The Role of Helicobacter pylori Outer Membrane Proteins in Adherence and Pathogenesis.* Biology (Basel), 2013. **2**(3): p. 1110-34.

219. Viala, J., et al., *Nod1 responds to peptidoglycan delivered by the Helicobacter pylori cag pathogenicity island.* Nat Immunol, 2004. **5**(11): p. 1166-74.

220. Suarez, G., et al., *Modification of Helicobacter pylori Peptidoglycan Enhances NOD1 Activation and Promotes Cancer of the Stomach.* Cancer Res, 2015. **75**(8): p. 1749-59.

221. Segal, E.D., et al., *Altered states: Involvement of phosphorylated CagA in the induction of host cellular growth changes by Helicobacter pylori.* Proceedings of the National Academy of Sciences of the United States of America, 1999. **96**(25): p. 14559-14564.

222. Bessede, E., et al., *Helicobacter pylori generates cells with cancer stem cell properties via epithelial-mesenchymal transition-like changes.* Oncogene, 2014. **33**(32): p. 4123-31.

223. Backert, S., et al., *Phosphorylation of tyrosine 972 of the Helicobacter pylori CagA protein is essential for induction of a scattering phenotype in gastric epithelial cells.* Molecular Microbiology, 2001. **42**(3): p. 631-644.

224. Murata-Kamiya, N., et al., *Helicobacter pylori CagA interacts with E-cadherin and deregulates the beta-catenin signal that promotes intestinal transdifferentiation in gastric epithelial cells.* Oncogene, 2007. **26**(32): p. 4617-26.

225. van Doorn, L.J., et al., *Clinical relevance of the cagA, vacA, and iceA status of Helicobacter pylori.* Gastroenterology, 1998. **115**(1): p. 58-66.

226. Malaty, H.M., *Epidemiology of Helicobacter pylori infection.* Best Pract Res Clin Gastroenterol, 2007. **21**(2): p. 205-14.

227. Lupetti, P., et al., *Oligomeric and subunit structure of the Helicobacter pylori vacuolating cytotoxin.* J Cell Biol, 1996. **133**(4): p. 801-7.

228. Szabo, I., et al., *Formation of anion-selective channels in the cell plasma membrane by the toxin VacA of Helicobacter pylori is required for its biological activity.* EMBO J, 1999. **18**(20): p. 5517-27.

229. Boquet, P. and V. Ricci, *Intoxication strategy of Helicobacter pylori VacA toxin.* Trends Microbiol, 2012. **20**(4): p. 165-74.

230. Smoot, D.T., et al., *Effects of Helicobacter pylori vacuolating cytotoxin on primary cultures of human gastric epithelial cells.* Gut, 1996. **39**(6): p. 795-9.

231. Atherton, J.C., et al., *Mosaicism in vacuolating cytotoxin alleles of Helicobacter pylori. Association of specific vacA types with cytotoxin production and peptic ulceration.* J Biol Chem, 1995. **270**(30): p. 17771-7.

232. Rudi, J., et al., *Diversity of Helicobacter pylori vacA and cagA genes and relationship to VacA and CagA protein expression, cytotoxin production, and associated diseases.* J Clin Microbiol, 1998. **36**(4): p. 944-8.

233. Clausen, T., et al., *HTRA proteases: regulated proteolysis in protein quality control.* Nat Rev Mol Cell Biol, 2011. **12**(3): p. 152-62.

234. Hoy, B., et al., *Helicobacter pylori HtrA is a new secreted virulence factor that cleaves E-cadherin to disrupt intercellular adhesion.* EMBO Rep, 2010. **11**(10): p. 798-804.

235. Balkovetz, D.F. and J. Katz, *Bacterial invasion by a paracellular route: divide and conquer.* Microbes Infect, 2003. **5**(7): p. 613-9.

236. Wroblewski, L.E. and R.M. Peek, *"Targeted disruption of the epithelial-barrier by Helicobacter pylori".* Cell Commun Signal, 2011. **9**(1): p. 29.

237. Senkovich, O.A., et al., *Helicobacter pylori AlpA and AlpB bind host laminin and influence gastric inflammation in gerbils.* Infect Immun, 2011. **79**(8): p. 3106-16.

238. Barczyk, M., S. Carracedo, and D. Gullberg, *Integrins.* Cell Tissue Res, 2010. **339**(1): p. 269-80.

239. Janeway, C.A. and R. Medzhitov, *Innate immune recognition.* Annu Rev Immunol, 2002. **20**: p. 197-216.

240. Akira, S. and K. Takeda, *Toll-like receptor signalling.* Nat Rev Immunol, 2004. **4**(7): p. 499-511.

241. Muotiala, A., et al., *Low biological activity of Helicobacter pylori lipopolysaccharide.* Infect Immun, 1992. **60**(4): p. 1714-6.

242. Appelmelk, B.J., et al., *Potential role of molecular mimicry between Helicobacter pylori lipopolysaccharide and host Lewis blood group antigens in autoimmunity.* Infect Immun, 1996. **64**(6): p. 2031-40.

243. Gewirtz, A.T., et al., *Helicobacter pylori flagellin evades toll-like receptor 5-mediated innate immunity.* J Infect Dis, 2004. **189**(10): p. 1914-20.

244. Bauer, S., et al., *Human TLR9 confers responsiveness to bacterial DNA via species-specific CpG motif recognition.* Proc Natl Acad Sci U S A, 2001. **98**(16): p. 9237-42.

245. Cornélie, S., et al., *Direct Evidence that Toll-like Receptor 9 (TLR9) Functionally Binds Plasmid DNA by Specific Cytosine-phosphate-guanine Motif Recognition.* Journal of Biological Chemistry, 2004. **279**(15): p. 15124-15129.

246. Takata, T., et al., *Phenotypic and genotypic variation in methylases involved in type II restriction-modification systems in Helicobacter pylori.* Nucleic Acids Res, 2002. **30**(11): p. 2444-52.

247. Castaño-Rodríguez, N., et al., *Genetic polymorphisms in the Toll-like receptor signalling pathway in Helicobacter pylori infection and related gastric cancer.* Human Immunology, 2014. **75**(8): p. 808-815.

248. Dundon, W.G., et al., *The neutrophil-activating protein of Helicobacter pylori.* Int J Med Microbiol, 2002. **291**(6-7): p. 545-50.

249. de Bernard, M. and C. Josenhans, *Pathogenesis of Helicobacter pylori Infection.* Helicobacter, 2014. **19**: p. 11-18.

250. Suzuki, T., et al., *Localization of antigen-presenting cells in Helicobacter pylori-infected gastric mucosa.* Pathol Int, 2002. **52**(4): p. 265-71.

251. Gobert, A.P., et al., *Helicobacter pylori arginase inhibits nitric oxide production by eukaryotic cells: a strategy for bacterial survival.* Proc Natl Acad Sci U S A, 2001. **98**(24): p. 13844-9.

252. Ramarao, N., et al., *Helicobacter pylori inhibits phagocytosis by professional phagocytes involving type IV secretion components.* Mol Microbiol, 2000. **37**(6): p. 1389-404.

253. Allen, L.A., L.S. Schlesinger, and B. Kang, *Virulent strains of Helicobacter pylori demonstrate delayed phagocytosis and stimulate homotypic phagosome fusion in macrophages.* J Exp Med, 2000. **191**(1): p. 115-28.

254. Molinari, M., et al., *Selective inhibition of Ii-dependent antigen presentation by Helicobacter pylori toxin VacA.* J Exp Med, 1998. **187**(1): p. 135-40.

255. Gebert, B., et al., *Helicobacter pylori vacuolating cytotoxin inhibits T lymphocyte activation.* Science, 2003. **301**(5636): p. 1099-102.

256. Sewald, X., et al., *Integrin subunit CD18 Is the T-lymphocyte receptor for the Helicobacter pylori vacuolating cytotoxin.* Cell Host Microbe, 2008. **3**(1): p. 20-9.

257. Schmees, C., et al., *Inhibition of T-cell proliferation by Helicobacter pylori gamma-glutamyl transpeptidase.* Gastroenterology, 2007. **132**(5): p. 1820-33.

258. Boanca, G., et al., *Autoprocessing of Helicobacter pylori gamma-glutamyltranspeptidase leads to the formation of a threonine-threonine catalytic dyad.* J Biol Chem, 2007. **282**(1): p. 534-41.

259. Ohkama-Ohtsu, N., et al., *Glutathione conjugates in the vacuole are degraded by gamma-glutamyl transpeptidase GGT3 in Arabidopsis.* Plant J, 2007. **49**(5): p. 878-88.

260. Okada, T., et al., *Crystal structures of γ-glutamyltranspeptidase from Escherichia coli, a key enzyme in glutathione metabolism, and its reaction intermediate.* Proceedings of the National Academy of Sciences of the United States of America, 2006. **103**(17): p. 6471-6476.

261. Brannigan, J.A., et al., *A protein catalytic framework with an N-terminal nucleophile is capable of self-activation.* Nature, 1995. **378**(6555): p. 416-419.

262. Boanca, G., A. Sand, and J.J. Barycki, *Uncoupling the enzymatic and autoprocessing activities of Helicobacter pylori gamma-glutamyltranspeptidase.* J Biol Chem, 2006. **281**(28): p. 19029-37.

263. Oinonen, C. and J. Rouvinen, *Structural comparison of Ntn-hydrolases.* Protein Sci, 2000. **9**(12): p. 2329-37.

264. Allison, R.D., *gamma-Glutamyl transpeptidase: kinetics and mechanism.* Methods Enzymol, 1985. **113**: p. 419-37.

265. Stromme, J.H. and L. Theodorsen, *Gamma-glutamyltransferase: Substrate inhibition, kinetic mechanism, and assay conditions.* Clin Chem, 1976. **22**(4): p. 417-21.

266. Meister, A., S.S. Tate, and O.W. Griffith, *Gamma-glutamyl transpeptidase.* Methods Enzymol, 1981. **77**: p. 237-53.

267. Keillor, J.W., et al., *Pre-steady-state kinetic studies of rat kidney γ-glutamyl transpeptidase confirm its ping-pong mechanism.* Journal of Physical Organic Chemistry, 2004. **17**(6-7): p. 529-536.

268. Wickham, S., et al., *Divergent effects of compounds on the hydrolysis and transpeptidation reactions of γ-glutamyl transpeptidase.* J Enzyme Inhib Med Chem, 2012. **27**(4): p. 476-89.

269. Hanigan, M.H. and H.F. Frierson, Jr., *Immunohistochemical detection of gamma-glutamyl transpeptidase in normal human tissue.* J Histochem Cytochem, 1996. **44**(10): p. 1101-8.

270. Lieberman, M.W., et al., *Growth retardation and cysteine deficiency in gamma-glutamyl transpeptidase-deficient mice.* Proc Natl Acad Sci U S A, 1996. **93**(15): p. 7923-6.

271. West, M.B., et al., *Novel insights into eukaryotic gamma-glutamyl transpeptidase 1 from the crystal structure of the glutamate-bound human enzyme.* J Biol Chem, 2013.

272. Lum, G. and S.R. Gambino, *Serum Gamma-Glutamyl Transpeptidase Activity as an Indicator of Disease of Liver, Pancreas, or Bone.* Clinical Chemistry, 1972. **18**(4): p. 358-362.

273. Corti, A., et al., *Gamma-glutamyltransferase of cancer cells at the crossroads of tumor progression, drug resistance and drug targeting.* Anticancer Res, 2010. **30**(4): p. 1169-81.

274. Hanigan, M.H., et al., *Altered expression of gamma-glutamyl transpeptidase in human tumors.* Hum Pathol, 1999. **30**(3): p. 300-5.

275. Candela, T. and A. Fouet, *Poly-gamma-glutamate in bacteria.* Molecular Microbiology, 2006. **60**(5): p. 1091-1098.

276. Zwartouw, H.T. and H. Smith, *Polyglutamic acid from Bacillus anthracis grown in vivo; structure and aggressin activity.* Biochem J, 1956. **63**(3): p. 437-42.

277. Kocianova, S., et al., *Key role of poly-gamma-DL-glutamic acid in immune evasion and virulence of Staphylococcus epidermidis.* J Clin Invest, 2005. **115**(3): p. 688-94.

278. Alkhuder, K., et al., *Glutathione provides a source of cysteine essential for intracellular multiplication of Francisella tularensis.* PLoS Pathog, 2009. **5**(1): p. e1000284.

279. Leduc, D., et al., *Coupled amino acid deamidase-transport systems essential for Helicobacter pylori colonization.* Infect Immun, 2010. **78**(6): p. 2782-92.

280. Wachino, J., et al., *Profile of Expression of Helicobacter pylori gamma-glutamyltranspeptidase.* Helicobacter, 2010. **15**(3): p. 184-92.

281. Rossi, M., et al., *Evidence for conserved function of gamma-glutamyltranspeptidase in Helicobacter genus.* PLoS One, 2012. **7**(2): p. e30543.

282. Ling, S.S.M., K.G. Yeoh, and B. Ho, *Helicobacter pylori γ-glutamyl transpeptidase: A formidable virulence factor.* World Journal of Gastroenterology : WJG, 2013. **19**(45): p. 8203-8210.

283. Ricci, V., et al., *Helicobacter pylori gamma-glutamyl transpeptidase and its pathogenic role.* World J Gastroenterol, 2014. **20**(3): p. 630-8.

284. Chevalier, C., et al., *Essential role of Helicobacter pylori gamma-glutamyltranspeptidase for the colonization of the gastric mucosa of mice.* Mol Microbiol, 1999. **31**(5): p. 1359-72.

285. Shibayama, K., et al., *Metabolism of glutamine and glutathione via gamma-glutamyltranspeptidase and glutamate transport in Helicobacter pylori: possible significance in the pathophysiology of the organism.* Mol Microbiol, 2007. **64**(2): p. 396-406.

286. Sommi, P., et al., *Significance of ammonia in the genesis of gastric epithelial lesions induced by Helicobacter pylori: an in vitro study with different bacterial strains and urea concentrations.* Digestion, 1996. **57**(5): p. 299-304.

287. McGovern, K.J., et al., *gamma-Glutamyltransferase is a Helicobacter pylori virulence factor but is not essential for colonization.* Infect Immun, 2001. **69**(6): p. 4168-73.

288. Flahou, B., et al., *Gastric epithelial cell death caused by Helicobacter suis and Helicobacter pylori gamma-glutamyl transpeptidase is mainly glutathione degradation-dependent.* Cell Microbiol, 2011. **13**(12): p. 1933-55.

289. Moss, S.F., et al., *Induction of gastric epithelial apoptosis by Helicobacter pylori.* Gut, 1996. **38**(4): p. 498-501.

290. Wagner, S., et al., *Regulation of gastric epithelial cell growth by Helicobacter pylori: offdence for a major role of apoptosis.* Gastroenterology, 1997. **113**(6): p. 1836-47.

291. Konturek, P.C., et al., *Helicobacter pylori induces apoptosis in gastric mucosa through an upregulation of Bax expression in humans.* Scand J Gastroenterol, 1999. **34**(4): p. 375-83.

292. Boonyanugomol, W., et al., *Effects of Helicobacter pylori gamma-Glutamyltranspeptidase on Apoptosis and Inflammation in Human Biliary Cells.* Dig Dis Sci, 2012. **57**(10): p. 2615-24.

293. Kim, K.M., et al., *Helicobacter pylori gamma-glutamyltranspeptidase induces cell cycle arrest at the G1-S phase transition.* J Microbiol, 2010. **48**(3): p. 372-7.

294. Shibayama, K., et al., *A novel apoptosis-inducing protein from Helicobacter pylori.* Mol Microbiol, 2003. **47**(2): p. 443-51.

295. Gong, M., et al., *Helicobacter pylori gamma-glutamyl transpeptidase is a pathogenic factor in the development of peptic ulcer disease.* Gastroenterology, 2010. **139**(2): p. 564-73.

296. Busiello, I., et al., *Helicobacter pylori gamma-glutamyltranspeptidase upregulates COX-2 and EGF-related peptide expression in human gastric cells.* Cell Microbiol, 2004. **6**(3): p. 255-67.

297. Ricciotti, E. and G.A. FitzGerald, *Prostaglandins and inflammation.* Arterioscler Thromb Vasc Biol, 2011. **31**(5): p. 986-1000.

298. Polk, D.B. and R.M. Peek, Jr., *Helicobacter pylori: gastric cancer and beyond.* Nat Rev Cancer, 2010. **10**(6): p. 403-14.

299. Yin, Y., et al., *Helicobacter pylori potentiates epithelial:mesenchymal transition in gastric cancer: links to soluble HB-EGF, gastrin and matrix metalloproteinase-7.* Gut, 2010. **59**(8): p. 1037-45.

300. Shirin, H., et al., *Chronic Helicobacter pylori infection induces an apoptosis-resistant phenotype associated with decreased expression of p27(kip1).* Infect Immun, 2000. **68**(9): p. 5321-8.

301. Xia, H.H. and N.J. Talley, *Apoptosis in gastric epithelium induced by Helicobacter pylori infection: implications in gastric carcinogenesis.* Am J Gastroenterol, 2001. **96**(1): p. 16-26.

302. Gerhard, M., et al., *A secreted low-molecular-weight protein from Helicobacter pylori induces cell-cycle arrest of T cells.* Gastroenterology, 2005. **128**(5): p. 1327-39.

303. Kluiver, J., et al., *BIC and miR-155 are highly expressed in Hodgkin, primary mediastinal and diffuse large B cell lymphomas.* J Pathol, 2005. **207**(2): p. 243-9.

304. Fontenot, J.D., M.A. Gavin, and A.Y. Rudensky, *Foxp3 programs the development and function of CD4+CD25+ regulatory T cells.* Nat Immunol, 2003. **4**(4): p. 330-6.

305. Oertli, M., et al., *Helicobacter pylori gamma-glutamyl transpeptidase and vacuolating cytotoxin promote gastric persistence and immune tolerance.* Proc Natl Acad Sci U S A, 2013. **110**(8): p. 3047-52.

306. Farzi, N., et al., *Genotype Diversity and Quasispecies Development of Helicobacter pylori in a Single Host.* Jpn J Infect Dis, 2014.

307. Kuipers, E.J., et al., *Quasispecies development of Helicobacter pylori observed in paired isolates obtained years apart from the same host.* J Infect Dis, 2000. **181**(1): p. 273-82.

308. Morrow, A.L., et al., *Characterization of Helicobacter pylori gamma-glutamyltranspeptidase reveals the molecular basis for substrate specificity and a critical role for the tyrosine 433-containing loop in catalysis.* Biochemistry, 2007. **46**(46): p. 13407-14.

309. Williams, K., et al., *Crystal structure of acivicin-inhibited gamma-glutamyltranspeptidase reveals critical roles for its C-terminus in autoprocessing and catalysis.* Biochemistry, 2009. **48**(11): p. 2459-67.

310. Sharath, B., Prabhune, A.A., Suresh, C.G., Wilkinson, A.J., Brannigan, J.A., *Crystal structure of gamma-glutamyl transferase from Bacillus subtilis.* to be published.

311. Rodríguez-Ortega, M.J., et al., *Characterization and identification of vaccine candidate proteins through analysis of the group A Streptococcus surface proteome.* Nat Biotechnol, 2006. **24**(2): p. 191-7.

312. Hanahan, D., *Studies on transformation of Escherichia coli with plasmids.* J Mol Biol, 1983. **166**(4): p. 557-80.

313. Zhang, Y., U. Werling, and W. Edelmann, *SLiCE: a novel bacterial cell extract-based DNA cloning method.* Nucleic Acids Res, 2012. **40**(8): p. e55.

314. Studier, F.W. and B.A. Moffatt, *Use of bacteriophage T7 RNA polymerase to direct selective high-level expression of cloned genes.* Journal of Molecular Biology, 1986. **189**(1): p. 113-130.

315. Alm, R.A., et al., *Genomic-sequence comparison of two unrelated isolates of the human gastric pathogen Helicobacter pylori.* Nature, 1999. **397**(6715): p. 176-80.

316. Baltrus, D.A., et al., *The complete genome sequence of Helicobacter pylori strain G27.* J Bacteriol, 2009. **191**(1): p. 447-8.

317. Diep, B.A., et al., *Complete genome sequence of USA300, an epidemic clone of community-acquired meticillin-resistant Staphylococcus aureus.* Lancet, 2006. **367**(9512): p. 731-9.

318. Schleifer, K.H. and R. Kilpper-Bälz, *Transfer of Streptococcus faecalis and Streptococcus faecium to the Genus Enterococcus nom. rev. as Enterococcus faecalis comb. nov. and Enterococcus faecium comb. nov.* International Journal of Systematic Bacteriology, 1984. **34**(1): p. 31-34.

319. Datsenko, K.A. and B.L. Wanner, *One-step inactivation of chromosomal genes in Escherichia coli K-12 using PCR products.* Proceedings of the National Academy of Sciences of the United States of America, 2000. **97**(12): p. 6640-6645.

320. Mullis, K., et al., *Specific enzymatic amplification of DNA in vitro: the polymerase chain reaction.* Cold Spring Harb Symp Quant Biol, 1986. **51 Pt 1**: p. 263-73.

321. Sanger, F., S. Nicklen, and A.R. Coulson, *DNA sequencing with chain-terminating inhibitors.* Proc Natl Acad Sci U S A, 1977. **74**(12): p. 5463-7.

322. Chung, C.T., S.L. Niemela, and R.H. Miller, *One-step preparation of competent Escherichia coli: transformation and storage of bacterial cells in the same solution.* Proceedings of the National Academy of Sciences of the United States of America, 1989. **86**(7): p. 2172-2175.

323. Inoue, H., H. Nojima, and H. Okayama, *High efficiency transformation of Escherichia coli with plasmids.* Gene, 1990. **96**(1): p. 23-8.

324. Noto, J.M. and R.M. Peek, Jr., *Genetic manipulation of a naturally competent bacterium, Helicobacter pylori.* Methods Mol Biol, 2012. **921**: p. 51-9.

325. Bolz, C.F., *Untersuchungen zum biochemischen Wirkungsmechanismus der Helicobacter pylori gamma-Glutamyltranspeptidase*, in *Lehrstuhl für Biologische Chemie*. 2013, Technische Universität München.

326. Selvaraj, P. and K.A. Balasubramanian, *Comparative structural and lectin-binding studies on gamma-glutamyltransferase from human adult liver, fetal liver and primary hepatoma.* Eur J Biochem, 1985. **153**(3): p. 485-90.

327. Smith, P.K., et al., *Measurement of protein using bicinchoninic acid.* Anal Biochem, 1985. **150**(1): p. 76-85.

328.   Laemmli, U.K., *Cleavage of structural proteins during the assembly of the head of bacteriophage T4.* Nature, 1970. **227**(5259): p. 680-5.

329.   Engvall, E. and P. Perlmann, *Enzyme-linked immunosorbent assay (ELISA). Quantitative assay of immunoglobulin G.* Immunochemistry, 1971. **8**(9): p. 871-4.

330.   Frankel, B.A., et al., *Vinyl sulfones: inhibitors of SrtA, a transpeptidase required for cell wall protein anchoring and virulence in Staphylococcus aureus.* J Am Chem Soc, 2004. **126**(11): p. 3404-5.

331.   Weissman, K.J. and R. Muller, *Myxobacterial secondary metabolites: bioactivities and modes-of-action.* Nat Prod Rep, 2010. **27**(9): p. 1276-95.

332.   Muller, R. and J. Wink, *Future potential for anti-infectives from bacteria - how to exploit biodiversity and genomic potential.* Int J Med Microbiol, 2014. **304**(1): p. 3-13.

333.   Jansen, R., et al., *Pyrronazols, metabolites from the myxobacteria Nannocystis pusilla and N. exedens, are unusual chlorinated pyrone-oxazole-pyrroles.* J Nat Prod, 2014. **77**(2): p. 320-6.

334.   Okanya, P.W., et al., *Hyaladione, an S-methyl cyclohexadiene-dione from Hyalangium minutum.* J Nat Prod, 2012. **75**(4): p. 768-70.

335.   Grote, A., et al., *JCat: a novel tool to adapt codon usage of a target gene to its potential expression host.* Nucleic Acids Res, 2005. **33**(Web Server issue): p. W526-31.

336.   Kabsch, W., *Xds.* Acta Crystallogr D Biol Crystallogr, 2010. **66**(Pt 2): p. 125-32.

337.   Vagin, A. and A. Teplyakov, *MOLREP: an Automated Program for Molecular Replacement.* Journal of Applied Crystallography, 1997. **30**(6): p. 1022-1025.

338.   Winn, M.D., et al., *Overview of the CCP4 suite and current developments.* Acta Crystallogr D Biol Crystallogr, 2011. **67**(Pt 4): p. 235-42.

339.   Murshudov, G.N., A.A. Vagin, and E.J. Dodson, *Refinement of macromolecular structures by the maximum-likelihood method.* Acta Crystallogr D Biol Crystallogr, 1997. **53**(Pt 3): p. 240-55.

340.   Emsley, P., et al., *Features and development of Coot.* Acta Crystallogr D Biol Crystallogr, 2010. **66**(Pt 4): p. 486-501.

341.   Stole, E., et al., *Interaction of gamma-glutamyl transpeptidase with acivicin.* J Biol Chem, 1994. **269**(34): p. 21435-9.

342.   King, J.B., et al., *A novel, species-specific class of uncompetitive inhibitors of gamma-glutamyl transpeptidase.* J Biol Chem, 2009. **284**(14): p. 9059-65.

343.   Wecke, T. and T. Mascher, *Antibiotic research in the age of omics: from expression profiles to interspecies communication.* Journal of Antimicrobial Chemotherapy, 2011. **66**(12): p. 2689-2704.

344.   Gengenbacher, M. and T. Dick, *Antibacterial Drug Discovery: Doing It Right.* Chemistry & Biology, 2015. **22**(1): p. 5-6.

345.   Carlsohn, E., et al., *HpaA is essential for Helicobacter pylori colonization in mice.* Infect Immun, 2006. **74**(2): p. 920-6.

346.   Loh, J.T., et al., *Helicobacter pylori HopQ outer membrane protein attenuates bacterial adherence to gastric epithelial cells.* FEMS microbiology letters, 2008. **289**(1): p. 53-58.

347. Derbise, A., et al., *A rapid and simple method for inactivating chromosomal genes in Yersinia.* FEMS Immunol Med Microbiol, 2003. **38**(2): p. 113-6.

348. Boivin, S., S. Kozak, and R. Meijers, *Optimization of protein purification and characterization using Thermofluor screens.* Protein Expression and Purification, 2013. **91**(2): p. 192-206.

349. Pantoliano, M.W., et al., *High-density miniaturized thermal shift assays as a general strategy for drug discovery.* J Biomol Screen, 2001. **6**(6): p. 429-40.

350. Call, E., et al., *Sortase-deficient lactobacilli: effect on immunomodulation and gut retention.* Microbiology, 2014.

351. Banerjee, S.K., et al., *Lysozyme-catalyzed Reaction of the N-Acetylglucosamine Hexasaccharide : Dependence of Rate on pH.* Journal of Biological Chemistry, 1973. **248**(13): p. 4786-4792.

352. Joseph-McCarthy, D., et al., *Fragment-based lead discovery and design.* J Chem Inf Model, 2014. **54**(3): p. 693-704.

353. Hann, M.M., A.R. Leach, and G. Harper, *Molecular complexity and its impact on the probability of finding leads for drug discovery.* J Chem Inf Comput Sci, 2001. **41**(3): p. 856-64.

354. Leach, A.R., et al., *Fragment screening: an introduction.* Mol Biosyst, 2006. **2**(9): p. 430-46.

355. Carr, R. and H. Jhoti, *Structure-based screening of low-affinity compounds.* Drug Discovery Today, 2002. **7**(9): p. 522-527.

356. Erlanson, D.A., R.S. McDowell, and T. O'Brien, *Fragment-Based Drug Discovery.* Journal of Medicinal Chemistry, 2004. **47**(14): p. 3463-3482.

357. Ferguson, F.M., et al., *Targeting Low-Druggability Bromodomains: Fragment Based Screening and Inhibitor Design against the BAZ2B Bromodomain.* Journal of Medicinal Chemistry, 2013. **56**(24): p. 10183-10187.

358. Ringe, D., *What makes a binding site a binding site?* Curr Opin Struct Biol, 1995. **5**(6): p. 825-9.

359. Tate, S.S. and M.E. Ross, *Human kidney gamma-glutamyl transpeptidase. Catalytic properties, subunit structure, and localization of the gamma-glutamyl binding site on the light subunit.* Journal of Biological Chemistry, 1977. **252**(17): p. 6042-5.

360. Muller, S.A., et al., *Stable isotope labeling by amino acids in cell culture based proteomics reveals differences in protein abundances between spiral and coccoid forms of the gastric pathogen Helicobacter pylori.* J Proteomics, 2015.

361. Azevedo, N.F., et al., *Coccoid form of Helicobacter pylori as a morphological manifestation of cell adaptation to the environment.* Appl Environ Microbiol, 2007. **73**(10): p. 3423-7.

Declaration

I, Christina Daschkin, hereby declare that I independently prepared the present thesis, using only the references and resources stated. This work has not been submitted to any examination board yet. Parts of this work will be published in scientific journals.

Ein besonderer Dank gilt Tobias Kruse für die intensive Zusammenarbeit zu immer wieder neuen Ideen sowie für die Möglichkeit, an seinem Projekt zu den HP-Kandidaten mitzuwirken.

Für das Zurverfügungstellen der Mausseren danke ich Dr. Florian Anderl und Tobias Kruse.

Ich danke Dr. Florian Anderl und Raphaela Semper für ihre Hilfe bezüglich Messung und Auswertung der Durchfluss-Zytometrie-Experimente.

Luca Formichella danke ich für die Bereitstellung serologisch charakterisierte Patientenseren zur Analyse der HP-Kandidaten.

Ich danke meinen Praktikanten Dennis Schöne und Lennart von Fritsch für ihre Unterstützung im Labor.

Dr. Stephanie Grubmüller, Dr. Phillipp Beck, Christine Öllig und Cardine Nokwe Nkumbe danke ich für die entspannte Zusammenarbeit und nette Atmosphäre bei der Betreuung von Saalpraktika.

Insbesondere danke ich der „Small-Molecule-Gruppe" für den anregenden Austausch und die vielen kleinen Hilfen mit herausfordernden Experimenten und Daten.

Für unvergessliche Erlebnisse auf Dienstreisen und Fortbildungen danke ich Dr. Hannelore Meyer, Tobias Kruse, Zohra Sahavi-Ouriaghi, Luca Formichella und Daniela Scheikl.

Der gesamten Arbeitsgruppe Gerhard möchte ich sehr für die angenehme Zusammenarbeit, gegenseitige Hilfe und die entspannte Atmosphäre, besonders in der Kaffeeküche, danken.

Ich danke Dr. Martin Steinborn, Dr. Hannelore Meyer und Ramona Nitiu für die aufmerksame Durchsicht meiner Arbeit.

★ ★ ★

Ein ganz besonderer Dank gilt meinem Freund Martin Steinborn, der mich stets unterstützt, motiviert und gestärkt hat. Das Vertrauen, die Geduld und das Verständnis, die mir von ihm, meinen Eltern und meiner gesamten Familie entgegengebracht wurden, haben mir die notwendige Kraft und Ruhe gegeben mir treu zu bleiben und meinen Weg zu gehen.